Anthropogenic Climate Change and Extreme Weather Events: Implications for Bangladesh



Ruksana Haque Rimi

Regent's Park College

Environmental Change Institute

School of Geography and the Environment

University of Oxford

A Thesis submitted to the Faculty of Social Sciences for the degree of Doctor of Philosophy at the University of Oxford

Trinity Term, 2019

Abstract

Probabilistic Event Attribution (PEA) quantifies the change in risk of extreme weather events due to external drivers of climate change. The regional climate model (RCM) of the weather@home system has been successfully used for this purpose. So far, most PEA based studies have focused on extreme events of mid-latitudes and developed countries, while the events occurring in tropical regions and developing countries have gained little attention. This thesis evaluates the performance of the RCM of weather@home over the complex tropical monsoon climate region of South Asia, with particular focus on Bangladesh. In a combined process-based and performance-based evaluation process, first the model's response to observed variability of sea surface temperatures (SSTs) are assessed. Second, the RCM's skill to simulate the extreme events in Bangladesh is evaluated against observations. The results suggest that the RCM performs well, capturing both, influence of observed natural SST variations and extreme weather events in Bangladesh. The thesis uses large ensembles of weather@home RCM simulations for two studies. PEA is first applied to attribute contributions of past and future greenhouse gas (GHG) emissions to extreme events under current climate conditions and future warmer worlds. In accordance with the targets set out in the Paris Agreement, 1.5 and 2.0 degrees warming scenarios are investigated. Results indicate that the risk of seasonal extreme rainfall events across Bangladesh will increase with additional global warming. Anthropogenic aerosols are found to be a significant influencing factor along with GHG concentrations and large-scale temperature in determining the climate change impacts. The RCM based results are found to be consistent with the findings based on simulations from four other Atmosphere Only Global Climate Models (AGCMs) under the Half a degree Additional warming, Prognosis and Projected Impacts (HAPPI) project. PEA is secondly applied for an extreme pre-monsoon rainfall event of 2017 that occurred over north-east Bangladesh and caused flash flood and severe crop damage. According to this analysis, anthropogenic climate change is assessed to have increased the risk of such event occurring by more than a factor of 2. Findings of this thesis show that the RCM of weather@home system may provide a sufficiently reliable tool for attributing human impacts on the likelihood of extreme events over the complex tropical monsoon climate region of South Asia in general and Bangladesh in particular. Since anthropogenic climate change is found to be of crucial importance with regard to extreme weather events, the conclusions of this thesis will facilitate further attribution studies over the region and help to provide guidance for local policy makers as far as climate change adaption is concerned.

Table of Contents

Abstract i

Table of Contents ii

Acknowledgements vii

List of Tables ix

List of Figures x

List of Abbreviations and Acronyms xxiv

1. **Introduction** 1

1.1. Motivation and aims 3

1.1.1. Background and Rational 3

1.1.2. Probabilistic Event Attribution 4

1.1.3. Extreme Event Attribution Approaches 9

1.1.4. The weather@home system 18

1.1.5. Research Aims and Key Questions 21

1.2. Study Area of Bangladesh 26

1.2.1. Regional Climate 27

1.2.2. Observed recent change in climate 29

1.2.3. Projected future change in climate 30

1.2.4. Extreme weather events 32

1.2.5. Significance of attribution assessments for Bangladesh 33

1.4 Organization of the Thesis 34

2. **Modelling frameworks, observation data sets and analytical methods** 37

2.1. Introduction 39

2.2. Modelling frameworks 39

2.2.1. The weather@home system 39

2.2.1.1. Volunteer Distributed Computing 41
2.2.1.2. Model configuration 42
2.2.2. Model scenarios 45
2.3. Observational Data sets 53
2.3.1. Overview 53
2.3.2. Justification for main reference data selection 57
2.4. Methods 61
2.4.1. Extreme Value distribution 61
3. **Model's response to observed variations in sea surface temperature** 69
3.1. Introduction 71
3.2. Data and methods 74
3.2.1. Model and Observation Data 74
3.2.2. Methods 75
3.3. Results and discussion 77
3.3.1. South Asian monsoon system 77
3.3.2. ENSO and IOD relationship 80
3.3.3. ENSO and IOD influence on rainfall 82
3.4. Conclusions 86
4. **Evaluation of a large ensemble regional climate modelling system for extreme weather events analysis over Bangladesh** 89
Authorship Declaration 92
Abstract.. 93
4.1. Introduction 94
4.2. The study region and subregions 96
4.3. Data and methods for model evaluation 98

4.3.1. Observational data sets 98
4.3.2. Model data 100
4.3.3. Extreme events 101
4.4. Results and discussion 103
4.4.1. Spatial variations in seasonal means 103
4.4.2. Annual cycle 106
4.4.3. Extreme events 112
4.5. Conclusions 121
Supplement of 124
5. **Risks of seasonal extreme rainfall events in Bangladesh under 1.5 and 2.0 degrees' warmer worlds – How anthropogenic aerosols change the story** 135
Authorship Declaration 138
Abstract.. 139
5.1. Introduction 140
5.2. Data and Methods 146
5.2.1. Observational data 146
5.2.2. Model setup and experimental design 146
5.2.3. Methods 149
5.3. Results and Discussion 155
5.3.1. Model Evaluation 155
5.3.2. Impact of Climate Change and Aerosol Reduction on Seasonal Mean Rainfall 157
5.3.3. Extreme Rainfall Events 164
5.4. Conclusions 171
Data/Code availability 177
Supplement 177

Author contributions 177
Competing interests 178
Acknowledgments 178
Supplement of 179
6. **Risks of pre-monsoon extreme rainfall events of Bangladesh: Is anthropogenic climate change playing a role?** 199
Authorship Declaration 202
Main Findings 203
6.1. Introduction 203
6.2. Data and methods 205
6.3. Results and discussion 207
6.4. Conclusions 210
Supplementary Materials 211
6.5. Additional notes of clarification 214
6.5.1. Reason behind no bias correction 214
6.5.2. Observational uncertainties 215
6.5.3. Does GPCC observation change the attribution statement? 216
6.5.4. Concluding remark 218
7. **Conclusion** 219
7.1. Synthesis of thesis findings 221
7.1.1. Model evaluation results 223
7.1.1.1. Process-based model evaluation 223
7.1.1.2. Performance-based model evaluation 224
7.1.2. Results from PEA-based studies 225
7.1.2.1. Present and future risks of seasonal extreme events 225

7.1.2.2. Extreme event attribution of 2017 226
7.2. Broader relevance and applicability 227
7.2.1. Contribution towards climate modelling for studying extremes 227
7.2.2. Better resilience and adaptation 227
7.2.3. Contribution to loss and damage 229
7.3. Potential future research avenues 230
7.3.1. Spatial resolution and domain size 232
7.3.2. Convection parameterisation at a coarse grid scale 233
7.3.3. Advanced correction techniques 234
7.3.4. Multi-model studies for attribution analysis 234
7.3.5. Aerosol-only forcings scenario 235
7.3.6. Use of Fixed versus variable SSTs 236
7.3.7. Physical mechanisms 236
7.3.8. Use of improved observational data 237
7.3.9. Extended attribution studies for impact assessments 238
7.4. Concluding remarks 238
8. Bibliography 241

Acknowledgements

Completing the journey for this DPhil was the greatest learning experience for me. I have realized that achieving the hardest ambition is possible with strong motivation, continuous support and lots of encouragement.

My deepest sense of gratitude goes to my supervisor, Professor Myles Allen for giving me the opportunity to work in his research group, and supporting me with his valuable insights, guidance, encouragement, and patience. Thank you for motivating me and allowing me to continue to try and achieve my goals, although it took much longer than expected.

I truly appreciate my supervisor Dr Karsten Haustein, without whose remarkable support I would have faced much more difficulty in completing this DPhil. Thanks for innumerable discussions, insightful comments and reassurance that I was going in the right direction. Learning how to write scripts in R programming language from you was the most vital stepping-stone towards my successful journey.

I would like to thank my supervisor Dr Emily Barbour, especially for her remote supervision from Australia, inspiration to complete tasks, long discussion sessions over skype, and all her constructive comments to improve this research activity. I will always carefully consider two aspects of research - its ‘novelty’ and associated ‘uncertainty’.

I would like to thank the Commonwealth Scholarship Commission, Department for International Development (DFID), United Kingdom, for funding my DPhil at University of Oxford for three years, without this financial support I would have been unable to study here.

I am grateful to my College Advisor, Dr Larry Kreitzer for his valuable guidance and significant help to overcome many difficulties. My heartfelt gratitude goes to Research Degrees Coordinator, Ruth Saxton for her ceaseless, extraordinary support with a great positive mind. Thanks to all IT technical support staff for dealing with the endless IT related problems.

I am grateful to Neil Massey for introducing me with the weather@home model outputs and helping with the very first data analysis and visualization. Thanks to Richard Jones from the Met Office for his guidance during the climate model evaluation process. I am grateful to Dr Sebastian Engelstaedter for helping me with coding and bash shell scripting. Thanks to Sebastian Sippel for guiding me through extreme value analysis method. Thanks to Lisa Schipper and Rachel James for discussing role of attribution in adaptation as well as loss and damage.

Thanks to Amy, Adnan, Boipelo, Callum, Emma, James, Lisa, Peter, Rachel, Sarah and others from the Climate Research Lab (CRL) and Environmental Change Institute for inspiring me to work harder, be more organized, and achieve goals. Special thanks to Emma, James and Victoria for doing the proof-reading. Thanks to Victoria for reminding me that it is more important to continue even with slow progress, because everyone has a different story.

No words can actually express my gratefulness to my parents. Thanks for believing in me, and giving the highest priority to my education. Thanks mom for having confidence that I could come to Oxford for my DPhil, all the way from Bangladesh. Thanks Dad for supporting me throughout my whole life. I am immeasurably grateful to my brothers Md. Erfanul Haque Raihan and Md. Enamul Haque Rimon for their encouragements and for taking care of my problems of all sorts.

I am grateful to my mother-in-law for her understanding and patience. I deeply miss my much-loved father-in-law, who had cared for me like his own daughter and loved to have a cup of tea with me. I am sure he would have been so proud to see my accomplishment.

Finally, I would like to thank my husband, the best life partner ever, my ultimate mentor and guide, Md. Zahidul Abedin for his continued love and support, for all his sacrifices, and for not giving up on me when I failed over and over again, for standing beside me determinedly until I did succeed. A lot of thanks to my lovely kids Zubayed Abedin and Zunayrah Abedin for their understanding, for waiting countless nights for me, and sometimes for hanging around with me at the CRL and even helping me at home whenever they could with their little activities. Without all your support I would have been unable to complete this extra-ordinary journey.

List of Tables

Table 2.1: The CMIP5 models used to calculate δSSTs.....48

Table 2.2: Basic information about the observational data sets used in this thesis. 54

Table 2.3: A summary of the model ensembles under different climate conditions 67

Table S4.1: Basic information about the five observation datasets……... 124

Table S5.1: Basic information about the two observation data sets…….. 179

Table S5.2: As per actual climate model ensemble during 2006-2015 - the wettest and driest two years over the four sub-regions.....179

Table S5.3: Basic information about the four HAPPI AGCMs used in this study (adapted from Chevuturi et al., 2018).....180

Table S5.4: The risk ratios with associated uncertainty ranges (in brackets) for four MAM rainfall events.....181

Table S5.5: The risk ratios with associated uncertainty ranges (in brackets) for four JJAS rainfall events.....183

List of Figures

Figure 1.1: This map shows all currently running regions under weather@home (source: https://www.climateprediction.net/weatherathome/regions/). The purple rectangle shows South Asia region. 19

Figure 1.2: The Ganges-Brahmaputra-Meghna (GBM) Basin and the downstream country of Bangladesh (red dotted rectangle indicates location) through which the rivers finally flow into the Bay of Bengal (source: Banglapedia 2012). 27

Figure 2.1: Schematic diagram for steps in the calculation of delta SSTs (adapted from http://climateprediction.net/wiki/lib/exe/fetch.php?media=wiki:natsst_doc_v2.pdf) 49

Figure 2.2: Return time plot for daily rainfall (mm/day) during monsoon season over north-east parts of Bangladesh..... 65

Figure 3.1: Schematic diagram showing the regions (in dark red coloured rectangles) used to monitor ENSO and IOD using SSTs in the Pacific and Indian Ocean, respectively. Image is adapted from http://www.bom.gov.au/climate/enso/indices/about.shtml..... 73

Figure 3.2: Winter (DJF, left column) and summer monsoon (JJA, right column) climatology of mean rainfall (mm/day) and 10 m wind are shown by the shading and vectors, respectively. The GCM outputs for wind and rainfall are compared with observations from GPCC and ERA-Interim (for rainfall and vector wind, respectively) datasets. 78

Figure 3.3: Winter (DJF, left column) and summer monsoon (JJA, right column) climatology of mean MSLP (hPa) and 10 m wind are shown by the shading and vectors, respectively. The GCM outputs for wind and MSLP are compared with observations from GPCC and ERA-Interim (for MSLP and vector wind, respectively) datasets. 79

Figure 3.4: Lagged correlations (by +6 to -6 months) between IOD and Niño3.4 indices with de-trended data for all months (Jan-Dec) during 1870-2018. Month indicates month of the year for the IOD index, while positive lags correspond to ENSO leading IOD, negative lags to ENSO lagging IOD. Correlation magnitudes are shown in red colour, while the strengths of correlations (from weakest to strongest) are indicated by the coloured contours. Where, purple is used for the strongest correlations and yellow for the weakest. Note that high correlations are only observed with SON IOD. Purple and dark blue contours correspond to correlations greater than 0.3 and 0.2, respectively.....81

Figure 3.5: Spatial distributions of correlation coefficients for the relationship between NINO3.4 and rainfall anomalies in observation (in right column) and model (in left column) in JJA, SON, DJF, and MAM (from top to bottom rows, respectively) during 1986-2015. The purple and orange shades (shading differs by 0.1) indicate statistically significant correlation coefficients (r>0.4) at 95% confidence level. The nonsignificant correlation coefficients are shown in olive green and brown shades. 83

Figure 3.6: Spatial distributions of correlation coefficients for the relationship between IOD and rainfall anomalies in observation (in right column) and model (in left column) in JJA, SON, DJF, and MAM (from top to bottom rows, respectively) during 1986-2015. The purple and orange shades (shading differs by 0.1) indicate statistically significant correlation coefficients (r>0.4) at 95% confidence level. The nonsignificant correlation coefficients are shown in olive green and brown shades. 84

Figure 4.1: The SAS50 domain of HadRM3P model uses the CORDEX region South Asia, which covers from north to south: The Himalayas as well as Lake Victoria; India; Bangladesh; the Bay of Bengal; and the surrounding ocean in the centre of the region and in west–east direction it ranges from the Horn of Africa and the Arabian Peninsula to Vietnam and Cambodia (left panel, CPDN, 2017). Here, the left panel shows the physical features with

darker shades on land area indicating high lands or mountains and lighter shades indicating the plains or low lands. The right panel shows the model evaluation domain with longitudes and latitudes ranging from 86°E to 96°E and 17°N to 27°N, respectively. The observed mean rainfall (in mm/day; from APHRODITE data set) of monsoon season is shown. The four subregional model evaluations are performed over the four areas of boxes (1–4) shown in the right panel within Bangladesh…….... 97

Figure 4.2: Spatial distributions of (a) mean daily surface temperature (°C), (b) rainfall (mm/day) in the APHRODITE observation data set; (c) mean daily surface temperature (°C) bias and (d) rainfall (mm/day) bias (model minus observation) over the study region in monsoon (JJA), post-monsoon (SON), winter (DJF) and pre-monsoon (MAM) season during 1988–2007. The coldest and driest season is winter (DJF), hottest seasons are both pre-monsoon and monsoon (MAM and JJA) and the wettest season is the monsoon (JJA). The highest warm and wet bias (in the north and east parts of the study region) is found in MAM, whereas, JJA has the highest dry bias with respect to APHRODITE observations. 105

Figure 4.3: The annual cycle of daily temperature (°C) (top panel) and rainfall (mm/day) (middle panel) during 1988–2007 and during 1998–2013 (bottom panel) over the study region — model ensemble mean (black line), with range of 10–90th percentile (grey) versus APHRODITE (red), GPCC (blue), TRMM (cyan) and CPC (orange) with range of 10–90th percentile in their respective light colours. There is nearly 2 weeks difference in the monsoon onset between the model and the observation.....107

Figure 4.4: Annual cycles of daily mean temperature (C) over the four subregions of Bangladesh during 1988–2007—model ensemble mean (black line), with range of 10–90th percentile (grey) versus APHRODITE (red) with range of 10–90th percentile (light red). The

amount of temperature bias among the four subregions is different, which is important to consider for local weather events.....109

Figure 4.5: Annual cycles of daily rainfall over the four subregions within Bangladesh during 1988–2007—model ensemble mean (black line), with range of 10–90th percentile (grey) versus APHRODITE (red), GPCC (blue) and CPC (orange). The amount of biases among these four subregions varies, and this variation is important to consider for local weather events. 110

Figure 4.6: Spatial distribution of mean daily surface temperature (_C) (top two panels) and rainfall (mm/day) (bottom two panels) in pre-monsoon (MAM) and shifted pre-monsoon (SMAM) season over the study region. The maximum hot bias (up to 4°C) and wet bias (up to 16 mm/day) appear in MAM. In SMAM the temperature bias is reduced by 1–2°C over most of the study region. For rainfall, the wet bias is reduced by nearly 7 mm/day in the northern parts; while a shift from wet bias to dry bias is noticed in the western parts of the study region.....111

Figure 4.7: Quantile-quantile plots for 5 days mean temperatures (°C) over the study region in the left column and daily temperatures over the sub-regions 2 and 4 in middle and right columns respectively during 1988-2007 in monsoon (JJA), post-monsoon (SON), winter (DJF) and pre-monsoon (MAM) season – model HadRM3P versus APHRODITE. The red dots represent from 1st to 99th percentile of the distribution of the variable, if the dot is directly overlying the 1:1 line of agreement (diagonal black line), the model perfectly simulates the observed event; if the dot is below the line, the model overestimates the observed event and if it is above the line, the model underestimates the observed event. 113

Figure 4.8: Same as Figure 4.7 but for rainfall – model HadRM3P versus APHRODITE (red), GPCC (blue) and CPC (orange) during 1988-2007. The wet bias in MAM is largely resolved in the distributions in the shifted pre-monsoon, SMAM. 115

Figure 4.9: Return time plots for GEV distributions fitted to maximum five days mean temperatures (°C) in the wet seasons over the study region during 1988-2007 – model HadRM3P (black) versus APHRODITE (red). The individual red dots represent the maximum 5 days mean temperatures (°C) during a season in a year (i.e., total 20 dots); shaded polygons represent 2.5-97.5% range of the confidence interval and the solid lines represent the best fit lines within the confidence interval for events from 2 to 100 years of return period. The black dots represent the maximum of five days mean temperatures (°C) during a season (i.e., 90 dots for 90 days) from all 200 members of the model ensemble....116

Figure 4.10: Return time plots for GEV distributions fitted to maximum 5-day mean temperatures (°C) in the wet seasons over the subregion 2 of Bangladesh during 1988–2007—model HadRM3P (black) versus APHRODITE (red). The individual red dots represent the maximum 5-day mean temperatures (°C) during a season in a year (i.e., total 20 dots); shaded polygons represent 2.5–97.5% range of the confidence interval and the solid lines represent the best fit lines within the confidence interval for events from 2 to 100 years of return period. The black dots represent the maximum 5-day mean temperatures (°C) taken from all 200 members of the model ensemble.....117

Figure 4.11: Return time plots for GEV distributions fitted to maximum 5-day mean temperatures (°C) in the wet seasons over the subregion 4 of Bangladesh during 1988–2007—model HadRM3P (black) versus APHRODITE (red). The individual red dots represent the maximum 5-day mean temperatures (°C) during a season in a year (i.e., total 20 dots); shaded polygons represent 2.5–97.5% range of the confidence interval and the solid

lines represent the best fit lines within the confidence interval for events from 2 to 100 years of return period. The black dots represent the maximum 5-day mean temperatures (°C) taken from all 200 members of the model ensemble.....118

Figure 4.12: Return time plots for GEV distributions fitted to maximum 5-day mean rainfall (mm) in wet seasons over the study region (shown in Figure 4.1, right panel) during 1988–2007—model HadRM3P (black), versus APHRODITE (red), GPCC (blue) and CPC (orange). The individual dots represent the maximum 5-day mean rainfall during a season in a year (i.e., total 20 dots per data sets); shaded polygons represent 2.5–97.5% range of the confidence interval and the solid lines represent the best fit lines within the confidence interval for events from 2 to 100 years of return period. The black line for the model that is in closest agreement with the APHRODITE observations (in red) during JJA and SON is comprised of the maximum 5-day mean rainfall (mm) taken from all 200 members of the model ensemble (i.e., 20 × 200 dots).....119

Figure 4.13: Same as Figure 4.10 but for the maximum 5-day mean rainfall events during MAM (left column) and JJA (right column) over the subregion 2 (top row) and subregion 4 (bottom row) of Bangladesh. The model-simulated extremes of 5-day mean rainfall events with return periods of 50–100 years are within the confidence intervals of at least one observation data set. MAM extremes are much better represented by the model and so a SMAM analysis is not required. The model underestimates the extremes during JJA when compared to APHRODITE and GPCC but lies within the confidence interval of CPC observations. 120

Figure S4.1: Histograms for 5 days mean surface temperature (°C) over the study region (left column) and daily surface temperature (°C) over subregion 3 (middle column) and subregion 4 (right column) during 1988–2007 in (a) monsoon (JJA), (b) post-monsoon (SON), (c) winter (DJF) and (d) pre-monsoon (MAM) season—model HadRM3P (black) versus

APHRODITE (red). The model gives cold biases during winter and post-monsoon seasons. There exists minimum bias during monsoon and maximum hot bias during pre-monsoon summer season. The amounts of seasonal daily temperature biases vary between the two subregions 3 and 4 in Bangladesh……. 128

Figure S4. 2: Same as Figure S1 but for rainfall (mm/day)—model HadRM3P (black) versus APHRODITE (red) and GPCC (blue). The model tends to simulate high density events of 1 mm/day rainfall in all three seasons except in the monsoon season; when the rainfall is underestimated at the higher ends.....129

Figure S4.3: Annual cycles of daily rainfall over the four subregions within Bangladesh during 1998–2013—model ensemble mean (black line), with range of 10–90th percentile (grey) versus TRMM (cyan), GPCC (blue) and CPC (orange). The amount of biases among these four subregions varies, and this variation is important to consider for local weather events. Subregions 2 and 4 experience the highest amounts of rainfall within Bangladesh, therefore looking at extremes can be useful in these two subregions.....130

Figure S4.4 : Quantile–quantile plots for 5-day mean rainfall over Bangladesh (left column) and daily rainfall (mm/day) over subregions 3 and 4 (middle and right column) during 1998–2013—model HadRM3P versus TRMM (cyan), GPCC (blue) and CPC (orange). The wet biases in (d) MAM is largely resolved in the distributions in (e) shifted pre-monsoon (SMAM).....131

Figure S4.5: Return time plots for GEV distributions fitted to maximum 5-day mean rainfall (mm) in wet seasons over the study region (shown in Figure 1, right panel) during 1998–2015—model HadRM3P (black), versus reference dataset of TRMM (cyan), GPCC (blue) and CPC (orange). The individual dots represent the maximum 5-day mean rainfall during a season in a year (i.e., total 16 dots per data sets); shaded polygons represent 2.5–97.5% range

of the confidence interval and the solid lines represent the best fit lines within the confidence interval for events from 2 to 100 years of return period. The black line for the model is comprised of the maximum 5-day mean rainfall (mm) taken from all 200 members of the model ensemble (i.e., 20 × 200 dots). 132

Figure S4.6 : Same as Figure S5 but for maximum 5-day mean rainfall events during MAM (left column) and JJA (right column) over subregion 2 (top row) and subregion 4 (bottom row). During MAM the model simulates the extreme rainfall events that are not highly overestimated and therefore a SMAM analysis is not required. During JJA, the model underestimates the maximum 5-day mean rainfall events of 2-16 years return periods but the extreme rainfall events of 50–100-year return period are within the confidence intervals of observations. 133

Figure 5.1: Seasonal cycles of five day mean rainfall under different forcing scenarios over the four sub-regions of Bangladesh. The ACT (black), NAT (green) and GHG-only (orange), HAPPI 1.5 (blue) and 2.0 (red) ensembles are compared with the observations from APHRODITE (dark purple) and CPC (dark purple). The model adequately captures the seasonal cycle of rainfall compared to observation but underestimates monsoon rainfall. Only over sub-region 2, rainfall is clearly shifting from NAT to ACT, from ACT to GHG-only, from ACT to HAPPI 1.5 and from HAPPI 1.5 to 2.0 forcing scenarios…….... 156

Figure 5.2: Percentage change (PC) in MAM mean rainfall between different forcing scenarios. The top row (panels a-d) shows the regional PC over central parts of the South Asia. a. ACT rainfall PC relative to NAT over SA b. ACT rainfall PC relative to HAPPI 1.5°C over SA c. HAPPI 1.5°C rainfall PC relative to HAPPI 2.0°C over SA d. ACT rainfall PC relative to GHG-only. Bottom row (panels e-h) shows PC in the same way but over

Bangladesh. The four boxes (1-4) on top of the panel e represent the four sub-regions of Bangladesh. 158

Figure 5.3: Same as Fig. 5.2, but for JJAS rainfall PC. This figure shows that the apparently non-linear response between panels of a, b, and c (or, e, f, g) can be explained by the response for GHG-only (anthropogenic aerosols reduced to pre-industrial levels) in the panel d (or, h) 160

Figure 5.4: Seasonal mean rainfall in MAM (left column) and JJAS (right column) over the sub-regions 1 and 2 (top and bottom row) of Bangladesh. Green, orange, grey, blue and red colours represent NAT, GHG-only, ACT, HAPPI 1.5 and HAPPI 2.0 ensembles respectively. Each panel has different y-scale range to clearly indicate the details of changes in the median values between different model ensembles. The horizontal black line in each box indicates the median value, the bottom and top limits of the box represents the 25^{th} and 75^{th} percentiles respectively. The figure shows that aerosol impacts over both sub-regions 1 and 2 are larger in MAM dry season than that in JJAS wet season. 162

Figure 5.5: Same as Fig. 5.4, but for sub-regions 3 and 4. During MAM over both sub-regions 3 and 4, aerosol effects repress the mean rainfall change between NAT and ACT (i.e., ACT rainfall is lower than NAT). On the other hand, during JJAS over both sub-regions 3 and 4, with lesser aerosol masking effects, ACT has higher mean rainfall than NAT and GHG-only would have noticeably much higher mean rainfall. 163

Figure 5.6: Return time plots for MAM daily rainfall under different forcing scenarios over the sub-regions 1 and 2 of Bangladesh. The ACT (black), ACT highest (sky-blue), ACT lowest (grey), NAT (green) and GHG-only (orange) ensembles are compared with the HAPPI 1.5 (blue) and HAPPI 2.0 (red) ensembles. Anthropogenic warming effects have not strongly influenced the present-day risks of extreme MAM rainfall over sub-region 1 (Fig. 5.6a). With

a 1.5 or 2.0 degrees' world, this sub-region might see extreme rainfall events with four-fold higher risks. 165

Figure 5.7: Same as Fig 5.6, but showing return time plots for MAM daily rainfall under different forcing scenarios over the sub-regions 3 and 4 of Bangladesh. 166

Figure 5.8: Return time plots for daily rainfall during monsoon (JJAS) season in different forcing scenarios over the sub-regions of 1 and 2 of Bangladesh. The HadRM3P ACT (black), ACT highest (upper grey with upward triangles), ACT lowest (lower grey with downward triangles), NAT (green) and GHG-only (orange) ensembles are compared with the HAPPI 1.5 (blue) and 2.0 (red) ensembles. The most significant changes in the risks of extreme monsoon rainfall take place in the sub-region2, which is already the wettest part of Bangladesh. 167

Figure 5.9: Same as Fig 5.8, but showing return time plots for daily rainfall during monsoon (JJAS) season in different forcing scenarios over the sub-regions of 3 and 4 of Bangladesh. 168

Figure 5.10: The risk ratios of four specific rainfall events with return periods of 10, 20, 50, and 100 years between ACT/NAT, HAPPI 1.5/NAT, HAPPI 2.0/NAT and GHG-only /ACT over the two northern sub-regions 1 and 2 during MAM (top two panels of a. & b.) and JJAS (bottom two panels of c. & d.). The error bars indicate the associated uncertainty range with 95% confidence level for individual event. 170

Figure 5.11: Same as Fig 5.10, but for MAM and JJAS risk ratios over the two southern sub-regions 3 and 4. 171

Figure 5.12: Comparative return periods (10-100 year events) of MAM daily rainfall (mm/day) over sub-region 1 during 1986-2015 as per (a) HadRM3P, (b) MIROC5, (c) ETH_CAM4, (d) CanAM4 and (e) NorESM1 models. ACT, NAT, GHG-only, plus 1.5°C

and 2.0°C model ensembles are shown in black, green, orange, blue and red colours respectively. 174

Figure 5.13: Comparative return periods (10-100 year events) of JJAS daily rainfall (mm/day) over sub-region 2 during 1986-2015 as per (a) HadRM3P, (b) MIROC5, (c) ETH_CAM4, (d) CanAM4 and (e) NorESM1 models. ACT, NAT, GHG-only, plus 1.5°C and 2.0°C model ensembles are shown in black, green, orange, blue and red colours respectively. 175

Figure S5.1: Relative change in SPI of MAM mean rainfall between different forcing scenarios. The top row (panels a-d) shows the regional SPI changes over central parts of the South Asia (SA) while, bottom row (panels e-h) shows the SPI changes over Bangladesh. The four boxes (1-4) on top of the panel e represent the four sub-regions of Bangladesh. a. ACT rainfall SPI relative to NAT over SA b. ACT rainfall SPI relative to HAPPI1.5 over SA c. HAPPI1.5 rainfall SPI relative to HAPPI 2.0 over SA d. ACT rainfall SPI relative to GHG-only over SA…….. 185

Figure S5.2: Same as Fig. S1, but for SPI changes in JJAS mean rainfall. This figure shows that the apparently non-linear response between panels of a, b, and c (or, e, f, g) can be explained by the response for aerosols in the panel d (or, h).....185

Figure S5.3: Return time plots for MAM five day mean rainfall under different forcing scenarios over the sub-regions 1 and 2 of Bangladesh. The ACT (black), ACT highest (sky-blue), ACT lowest (grey), NAT (green) and GHG-only (orange) ensembles are compared with the HAPPI 1.5 (blue) and HAPPI 2.0 (red) ensembles.....186

Figure S5.4: Same as Fig. S3, but for return time plots for MAM five day mean rainfall under different forcing scenarios over the sub-regions 3 and 4 of Bangladesh. 187

Figure S5.5: Return time plots for JJAS five day mean rainfall different forcing scenarios over the sub-regions 1 and 2 of Bangladesh. The ACT (black), ACT highest (sky-blue), ACT lowest (grey), NAT (green) and GHG-only (orange) ensembles are compared with the HAPPI 1.5 (blue) and HAPPI2.0 (red) ensembles. The risks of extreme rainfall events are evidently increasing between different forcing scenarios over sub-region 2. 188

Figure S5.6: Same as Fig. S5, but for return time plots for JJAS five day mean rainfall under different forcing scenarios over the sub-regions 3 and 4 of Bangladesh. 189

Figure S5.7: Comparative return periods (10-100 year events) of MAM daily rainfall (mm/day) over sub-region 2 during 1986-2015 as per (a) HadRM3P, (b) MIROC5, (c) ETH_CAM4, (d) CanAM4 and (e) NorESM1 models. ACT, NAT, GHG-only, plus 1.5°C and 2.0°C model ensembles are shown in black, green, orange, blue and red colours respectively. 190

Figure S5.8: Same as Figure S7 but for sub-region 3. 191

Figure S5. 9: Same as Figure S7 but for sub-region 4. 192

Figure S5.10: Comparative return periods (10-100 year events) of JJAS daily rainfall (mm/day) over sub-region 1 during 1986-2015 as per (a) HadRM3P, (b) MIROC5, (c) ETH_CAM4, (d) CanAM4 and (e) NorESM1 models. ACT, NAT, GHG-only, plus 1.5ºC and 2.0ºC model ensembles are shown in black, green, orange, blue and red colours respectively. 193

Figure S5.11: Same as Figure S9 but for sub-region 3. 194

Figure S5.12: Same as Figure S9 but for sub-region 4. 195

Figure S5.13: Prescribed field of high level and surface SO_2 emissions in the model in 1986 (top panel) and 2014 (bottom panel). 196

Figure 6.1: (a) Spatial distribution of CPC rainfall (mm day–1) over Bangladesh during 16 March–15 April 2017 relative to climatology (1979–2017). The red box indicates the study area of NEB. (b) Niño-3.4 (November–January) and IOD (February–April) indices during 1979–2017. The horizontal dashed black line in (c) indicates the threshold value for heaviest rainfall events. The vertical dashed black rectangles in (b) and (c) indicate the association between the heaviest rainfall events and IOD (Niño-3.4). (d) Return level plot of GP distribution fitted to CPC observed extreme 6-day rainfall events exceeding a 90th percentile threshold. (e)–(g) Annual cycles of 6-day rainfall over NEB as in models and observations (HadRM3P, ETH_CAM4 and MIROC5, respectively), with CPC (1979–2017 and 2004–16), GPCC (1988–2017), and APHRODITE (1979–2007)…… 204

Figure 6.2: Return periods for 6-day rainfall events in March over NEB showing (a) HadRM3P Actual 2017 (black) and Natural 2017 (dark green) vs Actual climatology 1986–2015 (gray) and Natural climatology 1986–2015 (light green) ensembles. (b) Actual climatology 2006–15 (gray), Natural climatology 2006–15 (light green), and GHG-only climatology 2006–15 (yellow). (c) Actual climatology 2006–15 (gray) and Natural climatology 2006–15 (light green) but as in MIROC5 (squares) and ETH_CAM4 (triangles) model ensembles. Each dot, triangle, or square represents one simulation of the HadRM3P, MIROC5, or ETH_CAM4 model, respectively, and the shaded polygon shows 95% confidence intervals. The horizontal dashed deep brown line in each panel indicates the extreme event of March 2017. 208

Figure 6.3: Annual cycles of 6-day rainfall over NEB as in HadRM3P model and observations of CPC (1979–2017 and 2004–2016 in dotted and solid sky-blue coloured lines respectively), GPCC (1988–2017 in blue), and APHRODITE (1979–2007 in pink). The green and red dotted rectangles indicate that in March model bias is very small but it is comparatively large in April. 214

Figure 6.4: Return level plot of GP distribution fitted to GPCC observed extreme 6-day rainfall events exceeding a 90th percentile threshold. 217

Figure S6.1: ENSO response in March rainfall anomalies during (left) post–El Niño, (middle) post-neutral and (right) post–La Niña conditions in (top) HadRM3P, (middle) CPC, and (bottom) GPCC in each composite..... 212

Figure S6.2: The left column shows global mean temperature (°C) anomaly averaged over a season [DJF, MAM, JJA, and SON in (a), (b), (e), and (f), respectively] and the months of (c) March and (d) June of 2017 relative to base climatological period of 1986–2015. Any gray areas in the maps signify missing data. The right column shows (g)–(i) Niño-3.4 and (j)–(l) IDMI regression with HadRM3P, CPC and GPCC rainfall in March during 1986–2015. ...213

List of Abbreviations and Acronyms

ADB	Asian Development Bank
AGCM	Atmosphere Only Global Climate Model
AOGCM	(Coupled) Ocean–Atmosphere Global Climate Model
APHRODITE	Asian Precipitation - Highly-Resolved Observational Data Integration Towards Evaluation of Water Resources
AR4	Fourth Assessment Report (of IPCC)
AR5	Fifth Assessment Report (of IPCC)
BMD	Bangladesh Meteorological Department
BWDB	Bangladesh Water Development Board
CanAM4	Canadian Fourth generation atmospheric global climate model
CI	Confidence Interval
CMIP5	Coupled Model Intercomparison Project Phase 5
CORDEX	Coordinated Downscaling Model Experiments
CPC	Climate Prediction Centre
CPDN	climateprediction.net
CPU	central processing unit
CRU	Climatic Research Unit
DJF	December January February
DMIC	Disaster Management Information Center
ECMWF	European Centre for Medium-Range Weather Forecasts
ENSO	El Niño-Southern Oscillation
ETH_CAM4	Eidgenössische Technische Hochschule_Community atmosphere model 4-2°
FAR	Fraction of Attributable Risk

GCM	General Circulation Model
GEV	Generalized Extreme Value
GEVD	Generalized Extreme Value Distribution
GHG	Greenhouse Gas
GoB	Government of Bangladesh
GPCC	Global Precipitation Climatology Centre
GTS	Global Telecommunication System
HAPPI	Half a degree Additional warming, Prognosis and Projected Impacts
IOD	Indian Ocean Dipole
IPCC	Intergovernmental Panel on Climate Change
JJA	June July August
JULES	Joint UK Land Environment Simulator
LBC	Lateral Boundary Condition
LPS	Low Pressure System
MAM	March April May
MIROC5	Model for interdisciplinary research on climate 5
MJO	Madden–Julian oscillation
MOSES	Met Office Surface Exchange Scheme
MSLP	Mean Sea Level Pressure
NAS	National Academy of Sciences
NASA	National Aeronautics and Space Administration
NOAA	National Oceanic and Atmospheric Administration
NorESM1	Norwegian earth system model 1
OSTIA	Operational Sea Surface Temperature and Sea Ice Analysis
PC	Percent Change

PEA	Probabilistic Event Attribution
PRECIS	Providing Regional Climates for Impacts Studies
RCM	Regional Climate Model
RCP	Representative Concentration Pathway
SI	Sea Ice
SON	September October November
SST	Sea Surface Temperature
SPI	Standardized Precipitation Index
TRMM	Tropical Precipitation Measuring Mission
UNFCCC	United Nations Framework Convention on Climate Change
UoD	University of Delaware
USD	United States Dollar
WB	World bank
WMO	World Meteorological Organization

1. Introduction

1.1. Motivation and aims

1.1.1. Background and Rational

For the public, scientists, and policy makers, extreme weather and climate-related events are of great concern and interest (Stott et al., 2013). Various extreme events, such as prolonged heatwaves, intense floods and droughts, and strong hurricanes can cause damaging impacts on the socio-economy, exacerbating the detrimental impacts of slow-onset events such as sea level rise in response to climate change.

For example, Europe's record-breaking heat wave in 2003 caused around 35-70,000 deaths (García-Herrera et al., 2010; Robine et al., 2008; Stott et al., 2004a) and Hurricane Katrina in 2005 led to more than $108 billion USD economic damages (Blake and Gibney, 2011). What causes these extreme events is therefore a matter of core interest for civil engineers and related infrastructural investments; to insurance companies for setting their instalment rates; and to communities, regions and nations who are struggling to adapt to climate change and make post-disaster recovery decisions.

According to McPhillips et al. (2018), an extreme event can be classified based on ‘thresholds’ that either indicate the probabilities of occurrence, or the point where they can cause potential impacts. Stott et al. (2016) defined an extreme event as: “discrete episodes of extreme weather or unusual climate conditions, often associated with deleterious impacts on society or natural systems, defined using some metric to characterize either the meteorological characteristics of the event or the consequent impacts”.

Therefore, an extreme event has two components to address, i) the meteorological hazard, and ii) the loss to life and property that results from the hazard. Meteorological hazards may include: unusually high or low temperatures, high or low rainfall, high wind speeds, and rapidly intensifying mid-latitudinal (or extra-tropical) low pressure systems causing storm surges (Stott et al., 2016) and these can vary in intensity (annual or all-time extreme) as well as duration (from hours to multi-annual). This thesis addresses the meteorological hazard component of extreme events.

By definition, extreme weather events are rare incidents and so observations depending on time series length, cannot provide an adequate sample size (National Academies of Sciences, Engineering, 2016) to detect changes in the frequency of occurrence or magnitude of the events, regardless of cause. A frequently asked question after an extreme event, from the public and the scientific community alike, is whether or not anthropogenic climate change made the event more or less likely, i.e. what probabilistic role climate change may have played in causing any given event.

1.1.2. Probabilistic Event Attribution

Probabilistic Event Attribution (PEA) (Allen, 2003) has become an important field of climate research to provide scientific evidence on how anthropogenic climate change has been influencing the likelihood of extreme weather events occurring. The first application of PEA revealed that the likelihood of occurrence of the 2003 European heatwave had very likely increased by a factor of at least two due to human influence on climate (Stott et al., 2004a).

Since then, the science of event attribution has advanced, with rapid development of event attribution methods, and better understanding of the mechanisms that produce extreme events (NAS, 2016). PEA has become an increasingly accepted tool to assess and quantify the role of human-induced climate change and other external drivers on changing risks for extreme weather events (Otto, 2017).

However, questions have been raised about the reliability of the attribution statements particularly when the extreme events are strongly influenced by the change in atmospheric circulations. Distinguishing the dynamic effect on circulation-related events is rather difficult due to small noise-to-signal ratios. Reliable attribution statements can be made with confidence when thermodynamics is the dominant factor in changing the probabilities of extreme events (Trenberth et al., 2015) .

Despite evidence of anthropogenic influence, natural variability can still play a substantial role in individual events. When addressing the associated complexities of the weather and climate processes involved, it is often difficult to evaluate how climate change has affected the strength and likelihood of individual extremes (Eckstein et al., 2015).

There exists an impression that attributing extreme and rare weather events to past greenhouse gas (GHG) emissions is impossible. The perception that attribution of specific events cannot be done, or that the relevant science is not robust (Surminski and Lopez, 2015) is generally based on one of three arguments.

1. Extreme weather is part of natural variability, and so we cannot actually say that a specific flood or drought would not have occurred without climate change. Event attribution research does not seek to specifically counter this statement, but rather explores to what extent anthropogenic climate change contributes to the probability of occurrence of specific events (Stott et al., 2013a).

2. Extreme events are by definition rare and so the relevant climate change signal cannot be detected. The technique of probabilistic event attribution overcomes this challenge by using very large ensembles of climate model simulations (Pall et al., 2011a). However, the model simulated data is not real; hence the uncertainty associated with this data needs to be quantified.

3. The dynamics associated with extreme weather events and the conditions in a hypothetical world without anthropogenic emissions, which are simulated to estimate the climate change signal, cannot adequately be reproduced in the climate model experiments (Pall et al., 2011a). In principle, the attribution experiments and the climate model experiments used for future projections, routinely employed by adaptation decision-makers, have similar limitations.

However, if uncertainties are well communicated, attribution results can be useful for policymakers despite this limitation (James et al., 2014). In its recent assessment, The National Academies of Science concludes that the science of attribution has advanced to the point that the perception that "attribution of specific events cannot be done" is no longer true (National Academies of Sciences, Engineering, 2016).

The attribution of individual extreme events is essential to understanding regional impacts of climate change. In a warmer atmosphere that can hold more water vapour, more extreme rainfall events are expected to happen when considering the thermodynamic effects only. However, higher ocean temperatures and GHG concentrations can also affect the atmospheric circulation.

Such dynamic effects can be either in the same direction as the thermodynamic effects and intensify the impacts of the event, or in the opposite direction (Otto, 2017). Other factors can also play a role, such as the declining risk of flooding related to spring snow-melt (Kay et al., 2011) despite a large-scale increase in the risk of heavy rainfall due to a warmer world (Otto, 2017).

The *Bulletin of the American Meteorological Society* (BAMS) started a special annual issue documenting event attribution studies of extreme weather events in the previous year (Peterson et al., 2012) in 2012. Since then, a total of 131 event attribution papers have been published in these special issues and about 65% of these studies have identified a role for climate change (Herring et al., 2017).

An event attribution study can have any one of the following outcomes: (i) anthropogenic climate change made the event more likely, (ii) made the event less likely, (iii) there is no detectable influence from anthropogenic climate change, or (iv) with our current understanding and available tools we are unable to analyse the role of external drivers in the event.

For example, PEA based studies have shown how global warming more made the 2011 Texas drought 20 times more likely (Rupp et al., 2012); and the extremely hot summer temperatures in Korea 10 times more likely (Min et al., 2014).

In contrast, climate change does not contribute to all extreme weather events, as there was no detectable influence on the events of the California droughts of 2012/13 and 2013/14 (Funk et al., 2014); the heavy rainfall event of 2013 in the upper Danube and Elbe basins (Schaller et al., 2014) or the extreme snow accumulation in the Western Spanish Pyrenees during the winter and spring of 2013 (Añel et al., 2014).

Christidis et al. (2013) emphasized that an attribution assessment can also be unreliable if the model does not reliably reproduce the event in the region; e.g., the flood in Pakistan of 2010 (Houze et al., 2011; Webster et al., 2011).

A PEA study has also shown that even though there was an increase in the risks of the prolonged drought in northeast Brazil during 2012-2016, anthropogenic climate change did not play a role in the increasing risks of this extreme event (Martins et al., 2018).

For the first time in 2017, three BAMS attribution papers reported that record global heat, the heat across Asia, and a marine heatwave off the coast of Alaska in 2016 were not possible in a preindustrial natural climate without climate change (Imada et al., 2017; Knutson et al., 2017; Walsh et al., 2017).

1.1.3. Extreme Event Attribution Approaches

The scientific interest in attributing an extreme event normally develops after the event has actually occurred, been associated with exceptional meteorological characteristics, and caused significant impacts on society and economy. Consequently, the public and media have often shown ample curiosity in the probable role of climate change behind such events (National Academies of Sciences, Engineering, 2016).

In case of unprecedented events that cause the most severe impacts, leading to national or even international concerns, governments and policymakers also become interested in possible link between climate change and the extreme event experienced (Stott and Walton, 2013).

In part, they wish to understand how climate change will affect future extreme events to inform post-disaster recovery decisions (for example, whether it makes sense to rebuild in the same vulnerable locations).

Event attribution assessments quantify to what extent anthropogenic or natural forcings influenced the probability of occurrence or magnitude of a particular type of event. The different approaches of extreme event attribution are reviewed in the following sections.

I. Coupled Model Approaches

Coupled ocean–atmosphere global climate model (AOGCM) runs for "natural", "historical", and "near-future" forcing scenarios that have been submitted to the CMIP5 archive (Taylor et al., 2012) are used to estimate attribution. The natural scenario excludes anthropogenic climate change, whilst the historical scenario is based on complete observed forcings up to 2005. The historical runs are then extended with the representative concentration pathway RCP4.5 near-future scenario. Both historical and near-future represent a world with climate change.

Multi-model ensembles for all scenarios are used to assess the distribution of the climate variable of interest. A comparative assessment of these distributions can indicate any shift in the probability of an extreme event occurring in past, present and near-future climate. Any shift in the probability of occurrence in the historical/near-future climate compared to the natural climate is attributed to the elevated GHG levels and other changes in atmospheric composition. This method has been widely used, for instance to attribute heatwaves and heavy rainfall in Australia (King et al., 2013; Perkins et al., 2014).

Because the model data is already available in the CMIP5 archive, an attribution assessment can be made soon after the event has occurred. This method depends, however, on the realism of the various models used in the multi–model ensemble: coupled models used for multi-century simulations often necessarily lack the atmospheric resolution to simulate some types of extreme weather events realistically. Structural differences between models can also be hard to distinguish from random variations.

II. Sea Surface Temperature Forced Atmosphere Only Model Approaches

Using a single atmosphere-only global climate model (AGCM), and running it many times with initial condition perturbations in a large ensemble to generate a different realisation of weather statistics in each ensemble member can be one way to obtain higher atmospheric resolution and reduce the uncertainty due to structural dissimilarity of the CMIP5 models.

Similar to the AOGCM approach, in the AGCM experiments, one forcing scenario uses the observed, anthropogenic levels of GHG (factual climate conditions), whilst the other forcing scenario removes the anthropogenic component (counter-factual climate conditions).

Prescribed sea surface temperatures (SSTs) are used to force the AGCMs for each of the scenarios. In the experiments described here, observed SST data set from the Operational Sea Surface Temperature and Sea Ice Analysis (OSTIA) system (Donlon et al., 2012) is used for the "factual" scenario.

To obtain the natural "counterfactual" scenario, the warming pattern due to elevated GHGs must be removed. This is done in two steps; first the modelled SST patterns resulting from the anthropogenic forcings (denoted as δSSTs) are obtained by subtracting CMIP5 historical natural SSTs from the CMIP5 historical SSTs (see equation 1.1).

Then the modelled SST responses to anthropogenic forcings (δSSTs) are removed from the observed OSTIA SSTs to obtain the counterfactual world's SSTs (see equation 1.2). These counterfactual world's SSTs are then used to force the AGCM for generating the natural scenario.

$$\delta SSTs = CMIP5\ Historical\ SSTs - CMIP5\ Historical\ Natural\ SSTs \quad (1.1)$$

$$Counterfactual\ World's\ SSTs = OSTIA\ Observed\ SSTs - \delta SSTs \quad (1.2)$$

During this process, either a multi-model ensemble mean of the SST anomalies, or a range of the SST anomalies, can be used to create an ensemble of natural (or non-anthropogenic) SSTs. A detailed description of the calculation method of the δSSTs is given in chapter 2, under section 2.2.1.3.

To estimate changes in the probability of occurrence of the extreme events, a Risk Ratio (RR) is used. Based on the numbers of factual and counterfactual ensemble members, where the event threshold is passed, the RR is calculated as:

$$RR = \frac{P_{factual}}{P_{counterfactual}} \quad (1.3)$$

Where the probability of the event in the factual climate is denoted by $P_{factual}$, and the probability of the same event in a counterfactual climate without anthropogenic climate change is denoted by $P_{counterfactual}$ (National Academies of Sciences, Engineering, 2016). Here the event threshold can either indicate the probabilities of occurrence, or the point where they can cause potential impacts (McPhillips et al. 2018).

Alternatively, the Fraction of Attributable Risk (FAR) approach (Allen, 2003) is used to measure how much of the event can be attributed to human influence from a probabilistic point of view. FAR is calculated as (National Academies of Sciences, Engineering, 2016):

$$FAR = \frac{P_{factual} - P_{counterfactual}}{P_{factual}} \qquad (1.4)$$

There are a number of advantages of using AGCMs for event attribution. AGCMs are less prone to bias than AOGCMS (He and Soden, 2016; Massey et al., 2015; Scaife et al., 2010) and are less computationally expensive. This allows many ensemble members to be run at higher spatial resolution, enabling better sampling of the tails of the distributions of the climate variables.

The volunteer distributed computing method of computing AGCMs can produce many thousands of model runs (Massey et al., 2015; Rowlands et al., 2012), producing an improved signal-to-noise ratio when compared to smaller ensembles.

The main disadvantage of this method is that atmosphere-ocean coupling is not represented in the model, which may lead to a poorer representation of extreme events which are particularly influenced by atmosphere-ocean dynamics (Stott et al., 2016). Studies that have used this setup include, for example, Pall et al. (2011), Otto et al. (2012), Lewis and Karoly (2013) and Schaller et al. (2014).

III. Analogue-Based Approaches

In this approach, first the synoptic situation (the large-scale circulation pattern associated with the event of interest) is analysed, and then historical analogues with similar circulation states are identified from observations or reanalysis data. Based on these historical analogues, any changes in the local impacts of meteorologically similar events may be examined (National Academies of Sciences, Engineering, 2016). Examples of studies conducted using this approach include Cattiaux et al., (2012) and Yiou and Cattiaux (2013, 2014).

The advantage of this approach is that no model simulations are required; as an alternative a readily available reanalysis product is used. The disadvantage is that alternative climate scenarios such as a natural climate without anthropogenic GHG emissions cannot be explored. The historical record also needs to be long enough to exclude any effects of internal variability of the climate system.

IV. Empirical Approaches

With the increase in mean temperatures, increase in the risk of extreme temperature and rainfall events can take place because higher mean temperatures allows more moisture to be held in the air (Stott et al., 2016). This fundamental concept forms the basis for many empirical approaches to attribution.

In these empirical methods, a generalized extreme value distribution (GEVD) is fitted to observed data and then the location parameter of the GEVD is modified by modelling it as a linear function of global mean surface temperature (GMST) change.

From the GEVD, the relative increase in risk, or the FAR, associated with that GMST change can be computed for an extreme event that exceeded a predefined threshold (Van Oldenborgh et al., 2012).

The advantage of this method is simple computation and reliance on a small amount of data. As a consequence, an attribution assessment is possible directly after the event occurs. Using reliable seasonal forecasts, this method can even provide attribution statements prior to the actual occurrence of the event.

The disadvantages include the possibility of false positives (or negatives) due to spurious correlations and the inability to provide any information about the atmospheric state causing the event. Furthermore, any change in risk can only formally be attributed to the change in climate, but not to GHG emissions, which is possible in the modelling approaches (Massey, 2015).

V. Broad-Scale Approaches

Unlike other approaches, broad-scale approaches do not focus on specific extreme events with unusually high impacts, magnitudes or media interest. Rather, large-scale metrics of global change in temperature and rainfall are attributed to increased GHG levels using an adapted global detection and attribution method (Massey, 2015).

For instance, global daily minimum and maximum temperature observations over recent decades are fitted to GEVDs. The shape and location parameters of the GEVD are then modified based on GCM runs with various combinations of anthropogenic and natural forcings.

By comparing the modified GEVDs, one study reported globally an increase in the risk of very hot days and a decrease in the risk of very cold nights (Zwiers et al., 2011).

The advantages of broad-scale approaches include the ability to do such studies at any time with available data, preserving the link between detection and attribution methods and extreme event attribution, and the prospect of providing future projections of changes in the risks using the future RCP projections from CMIP5. The disadvantages are that these approaches are suitable only for global scale studies and work primarily with temperature-related variables (Stott et al., 2016).

VI. Choice of Approach for this Thesis

There is no single right attribution approach to quantify the changes in the likelihood of the extreme events. The framing of the question, available resources and the amount of time available to answer it largely control the choice of method or set of assumptions for event attribution (National Academies of Sciences, Engineering, 2016).

All of the approaches discussed above have their own limitations and benefits. The main limitation of each approach is as follows: the broad-scale approach is not suitable regional or local scale studies; the empirical approach cannot attribute the change in risks to GHG emissions; the analogue-based approach depends on reliable long-term observations, which is not available in many regions.

The atmosphere-only-model approach, forced by prescribed SSTs, overcomes many of the limitations of the other approaches by using high resolution regional climate model

ensembles consisting of thousands of model runs that can simulate required alternative counterfactual scenarios, and can be used for many climate variables.

However, there are some uncertainties in this approach that need to be carefully considered. For example, single-model ensemble based assessment that is widely applied in event attribution studies (e.g., Black and Karoly, 2016; Mitchell *et al.*, 2016; Schaller *et al.*, 2016; Sippel *et al.*, 2016) has a potential risk of either detecting a false signal or, overlooking a true signal (Hauser et al., 2017).

The atmosphere-only models may possibly incline to overestimate extreme tropical rainfall compared to the coupled model as a function of SST-forced rainfall variability (Hirons et al., 2018). The coarse resolution models may provide with imperfect simulations for the fine-scale atmospheric convection process (National Academies of Sciences, Engineering, 2016) and this in turn may cause underestimation of convective rainfall at regional levels.

Quantifying model bias for extreme events can be difficult when uncertainty in the observation data largely hinders the ability to compare to the truth (Kharin et al., 2007, 2013). Evaluation of the counterfactual scenario can be even more difficult due to lack of pre-industrial observations.

This thesis uses the SST forced atmosphere-only-model approach and the weather@home system to generate the necessary model ensembles. The potential sources of uncertainties in the SST forced atmosphere-only-model approach are

carefully considered and if, it is within the scope of this research project, those uncertainty issues are addressed.

For example, to address the observational uncertainty, multiple sources of observation data are used and to test robustness of model results from weather@home modelling system, additional model ensembles from different models are used. The possible ways forward to address the uncertainty issues beyond the scope of this thesis are discussed in the concluding chapter.

1.1.4. The weather@home system

The weather@home (Guillod et al., 2017; Massey et al., 2015) climate modelling system is a part of climateprediction.net (Allen, 1999), a climate modelling project based on volunteer computing. A set of regional climate modelling experiments are run through the weather@home system for different regions including Europe, Western US, Central America, South America, Australia & New Zealand, South Asia, East Asia, and Africa (figure 1.1).

For a specific region of interest, an AGCM, HadAM3P, is downscaled to a higher resolution (50 or 25 km) over a limited domain by its RCM equivalent, HadRM3P. The RCM cannot impact on the GCM during the downscaling process because the coupling is strictly one-way. Both GCM and RCM share the same physics and are based on the atmospheric component of the coupled climate model of the UK Met Office Hadley Centre, HadCM3 (Gordon et al., 2000).

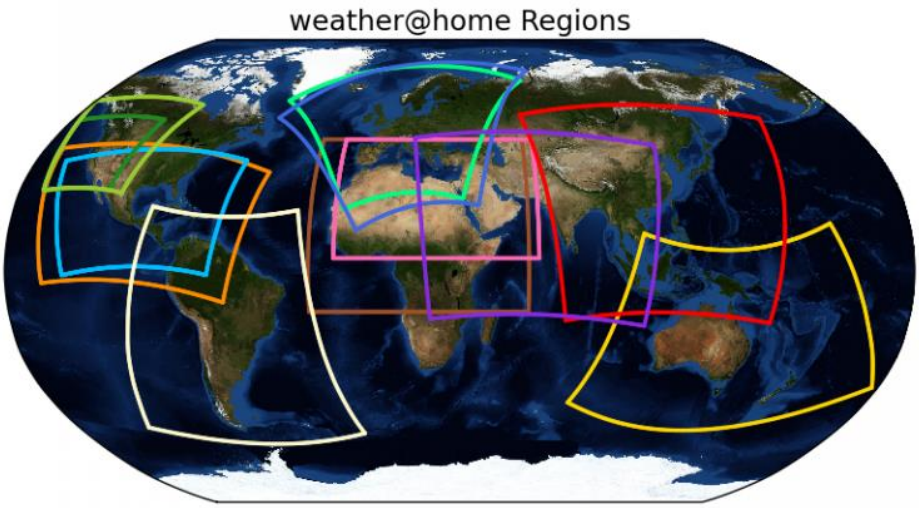


Figure 1.1: This map shows all currently running regions under weather@home (source: https://www.climateprediction.net/weatherathome/regions/). The purple rectangle shows South Asia region.

Both models are forced with prescribed sea surface temperature (SST), sea ice, atmospheric composition, SO_2 emissions (including volcanoes), and solar forcing, as well as initial conditions for all model variables. The advantages of using the prescribed SSTs are that there is no ocean-component of the model that would otherwise require a long spin–up period, and there are no ocean-induced biases in the atmospheric circulation (Scaife et al., 2010) apart from due to observed SST biases. Chapter 2, section 2.3.1, discusses more about the modelling framework and methodological aspects of the weather@home system for South Asia region that is used to generate the required model ensembles for this thesis.

The HadAM3P-HadRM3P modelling setup of the weather@home system successfully applies PEA to assess whether, and to what extent, external drivers change the likelihood of a specific extreme weather event occurring in different regions of the world (e.g., Black and Karoly 2016; Lott et al. 2013; Marthews et al. 2015; Schaller et

al. 2016). However, as a result of differences in regional climates, availability of long-term observational data, and modelling capability, the ability to attribute events in different regions varies substantially. Consequently, there exists disparity between the different regions covered in attribution studies.

An independent assessment (Angélil et al., 2017) done for the first three BAMS annual reports (Herring et al., 2015; Peterson et al., 2012, 2013) on attribution of extreme events pointed out that the events analysed in these reports are biased in two ways: (i) the authors' proximity to the location of event examined and (ii) the degree of anticipated media and public interest. These factors contributed to a strong focus on events (49 from a total of 63 events) that occurred in Europe, the United States, and Australia.

Very few of these studies have been done for tropical regions (Marthews et al., 2015; Otto et al., 2015c), or developing countries (e.g., Philip et al. 2018), even though these countries are highly vulnerable to climate change, particularly susceptible to extreme weather events, and have the least capacity to adapt to the consequent impacts (IPCC, 2013a).

Scientists are exploring promising approaches to conduct robust attribution studies in regions where observational data is scarce (Otto et al., 2013), and this has led to recent progress with regard to PEA studies in tropical regions and developing countries being made (e.g., Imada et al. 2017; Sun and Miao 2017; X. Yuan, Wang, and Wood 2017; Xing Yuan, Wang, and Hu 2017; Christidis et al. 2017).

1.1.5. Research Aims and Key Questions

Bangladesh is one of the countries that are most critically affected from climate change and extreme weather events. The consequent impacts are already affecting water resources, agriculture, health, ecosystems, and economic development (Dasgupta et al., 2011; Sarraf et al., 2011). Despite considerable public and governmental interest in recognizing and quantifying the possible role of climate change, attribution studies for local sub-regional scale events in Bangladesh are sorely missing.

Recognizing this gap, this DPhil research project addresses the meteorological hazard aspects of extreme events in Bangladesh at sub-regional scale, aided by the HadAM3P-HadRM3P model set-up of weather@home for the first time. Prior to this PEA analysis, the responses of the model to external radiative forcings factors and observed natural modes of SST variability relevant for South Asian climate is assessed, and the overall performance of the model in simulating extremes is evaluated using a combination of process-based and performance-based metrics.

Hence, this DPhil thesis has two fundamental aims. The first aim is to provide a detailed evaluation of the HadAM3P-HadRM3P modelling system of weather@home for the South Asia region. The work will constitute a thorough model evaluation over South Asia in general and Bangladesh in particular, with emphasis on the model's ability to simulate the frequency and magnitude of observed extremes.

The second aim of this thesis is to quantify the changes in the probable risks of extreme weather events under different climate change scenarios in Bangladesh, and to attribute a recent extreme event (an extreme pre-monsoon rainfall event of 2017 that caused

flash flooding in northeast Bangladesh) to anthropogenic climate change forcings using very large ensembles of thousands of model simulations from weather@home. To attain the aforementioned two broad research aims, the key questions asked in this thesis are the following:

1. What is the model's response to observed natural modes of SST variability?
2. How does the model perform in capturing the observed weather features and in particular the extreme events in Bangladesh?
3. How different are the risks of extreme rainfall events under the scenarios of past (pre-industrial, natural or non-anthropogenic), present and future climate conditions consistent with the Paris Agreement global temperature goals?
4. Did anthropogenic climate change drivers influence the likelihood of occurrence of the most recent unusual and extreme rainfall event of 2017 in Bangladesh?

The contexts for each of these key questions are briefly discussed here. El Niño-Southern Oscillation (ENSO) and the Indian Ocean Dipole (IOD) are the two important modes of observed natural SST variability that impact on rainfall patterns over the South Asian monsoon region (Ashok et al., 2004; Ropelewski and Halpert, 1987; Saji et al., 1999b, 1999a; Saji and Yamagata, 2003a).

ENSO has also been shown to affect the intensity and occurrence of extreme weather events (King et al., 2016; Yeh et al., 2018). IOD influences the Indian summer monsoon rainfall, and reduces the impact of ENSO on the Indian summer rainfall (Ashok et al., 2004; Li et al., 2016c). Hence these two modes need to be considered while assessing the model's suitability for PEA applications. The first key question comes under this context.

Equally important, the question of whether or not IOD is an independent mode of true internal variability is addressed, as it may very well co-vary with ENSO. In numerous studies, the variability of IOD is attributed to ENSO (e.g., Baquero-Bernal et al., 2002; Dommenget and Latif, 2002; Lau and Yu, 2005; Li et al., 2003; Yang et al., 2015). This thesis therefore reviews their relationship for the recent period of 1986-2015 and then explores how they impact on rainfall events. Chapter 3 provides more a detailed discussion about the variable aspects of ENSO and IOD.

The most commonly used and straightforward approach for evaluating the model's performance in simulating historical climate is done by quantifying the difference between model simulated and observation-based data, to determine model biases (Flato et al., 2013).

Regional climate models have been evaluated in a number of studies against selected observational datasets over South Asia (Bhaskaran et al., 1996; Caesar and Janes, 2018; Janes and Bhaskaran, 2012; Lucas-Picher et al., 2011; Macadam and Janes, 2017; Saeed et al., 2012) but very few studies have focused on Bangladesh (Caesar et al., 2015; Fahad et al., 2017; Hasan et al., 2013).

Previous studies have mainly looked at climatological means, including seasonal or monthly means, to evaluate the credibility of the model simulations for future prediction purposes. Evaluation of model-simulated extreme events is commonly done by looking at the higher percentiles of the distributions (for example, 90, 95 or, 99th percentiles) of the climate variables (e.g., Black et al., 2016; Caesar et al., 2015).

However, none of the previous studies examined model simulated exceptionally rare extreme events of 100-year return period against observations in Bangladesh using very large model ensembles of a high-resolution regional climate model. The second key question takes on this challenge of evaluating not just the modelled means, but also the extremes at local sub-regional scales in Bangladesh. Chapter 4 presents a paper on model evaluation of the RCM, HadRM3P, focusing on the extreme events in this country.

The first key question deals with the physical processes and model responses to internal variability of teleconnections that are important for this tropical monsoon region. The second key question judges the model's performance, particularly for capturing the observed extreme events to establish its suitability for PEA experiments. The first two research questions are important to build confidence in the attribution results, while the latter two questions are designed for the application of the model to quantify changing risks of seasonal extreme events under different climate change scenarios (key question 3), and to attribute a recent extreme event to anthropogenic climate change drivers (key question 4) in Bangladesh.

Northeast Bangladesh (NEB; 90.5°-92.5°E, 24°-25.5°N) is an important agricultural region, contributing 15% of the total 'Boro' rice production during the 2011-2016 period (FAO, 2017). On 27 March 2017, an extreme rainfall event triggered the earliest flash flood since 2000 (Ahmed et al., 2017). Subsequently, around 850,000 households were affected and 220,000 hectares of nearly-harvestable Boro rice crop were damaged. Such crop failure in 2017 contributed to a record 30% rice price hike compared to 2016

(FAO, 2017). This extreme event has been selected for an attribution study in this thesis.

Additionally, as an interesting part of the key questions 3 and 4, the effects of GHGs as the major contributor in a climate scenario are explored in simulations where anthropogenic aerosols are reduced to pre-industrial levels. Radiative forcing and micro physical effects from aerosols can cause changes in the radiation, monsoon rainfall and regional climate (Guo et al., 2016; Huang et al., 2014; Li et al., 2011a, 2011b; Nakajima et al., 2007; Rosenfeld, 2000). Elevated deep layers of light-absorbing aerosols that significantly change the energy balance can potentially affect the water cycle (Lau et al., 2006; Lau and Kim, 2006; Ramanathan et al., 2005).

Many studies reported climate implications of the high aerosol loading over the Indian subcontinent, a fraction of which is absorbing black carbon (Bollasina et al., 2011; Manoharan et al., 2014; Ramanathan and Carmichael, 2008; Ramanathan and Feng, 2009). The trend in total monsoon rainfall is relatively stable but the frequency and intensity of rainfall has changed radically (Ganguly et al., 2012; Goswami et al., 2006).

India and China are rapidly scaling up renewable energies and are both on track to meet their climate targets set for the Paris Agreement (Liesch et al., 2017). Consequent reductions in air pollution, due to the use of clean energy resources, will rapidly reduce the anthropogenic aerosol concentrations. Such committed reductions in aerosols, together with existing GHGs, can impact regional climate and rainfall patterns and change risks of extreme events in different ways.

There are three possible impacts of GHG and aerosol interactions on attribution results: (i) the warming effects from GHG and cooling effects from the aerosols counter-balance each other, leading to no climate change signals in the attribution results (ii) a stronger GHG influence with a reduced aerosol impact, leading to an intensification of the potential risks of intense and extreme events or, (iii) a stronger aerosol impact with small GHG influence, leading to a reduction in the risks. Shortwave aerosol forcing also has different impacts on the hydrological cycle than longwave GHG forcing (Allen and Ingram, 2002). Therefore, it is important to consider these interactions and examine how this can change the overall climate change impacts particularly for extreme events.

1.2. Study Area of Bangladesh

Bangladesh (20.34°-26.38°N and 88.01°-92.41°E) is a South Asian country with an area of ~144000 km^2, criss-crossed by ~700 hundreds of rivers and their tributaries (Banglapedia, 2012). The confluence of three great rivers - the Ganges, the Brahmaputra, and the Meghna - makes the country a giant deltaic plain. An average flow of 1,350 billion m^3 of water drains through the country each year from the Ganges-Brahmaputra-Meghna (GBM) basin.

The main physiographic features are characterised by extensive floodplains, which form about 80% of the land. These are mainly formed by sediments carried by the Ganges and the Brahmaputra River systems (Rashid, 1991). Two-thirds of the land area of Bangladesh is less than 5m above sea level, which makes the country extremely susceptible to riverine flooding and sea level rise (Dasgupta et al., 2011).

1.2.1. Regional Climate

Bangladesh is located in the sub-tropical monsoon region. Consequently, high temperatures, heavy rainfall, high humidity, and distinctive seasonal variations characterize its climate (Rashid, 1991).

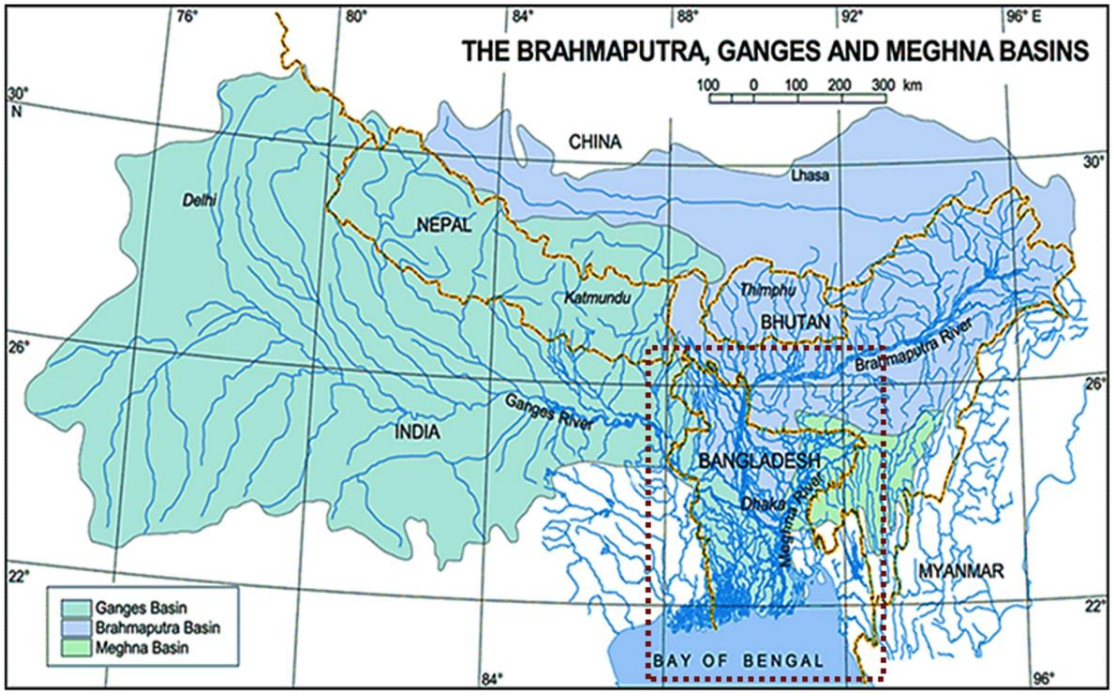


Figure 1.2: The Ganges-Brahmaputra-Meghna (GBM) Basin and the downstream country of Bangladesh (red dotted rectangle indicates location) through which the rivers finally flow into the Bay of Bengal (source: Banglapedia 2012).

Four distinctive seasons of this country can be characterized as: i) hot summer pre-monsoon season from March to May; ii) rainy monsoon season from June to September; iii) post-monsoon autumn season from October to November and iv) dry winter season from December to February (Shahid, 2010a).

During the summer monsoon season from June to September, when the country receives more than 75% of its annual rainfall (Shahid, 2010a), the three rivers have a combined peak flow of 180,000 m^3 per second, which is surpassed only by that of the Amazon (Sarraf et al., 2011).

Being a downstream country through which the river-runoff finally flows into the Bay of Bengal (Figure 1.2), Bangladesh is an extremely flood-prone nation. Apart from its topography, uncertain transboundary flow from 57 international rivers, heavy monsoon rainfall, high vulnerability to tsunamis and marine storm surges, and congested drainage channels are also contributing factors for the high flood risk (Dasgupta et al., 2011).

Closely linked with the four classes of rainfall seasons, four types of floods are experienced in Bangladesh: (i) flash floods that occur during mid-April before the on-set of the south-westerly monsoon; (ii) rain-fed floods that occur in the deltas in the south-western part of the country; (iii) river floods that occur during the monsoon season (these are the most common floods), when areas are inundated along the river and sometimes far beyond the riverbanks and (iv) coastal floods that occur due to storm surges or tidal effects along the northern part of Bay of Bengal (Hossain, 1998). Pre-monsoon flash floods are particularly damaging for crop production because crops nearly ready for harvest are flooded. Consequent crop damages can affect the local or even national food supply system (Ahmed et al., 2017).

In an average year, nearly 25% of the country is inundated (Ahmed and Mirza, 2000). A severe flood occurs every four or five years during the monsoon season, submerging more than 60% of the total land (GoB, 2014). The frequency of above-normal floods (exceeding 21% inundation area) has increased since 1950 (Höfer and Messerli, 2006).

About 50% (Basak, 2014) of the 158.5 million (UNFPA, 2014) Bangladeshi people are directly or indirectly dependent on agricultural livelihoods.

The agricultural sector, which largely depends on weather, contributes significantly to major macroeconomic objectives like employment generation, poverty alleviation, and food security (GoB, 2014). Therefore reliable weather and climate information, particularly concerning rainfall and temperature extremes, and their effects on water-related hazards and subsequent implications towards management of agriculture is enormously important (Ahmed and Mirza, 2000).

1.2.2. Observed recent change in climate

Immerzeel (2008) analysed historical monthly temperature and rainfall data for the period of 1901-2002 from the global database of Climate Research Unit (CRU) and found that temperatures are increasing at an average rate of 0.06°C per decade over the Brahmaputra basin but that no changes in the trends of observed rainfall over the last 100 years can be detected.

Based on station data analysis for the period of 1958-2007, Shahid (2010b) reported that the mean temperatures over Bangladesh are increasing at a rate of 0.103°C per decade. They also found a significant increase in the observed average annual rainfall

over Bangladesh (Shahid, 2010a). Another recent study conducted by analysing 50 years (1964-2013) of station data for northern Bangladesh revealed that pre-monsoon and post-monsoon rainfall is increasing, while monsoon rainfall is decreasing at most of the stations (Bari et al., 2016).

A few potential reasons behind the existing discrepancies in these findings could be differing analysis methods, a low signal-to-noise ratio, or high sensitivity to spatio-temporal variations. These seemingly contradicting results deserve closer inspection, hence calling for a more rigorous model analysis, as carried out in this thesis.

1.2.3. Projected future change in climate

There are numerous climate model studies that have projected changes in future climate over the wider South Asia region, including a few over Bangladesh (e.g., Agrawala et al. (2003); May (2004); Immerzeel (2008); Islam et al. (2008); Kumar et al. (2013); Mathison et al. (2013); Caesar et al. (2015); Fahad et al. (2017).

However, there exist large uncertainties in these model projections, partly due to the differences in the climate model characteristics (e.g., using 'perturbed physics ensembles' or, 'perturbed initial condition ensembles'); experimental methods (e.g., using 'multi-model ensembles' or 'multi-members ensemble' from a single model) and partly because of the integral uncertainties in the possible future GHG emissions scenarios (Collins et al., 2006, 2011; Immerzeel, 2008; IPCC, 2013a; Islam et al., 2008a; Massey et al., 2015).

Discrepancies between model results may also exist partially because of (i) uncertainty in representation of processes (parameterizations); (ii) error in propagation (e.g., biases in mean states can lead to some biases in variability or trend); (iii) sensitivity to model resolution (models with higher horizontal and/or vertical resolution better simulate some aspects of climate); and (iv) observational uncertainty (due to insufficient length or quality of observational data) (Flato et al., 2013).

Using the same UK Met Office Hadley Centre HadRM3P model that is also used in weather@home, Caesar et al. (2015) provided future projections of temperature and rainfall over Bangladesh and upstream Ganges, Brahmaputra and Meghna system. According to their study, the temperatures are projected to increase between 2.6°C and 4.8°C in Bangladesh by 2100 under the "RCP8.5" scenario (the Representative Concentration Pathway that assumes continued increasing fossil fuel use throughout this century). Future changes in rainfall are more variable; however from 8% to 28% increases are projected by the end of the century (Caesar et al., 2015).

Here, it can be noted that unlike the weather@home system that uses the HadRM3P model with 50 km horizontal grid resolution and the model ensembles of thousands of simulations with initial condition perturbations; the HadRM3P model used in Caesar et al., (2015) is at 25 km grid resolution and the future projections are based on a 17 member ensemble using a perturbed physics ensemble (PPE) approach (Collins et al., 2006).

Based on a multi-model ensemble from 11 RCMs of the Fifth Phase Coupled Model Inter-comparison Project (CMIP5), Fahad et al. (2017) estimated possible high end

future changes in mean temperature and rainfall under the high-emission RCP8.5 scenario. According to their findings, mean temperature increase can range from 3.24°C to 5.77°C in Bangladesh by 2100. The winter months of January and February are projected to warm the fastest.

In case of the projected future changes in the mean rainfall, Fahad et al. (2017) reports up to 12% increase over northeast and southeast regions, and up to 20% increase over the eastern hilly region, but a decrease in rainfall by up to 8% over south-west region of Bangladesh. The analysis of seasonal rainfall change suggests an increase during winter and pre-monsoon seasons, and a decrease in monsoon seasonal rainfall, indicating why there has not been found a consistent trend in the observational analyses as highlighted above.

1.2.4. Extreme weather events

Very few studies have explored how temperature and rainfall extremes may change under current and future climate change scenarios specifically in Bangladesh. Using a 17-member ensemble of HadRM3P at 25km grid resolution under the SRES A1B scenario (Solomon et al., 2007), one study by Nowreen et al. (2015), which did attempt to quantify the change in rainfall extremes, found a significant increase in both the 1-day and 5-day maximum rainfall over the Surma-Kushiyara river basin in north-east Bangladesh during pre-monsoon season by 2080, compared to baseline period of 1971–2000. Yet owing to the small sample size, a robust evaluation of the change in extreme event occurrence under current conditions was not feasible.

The sore lack of risk analyses of extreme events in Bangladesh highlights the importance of this thesis. Key challenges such as quantification of uncertainty are resolved by using a very large model ensemble. A carefully designed experimental setup allows for the investigation of the competing drivers of change, with particular focus placed on rainfall change.

1.2.5. Significance of attribution assessments for Bangladesh

As regional climates change, many extreme weather events are either becoming more intense, more likely, or both. It is important to recognise that neither of these changes represents "the new normal" implying a changed but stationary climate. As long as the GHG emissions continue to elevate global temperatures, these extreme weather events may continue to become more extreme in their intensities and increasingly more common in their frequencies (Christian Aid, 2018; Masson-Delmotte et al., 2018).

Bangladesh will be no exception from this context of climate change. Communities living in this country are already highly vulnerable to the impacts of global and regional climate change. In the global climate risk index of 2018 (Eckstein et al., 2018), Bangladesh is ranked 6th amongst the 10 most affected countries during the last two decades (1997-2016). With extreme weather events occurring even more frequently, the situation becomes more challenging due to limited capacity to adapt.

Robust attribution statements can be significant for Bangladesh to raise public awareness of the human impacts on extreme weather events, and support better

adaptation strategies to tackle climate change consequences (Stott et al., 2013b). Attribution results can also potentially contribute to the Warsaw International Mechanism (WIM) to deal with Loss and Damage (L&D) associated with climate change impacts, including extreme events. However, extensive dialogue is required between scientists and stakeholders to establish whether, and how, this science could play a role in the WIM (Parker et al., 2015).

1.4 Organization of the Thesis

This current chapter develops the case for the DPhil research, sets the background, identifies the knowledge gaps and challenges and informs the aims and key questions of the thesis.

Chapter 2 presents the experimental methods, modelling frameworks and observation datasets used in this thesis. Further details of the data and methods are presented in the relevant papers as appropriate.

Chapter 3 discusses process based model evaluation results by looking at the key monsoon mean state features in the model compared to observed ones and the model's response to observed variations of sea surface temperatures.

Chapter 4 presents a paper that evaluates the RCM's performance in simulating extreme events compared to available gridded observational datasets and satellite data.

Chapter 5 presents a paper that compares risks of seasonal extreme rainfall events in Bangladesh under different climate change scenarios relevant to the long-term

temperature goals set out in the Paris Agreement. Interesting results are reported for changes in risks when anthropogenic aerosols are reduced to pre-industrial levels.

Chapter 6 presents an event attribution paper to reveal whether or not climate change contributed to an extreme rainfall event during pre-monsoon season at northeast parts of Bangladesh in 2017.

Finally, **chapter 7** presents the thesis conclusions by discussing implications and potential avenues for future research.

Although the core thesis chapters of 4-6 are independent and present distinct findings in the form of three journals papers, collectively they form a coherent basis for the thesis. The content of each chapter (of 4-6) is the same as it appears in the published (in chapter 4 and 6) or revised version of the paper (in chapter 5); though figure and table numbers are modified to attain coherency throughout the thesis.

To improve readability, the figure layouts are also changed. Supplementary material of each paper is given at the end of relevant chapter. After supplementary materials, additional section is given when extra information is needed for better clarification of the context and any other aspect of the study.

Papers published/in review

1. **Rimi R.H.,** Haustein K., Barbour E.J., Jones R.G., Sparrow S.N., and Allen M.R. 2019. Evaluation of a large ensemble regional climate modelling system for extreme weather events analysis over Bangladesh. *International Journal of Climatology* 39(6): 2845–2861. DOI: 10.1002/joc.5931 (Forming Chapter 4).

2. **Rimi R.H.,** Haustein K., Barbour E.J., Sparrow S.N., Li S., Wallom D.C.H., and Allen M.R. 2018. Risks of seasonal extreme rainfall events in Bangladesh under 1.5 and 2.0 degrees' warmer worlds - How anthropogenic aerosols change the story. *Hydrology and Earth System Sciences Discussions* (in review). 1–23. DOI: 10.5194/hess-2018-400 (Forming Chapter 5).

3. **Rimi R.H.,** Haustein K., Barbour E.J., and Allen M.R. 2019. Risks of Pre-Monsoon Extreme Rainfall Events of Bangladesh: Is Anthropogenic Climate Change Playing a Role? *Bulletin of the American Meteorological Society* 100(1): S61–S65. DOI: 10.1175/BAMS-D-18-0152.1 (Forming Chapter 6).

2. Modelling frameworks, observation data sets and analytical methods

2.1. Introduction

This chapter first introduces the details of model configuration and necessary inputs for the two modelling frameworks: (i) weather@home system and (ii) Half a degree Additional warming, Prognosis and Projected Impacts (HAPPI) project. The weather@home system is used to generate regional model ensembles over South Asia region. The climate variables are simulated under different forcing scenarios including historical (actual), counterfactual (natural), greenhouse (GHG)-only, and projected future scenarios of 1.5° and 2.0° of warming compared to pre-industrial levels.

Secondly, the observational datasets from surface, satellite, and reanalysis sources which are used as the reference to evaluate model's performance in this thesis are briefly discussed. The analytical methods presented at the end of this chapter explain the different statistical and graphical methods applied in this thesis. Additional information regarding case-specific data and methods are also present in chapters 3-6.

2.2. Modelling frameworks

2.2.1. The weather@home system

As mentioned in chapter 1 section 1.1.4, the regional climate modelling system known as weather@home (Guillod et al., 2017; Massey et al., 2015) is a part of the climateprediction.net (CPDN; Allen, 1999) project. Weather@home uses the Met Office Hadley Centre's atmospheric GCM, HadAM3P, which is downscaled to a higher resolution over a limited domain (i.e., South Asia for this thesis) by its RCM counterpart, HadRM3P.

HadRM3P has been used across a range of experiments and forms the basis of the Providing Regional Climates for Impacts Studies (PRECIS) modelling system. The South Asia domain of weather@home is similar to the Coordinated Downscaling Model Experiments (CORDEX) South Asia domain (Massey et al., 2015). Both HadRM3P and HadAM3P share the same physics and are based on the atmospheric component of HadCM3, a well-documented and widely used ocean-atmosphere coupled general circulation model (Gordon et al., 2000) with a number of improvements (Massey et al., 2015).

These improvements include a better representation of cloud cover, relative humidity, radiative effects of convection, and the inclusion of a sulphur cycle scheme (Jones et al., 2001) which models the interactions of both natural and anthropogenic sulphate aerosol emissions. The model also uses a more recent sulphur dioxide (SO_2) data from the ECLIPSE v5a global emissions dataset (Klimont et al., 2013) to prescribe the SO_2 fields in the model with emissions varying at the surface and at high levels.

HadAM3P has 19 vertical levels, a regular latitude–longitude grid (1.25° latitude by 1.875° longitude) with regular poles (which approximates grid boxes of length of ~150 km at mid-latitudes and ~200 km in the tropics), and operates using a 15 minute timestep. HadRM3P shares the same vertical resolution, but has a 5 minute timestep and a horizontal resolution of 50 km on a rotated latitude-longitude grid for extratropical domains, ensuring that each grid box in the region has approximately the same area (Jones et al., 2004; Massey et al., 2015). The different inputs necessary to successfully run the coupled model under the distributed network of the volunteers' computers are briefly discussed in the following sub-sections.

2.2.1.1. Volunteer Distributed Computing

Volunteer Distributed Computing (VDC) allows for the computation of very large ensembles of the GCM and RCM. The Berkeley Open Infrastructure for Network Computing (BOINC; Anderson, 2004) allows to utilize the idle computing power of volunteers in a client/server model. A volunteer first needs to sign up to the CPDN project via the BOINC client software.

After completing this step, the GCM and RCM are downloaded to the volunteer's home computer. Designated CPDN scientists then hand out the 'workunits' to the volunteers' computers through a controlled project server. Each workunit provides fundamental information for the climate models to run an experiment under a specified climate scenario and for a certain period of model time (Massey et al., 2015).

Following CPDN's success in using VDC through BOINC system, weather@home uses the identical infrastructure to compute very large ensembles of the HadAM3P-HadRM3P models. The meteorological variables of interest can be retained in the post-processed outputs upon completion of the runs of each model month as specified in the header file of each workunit. The final results are returned after post-processing to the host server.

A standard home computer can take around 4 to 5 days to integrate over the model year but this can vary depending on the domain size. When a model year is completed, the final state of the atmosphere is returned in an additional file called the 'restart file'. The following year of the climate scenario is run with a new workunit that incorporates the

restart file representing the previous year's final state. Hence, it is possible to generate an extended time series of climate model integrations by running the system for a year at a time, in a time-slice manner, generating multi-thousand ensemble members for the time period of interest. Completed results are converted to netCDF format, compressed to reduce size (gzipped) and then returned to the result upload server.

Usually, 80% of the submitted workunits are successful, corresponding to a failure rate of 20% due to various factors related to volunteers computer usage or transfer failures (see Massey *et al.* (2015) for details). The model can be run over time periods longer or shorter than one year, but 12 months at the current spatial resolution provide a sensible balance between failures in data exchange and failures in running the model at the volunteer's computer.

2.2.1.2. Model configuration

In the weather@home system, the HadAM3P-HadRM3P models run on the same client computer with HadAM3P providing the lateral boundary conditions (LBCs) for the HadRM3P. The coupling is strictly one way, meaning that the GCM feeds the RCM but there is no feedback from the regional model to the global model.

The RCM defines a four-point buffer zone around the perimeter of the region. The main variables of the LBCs (atmospheric pressure at the surface along with horizontal winds, temperature and humidity for all atmospheric layers) are relaxed across the buffer zone to values temporally interpolated from 6 hourly outputs from the global model.

This relaxation technique is implemented across the four point buffer zone at each vertical level (Guillod et al., 2017; Massey et al., 2015). Before the model can be used for simulating the climate, the atmosphere and land surface have to adjust, or "spin up" to a mutual equilibrium state in the model. The atmosphere of the regional model interior may take from few model days to two weeks to achieve equilibrium with its LBCs depending on the region under study, but the temperature and moisture in the deep soil levels can take many model months to years to reach equilibrium.

Consequently, the spin up period should be region specific, at least a year or more which is then discarded for the actual model run. The model is started with a pool of workunits, containing the same generic initial conditions. The generic condition resembles the state of the model at 1 December after ten year spin-up period to ensure that the deep soil of the model region is properly spun-up.

With the initial condition and the subsequently produced restart files, the model climatology is generated. The time-slices consist of over-lapping 13-month model runs for the 1986–2015 period. The first year (1985) as well as every first month (December) in each model year is discarded due to the above mentioned spin-up effects.

Initial condition (IC) perturbations are required to produce model simulations with the full range of possible internal variability. This is achieved using slight changes to the three-dimensional potential temperature field in the GCM.

The perturbations are fully three-dimensional fields with a scaling function (S) that is applied in a way that ensures that the top of atmosphere flux is not influenced significantly. It is calculated as follows:

$$S = 1 - \frac{\sin(Z_c - Z_0)}{N_z - Z_0} \qquad (2.1)$$

Where, Z_c is the level at which the scaling is applied, Z_0 is the level above which no perturbation occurs and N_z is the number of levels in the model's atmosphere (Massey, 2015). In order to minimize the risk of making the model unstable, the maximum amplitude of the perturbation in potential temperature is set to 5 Kelvin. 1,740 different IC perturbations are generated, available for the pool of workunits. No perturbations are applied to the RCM, as the GCM drives the RCM simulations through the transfer of LBCs at the end of the first global model day.

An updated version of weather@home (known as weather@home 2), which includes a more recent land surface scheme, the Met Office Surface Exchange Scheme (MOSES 2, Essery and Clark, 2003), is used in this thesis. MOSES is a third generation land surface model that can incorporate the direct physiological effect of CO_2 on photosynthesis and stomatal conductance (Sellers et al., 1997).

MOSES 2 explicitly considers land surface heterogeneities within each grid cell through a tiling scheme (Essery and Clark, 2003) and consequently the weather@home 2 system provides a better representation of the land surface features than the earlier version.

In the RCM of the weather@home 2 system, the use of Top-Down Representation of Interactive Foliage and Flora Including Dynamics model (TRIFFID; Cox, 2001) also improves the representation of the land surface. For more details about these model developments see Guillod *et al.*, (2017). For conciseness, the updated weather@home 2 that used in South Asia model domain is simply referred to as weather@home in the rest of this thesis.

2.2.2. Model scenarios

Here, the technical details of the different model scenarios that are used in this thesis are provided. First the historical scenario, which can also be referred to as default setup; followed by the natural (counter-factual), GHG-only, and finally the two future scenarios of 1.5°C and 2.0°C warmer worlds than pre-industrial. The latter two scenarios are equivalent to HAPPI, but generated independently by the weather@home system. Brief discussions on the pertinent climate scenarios also exist in the papers presented at chapter 4, 5 and 6.

(1) Historical scenario

The GCM (HadAM3P) and RCM (HadRM3P) used in the weather@home system are atmosphere-only models, hence they both require forcing at the surface boundary between the atmosphere and ocean in the form of sea surface temperatures (SSTs) and sea ice fractions (SIFs).

For the 30-year historical climate scenario of 1986–2015, lower boundary conditions of SSTs and SIFs fields are taken from the UK Met Office Operational Sea Surface

Temperature and Sea Ice Analysis (OSTIA) dataset (Donlon et al., 2012). OSTIA is re-gridded using an area-weighted average to HadAM3P's spatial resolution of 1.875° x 1.25°.

The radiative forcings follows the Coupled Model Intercomparison Project Phase 5 (CMIP5; Taylor *et al.*, 2012) protocol, with prescribed GHG concentrations (CO_2, CH_4 and N_2O), ozone, halocarbons, and sulphur species. The halocarbon gases (CFC113, CFC11, CFC12, HCFC22, HFC124 and HFC134A) are represented as a single value per time point in the time series in a way that produces the equivalent radiative forcings as if all six gases were modelled (Massey et al., 2015).

Beyond the year 2005, the GHG concentrations and aerosol emissions follow the Representative Concentration Pathway (RCP) 4.5 scenario of CMIP5 (IPCC, 2013c). While solar and volcanic forcings are kept the same across all forcings scenarios; anthropogenic radiative forcings contributions and lower boundary conditions are a function of the respective climate scenario.

The sulphur cycle scheme of the HadAM3P-HadRM3P models is supplied with the standard inputs of the surface anthropogenic emissions of SO_2 including elevated emissions of SO_2, which are released at a higher model layer than the surface (e.g. from a chimney stack). Other non-anthropogenic sources are also incorporated in the model, including regular but small-scale natural emissions of SO_2, and natural emissions of dimethyl sulphide, primarily from phytoplankton in the ocean. In addition, explosive volcanic eruptions are setup such they also emit tropospheric SO_2 in addition to the actual prescribed radiative forcing.

A small modification also enables the HadAM3P model to account for variations in solar activity. These solar anomalies take into account the 11-year solar cycle as well as longer time-scale solar activity.Based on this historical scenario, 200 model ensemble members are generated for each year during the period of 1986-2015 that constitute the 30-year climatology period for this thesis. Using this same standard setup of weather@home, an actual climate scenario based on observed SSTs of the year 2017 is generated with 2500 model ensemble members for the attribution study of 2017 extreme event in Bangladesh. Such a large model ensemble with initial condition perturbations provides an adequate sample for examining the tails of the distribution for studying extreme events.

(2) Natural scenario

For the counterfactual natural climate scenario, different lower boundary conditions are required to drive the weather@home model. Pre-industrial levels of GHGs, ozone and aerosols, following the IPCC historical forcing for the year 1900 are used. The sea ice fraction (SIF) extent that corresponds to the year of maximum SIF extent in each hemisphere of the OSTIA record is used. This corresponds to 1986 SIF in the Arctic and 2007 SIF in Antarctica.

Natural SST patterns without anthropogenic warming are used for the counterfactual world scenario. To calculate the natural SST patterns, the modelled anthropogenic warming is subtracted from the observed SSTs (as mentioned earlier in equation 1.1 and 1.2). For this purpose, 11 GCM simulations (listed in Table 2.1) from the CMIP5 archive are used.

Global daily SST fields of OSTIA data set have a spatial resolution of 0.05° latitude x 0.05° longitude. The GCM, HadAM3P has a different spatial resolution of 1.875° latitude x 1.25° longitude. Therefore, the OSTIA SST data are regridded using an area-weighted averaging method so that these fields can be defined per grid box of HadAM3P model. The mean of surrounding ocean grid points is used to resolve any discrepancies between the HadAM3P and OSTIA land-sea mask. Figure 2.1 shows a flow diagram for the steps involved in the calculation of SSTs.

Table 2.1: The CMIP5 models used to calculate δSSTs

CMIP5 model	**Ensemble member (i1p1)**
CanESM2	r1 r2 r3 r4 r5
CCSM4 Nat	(r1 r2 r4 r6) / all (r1 r2 r3 r4 r5 r6)
CNRM-CM5 Nat	(r1 r2 r3 r4 r5 r8) / all (r1 r2 r3 r4 r5 r6 r7 r8 r9 r10)
CSIRO-Mk3-6-0 Nat	(r1 r2 r3 r4 r5) / all (r1 r2 r3 r4 r5 r6 r7 r8 r9 r10)
GFDL-CM3 Nat	(r1 r2 r3) / all (r1 r2 r3 r4 r5)
GISS-E2-H	r1 r2 r3 r4 r5
GISS-E2-R Nat	(r1 r2 r3 r4 r5) / all (r1 r2 r3 r4 r5 r6)
HadGEM2-ES Nat	(r1 r3 r2 r4) / all (r1 r2 r3 r4)
IPSL-CM5A-LR Nat	(r1 r2 r3) / all (r1 r2 r3 r4 r5r6)
IPSL-CM5A-MR	r1 r2 r3
MIROC-ESM	r1 r2 r3

To represent the climatological mean of the delta SST pattern, 10-year running means of the natural (HistoricalNat) SSTs are subtracted from the actual (Historical) SST simulations. The moving window of these running means encompasses the 1976-2005 period, which in essence fits the 1986-2015 period best as far the agreement between observed SSTs and the resulting delta SSTs are concerned.

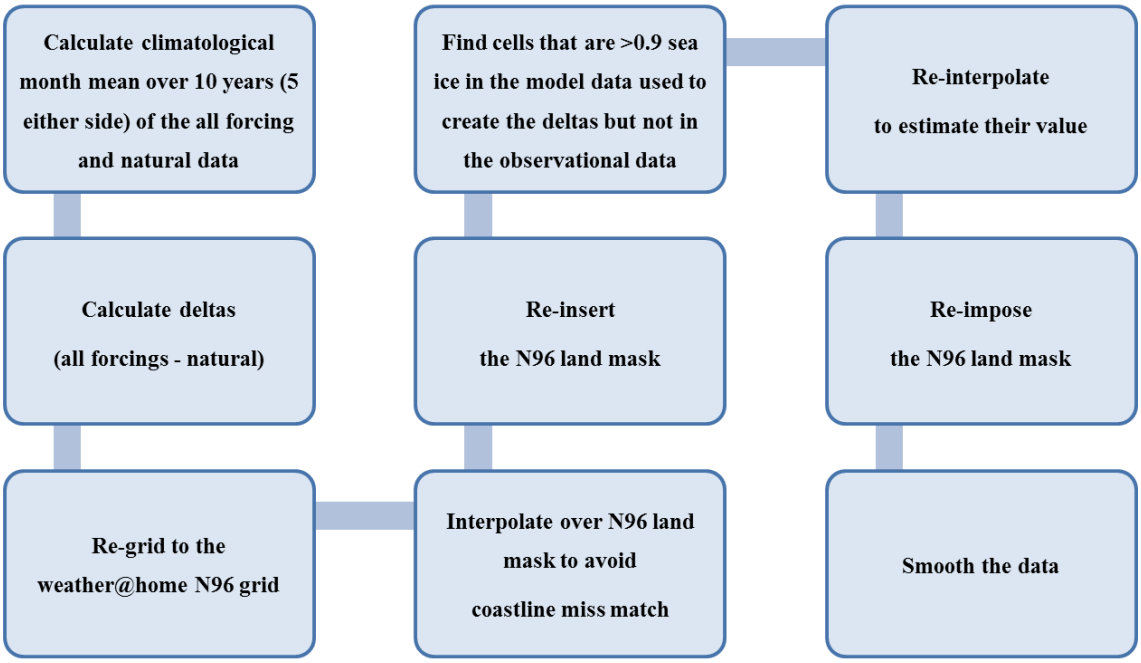


Figure 2.1: Schematic diagram for steps in the calculation of delta SSTs (adapted from http://climateprediction.net/wiki/lib/exe/fetch.php?media=wiki:natsst_doc_v2.pdf)

The delta SST patterns thus represent 11 estimates of the possible impact of human GHG emissions on SSTs. These anomalies are then subtracted from the OSTIA observed SSTs to generate the natural SSTs which are then used to run the associated counterfactual world experiments, along with pre-industrial atmospheric GHG concentrations (Schaller et al., 2016).

For the natural 30 year climatology period, 200 model ensemble members are generated for each year during the historical period of 1986-2015 for this thesis. Following the same method, the natural counterfactual scenario of 2017 is generated with 5250 model ensemble members to assess the risks of extreme rainfall event in Bangladesh without human impacts on climate change.

(3) GHG-only scenario

For generating the GHG-only scenario, the SST forcings are constructed in a similar way to the counterfactual SSTs. Except this time, the CMIP5 historical SSTs are subtracted from the combined SSTs of GHG-only plus natural. The addition of the natural SSTs (HistoricalNat) to GHG-only is necessary to account for the fact that the GHG-only scenario in CMIP5 does not include natural forcings. Yet they need to be represented when compared with the historical simulations.

As before, a moving 10-year running mean between the 1976-2005 period is used to derive the delta SST pattern, of which there are 11 estimates based on the same CMIP5 models as in the natural scenario. Correspondingly, in this scenario the anthropogenic aerosol concentration is reduced to pre-industrial levels in order to simulate a hypothetical climate, where impacts of anthropogenic aerosols are removed.

Hence, the difference between historical and GHG-only scenarios simulates the net aerosol effect under current conditions assuming additive behaviour of different radiative forces. The GHG-only scenario is used to the attribute changing risks of extreme weather events to a variable loading of anthropogenic aerosols.

For the GHG-only 30 year climatology period, 200 model ensemble members are generated for each year during the historical period of 1986-2015.

(4) Future warming scenario of 1.5°C and 2.0°C

The HAPPI project provides a modelling framework to generate climate data that can be used to study extreme weather events and quantify the difference between the probability of occurrence of those events in the present climate condition, and in the worlds that are 1.5°C and 2.0°C warmer than pre-industrial conditions (Mitchell et al., 2017).

HAPPI experiments are designed to generate large model ensembles of simulations (50-100 members) from atmosphere-only models for three time slices. Each of these three time slices is a decade in length. The first scenario represents the most recent observed 10-year period (2006–2015), while the second two scenarios are the two future decades under 1.5°C and 2.0°C warmer than pre-industrial conditions. The CMIP5 models under RCP2.6 forcings scenario provide a global average temperature response at 1.55°C relative to preindustrial. Therefore, the HAPPI 1.5°C experiment basically uses the RCP2.6 scenario for the model boundary conditions. For each of the years within the decade of the 1.5°C experiment, forcings values for the year 2095 for GHGs, aerosol, land-use, and land-cover changes are used.

Because no analogous CMIP5 simulations are available for the 2°C experiment, a weighted combination of RCP2.6 and RCP4.5 is used. The weights are calculated in such a way that the global mean temperature response is 2.05°C, which is exactly half a degree above the 1.55°C response from the 1.5°C experiment. The natural radiative

forcings are set to the same values as in the current decade experiment and in the 1.5°C experiment (Mitchell et al., 2017). The weather@home system is used to generate the large model ensembles for each of these HAPPI scenarios using the VDC. By means of the initial condition perturbation model ensemble, each simulation within an experiment differs from the others in its initial weather state. For each model experiment, the 10-year time slices are generated with 98 ensemble members per year for this thesis.

(5) Additional simulations from other AGCMs under the HAPPI project

Along with these model simulations from weather@home system, available simulations from additional four AGCMs under the HAPPI project are used in chapter 5 (downloaded from http://portal.nersc.gov/c20c/data/.) for a multi-model assessment of the changes in the risks of extreme rainfall events in Bangladesh.

These AGCMs have the same HAPPI experimental set-up to provide with decadal simulations with initial conditions perturbations and have ≥100 members per year. Available forcings scenarios include natural, actual, and 1.5°C and 2.0°C warmer worlds (i.e., no GHG-only scenario). Such short duration (10-year) of model ensembles require less computational expense, and allow for the analysis of interannual variability and extremes (Mitchell *et al.*, 2017). More details of the AGCMs can be found in the recent study by Chevuturi et al., (2018).

2.3. Observational Data sets

2.3.1. Overview

For each of the climate variables, there are numerous observational datasets available for model evaluation. Different sources of observational datasets can have inconsistencies in the magnitude of the climate variables. Appropriate choice of the reference dataset is therefore important and can lead to highly contrasting model evaluation results. Possible reasons behind such discrepancies may include: different analysis methods and inputs to derive the observational data set; temporal and spatial scales; and density of the meteorological stations.

In order to address this observational uncertainty, a range of available observation data sets are initially used to compare with the model data. After considering the preliminary results (not shown) and also reviewing previous studies reporting comparative strengths and weaknesses of the observation datasets, a subset was selected for the final analysis. Section 2.4.2 gives the justification for using each of the selected observation data sets and also reports their limitations.

Observational data sets used in this thesis include high resolution gridded observation-based datasets of: Asian Rainfall - Highly-Resolved Observational Data Integration Towards Evaluation of Water Resources (APHRODITE), Global Rainfall Climatology Centre (GPCC), Climate Prediction Centre (CPC), reanalysis data from the European Centre for Medium-Range Weather Forecasts (ECMWF) interim reanalysis (ERAI-interim) data sets, and one satellite-based dataset from the Tropical Rainfall Measuring

Mission (TRMM). Table 2.2 presents basic information for these data sets, followed by an overview of each.

Table 2.2: Basic information about the observational data sets used in this thesis.

Product name and version	Temporal coverage	Spatial coverage	Temporal resolution	Spatial resolution	Reference
APHRODITE Rainfall V1003R1 and V1901	1951-2007 and 1998-2015	0.5°x0.5°	Daily	Asia	Yatagai et al., 2012
APHRODITE Temperature V1204R1	1973-2007	0.5°x0.5°	Daily	Asia	Natsuko et al., 2011
GPCC V1.0	1988-2013	1.0°x1.0°	Daily	Global land	Schamm et al., 2015
GPCC V8	1891-2016	0.5°x0.5°	Monthly	Global land	Anja M-C et al., 2018
CPC	1979-present	0.5°x0.5°	Daily	Global land	Chen and Xie, 2008
TRMM 3b42 V7	1998-2013	0.25°x0.25°	Daily	50°N-50°S	Huffman, G.J. et al., 2007
ERAI-interim	1979-present	0.79°x0.79°	Monthly	Global	Dee D.P. et al., 2011

APHRODITE daily rainfall data set provides the only long-term (1951-2007) continental-scale gridded product over Asia, including the Himalayas, and South and Southeast Asia. Most daily gridded rainfall products are based on data available through the Global Telecommunication System (GTS) network. APHRODITE has a dense network of daily rain-gauge data from 5000-12,000 stations and so this product can use 2.3-4.5 times more data compared to other GTS network-based products. Spatial interpolation is done using a Sheremap-type scheme (Willmott et al., 1985) by employing angular distance weighting to yield better representation of the orographic rainfall pattern (Yatagai et al., 2012).

Recently this observation data is updated (latest version V1901) for the duration of 1998-2015 with improved quality control to represent extreme rainfall events more precisely. This updated version of APHRODITE data is used in chapter 5 while, the older version is used in chapter 4.

APHRODITE daily temperature data set has 1.5 to 3 times more data than other temperature products based on GTS data. This temperature data is corrected for mean sea level and elevation influences and is then interpolated using area-weighted means (Natsuko et al., 2011).

GPCC daily global land surface rainfall data set is based on observation data provided by National Meteorological and Hydrological Services, regional and global data collections, and the World Meteorological Organization (WMO) GTS data. Ordinary block kriging method is used to interpolate irregularly spaced observations of rainfall to a regular grid (Schamm et al., 2014).

When the analysis is focused on the daily rainfall, the GPCC daily product is recommended for use, e.g., for analyses of extreme events and related statistics at a daily resolution (Schamm et al., 2015).

GPCC monthly global land surface rainfall product is based on both near-real-time and non-real-time stations thereby including the data from National Meteorological and Hydrological Services and historical data collections (Schneider et al., 2014). As a result, this product has much higher accuracy compared to the GPCC near-real-time products. The stations which contribute to the data coverage every month range from less than 10,000 to more than 50,000. GPCC monthly data is recommended for model evaluation at global and regional scales, climate variability analysis, and water resources assessment studies (Anja et al., 2018).

TRMM daily rainfall is a joint product of an independent agency of the United States Federal Government - the National Aeronautics and Space Administration (NASA) and the Japan Aerospace Exploration Agency. TRMM rainfall measurements in the tropical and subtropical regions are targeted towards weather and climate research and provide critical inputs to tropical cyclone forecasting, numerical weather prediction, and rainfall climatology studies (Huffman et al., 2007). Among the five high-resolution satellite based rainfall products, TRMM is reported to provide the second best performance (after RFE2.0-Modified data) to capture observed rainfall over the Brahmaputra river basin (Bajracharya et al., 2015).

CPC daily global rainfall data set is based on unified gauge-based analysis. Rainfall data from over 30,000 global land rainfall gauge stations contributed to construct this product. CPC data set uses optimal interpolation (OI) with orographic consideration (Chen and Xie, 2008).

ERA-Interim monthly data set is a global atmospheric reanalysis produced by the ECMWF. Reanalysis data is a model product where model variables are nudged towards observed values (on average ~10^6 per day in 1989, and ~10^7 per day in 2010). The majority of observation data comes from satellites. In situ measurements of upper-air temperatures (T), wind (u/v), and specific humidity (q) are taken from radiosondes, pilot balloons, aircraft, and wind profilers. Observations of surface pressure (Ps), 2 m temperature, 2 m relative humidity (RH), and near-surface (10 m) winds (u/v) taken from ships, drifting buoys, and land stations are also assimilated. The atmospheric model used by the ERA-Interim reanalysis system is ECMWF's Integrated Forecast System (Dee et al., 2011).

2.3.2. Justification for main reference data selection

For the process-based model evaluation, when monthly observational data can be used for the analysis of the physical processes at seasonal scales, the selected main reference data sets are GPCC (for rainfall) and ERA-Interim reanalysis (for sea level pressure and wind). The two natural modes of climate variability that are used in this model evaluation process are NINO3.4 and IOD indices, and both indices have monthly time-scales.

As mentioned in section 2.3.1., GPCC monthly data has high accuracy, and is recommended for model evaluation at regional scales. GPCC monthly data is available for the same period as model data (1986-2015) and allows for a straightforward evaluation of the model. ERA-Interim global data is of particular importance when regional observation data sets are scarce. Use of the wind and mean sea level pressure data from ERA-Interim data set allows looking at key features of the South Asian monsoon system during the 30 years study period of 1986-2015. Specific details regarding this process-based model evaluation is given at chapter 3, section 3.3.

APHRODITE is selected as the main reference observational dataset for the performance-based model evaluation when using daily observation data with high quality is crucial. The density of stations contributing to the calculation of rainfall in APHRODITE is relatively good across South Asia, particularly over India, Bangladesh and Nepal (Mani et al., 2018). Consequently, APHRODITE is useful for improved evaluation of daily series of model outputs and for statistical analysis of extreme weather events (Yatagai et al., 2012) in this region.

Numerous studies have quantitatively evaluated the accuracy of APHRODITE's rainfall data over the South Asia region. For example, Andermann et al. (2011) reported that APHRODITE provides the best estimates among five gridded rainfall data sets when compared to independent ground observations at daily scales over Nepal. Khandu et al. (2016) found that APHRODITE adequately captures the spatio-temporal variability of rainfall over Bhutan including the extreme events (with correlation coefficients >0.5).

APHRODITE is well correlated with daily gridded rainfall data (with correlation coefficients >0.6) from the Indian Meteorological Department (Prakash et al., 2015; Rajeevan and Bhate, 2008).

The climatology data and monthly means of the APHRODITE daily temperature dataset and other monthly mean gridded temperature data sets (e.g., Climate Research Unit (CRU) and University of Delaware (UoD) temperature data) have minimal difference. APHRODITE daily temperature data set is useful for the improved monitoring of long-term change, as well as statistical analysis of temperature related extreme weather events (Natsuko et al., 2011).

Islam et al., (2018) verified the performance of APHRODITE rainfall over Bangladesh against data from 34 stations of the Bangladesh Meteorological Department (BMD) for the period of 2003-2005. For a rainfall event in the 1-50 mm range, APHRODITE shows very good correlation with the BMD station data (correlation coefficient 0.82). But for ≥50 mm and ≥100 mm rainfall events, APHRODITE shows poorer performance with correlation coefficients of 0.53 and 0.32, respectively. Underestimation of extreme rainfall accumulations is a limitation of APHRODITE according to their study.

Nevertheless, APHRODITE rainfall and temperature data sets are the most commonly used products in different studies that focus on Bangladesh (e.g., Hatsuzuka et al. 2014; Caesar et al. 2015; Sugimoto and Takahashi 2017; Fahad et al. 2017; Caesar and Janes 2018; Hasan and Islam 2018).

Temperature data from APHRODITE is nearly identical when compared with UoD data, hence only APHRODITE daily temperatures are used in the model evaluation. But for rainfall, other sources from gauge (GPCC, CPC), and satellite (TRMM) data sets are included to address the observational uncertainty. More details about how these observation data sets are used to evaluate the model's performance in capturing the extreme events are presented in chapter 4, section 4.3.

Regions with poor observational records or without long-term data are usually considered with caution by researchers in their PEA analyses, because observational data needs to be adequate for assessing long-term trends for characterizing an event as extreme, or for evaluating climate models that are used for the assessments (Angélil et al., 2017).

In chapter 6, attribution assessment of the 2017 pre-monsoon extreme rainfall event in Bangladesh is presented. In this study, the observation data is used to characterize the event as a rare occurrence and to evaluate the model's performance in simulating the observed event. In this case, the selected main reference data set is CPC given it is the only high-resolution gridded daily rainfall data set from 1979 to present over the study region. Although other observation data sets including APHRODITE (1979-2007) and GPCC (1988-2017) are used in the analysis of the 2017 extreme event, the longer temporal coverage of CPC provides a larger sample to fit extreme value distribution in order to determine the event's rarity. For details see chapter 6, section 6.2.

2.4. Methods

The statistical concepts and methods that are used in different chapters of this thesis are briefly discussed in the following sections:

2.4.1. Extreme Value distribution

Extreme Value distribution analysis particularly focuses on the model's ability to capture extreme events with up to 100 years of return periods. Because the quantitative assessment of the model's quality with regards to infrequent events, it can build necessary confidence in PEA studies (National Academies of Sciences, Engineering, 2016).

The large model ensembles from weather@home can provide adequate model data to look at the tails of the distributions, where the extreme events lie. But the short temporal coverage of the available high resolution gridded observational datasets cannot provide necessary statistical sample data to examine infrequent rare events with long return periods.

Generalized Extreme Value (GEV) theory is applied to solve the problem associated with very long return periods. The Extreme Value Distributions (EVDs) is fitted to the observation and model data before doing an evaluation of the model simulated extreme events.

The events (z) of maximum temperature and rainfall are fitted to the GEV distribution following the equation (Coles et al., 2001):

$$G(z) = \exp\left(-\left[1+\xi\frac{z-\mu}{\sigma}\right]^{-\left(\frac{1}{\xi}\right)}\right) \qquad (2.3)$$

Here, G is a non-degenerate distribution function; μ, σ and ξ denote the location, scale and shape parameter of the GEV distribution, respectively.

For the observations, the confidence intervals (CIs) are also estimated by applying a parametric bootstrap (Gilleland and Katz, 2011) for events with return periods ranging from 2 to 100 years.

3. Bootstrap method, first introduced by B. Efron (1979) relies on sampling with replacement from sample data to provide inference about a population. This technique is used to estimate the standard error of any statistic and to obtain a confidence interval (CI) for it. Bootstrap method is particularly useful for estimating CIs that are very complicated or do not have a closed form.

   The calculation method involves the following steps:

   For a sample of n elements: $X = \{x_1, x_2, \ldots, x_n\}$ and for some statistic of interest $T = t(X)$; the following scheme is repeated for R times:

   (i) For i-th repetition, sample with replacement n elements from the available sample and call this new sample i-th bootstrap sample, X_i

   (ii) Calculate desired statistic $T_i = t(X_i)$

(iii) From the above mentioned steps (i) and (ii), a bootstrap distribution of T is obtained as: $T_1, T_2, \ldots, T_R$.

(iv) Based on this distribution, CI for T is calculated using the percentile method (Efron and Gong, 1983; Efron and Tibshirani, 1993) by taking the Alpha/2 and 1 - Alpha/2 quantiles of the sample in following manner:

$$\textbf{Percentile CI} = (\theta_{(1-\alpha)/2},\ \theta_{1-(1-\alpha)/2}) \qquad \textbf{(2.4)}$$

Where, α is a confidence level, typically $\alpha = 0.95$, θ_α is an α-percentile of distribution of bootstrap realizations.

For calculating the lower and upper bounds of the CIs, the 'Alpha' numeric parameter between 0-1 that gives the desired significance level is used. An Alpha value of 0.05 corresponds to a 95 per cent confidence level, which is used to calculate the lower and upper CIs for the observations by following equations:

$$\textit{Lower CI} = \frac{\textit{Alpha}}{2} \textit{ x 100} = \frac{0.05}{2} \textit{ x 100} = 2.5 \qquad \textbf{(2.5)}$$

$$\textit{Upper CI} = \frac{\textit{1-Alpha}}{2} \textit{ x 100} = \frac{1-0.05}{2} \textit{ x 100} = 97.5 \qquad \textbf{(2.6)}$$

The range of CI for GEV fitted distributions of the observations presented in the figures 4.9-4.13 (and supplementary figures S4.5-S4.6) in chapter 4, are therefore, from 2.5 to 97.5.

(1) **Peak Over Threshold (POT)** model, another type of EVD is fitted to estimate the return period of the observed event, mainly to determine its rarity. The POT model is used, where the data points (or excesses) over a threshold can be used to estimate the parameters of the distribution function. This approach is useful

when the observations are not long enough to assess exceptionality of an extreme event with conventional methods. More details can be found at the supplementary material of chapter 6.

(2) **Return time plots** assist in analysing the "tail" of a distribution where the extreme events exist. These plots provide one suitable way of graphically representing extreme events in a big sample of data, such as weather data. The "return time" of an event, also known as the "return period" or "recurrence interval", is the likelihood of an event occurring, defined by a particular variable exceeding a certain threshold in a certain time interval. For example, figure 2.2 indicates that rainfall event exceeding a threshold of 240 mm during the monsoon season is an extreme event of 100 year return period (see black dots for actual climate model ensemble in figure 2.2).

Each coloured dot on this return time plot represents a single model simulation. The logarithmic x-axis of the plot indicates the chance of an event occurring in a given year, such as seasonal rainfall, exceeding a particular threshold. For instance, a "1 in 10 year event" is a frequent event with the chance of occurring 1 in 10, or 10%, in any given year. On the contrary, the rarest event is a "1 in 1000 year event", with a 0.1% chance of occurring in a given year.

The y-axis shows the magnitude of the weather event in the form of a threshold. In this example, the y-axis shows the total rainfall per day that exceeded a certain threshold during monsoon season.

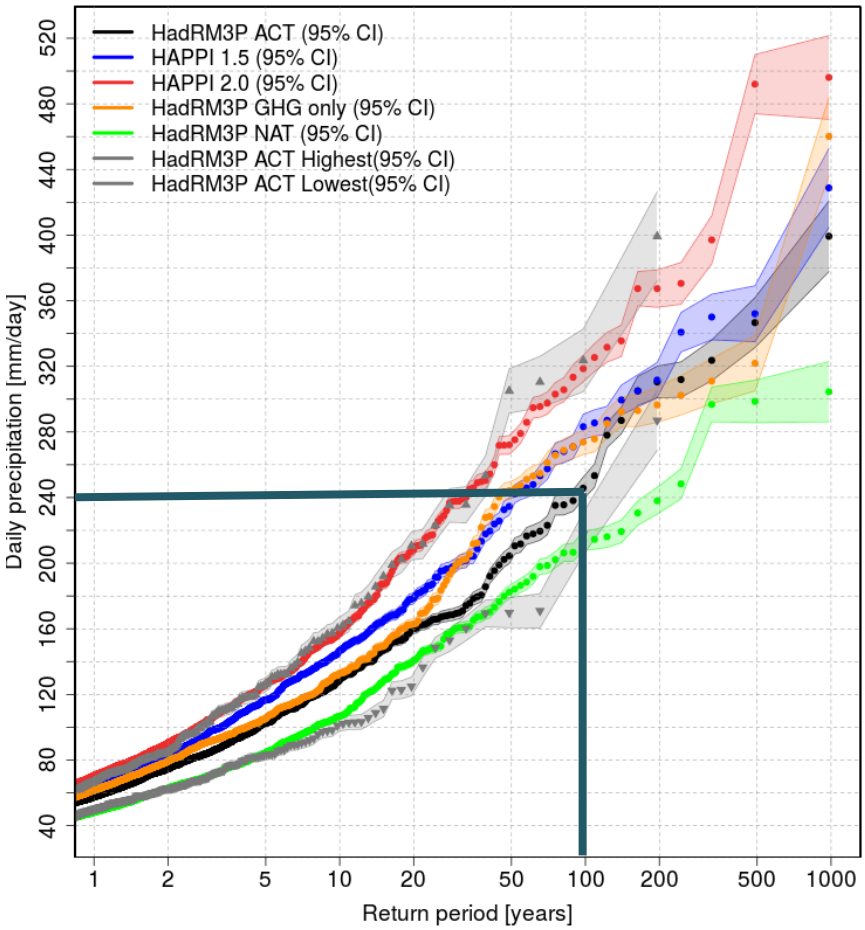


Figure 2.2: Return time plot for daily rainfall (mm/day) during monsoon season over north-east parts of Bangladesh.

For calculating the confidence intervals of the return periods of rainfall events, a bootstrapped distribution sample data from the original data is used. Specifically, for R=1000 times, the booted sample distributions of all rainfall values are ranked. Then the confidence intervals are calculated using quantile score, Z between -1.96 to +1.96, which is equivalent to 2 sigma standard deviations (giving the ~5th and ~95th percentile data). The estimated 95% CIs are shown in figure 2.2 by the light coloured shading for each ensemble data. This is how the uncertainty is estimated in the return times of extreme events in chapter 5 and 6 of this thesis.

For assessing the risks of seasonal extreme rainfall in Bangladesh, the changes in the risks of extreme seasonal rainfall under (i) factual present climate condition, (ii) counterfactual pre-industrial climate condition (without anthropogenic GHG emissions), (iii-iv) future 1.5°C and 2.0°C warmer than pre-industrial climate conditions, and (v) GHG-only climate condition without anthropogenic aerosols, are quantified. By the virtue of the very large RCM ensembles, the model simulated rainfall events can have return periods ranging from 1 to 1000 years thus allowing for examining very rare extreme events under the aforementioned five climate scenarios.

However, extreme events with up to 100 year return periods are given emphasis for adaptation and policy implications. In figure 2.2, five colours of dots represent individual model simulations under these five scenarios. The figure also shows two sub-sampled actual model ensembles in grey colour as an approximate measure of the response to natural SST variations. A summary of the model ensembles under different climate conditions that are used in this thesis are presented in table 2.3.

Table 2.3: A summary of the model ensembles under different climate conditions

model ensemble	members per year	Climate conditions used in the model ensembles
Actual Climatology (1986–2015)	200	Actual climatic conditions, using observed SST data from the Operational Sea Surface Temperature and Sea Ice Analysis (OSTIA) data set and present day atmospheric GHG and aerosol concentration.
Natural Climatology (1986–2015)	200	Natural climate condition, but here the modelled SST patterns of anthropogenic forcings are removed from the observed SSTs to simulate a counterfactual world.
GHG-only (1986–2015)	200	Current climatic conditions, but with anthropogenic aerosol concentrations reduced to pre-industrial levels to simulate a hypothetical climate, where impacts of aerosols are removed.
Actual (2017)	2500	Actual climatic condition forcing for 2017
Natural (2017)	5250	Natural climate condition forcing for 2017
HAPPI 1.5 (2091–2100)	98	representing 1.5°C warmer than pre-industrial (1861–1880) climatic conditions
HAPPI 2.0 (2091–2100)	98	representing 2.0°C warmer than pre-industrial (1861–1880) climatic conditions

3. Model's response to observed variations in sea surface temperature

3.1. Introduction

Later chapters of this thesis will use numerical modelling tools to address the question of how extreme weather, particularly rainfall, in Bangladesh may be responding to anthropogenic climate change. Attribution experiments as conducted here rely on prescribing in models changes in sea surface temperature (SST) that are thought to be due to human influence on climate, but because we have no direct observations of a world without human influence, validating these models is challenging.

This chapter explores the response of one of the models used in later chapters to two major natural modes of SST variability. These are not perfect proxies of the anthropogenic signal, so realistic simulation of the response to these natural modes does not guarantee a realistic response to anthropogenic forcing, but the opposite is true: an unrealistic response to internal modes of variability would reduce our confidence in the use of this model for attribution, so it is important to explore it.

The monsoon in South Asia is driven by the natural seasonal variation of incoming solar radiation (Wu et al., 2007; Xu et al., 2010). Strong pressure gradients between the land and ocean are produced as a consequence of different rates of surface heating, with the land heating up much more quickly than the ocean. Large-scale circulation patterns driven by these pressure gradients subsequently lead to the development of the monsoon (Li et al., 2016a). It is characterised by a prominent seasonal reversal of wind circulation, (Ramage, 1971) associated with seasonal changes in multiple meteorological variables including strong seasonal rainfall anomalies (Wang, 1994; Wang and Ding, 2008; Webster, 1987; Webster et al., 1998).

One of the earliest reported observed teleconnections in global climate studies recognized the relationship between El Niño Southern Oscillation (ENSO) and South Asian monsoon summer rainfall (G. T. Walker, 1925). ENSO is a significant source of inter-annual variability in the climate system and can trigger extreme hydro-climatological events, such as floods, droughts and intense cyclones (Agilan and Umamahesh, 2018).

In recent years, the scientific community has given more emphasis to exploring ENSO's influence on the large scale circulation in general, and weather and climate extremes in particular (e.g., Bothale and Katpatal, 2016; Geethalakshmi et al., 2009; Kenyon and Hegerl, 2010; Zhang et al., 2013, 2010). The influence of rising GHG levels on the frequency of the warm/cold phase of the ENSO cycle, known as the El Niño/La Niña events, has also been increasing (e.g., Cai *et al.*, 2014, 2015).

Figure 3.1 shows the NINO regions over Pacific Ocean which are used to monitor ENSO, with NINO3 and NINO3.4 typically used to identify El Niño and La Niña events. El Niño (La Niña) is the warm (cold) phase of ENSO, characterised by anomalously high (low) SSTs in the equatorial Pacific Ocean. The El Niño (La Niña) threshold is considered to be exceeded when the 3-month running mean of the SSTs in the Niño3.4 region (Rayner et al., 2003) are above(below) 0.5°C with respect to the climate mean state for five consecutive months.

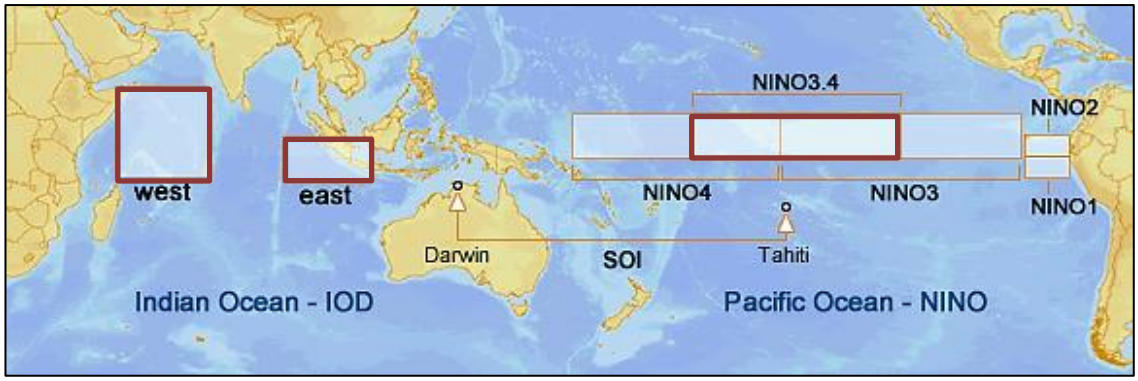


Figure 3.1: Schematic diagram showing the regions (in dark red coloured rectangles) used to monitor ENSO and IOD using SSTs in the Pacific and Indian Ocean, respectively. Image is adapted from http://www.bom.gov.au/climate/enso/indices/about.shtml.

Saji et al. (1999a) first described the Indian Ocean Dipole Mode Index (IODMI), another important mode of variability that impacts the South Asian region. The associated IOD events are defined as the SST anomaly difference between the tropical western Indian Ocean (50°E-70°E, 10°S-10°N) and the tropical south eastern Indian Ocean (90°E-110°E, 10°S-equator). The 'west' and 'east' dark red coloured rectangles in figure 3.1 indicate the locations of these regions in the Indian Ocean. A positive IOD event is associated with warmer waters than normal in the west and cooler waters in the east of the Indian Ocean basin (Huang et al., 2017).

A process-based model evaluation approach assesses how well the models can capture the physical processes that play important roles behind the generation of regional weather and climate (Creese and Washington, 2018; James et al., 2018). This chapter presents a process-based evaluation of the GCM/RCM outputs from the weather@home system by focusing on the model's ability to capture the South Asian monsoon system's key features such as the reversal of the surface wind regime between

winter and summer season; mean sea level pressure (MSLP) patterns; and the seasonal rainfall cycle.

The model's ability to capture the historical teleconnections between rainfall patterns and two climate modes of ENSO/IOD is assessed. A realistic response to SST anomalies is particularly important when applying these models to attribution and prediction studies that involve imposing an SST change.

3.2. Data and methods

3.2.1. Model and Observation Data

Daily climate variables of wind (both zonal (u) and meridional wind (v) components), MSLP and rainfall for the 30-year period 1986-2015 are used from the global and regional model driven with full forcings ("actual") and observed (OSTIA) SSTs. Rainfall outputs are taken directly from the RCM, whilst wind and MSLP are taken from the driving AGCM to investigate global teleconnections. GPCC monthly data is used for observed rainfall because this data is recommended for model evaluation at global and regional scales (Anja et al., 2018). ERA-Interim monthly reanalysis data (Dee et al., 2011) for wind and MSLP are used for comparison with the AGCM.

Both model and observational data are post-processed so that the outputs are comparable. For example, a bi-linear interpolation is performed to ensure the data has consistent grid resolution; and monthly mean statistics are analysed for each season. The two indices used in this chapter are the Niño3.4 index as an indicator for ENSO and the IODMI index to represent the IOD.

3.2.2. Methods

The climatological mean states of wind, MSLP, and rainfall (during 1986-2015) over South Asia are compared in the model and observations during winter (DJF) and summer (JJA) seasons. The pre- (MAM) and post-monsoon (SON) seasons are transitional periods and hence less suitable for a process based assessment with regard to the fundamental monsoon dynamics, which is why they are not shown here.

Given the uncertainty in the relationship between ENSO and IOD, this chapter explores the ENSO-IOD relationship using lagged correlations. Lag correlation is a simple and common analysis method in climate research that is used to gain insights into interaction mechanisms between climatological processes, in particular to assess time delays and to quantify the strength of a mechanism (Runge et al., 2014).

Rainfall patterns in South Asia region are correlated with both Niño3.4 (as the chosen ENSO index) and IOD, but ENSO and IOD are themselves also closely related to each other. An event-specific analysis performed for the pre-monsoon season in chapter 6 reveals that ENSO leads most IOD changes, particularly during strong El Niño events. The correlation between NINO3.4 during November to January and IOD during February and March is found to be significant at 95% confidence level, with 4 months' lead time.

In this chapter an extended analysis of the ENSO (IOD) relationship with rainfall anomalies aggregated over South Asia during all four seasons – winter (DJF), pre-monsoon (MAM), monsoon (JJA) and post-monsoon (SON) - is presented. This

extended analysis provides a broader understanding of the model's ability in capturing the teleconnections for different seasons over South Asia.

Pearson Correlation analysis is used to assess the association between ENSO (IOD) and seasonal rainfall anomalies. The correlation coefficient, r_{xy} for variables x and y with total n number of observations, is calculated as (Wilks, 2011):

$$r_{xy} = \frac{\frac{1}{n-1}\sum_{i=1}^{n}(x_i - \bar{x})(y_i - \bar{y})}{\sqrt{\frac{1}{n-1}\sum_{i=1}^{n}\left\{(x_i - \bar{x})^2 . \frac{1}{n-1}\sum_{i=1}^{n}(y_i - \bar{y})^2\right\}}}$$

The value of correlation coefficient, r_{xy} can range from -1 to +1. A value of r_{xy} = 0 corresponds to no linear relationship, but other nonlinear associations may exist. Values near 0 indicate weak correlations and values close to ±1 indicate strong correlations.

Correlation coefficients for each grid point of two fields over all time steps in a season are computed using this equation. One seasonal mean value is used for each season (DJF, MAM, JJA and SON) over 30 year (1986-2015) study period means, n=30 in both model and observation data. Because the model ensemble data consists of 200 members per year, at first correlation coefficients are computed for individual ensemble members and then the average of 200 correlation coefficients is used to compare with the observed correlation coefficient found in the respective season. Note that the average correlation coefficients calculated for the model data are therefore smaller than if they were calculated with the model ensemble means (not shown). The significance

of the correlation coefficients is assessed at 95% confidence levels using the two-tailed Student's t-test based on the following equation: $\boldsymbol{t = r_{xy}\sqrt{\frac{n-2}{1-r_{xy}^2}}}$

For n = 30, and r_{xy} = 0.4, the calculated t value is 2.3, which corresponds to p value of 0.029. Therefore, correlation coefficients that are greater than ±0.4 are statistically significant at approximately 95% confidence using the two-tailed Student's t-test.

These correlation coefficients and particularly significance levels are only indicative of the association between the two variables x and y and do not necessarily point toward causation. Significance levels in particular test again the null hypothesis of random, uncorrelated interannual variability. Clearly there is some lag-correlation, although lower from year to year than from month to month. The aim of this chapter is to assess the realism of relationships within the models used, so correlation coefficients represent a simple and transparent way of doing so, and the significance levels are only used to highlight potentially interesting relationships.

3.3. Results and discussion

3.3.1. South Asian monsoon system

Figure 3.2 and 3.3 shows a comparison between climatological mean modelled and observed wind, MSLP and rainfall averaged over the winter (DJF) and summer (JJA) seasons over South Asia. The change in the wind circulation regime that characterizes the South Asian monsoon system is adequately captured by the model as compared to the reanalysis (compare vectors in right and left column, figure 3.2).

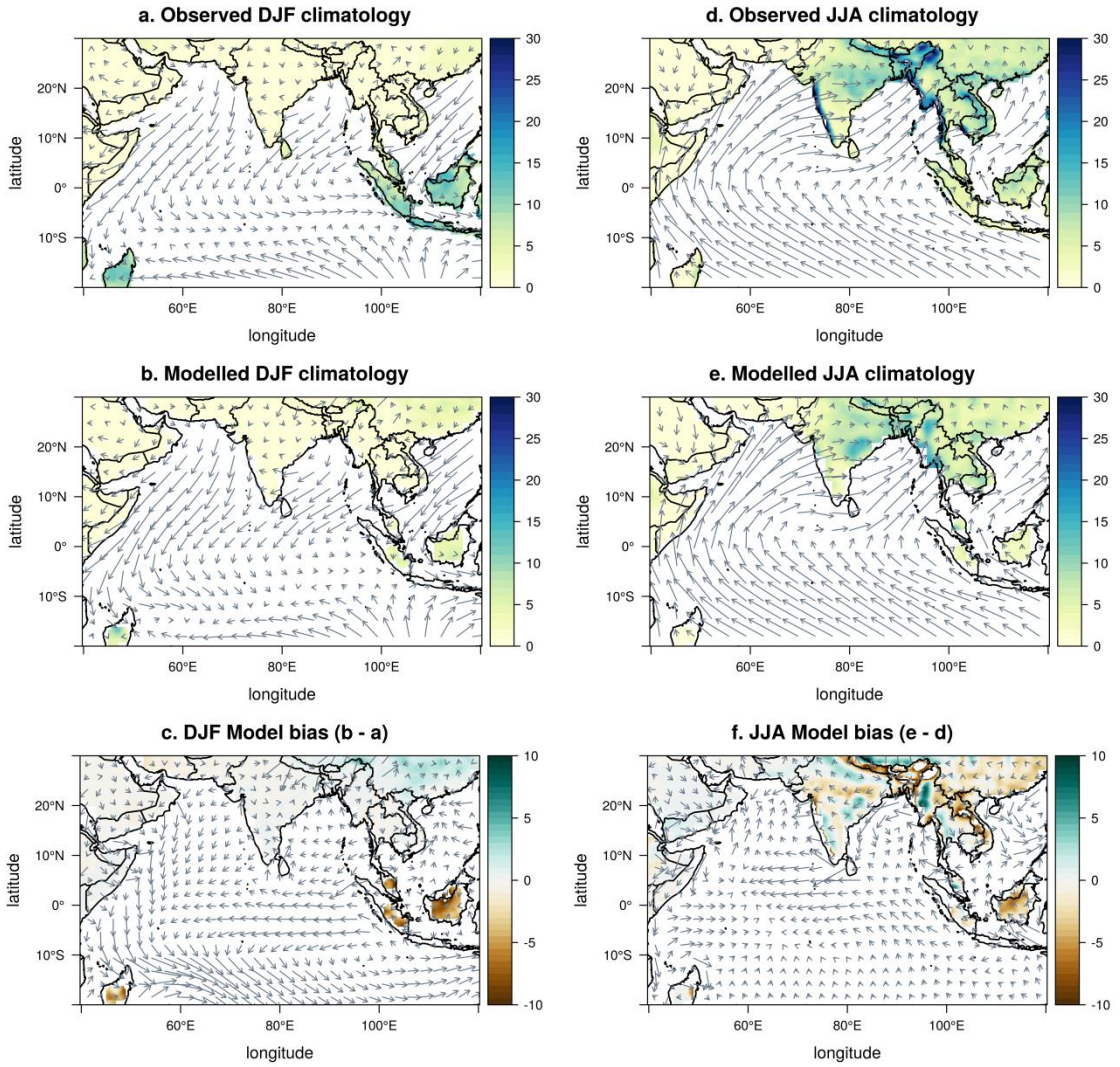


Figure 3.2: Winter (DJF, left column) and summer monsoon (JJA, right column) climatology of mean rainfall (mm/day) and 10 m wind are shown by the shading and vectors, respectively. The GCM outputs for wind and rainfall are compared with observations from GPCC and ERA-Interim (for rainfall and vector wind, respectively) datasets.

The model simulated mean winter rainfall pattern is representative of the observed dry season over most parts of South Asia, however there exists some dry biases over the south-east parts (figure 3.2, panel e). There is a noticeable dry bias in the monsoon mean rainfall, particularly over parts of India and Bangladesh (figure 3.2, panel f).

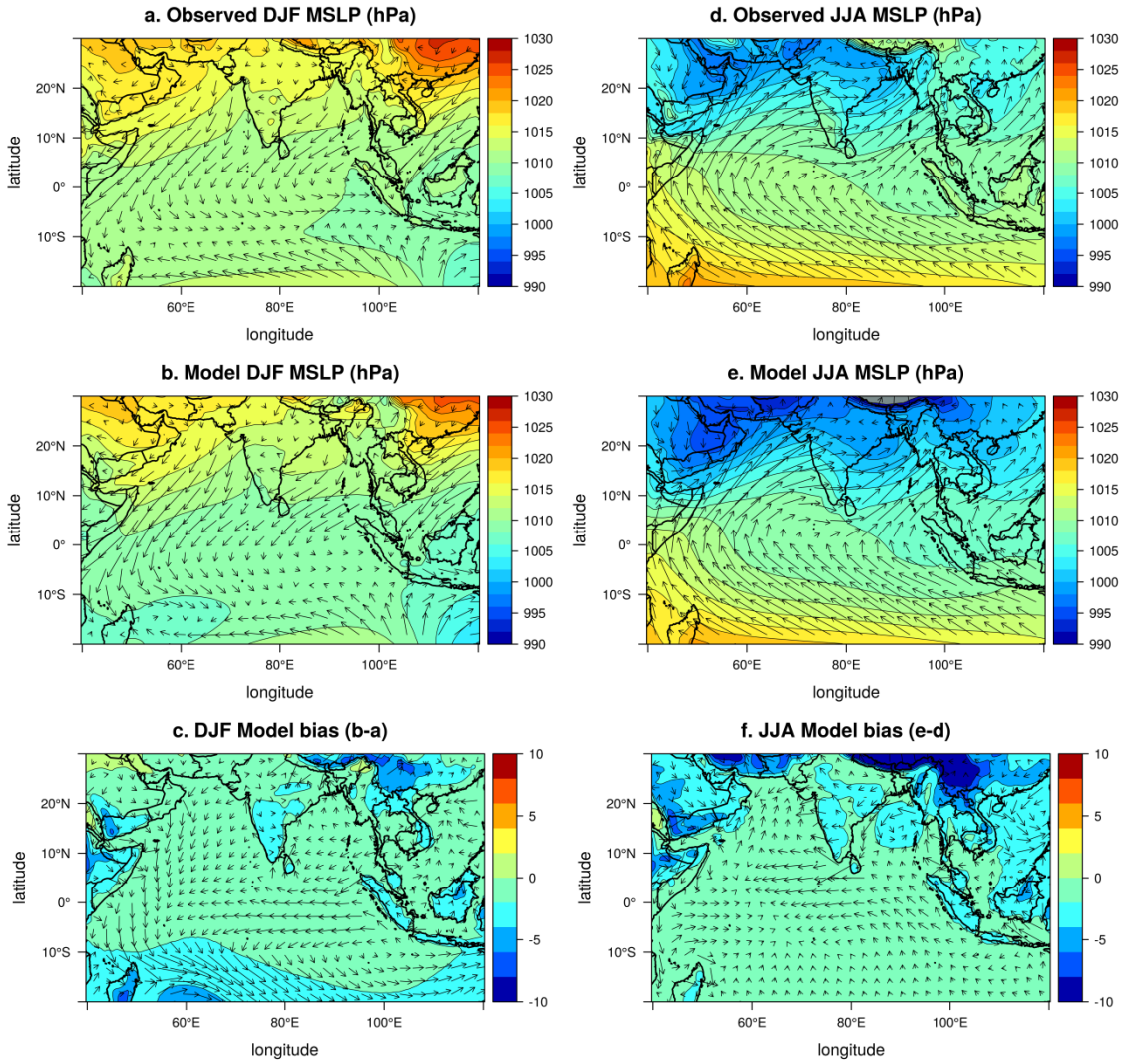


Figure 3.3: Winter (DJF, left column) and summer monsoon (JJA, right column) climatology of mean MSLP (hPa) and 10 m wind are shown by the shading and vectors, respectively. The GCM outputs for wind and MSLP are compared with observations from GPCC and ERA-Interim (for MSLP and vector wind, respectively) datasets.

A similar dry bias in the monsoon season is also reported in previous studies (e.g., Islam 2009; Macadam and Janes, 2017). Such a dry bias can potentially be caused by difficulties in simulating deep convective rainfall over areas of complex topography (Caesar et al., 2015).

The spatial pattern of model-simulated winter and summer MSLP (shading in figure 3.3) over the Indian Ocean is broadly similar to observations; however there are strong biases in summer at higher latitudes (figure 3.3, panel f), particularly near the Himalaya region. These MSLP biases at high latitudes are most likely to be linked to differences between interpolation methods used in the model and reanalysis to obtain MSLP based on the surface pressure values in high-altitude regions, and hence do not necessarily indicate a deficiency in the model itself.

3.3.2. ENSO and IOD relationship

Numerous studies have claimed that in the tropical Indian Ocean, the IOD represents an independent mode of climate variability (Meyers et al., 2007; Saji et al., 1999b; Saji and Yamagata, 2003b; Webster et al., 1999). However, during boreal autumn (September to November, SON), a positive correlation is observed between ENSO and IOD events, manifested by the co-occurrence of positive/negative IOD and El Niño/La Niña events respectively (Allan, R. J. et al., 2001; Annamalai et al., 2003; Baquero-Bernal et al., 2002; Xie et al., 2002; Zhang et al., 2015).

Variability of the IOD has been often partially attributed to ENSO (e.g., Baquero-Bernal et al., 2002; Dommenget and Latif, 2002; Lau and Yu, 2005; Li et al., 2003; Yang et al., 2015). However, it is also possible that IOD may modulate ENSO, as suggested by Lim and Hendon (2017). Their study claims to have shown that the weak La Niña of 2016 was caused by the strong negative IOD to some extent. The exceptionally long-lasting warm surface condition from the tail end of the strong El Niño of 2015–16 may have made this La Niña substantially weaker than it may have been otherwise (Lim and Hendon, 2017).

A large body of literature based on observational evidence and modelling results indicate that IOD is a relatively weak natural mode, which can be excited by external forcings (Li et al., 2003; Schott et al., 2009; Zhang et al., 2015).

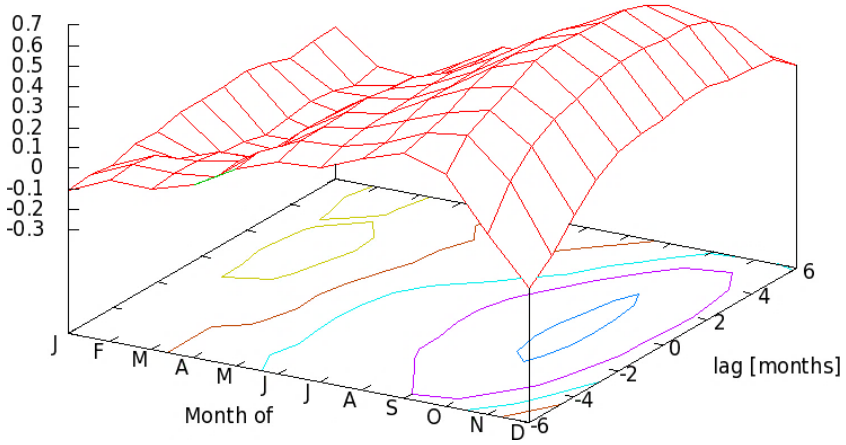


Figure 3.4: Lagged correlations (by +6 to -6 months) between IOD and Niño3.4 indices with de-trended data for all months (Jan-Dec) during 1870-2018. Month indicates month of the year for the IOD index, while positive lags correspond to ENSO leading IOD, negative lags to ENSO lagging IOD. Correlation magnitudes are shown in red colour, while the strengths of correlations (from weakest to strongest) are indicated by the coloured contours. Where, purple is used for the strongest correlations and yellow for the weakest. Note that high correlations are only observed with SON IOD. Purple and dark blue contours correspond to correlations greater than 0.3 and 0.2, respectively.

A simple lag-lead correlation analysis is performed to visualise the relationship between Niño3.4 and IOD prior to using these modes for model validation. Based on de-trended long-term IOD and Niño3.4 data (1870-2018) for all 12 months (Jan-Dec), the correlation patterns with +6 to -6 months' lag demonstrate a strongest correlation during SON with a negative lag of one month, indicating that ENSO is likely the causal factor for the respective IOD phase (purple contour line in figure 3.2): this is also the season of strongest IOD variability.

This indicates a strong effect of seasonality on the relationship between IOD and Niño3.4. Given the atmosphere-only setup of the weather@home model, the relationship is exactly the same in the model simulations by construction.

3.3.3. ENSO and IOD influence on rainfall

Given the large year-to-year variability of the strength of the monsoon cycle, it is important to understand variations due to stochastic weather variability and the influence of ENSO (IOD) related teleconnections in the model and the real world.

Figure 3.5 demonstrates that the observed summer monsoon (JJA) rainfall anomalies have significant negative correlations with NINO3.4 (correlation coefficient, r = 0.4, with p value = 0.029) over some parts of India (figure 3.5, orange shades in panel a). The spatial distributions of correlation coefficients in the model differ from the observed distributions. The significant positive correlations (correlation coefficient, r=0.5, with p value=0.004) for SON rainfall anomalies are captured by the model over the south-east parts of Indonesia but not adequately over India (compare panel c & d).

During the winter season (DJF), the north and west regions exhibit significant positive correlations in the observations. However, only the correlations at the northern region are captured in the model (compare panel e & f). The strengths of observed association between NINO3.4 and MAM rainfall anomalies are mostly underestimated by the model (compare panel g & h).

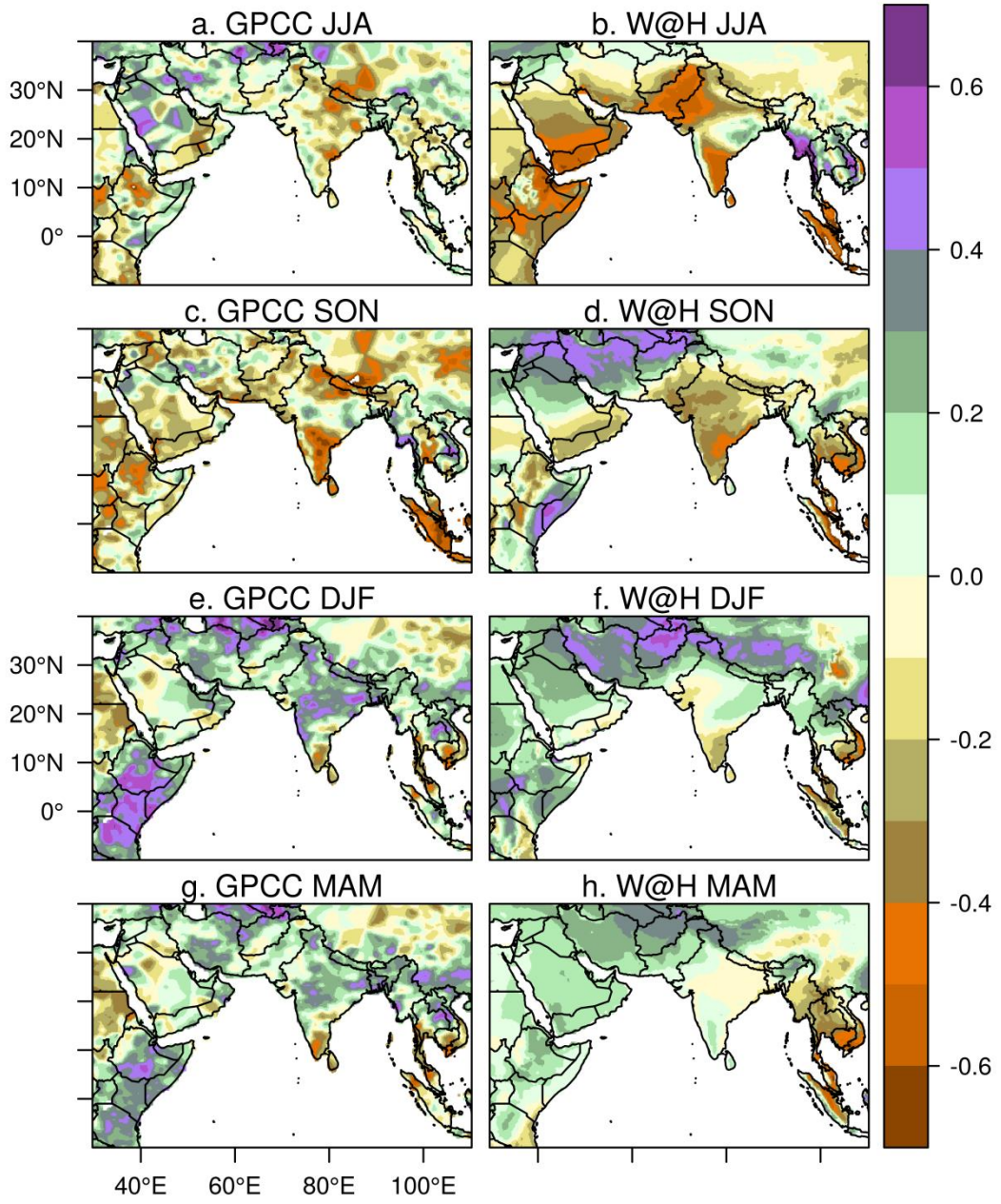


Figure 3.5: Spatial distributions of correlation coefficients for the relationship between NINO3.4 and rainfall anomalies in observation (in right column) and model (in left column) in JJA, SON, DJF, and MAM (from top to bottom rows, respectively) during 1986-2015. The purple and orange shades (shading differs by 0.1) indicate statistically significant correlation coefficients (r>0.4) at 95% confidence level. The non-significant correlation coefficients are shown in olive green and brown shades.

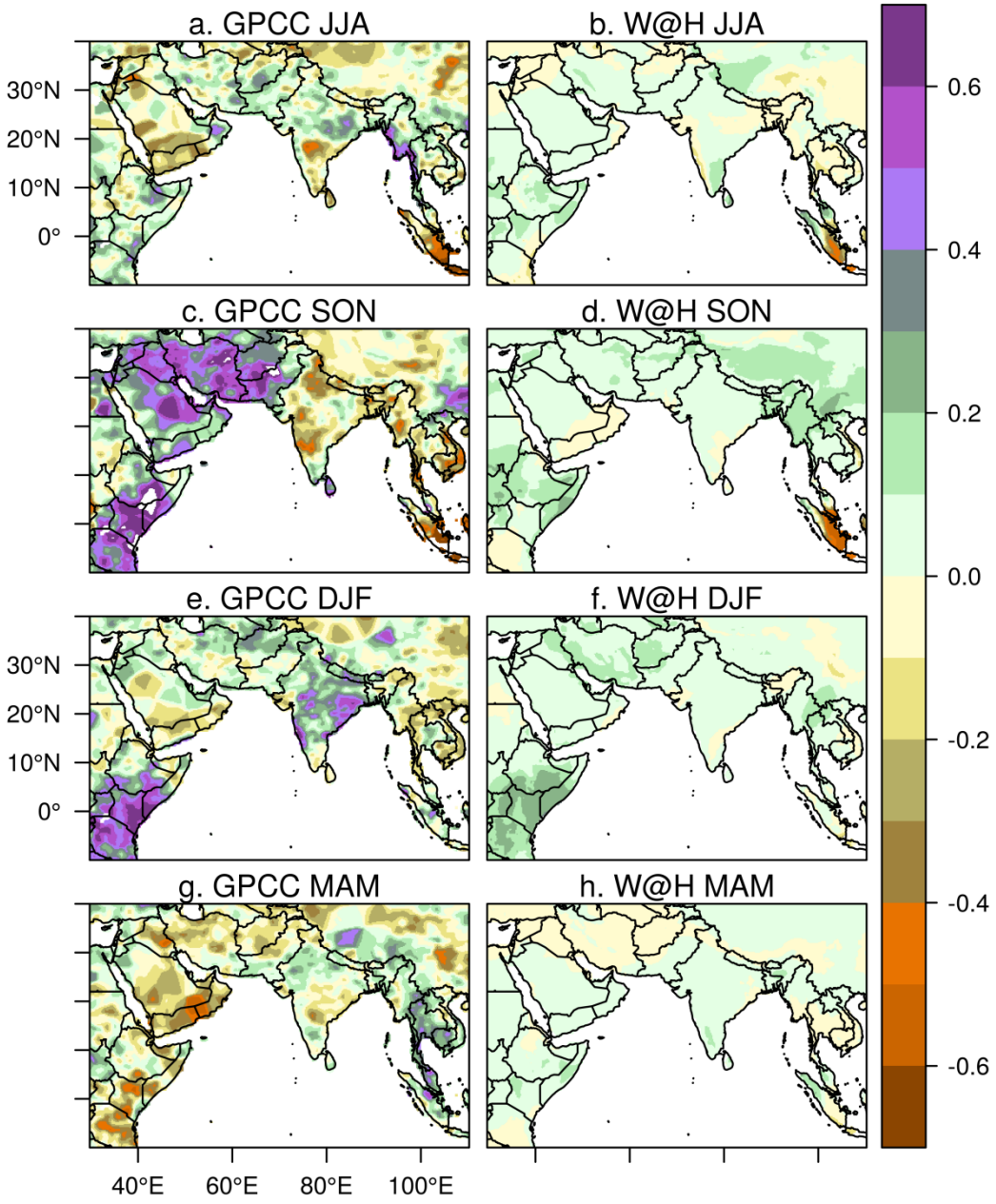


Figure 3.6: Spatial distributions of correlation coefficients for the relationship between IOD and rainfall anomalies in observation (in right column) and model (in left column) in JJA, SON, DJF, and MAM (from top to bottom rows, respectively) during 1986-2015. The purple and orange shades (shading differs by 0.1) indicate statistically significant correlation coefficients (r>0.4) at 95% confidence level. The non-significant correlation coefficients are shown in olive green and brown shades.

Overall, the model reasonably captures the associations (correlation coefficient, r<0.4, shown in olive green shades) between NINO3.4 and rainfall anomalies over Bangladesh and surrounding areas in all four seasons. However, these associations are not statistically significant (at p-value of 0.05).

Figure 3.6 shows the associations between IOD and seasonal rainfall anomalies. The model performs well in capturing the significant negative relationship between JJA (figure 3.6, panel a, b) and SON (figure 3.6, panel c, d) rainfall anomalies over Indonesia. But over the western parts of South Asia region, the model fails to capture any of the significant positive correlations found in the observed SON rainfall anomalies. The noisiness of these patterns of correlation in the observations suggests, however, that some of these apparently significant positive correlations may have occurred by chance. In the model, correlation patterns are averaged over a large ensemble, giving a much smoother pattern and lower absolute correlations overall.

Over most parts of Bangladesh and India, a weak positive relationship is found for SON rainfall anomalies, which is different from the observed relationship (figure 3.6, panel c & d). Although the sign of the correlations during DJF and MAM agree between observation and model (figure 3.6, panels e-h), none of these correlations over Bangladesh are statistically significant.

3.4. Conclusions

The process-based model evaluation presented in this chapter suggests that the model performs adequately well in capturing the key features of the mean state of the monsoon climate in winter and summer. The reversal of wind circulation patterns between winter and summer and the MSLP gradients over the ocean that drive the monsoon system are satisfactorily simulated by the model.

The spatial distributions of the correlation coefficients for seasonal mean rainfall anomalies and NINO3.4 over South Asia region indicate that most of these correlations are not statistically significant in either the observations or the climate model. Based on CAM5, MIROC5 and ACCESS1.3 model simulations, for extreme rainfall (95^{th} percentile) events, Dittus *et al.*, (2018) also found that the NINO3.4 and rainfall correlations are not significant over south Asia region and the pattern correlation on a global scale, vary from 0.21 to 0.30.

It is important to consider that the model's response to observed modes of SST variability such as ENSO and IOD is variable as a function of different season and region of South Asia, when compared to corresponding observed responses. Although the relationship between ENSO/IOD and seasonal rainfall anomaly over Bangladesh is not statistically significant, that does not imply that the model is not capable of simulating the regional scale response to SST anomalies.

Finding a less confidence in the association, as a result of statistical testing cannot certainly deduce that there is absolutely no causal link. The significant correlations,

those agree in the model and observation for NINO3.4 and rainfall indicate that the model has capability of responding to SST variability by showing representative ENSO influence on rainfall anomalies. The pattern of SST change has little impact on climate change over the extra-tropics and land (He et al., 2014; He and Soden, 2016). In contrast, the change in SST pattern over tropical oceans has a large climate impact and drives changes in rainfall and atmospheric circulation (He and Soden, 2016; Ma et al., 2012; Xie et al., 2010; Zheng et al., 2010).

This chapter evaluates the model for its response to observed SST variability modes of ENSO and IOD and finds that the model better simulates the relationship between seasonal rainfall anomalies and NINO3.4 than that with IOD. Such model performance is anticipated given that ENSO is the dominant driver of SST variability in the Indian Ocean, explaining 37% of the variability in the Indian Ocean SST anomalies, while IOD explains only 12% SST variability (Saji *et al.*, 1999). Equally, shorter-term Madden-Julian Oscillation (MJO) variability may play a major role in modulating the IOD phase (Zhang, 2013).

A more thorough investigation of the physical mechanisms behind these relationships is necessary in order to fully understand the teleconnections and to draw more robust conclusions. While the findings of this chapter have not revealed any fundamental obstacles to applying this model to simulating the rainfall response to SST anomalies in attribution and prediction studies, the comparison of model with observed relationships with IOD variability in particular give reason for caution in interpreting model-simulated responses to the patterns of anthropogenic climate change.

4. Evaluation of a large ensemble regional climate modelling system for extreme weather events analysis over Bangladesh

Evaluation of a large ensemble regional climate modelling system for extreme weather events analysis over Bangladesh

RUKSANA H. RIMI[1], KARSTEN HAUSTEIN[1], EMILY J. BARBOUR[1], RICHARD G. JONES[1,2], SARAH N. SPARROW[3] AND MYLES R. ALLEN[1]

[1]Environmental Change Institute, School of Geography and the Environment, University of Oxford, Oxford, OX1 3QY, UK.

[2]Met Office Hadley Centre, Exeter, UK.

[3]Oxford e-Research Centre, University of Oxford, Oxford, UK.

Submitted to *International Journal of Climatology (IJC)* 02 March, 2018

Accepted 14 November 2018, Published 18 March, 2019

Available at https://doi.org/10.1002/joc.5931

Authorship Declaration

I, Ruksana H. Rimi, hereby declare that I conducted all of the analyses and writing for this paper with advice from Myles R. Allen, Karsten Haustein and Emily Barbour. The manuscript was finalized with edits from all co-authors including Richard G. Jones and Sarah N. sparrow.

Abstract

Potential increases in the risk of extreme weather events under climate change can have significant socio-economic impacts at regional levels. These impacts are likely to be particularly high in South Asia where Bangladesh is one of the most vulnerable countries. Regional climate models (RCMs) are valuable tools for studying weather and climate at finer spatial scales than are typically available in global climate models. Quantitative assessment of the likely changes in the risk of extreme events occurring requires very large ensemble simulations due to their rarity. The weather@home setup within the climateprediction.net distributed computing project is capable of providing the necessary very large ensembles at regionally higher resolution, but has only been evaluated over the South Asia region for its representation of seasonal climatological and monthly means. Here, we evaluate how realistically the HadAM3P-HadRM3P model setup of weather@home can reproduce the observed patterns of temperature and rainfall in Bangladesh with focus on the modelled extreme events. Using very large ensembles of regional simulations, we find that there are substantial spatial and temporal variations in rainfall and temperature biases compared with observations. These are highest in the pre-monsoon, which are largely caused by timing issues in the model. Modelled mean monsoon and post-monsoon temperatures are in good agreement with observations, whereas there is a dry bias in the modelled mean monsoon rainfall. The rainfall bias varies both spatially and with the data set used for comparison. Despite of these biases, the model-simulated temperature and rainfall extremes in summer monsoon over Bangladesh are approximately representative of the observed ones. At the wettest parts of northeast Bangladesh, rainfall extremes are underestimated compared to GPCC and APHRODITE but are within the range of CPC

observations. Therefore, the weather@home RCM, HadRM3P may provide a sufficiently reliable tool for studying the extreme weather events in Bangladesh.

Key words: Bangladesh, climate change, extreme weather events, model evaluation, regional climate model.

4.1. Introduction

For the public, scientists and policy makers, extreme weather events are of great concern and interest due to their impact on the environment, economy and society. Whenever an extreme event occurs, a commonly asked question is to what extent human-induced climate change has played a role (Otto, 2017), information that can help motivate action to adapt or to build resilience in impacted systems.

Using Probabilistic Event Attribution (PEA; Allen, 2003), climate scientists are progressively able to provide robust quantitative answers to this question. However, the geographical coverage of events that are attributed is not uniform (Stott et al., 2016). To date, most of the PEA studies have focused on extreme weather events of mid-latitudes and predominantly events that have occurred in developed countries (Black and Karoly, 2016; Otto et al., 2012, 2015b; Pall et al., 2011a; Schaller et al., 2016; Stott et al., 2004b). A few studies have been performed for tropical regions and developing countries (Marthews et al., 2015; Otto et al., 2015c), though there is significant scope to focus more of this work in these countries because they are highly susceptible to extreme weather events, and have least capacity to adapt with the consequent impacts (IPCC, 2013c).

Bangladesh, a subtropical developing country, and one of the most climate vulnerable nations in the world, is of relevance for examining extreme weather events. It is exposed to damaging storms, rainfall extremes and sea level rise from its unique geographical location, and flat and low-lying topography. It has a high population density (Dasgupta et al., 2011) and an agrarian economy with limited capacity to address impacts of climate change (IPCC, 2013c).

Bangladesh is already experiencing temperature extremes, erratic seasonal rainfall (Rahman and Lateh, 2017) and more frequent events of intense floods (Thiele-Eich et al., 2015) and droughts (Habiba and Shaw, 2013). Increased occurrences of extreme weather events has led to the question of whether and to what extent changes in frequency and/or magnitude of such extreme events are attributable to anthropogenic drivers of climate change. While, this paper does not attempt to answer these questions but establishes the credibility of the very large ensemble regional modelling experiment, weather@home, to be used for such attribution analyses.

Using large ensemble simulations for extreme event attribution can only generate credible results if the model used is fit for purpose. As climate change is likely to modify the probability of occurrence of extreme weather events (IPCC, 2013c; National Academies of Sciences, Engineering, 2016), we need to evaluate how well the existing climate models perform in replicating such events. The model configuration used in the weather@home system has been evaluated and successfully used for attribution studies over Europe (Guillod et al., 2017; Massey et al., 2015), the western United States (Li et al., 2015; Mote et al., 2016), Africa (Marthews et al., 2015) and Australia and New Zealand (Black et al., 2016; Black and Karoly, 2016).

In this paper, we evaluate weather@home model set up for a new study area of Bangladesh, which is part of the wider 50 km South Asia regional model domain (hereinafter referred to as SAS50). This study also enables us to evaluate the model-simulated extreme events in the complex tropical monsoon system where, unique atmosphere–land–ocean interactions largely determine the weather features.

We draw on the availability of a large ensemble of 50-km horizontal resolution RCM simulations, which provide sample sizes of realistic weather events sufficient to estimate the occurrence of a rare event with high statistical confidence (Guillod et al., 2017; Otto et al., 2013). This evaluation assesses model bias, with a focus on short-term extreme events thereby informing on the applicability of this model setup to study high impact weather in Bangladesh.

The following sections describe the model evaluation domain and subregions (section 2); the observation data sets, the model data and evaluation process (section 3); the results of model evaluation (section 4); and the main conclusions (section 5).

4.2. The study region and subregions

The model evaluation domain extends from 86°E to 96°E and 17°N to 27°N (Figure 4.1, right) covering Bangladesh with some of the surrounding areas. We refer to this model evaluation domain as “study region” in the rest of the paper. We also use four subregions (shown by boxes 1–4 in right panel of Figure 4.1) within Bangladesh to investigate smaller-scale local weather features.

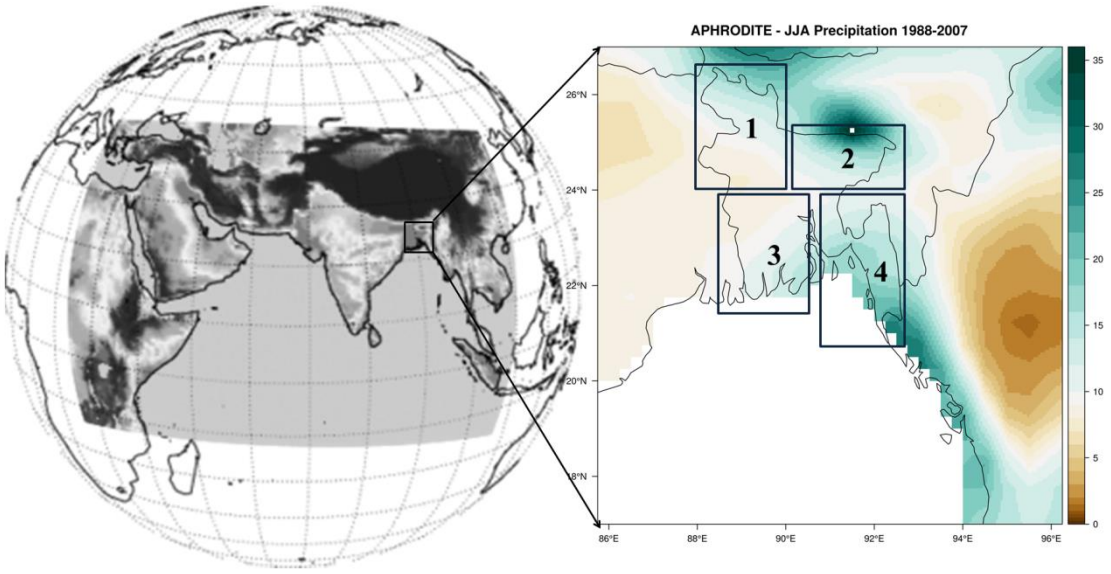


Figure 4.1: The SAS50 domain of HadRM3P model uses the CORDEX region South Asia, which covers from north to south: The Himalayas as well as Lake Victoria; India; Bangladesh; the Bay of Bengal; and the surrounding ocean in the centre of the region and in west–east direction it ranges from the Horn of Africa and the Arabian Peninsula to Vietnam and Cambodia (left panel, CPDN, 2017). Here, the left panel shows the physical features with darker shades on land area indicating high lands or mountains and lighter shades indicating the plains or low lands. The right panel shows the model evaluation domain with longitudes and latitudes ranging from 86°E to 96°E and 17°N to 27°N, respectively. The observed mean rainfall (in mm/day; from APHRODITE data set) of monsoon season is shown. The four subregional model evaluations are performed over the four areas of boxes (1–4) shown in the right panel within Bangladesh.

The four subregions consist of: subregion 1: 88°–90°E, 24°–26°N covering northwest parts; subregion 2: 90.5°–92.5°E, 24°–25.5°N covering the northeast parts; subregion 3: 89°–91°E, 21.5°–23.5°N covering the southwest and subregion 4: 91°–93°E, 20.5°–24°N covering southeast parts of the country. These four subregions reflect large spatial variability in both observed temperature and rainfall(Syed and Al Amin, 2016). For instance, the eastern parts of Bangladesh at subregions 2 and 4 receive considerably more annual average rainfall (3,000–6,400 mm) than the western parts at subregions 1 and 3 (1,500–2,500 mm) (BARC, 2014).

The highest annual average rainfall of 6,400 mm occurs at Sylhet (Ahmed, 2012), which is in subregion 2. These spatial differences require the evaluation of the model's performance over each of the specified subregions to have confidence in the model-simulated local-scale weather events. Both northern subregions of 1 and 2 are likely to be influenced by the orographic effects coming from the Himalayan Foothills and Meghalaya Hill ranges. While both southern subregions of 3 and 4 are located near the coasts of the Bay of Bengal and are likely to be influenced by the land-sea interactions.

4.3. Data and methods for model evaluation

We primarily focus on the evaluation of the distributions of daily and 5-day mean values because extreme weather events within this temporal range are a major cause of climate impacts within the study region. The model and observational data are processed in a way so that both data sets have the same temporal and spatial characteristics. We use bilinear interpolation method to re-grid all data and then use area-averaged daily and 5-day rainfall and temperature data over the study region and each of the subregions of Bangladesh to evaluate model's performance against the observations.

4.3.1. Observational data sets

The reference data sets of observation from Asian Precipitation Highly Resolved Observational Data Integration Towards Evaluation of Water Resources (APHRODITE), Climate Prediction Centre (CPC), Global Rainfall Climatology Centre (GPCC) and The Tropical Rainfall Measuring Mission (TRMM) are used to evaluate

the RCM. Table S1, Supporting Information briefly presents some basic information about these data sets.

APHRODITE is the only long-term continental-scale daily product (1951–2007) that provides gridded temperature and rainfall data at high spatial resolution for Asia including the Himalayas, South and Southeast Asia. This data set is useful for improved evaluation of daily series of model outputs and for statistical analysis of extreme weather (Yatagai et al., 2012).

GPCC provides daily global land surface rainfall data based on observations provided by national meteorological and hydrological services, global and regional data collections as well as WMO GTS data. This product contains the daily totals on a regular grid with a spatial resolution of 1.0 × 1.0°. Relative rainfall anomalies at the stations are interpolated by means of ordinary block kriging and then superimposed on the GPCC Full Data Reanalysis V7. This GPCC product is recommended to be used when the daily rainfall information is of highest importance, for example, for analyses of extreme events and related statistics at daily resolution (Schamm et al., 2015).

TRMM, a joint mission of National Aeronautics and Space Administration (NASA) and the Japan Aerospace Exploration Agency, was operational from 1997 to 2015 to study rainfall in the tropical and subtropical regions for weather and climate research. TRMM rainfall measurements have made critical inputs to tropical cyclone forecasting, numerical weather prediction and rainfall climatology (Huffman et al., 2007).

CPC Unified Gauge based Analysis is a global daily rainfall data set that is constructed through from over 30,000 global land rainfall gauge stations. This CPC data set consists of daily rainfall fields from 1979 to present, uses optimal interpolation with orographic consideration and has a resolution of 0.5° over global land (Chen and Xie, 2008).

APHRODITE is only available until 2007, so the model evaluation period presented here is 1988–2007. To evaluate the model's performance beyond 2007, we compare the model simulated rainfall statistics with the observations from CPC, GPCC (ends in 2013) and TRMM (starts only in 1998) satellite data. Hence, the evaluation period for these data sets is 1998–2013. For brevity, model evaluation results for this period (1998-2013) are presented at the supporting information.

4.3.2. Model data

The weather@home system uses the Met Office Hadley Centre's RCM, HadRM3P, nested in the global atmosphere-only model HadAM3P (Guillod et al., 2017; Massey et al., 2015). This study uses an updated version of weather@home (weather@home 2), which includes a more recent land surface scheme, the Met Office Surface Exchange Scheme (MOSES 2; Essery and Clark, 2003), providing an improved physical representation of the land surface compared with the previous version (Guillod et al., 2017).

We denote the "weather@home 2" system as "weather@home" in the rest of this paper. Description of this HadAM3P-HadRM3P model setup of the weather@home system is presented in Supporting Information. Actual climate model scenarios are

simulated by driving the model with observed sea surface temperatures (SSTs), sea ice from Operational Sea Surface Temperature and Sea Ice Analysis (OSTIA; Donlon *et al.*, 2012) and present-day atmospheric compositions.

We use weather@home regional model domain of SAS50 to simulate 30 years (1986–2015) climatology period with 200 plausible realizations with initial condition perturbations for each day of the year. The model has a 360-day calendar and our model evaluation period is mainly 20 years (1988–2007). Therefore, we use (360 × 20 × 200)/4 = 360,000 model-simulated daily plausible values per season.

Such large sample size allows us to sample an acceptable range of model-simulated physically plausible climate conditions and hence the tails of the distribution can be resolved with higher confidence. Using this large model data set, we can closely look at the "tail" of a distribution where, the extreme events lie and can quantitatively assess the model bias compared to the observed weather events at a specific season for a particular threshold for the extreme event.

4.3.3. Extreme events

To investigate the fidelity of the model to capture the frequency of extreme weather events further, block maxima of 5-day means of temperature and rainfall are fitted to a generalized extreme value (GEV) distribution. This is performed by first dividing the data into seasonal blocks (i.e., 90 days) of equal length (i.e., monsoon, pre- or post-monsoon season under observed or model-simulated climate conditions).

GEV distributions of the form shown in Equation (1) (Coles et al., 2001) are then fitted to a sample of maximum temperatures and rainfall events (z) for each season for each area-averaged region,

$$G(z) = \exp\left(-\left[1 + \xi\frac{z-\mu}{\sigma}\right]^{-\left(\frac{1}{\xi}\right)}\right) \qquad (3.1)$$

Here G is a nondegenerate distribution function; μ, σ and ξ denote the location, scale and shape parameter of the GEV distribution, respectively.

The GEV parameter estimation is performed using the L-moment method, which is conducted using the "extRemes" software package (Gilleland and Katz, 2011). L-moments are defined as linear combinations of expected values of order statistics of a variable and are estimated from samples using functions of weighted means of order statistics.

The L-moments method has several advantages over classical moments. It can characterize a wider range of distributions, is more robust to the presence of outliers in the data when estimated from a sample and is less subject to bias in estimation and approximates its asymptotic normal distribution more closely (Hosking, 1990). In the return time plots, we also include the 95% confidence intervals (CI) for the observations by using a parametric bootstrap (Gilleland and Katz, 2011).

4.4. Results and discussion

In the following sections, we present the model evaluation results for (a) spatial variation of the seasonal mean temperature and rainfall, (b) annual cycles of daily temperature and rainfall, (c) distributions of the quantiles of the daily (5-day mean) values, and finally (d) return periods of seasonal 5-day maximum temperature and rainfall. MAM (March–April–May), JJA (June–July–August) and SON (September–October–November) represent the pre-monsoon, monsoon and post-monsoon season, whereas DJF (December–January–February) represents the dry (winter) season.

4.4.1. Spatial variations in seasonal means

Figure 4.2 illustrates the spatial variation of seasonal mean surface temperature (a) and rainfall (b) during monsoon (JJA), post-monsoon (SON), winter (DJF) and pre-monsoon (MAM) over the period of 1988–2007 according to the APHRODITE data set. The observed patterns of seasonal mean temperature and rainfall from Figure 4.2 indicate that both pre-monsoon and monsoon seasons are the hottest time of the year, with average daily temperatures reaching >30°C. Temperatures gradually decrease during post-monsoon and become 19–27°C and then drop to ~12°C in winter. Mean rainfall during monsoon season reaches >35 mm/day, on the contrary, the driest conditions prevail during winter with minimal recorded rainfall (<1 mm/day).

Model biases for temperature and rainfall relative to the observations (in Figure 4.2a, b) are shown in Figure 4.2c, d, respectively. The maximum warm bias (up to +3.5°C) occurs in the pre-monsoon season (MAM) whereas, the maximum cold bias (up to −3.5°C) occurs during winter (DJF) in Bangladesh. The warm bias is relatively lower

over the eastern parts of Bangladesh (0.5–2.0°C). The lowest temperature bias occurs during the monsoon (JJA) season with only ~1°C warm and cold bias at the eastern and western parts of the country.

The model bias maps for seasonal mean rainfall presented in Figure 4.2d show a predominantly dry bias over Bangladesh during the wet seasons (JJA and SON), following a wet bias in the pre-monsoon season (MAM) with the model producing an early arrival of the monsoon. This dry bias during monsoon season is also present in other RCMs (e.g., Islam, 2009; Macadam and Janes, 2017), and is likely to be caused by difficulties in simulating deep convective rainfall over orographic terrain (Caesar et al., 2015).

The maximum dry bias occurs during the height of the monsoon, with up to −10 mm/day over eastern Bangladesh, and up to −16 mm/day in the northeast parts as far as APHRODITE observation data is concerned. It is worth mentioning that the northeast parts of the study region includes the top two wettest places on earth, Mawsynram (25.30°N, 91.58°E; 2,000 m above sea level) and Cherrapunji (25.30°N, 91.70°E; 1,484 m above sea level), with a yearly rainfall average of 11,873 and 11,777 mm, respectively (Sawe, 2017).

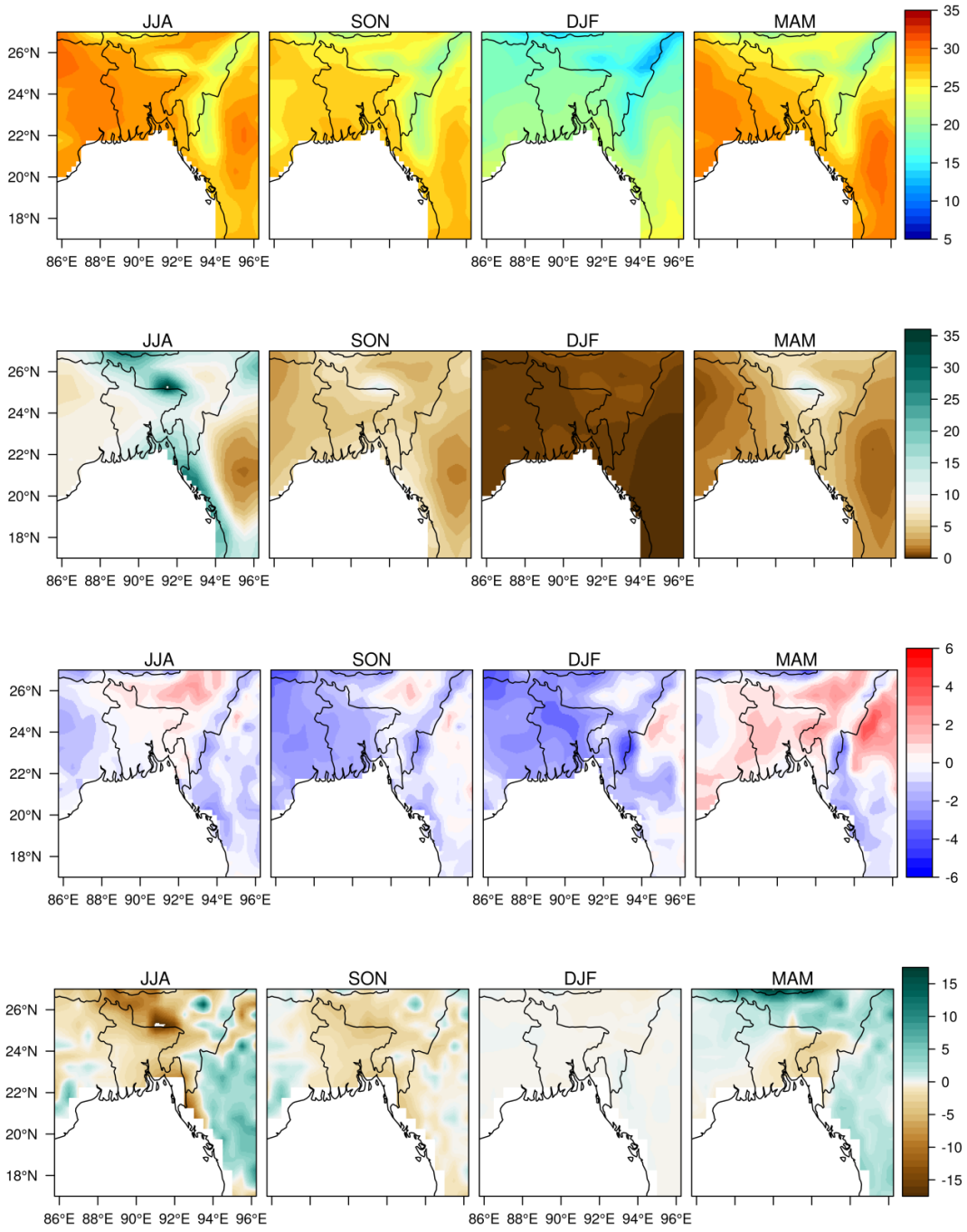


Figure 4.2: Spatial distributions of (a) mean daily surface temperature (°C), (b) rainfall (mm/day) in the APHRODITE observation data set; (c) mean daily surface temperature (°C) bias and (d) rainfall (mm/day) bias (model minus observation) over the study region in monsoon (JJA), post-monsoon (SON), winter (DJF) and pre-monsoon (MAM) season during 1988–2007. The coldest and driest season is winter (DJF), hottest seasons are both pre-monsoon and monsoon (MAM and JJA) and the wettest season is the monsoon (JJA). The highest warm and wet bias (in the north and east parts of the study region) is found in MAM, whereas, JJA has the highest dry bias with respect to APHRODITE observations.

During the pre-monsoon season, the wet bias is up to 16 mm/day caused by an overly aggressive convective signal in the model due to the high pre-monsoon temperatures. Histograms of seasonal temperature and rainfall distributions for HadRM3P and APHRODITE (and GPCC) are shown in Figures S4.1 and S4.2.

4.4.2. Annual cycle

Figure 4.3 compares the model-simulated annual cycle of climatological mean daily temperature (top panel), and rainfall (middle panel) with reference observational data sets over the study region during 1988–2007. The bottom panel of Figure 4.3 also shows the climatological mean annual cycle of daily rainfall but for the more recent years of 1998–2013 and in this case model-simulated rainfall is compared with TRMM satellite data instead of APHRODITE. The RCM represents the daily mean temperature best during June–October (top panel of Figure 4.3).

There are warm biases (up to +2°C) during Mar–May and cold biases (up to −2°C) during November–January. Both Islam et al. (2008) and Caesar et al. (2015) reported similar patterns of temperature biases in the monthly mean temperatures based on the HadRM3P model outputs. While Fahad et al. (2017) used 11 RCMs of the Fifth Phase Coupled Model Inter-comparison Project (CMIP5) and found extended warm biases (March–October) in the annual cycle of monthly mean temperatures over Bangladesh. According to the middle and bottom panel of Figure 4.3, the mean daily rainfall based on the three observational data sets of APHRODITE, GPCC, and TRMM (indicated by red, blue, and sky blue solid lines) are mostly within the 10–90th percentiles (indicated by the grey shaded polygon) of the model simulated rainfall throughout the year.

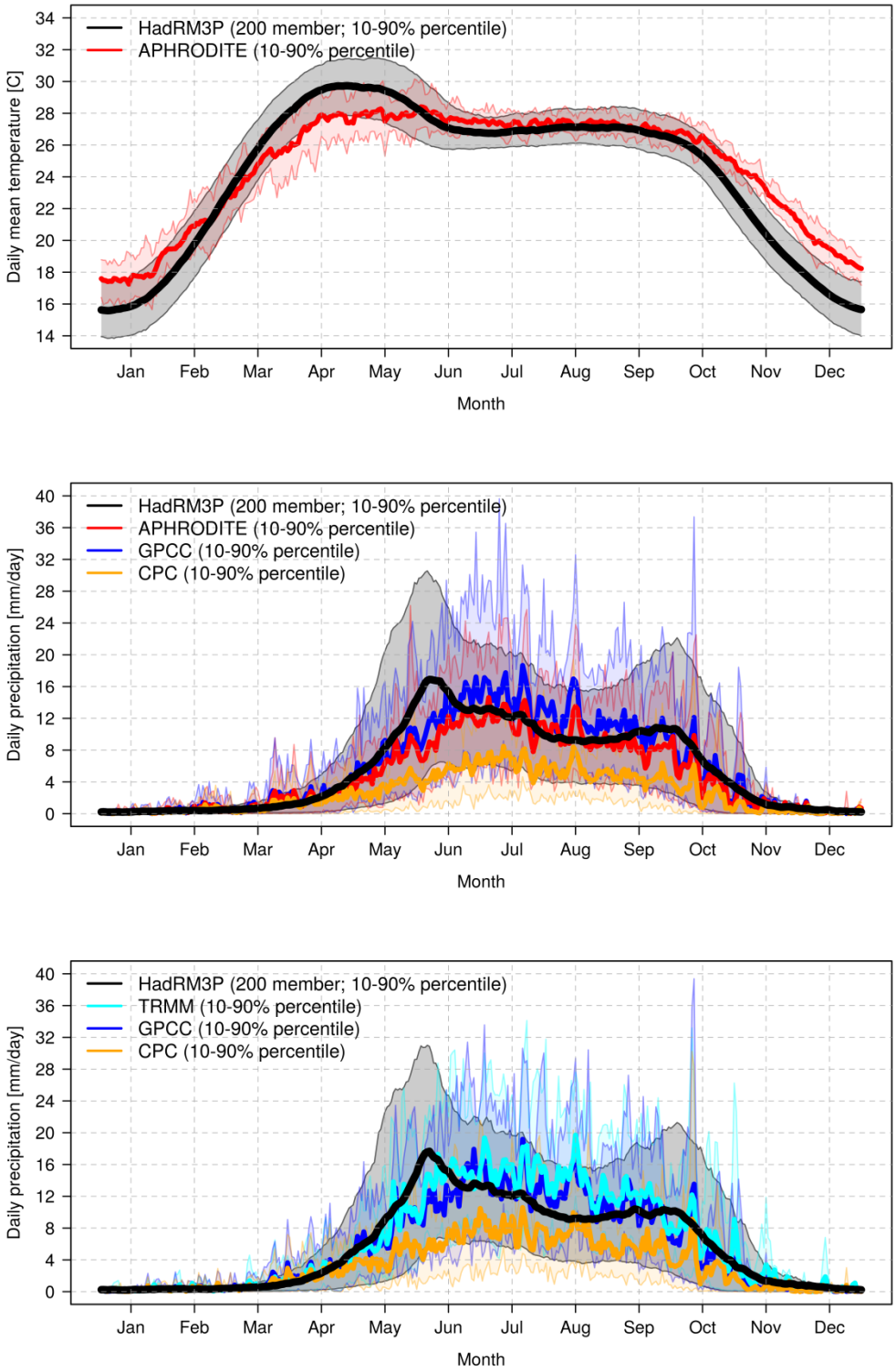


Figure 4.3: The annual cycle of daily temperature (°C) (top panel) and rainfall (mm/day) (middle panel) during 1988–2007 and during 1998–2013 (bottom panel) over the study region — model ensemble mean (black line), with range of 10–90th percentile (grey) versus APHRODITE (red), GPCC (blue), TRMM (cyan) and CPC (orange) with range of 10–90th percentile in their respective light colours. There is nearly 2 weeks difference in the monsoon onset between the model and the observation.

However, the model ensemble mean (black solid line) indicates that monsoon rainfall during June–September is underestimated when compared to observations, except to CPC, which appears to have a dry bias throughout the year.

Macadam and Janes (2017) used the PRECIS 2.1 regional climate modelling system to downscale three global climate models (HadGEM2-ES, CNRM-CM5, GFDL-CM3) dynamically over the South Asia domain to a horizontal resolution of 0.22 × 0.22° (~25 × ~25 km). Simulations for the period of 1960–1999 from all three models have shown extensive dry biases during the height of the summer monsoon season (June–September) in Bangladesh and eastern India (Macadam and Janes, 2017).

The ICTP RCM version RegCM4.3 with a horizontal resolution of 50 km is evaluated against the observed data sets of Climate Research Unit (CRU) and University of Delaware (UDEL) over South Asia for seasonal mean climatology and annual cycle for the period of 1971–2000. This study reported that the model underestimates the monsoon rainfall over the Bay of Bengal and Bangladesh (Hassan et al., 2014). Similar dry biases are also reported in Janes and Bhaskaran (2012), Islam (2009) and Islam et al. (2008).

Although the model exhibits similar patterns of temperature biases in the annual cycle of climatological mean daily temperature over the four different subregions within Bangladesh (Figure 4.4); the magnitude of the biases are not the same. There exist cold biases during November–February, warm biases during March–May and almost identical temperatures during June–September months in all four subregions.

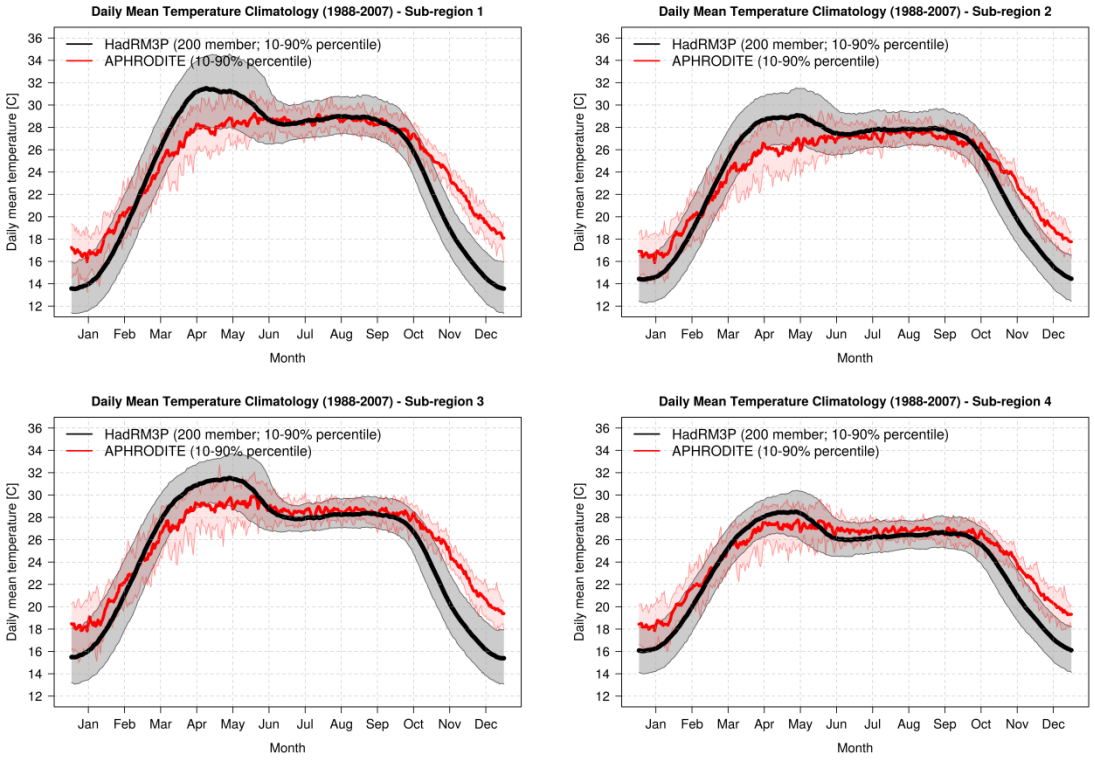


Figure 4.4: Annual cycles of daily mean temperature (C) over the four subregions of Bangladesh during 1988–2007—model ensemble mean (black line), with range of 10–90th percentile (grey) versus APHRODITE (red) with range of 10–90th percentile (light red). The amount of temperature bias among the four subregions is different, which is important to consider for local weather events.

But subregion 4 exhibits the lowest temperature bias throughout the year (bottom right panel of Figure 4.4). On the other hand, both the highest negative and positive temperature biases are found at subregion 1 (top left panel of Figure 4.4).

As per observations, Figure 4.5 demonstrates that the eastern parts of Bangladesh (subregions 2 and 4) receive relatively more rainfall compared to the western parts of the country (subregions 1 and 3). The underestimation of monsoon rainfall is consistent across all four subregions, although with varying magnitudes.

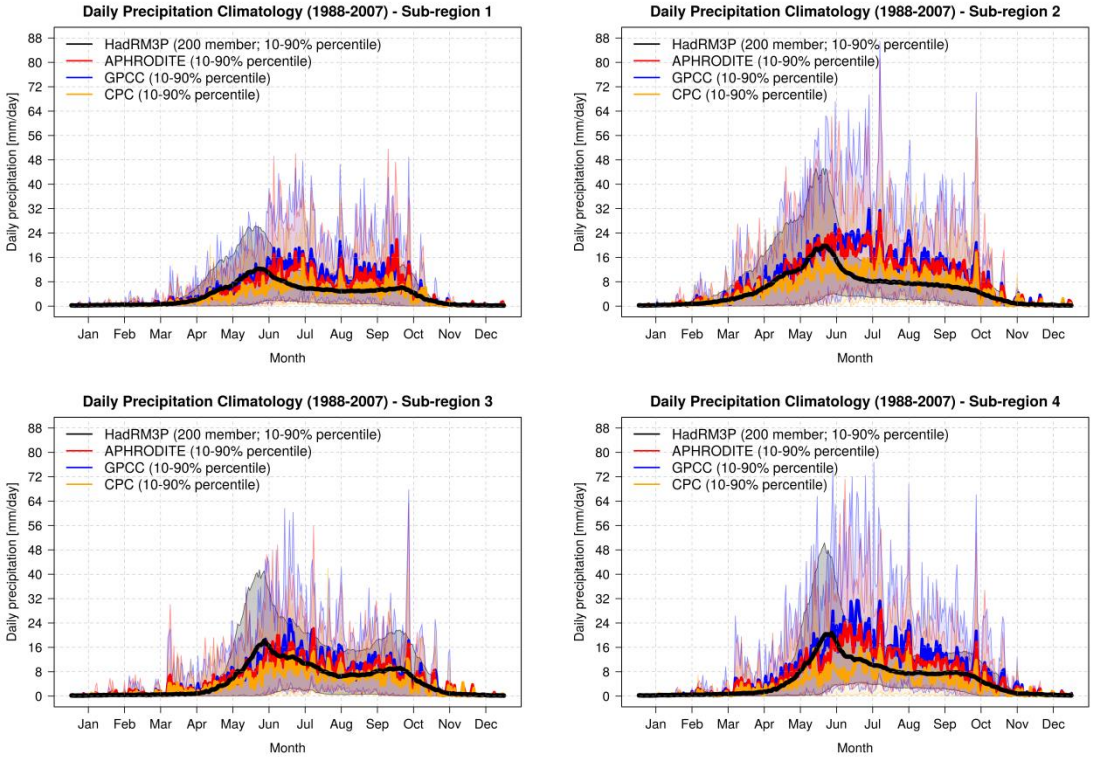


Figure 4.5: Annual cycles of daily rainfall over the four subregions within Bangladesh during 1988–2007—model ensemble mean (black line), with range of 10–90th percentile (grey) versus APHRODITE (red), GPCC (blue) and CPC (orange). The amount of biases among these four subregions varies, and this variation is important to consider for local weather events.

The weaker dry biases are found in the western subregions 1 and 3 (top and bottom left panels of Figure 4.5); while the eastern subregions 2 and 4 have much stronger dry biases (top and bottom right panels of Figure 4.5). These findings are corroborated by the annual cycles for sub-regional rainfall during 1998-2013 (Figure S4.3). Both Figure 4.3 (middle and bottom panels) and Figure 4.5 (including Figure S4.3) for the four subregions indicate that the onset of the monsoon differs between observations and the model by approximately 2 weeks. Given this difference in the onset, we consider redefining the pre-monsoon season in the model as a "shifted MAM" (SMAM) as a way of correcting for biases in climatological averages over this season.

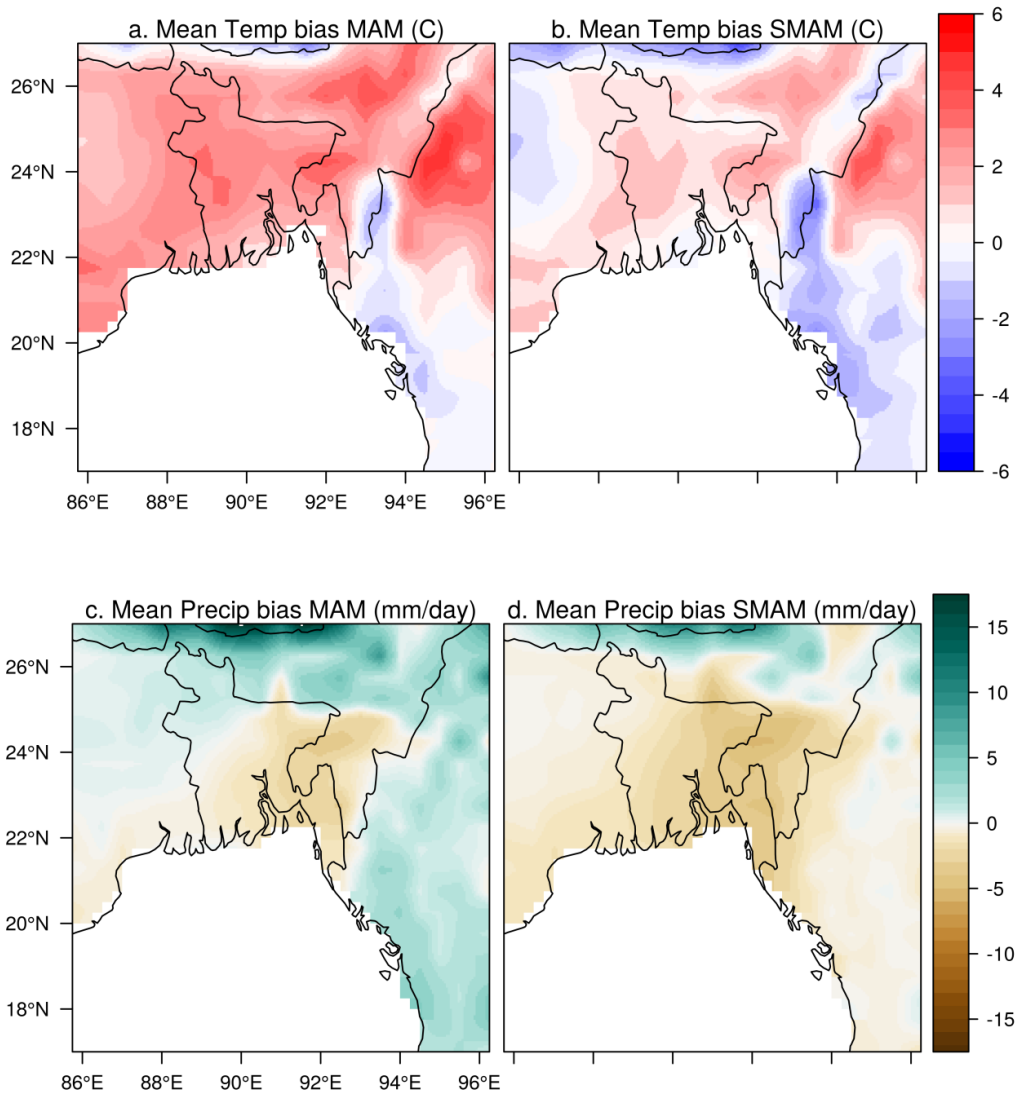


Figure 4.6: Spatial distribution of mean daily surface temperature (_C) (top two panels) and rainfall (mm/day) (bottom two panels) in pre-monsoon (MAM) and shifted pre-monsoon (SMAM) season over the study region. The maximum hot bias (up to 4°C) and wet bias (up to 16 mm/day) appear in MAM. In SMAM the temperature bias is reduced by 1–2°C over most of the study region. For rainfall, the wet bias is reduced by nearly 7 mm/day in the northern parts; while a shift from wet bias to dry bias is noticed in the western parts of the study region.

In SMAM, the dates are changed from 1 March to 30 May to 15 February to 16 May for each year of the evaluation period and then compared with MAM in the observations. Comparison between the model biases in the seasonal mean temperature

and rainfall in MAM and SMAM (Figure 4.6) demonstrates that using SMAM reduces warm biases over the study region. The impact on rainfall is spatially variable, with a reduction in the wet bias in western subregion, but at the cost of some increase in the dry bias to the east.

Using the SMAM approach as a simple temporal modification technique conserves both the model's ensemble size and model's physical parameterizations given that no subsampling or parameter specific bias correction is required. However, the effectiveness of this method for improving rainfall bias requires further investigation especially with regard to soil moisture conditions.

4.4.3. Extreme events

Model representation of extreme events is evaluated using two approaches; (a) the quantile-quantile (QQ) plots that are useful to look at the tails of the distributions and (b) return time plots that can specifically look at extreme events with up to 100 years of return periods.

In the QQ approach, we use 5-day means over the study region of Bangladesh, and then daily values over the eastern parts of the country (i.e., subregions 2 and 4). QQ plots are commonly used to quantitatively compare two distributions by plotting the corresponding percentiles of the data (Wilks, 2011). The overall model evaluation results vary depending on the season of interest and more importantly which observation data set is taken as the reference.

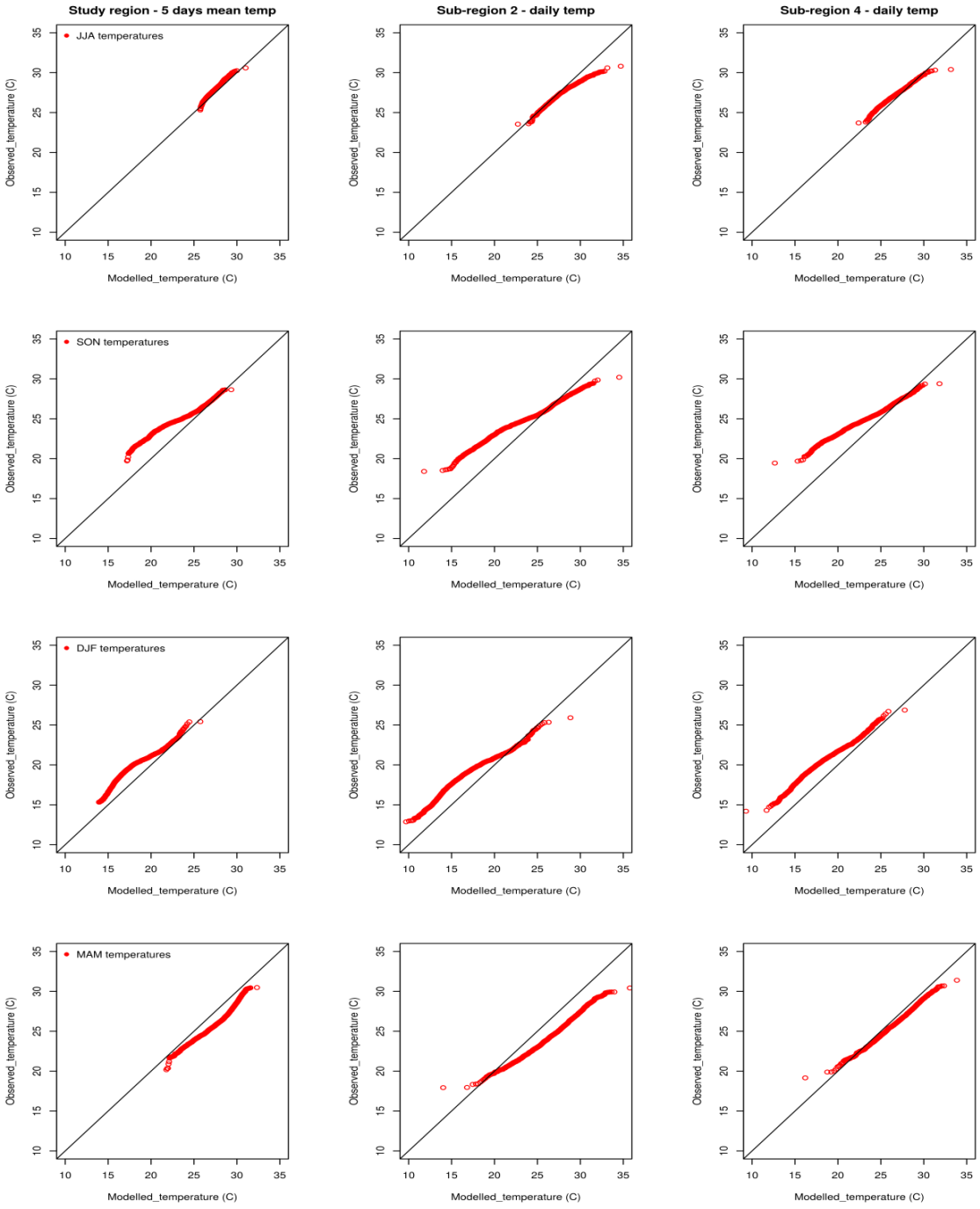


Figure 4.7: Quantile-quantile plots for 5 days mean temperatures (°C) over the study region in the left column and daily temperatures over the sub-regions 2 and 4 in middle and right columns respectively during 1988-2007 in monsoon (JJA), post-monsoon (SON), winter (DJF) and pre-monsoon (MAM) season – model HadRM3P versus APHRODITE. The red dots represent from 1st to 99th percentile of the distribution of the variable, if the dot is directly overlying the 1:1 line of agreement (diagonal black line), the model perfectly simulates the observed event; if the dot is below the line, the model overestimates the observed event and if it is above the line, the model underestimates the observed event.

The left column of Figure 4.7 corroborates our earlier findings based on the evaluation of the annual cycle in Figure 4.3 (top panel)—with very good agreement of JJA temperatures, partial overestimations in MAM (warm extremes) and partial underestimations in DJF and SON (cold extremes). The middle and right columns present the model evaluation results for subregions 2 and 4, respectively. The model performs marginally better in capturing the tails of the distributions of temperatures over the subregion 4, with greater improvement in the small warm bias in MAM.

Figure 4.8 demonstrates more variation in the evaluation results in terms of rainfall. For the study region, the distribution of 5-day mean rainfall events (using APHRODITE as a reference data set) is well represented in the model during monsoon (JJA), post-monsoon (SON) and dry winter (DJF) seasons. While pre-monsoon (MAM) rainfall is overestimated in the model, the SMAM results (see bottom row of Figure 4.8) reduce the bias for the study area and subregion 2, despite resulting in a slight underestimation for subregion 4.

As far as the observations are considered, GPCC is essentially wetter than APHRODITE across the rainfall distributions, while CPC is drier. QQ plots for model simulated rainfall compared to TRMM satellite data, GPCC and CPC gridded observation datasets for the evaluation period of 1998-2013 exhibited similar results (see Figure S4.4).

Figures 4.9–4.13 present the model evaluation results for extreme events of 5-day mean temperatures and rainfall with up to 100 years return periods for JJA, SON, MAM and SMAM.

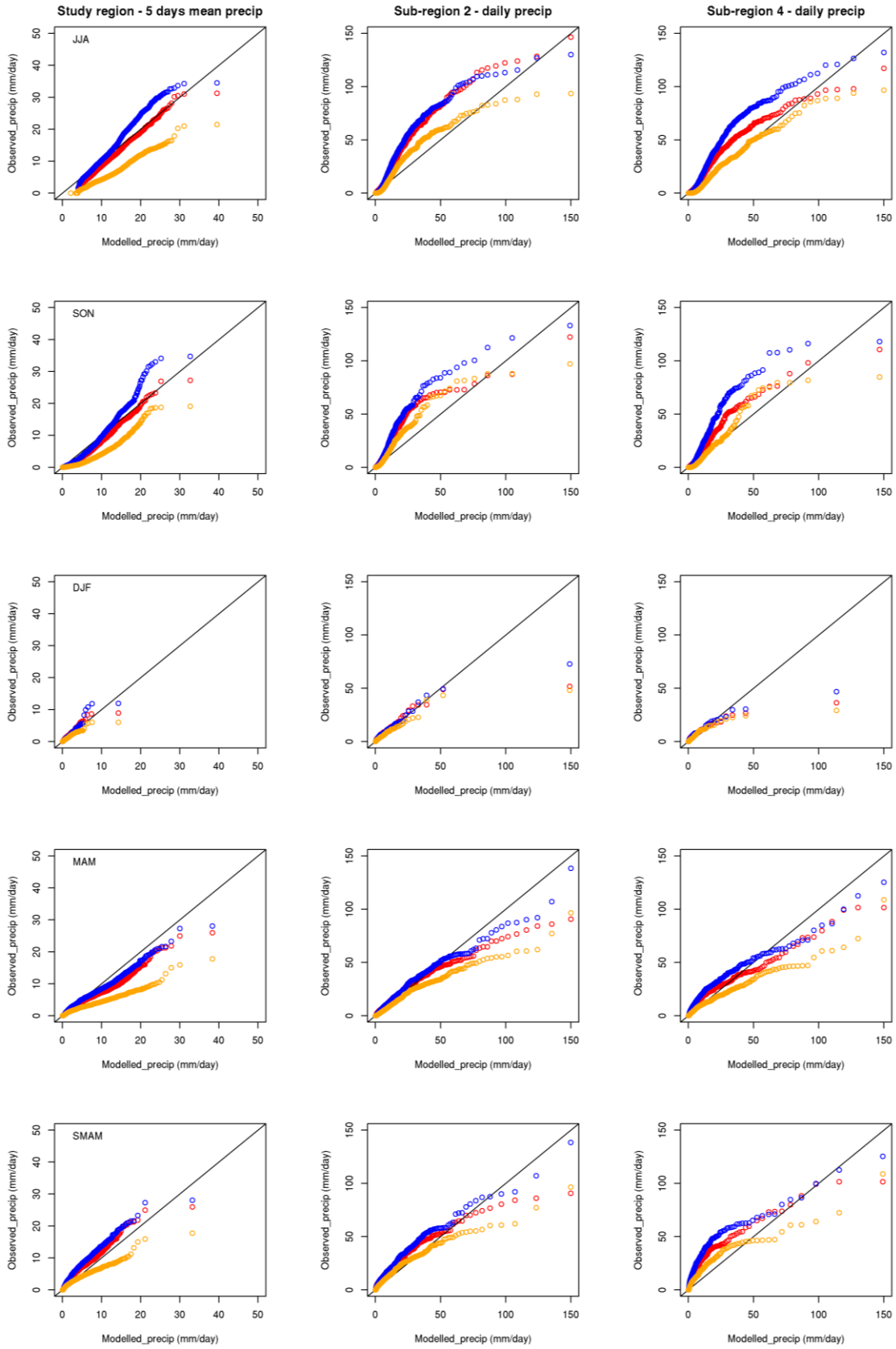


Figure 4.8: Same as Figure 4.7 but for rainfall – model HadRM3P versus APHRODITE (red), GPCC (blue) and CPC (orange) during 1988-2007. The wet bias in MAM is largely resolved in the distributions in the shifted pre-monsoon, SMAM.

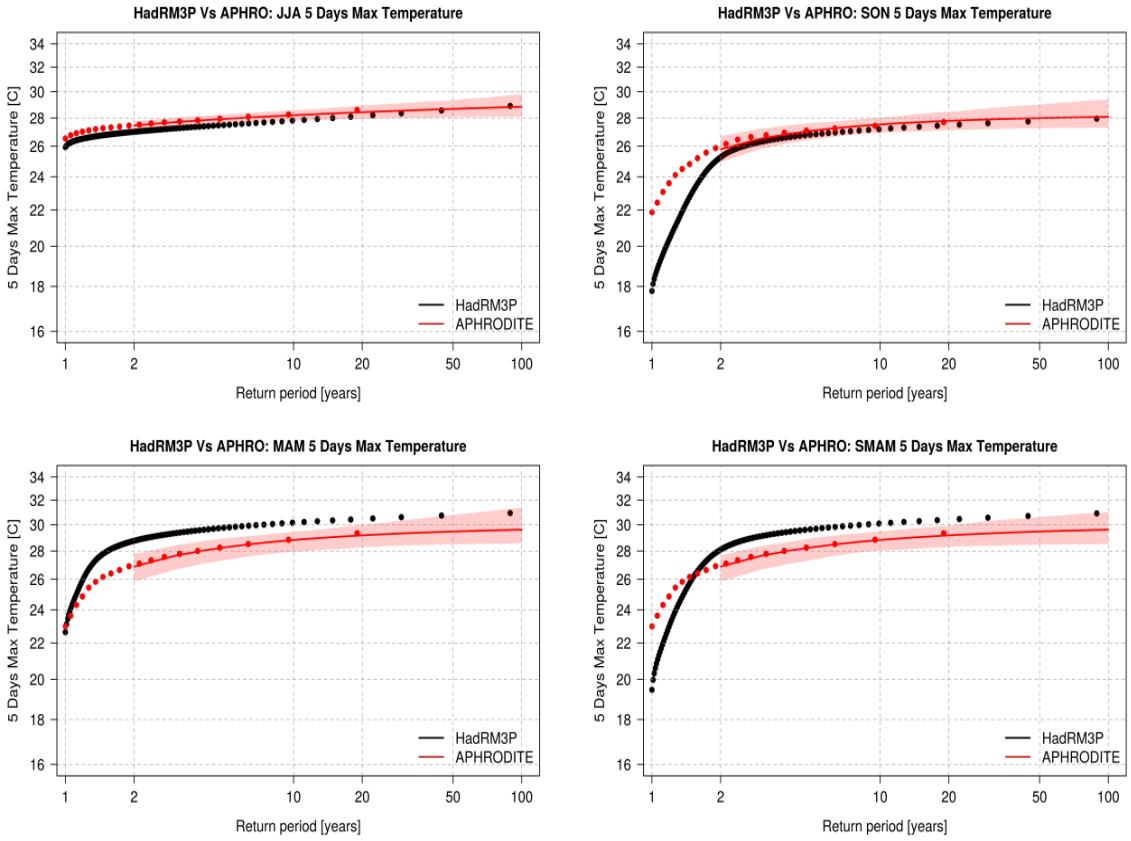


Figure 4.9: Return time plots for GEV distributions fitted to maximum five days mean temperatures (°C) in the wet seasons over the study region during 1988-2007 – model HadRM3P (black) versus APHRODITE (red). The individual red dots represent the maximum 5 days mean temperatures (°C) during a season in a year (i.e., total 20 dots); shaded polygons represent 2.5-97.5% range of the confidence interval and the solid lines represent the best fit lines within the confidence interval for events from 2 to 100 years of return period. The black dots represent the maximum of five days mean temperatures (°C) during a season (i.e., 90 dots for 90 days) from all 200 members of the model ensemble.

Over the study region of Bangladesh (Figure 4.9), the high-temperature extremes are adequately captured by the model (model-simulated black dots for extreme events overlap with the red best fit line of observations) during monsoon (JJA) and post-monsoon (SON) seasons. The extreme temperatures during the pre-monsoon (MAM) season are biased warm, which is not effectively resolved using our SMAM bias correction method.

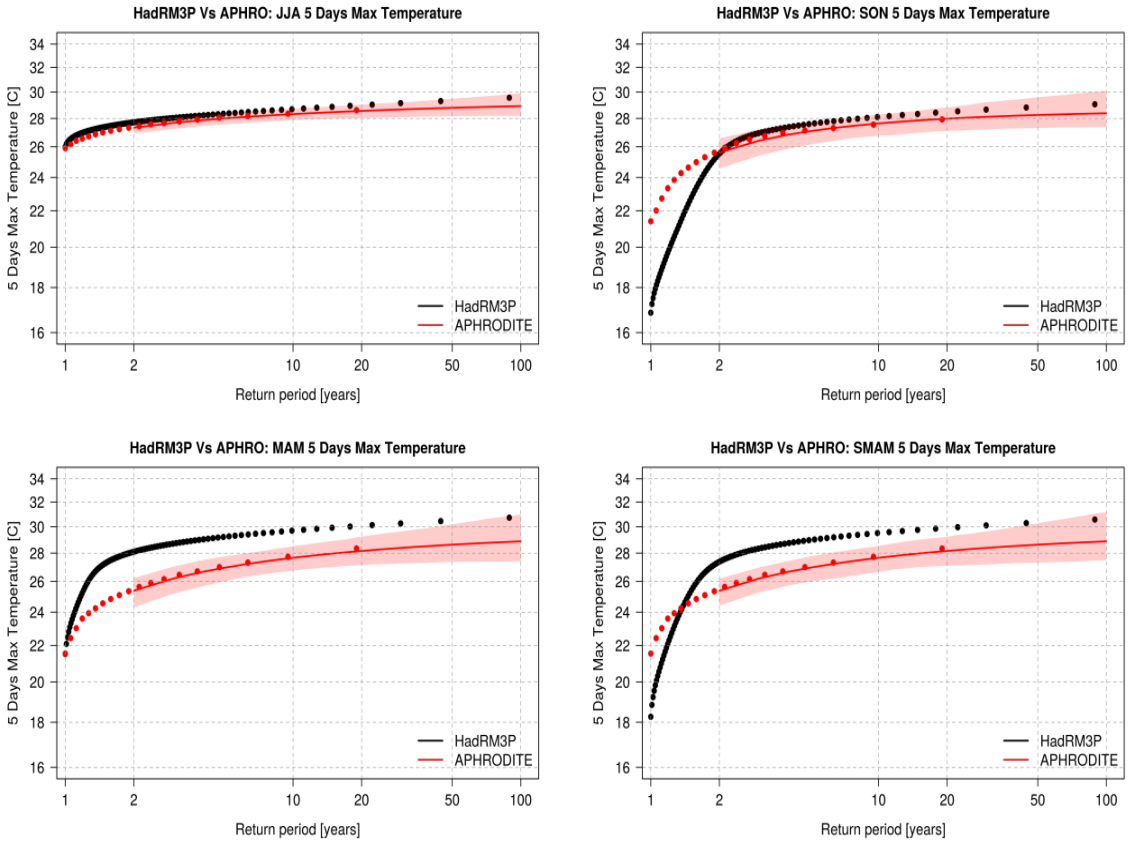


Figure 4.10: Return time plots for GEV distributions fitted to maximum 5-day mean temperatures (°C) in the wet seasons over the subregion 2 of Bangladesh during 1988–2007—model HadRM3P (black) versus APHRODITE (red). The individual red dots represent the maximum 5-day mean temperatures (°C) during a season in a year (i.e., total 20 dots); shaded polygons represent 2.5–97.5% range of the confidence interval and the solid lines represent the best fit lines within the confidence interval for events from 2 to 100 years of return period. The black dots represent the maximum 5-day mean temperatures (°C) taken from all 200 members of the model ensemble

At subregional scale, we find 2-3°C warm biases in the model simulated temperature extremes during JJA, SON and MAM over subregion 2. The model captures temperature extremes in all three seasons of pre-monsoon, monsoon and post-monsoon (cold winter season is excluded as we are interested in the hot extremes) well over subregion 4 (Figure 4.11).

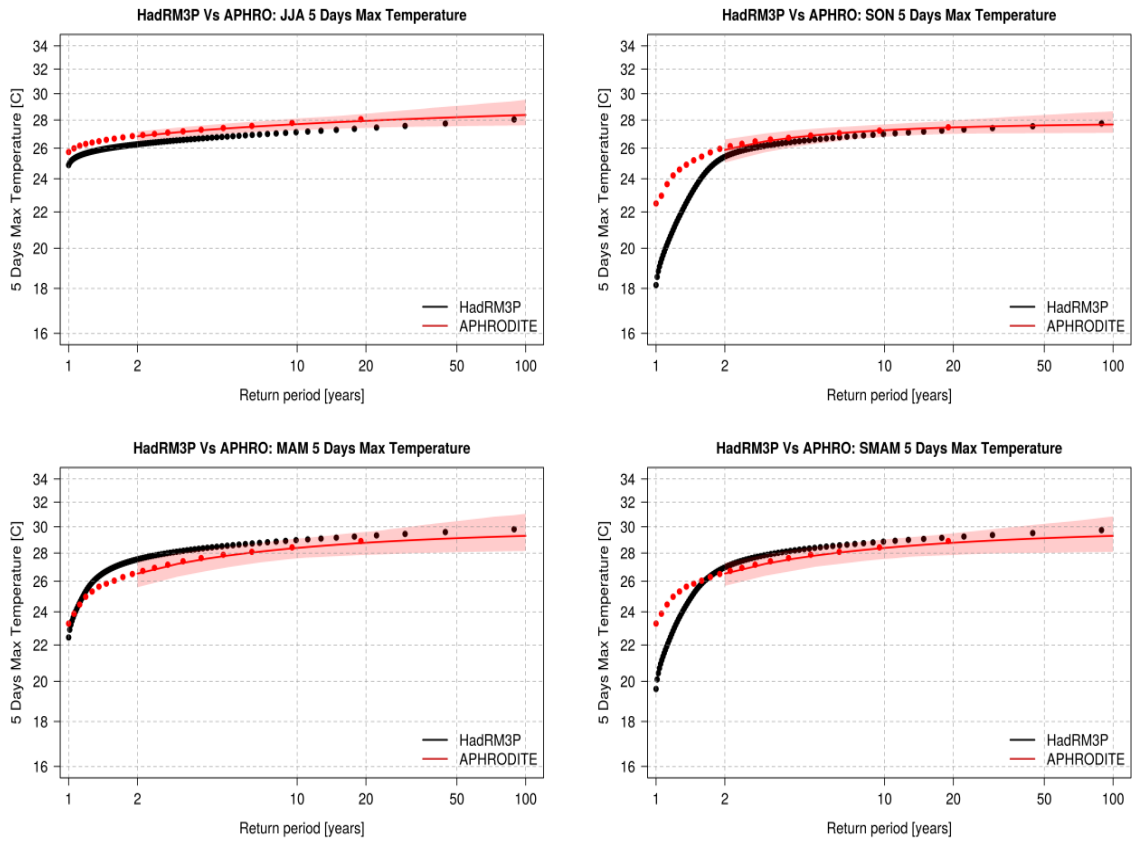


Figure 4.11: Return time plots for GEV distributions fitted to maximum 5-day mean temperatures (°C) in the wet seasons over the subregion 4 of Bangladesh during 1988–2007—model HadRM3P (black) versus APHRODITE (red). The individual red dots represent the maximum 5-day mean temperatures (°C) during a season in a year (i.e., total 20 dots); shaded polygons represent 2.5–97.5% range of the confidence interval and the solid lines represent the best fit lines within the confidence interval for events from 2 to 100 years of return period. The black dots represent the maximum 5-day mean temperatures (°C) taken from all 200 members of the model ensemble

For the study region of Bangladesh, the model-simulated 5-day rainfall extremes during SMAM, JJA and SON (dry winter season of DJF months is excluded as we are interested in the wet extremes) are well reproduced when compared with APHRODITE (Figure 4.12) and TRMM (Figure S4.5). Caesar et al. (2015) also reported that the RCM, HadRM3P can approximately capture the spatial pattern of the daily extreme rainfall events (>99th percentile) during JJAS months over this region compared with APHRODITE observations.

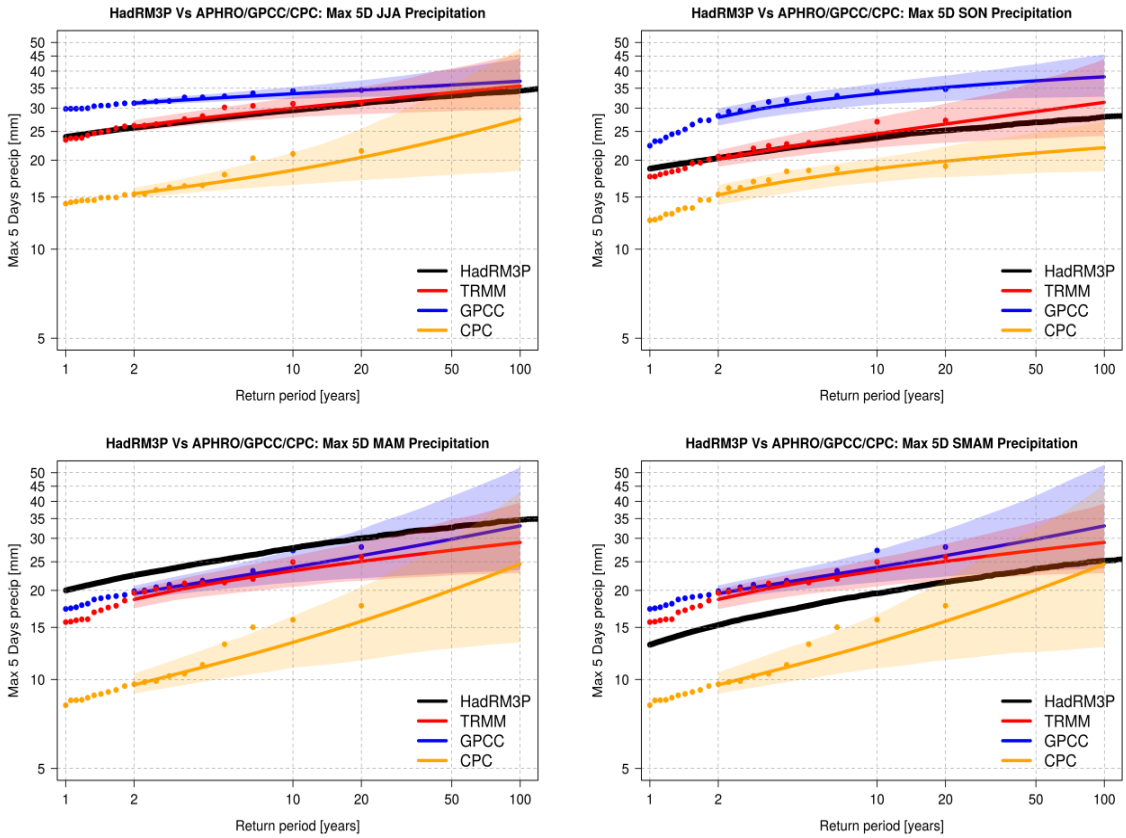


Figure 4.12: Return time plots for GEV distributions fitted to maximum 5-day mean rainfall (mm) in wet seasons over the study region (shown in Figure 4.1, right panel) during 1988–2007—model HadRM3P (black), versus APHRODITE (red), GPCC (blue) and CPC (orange). The individual dots represent the maximum 5-day mean rainfall during a season in a year (i.e., total 20 dots per data sets); shaded polygons represent 2.5–97.5% range of the confidence interval and the solid lines represent the best fit lines within the confidence interval for events from 2 to 100 years of return period. The black line for the model that is in closest agreement with the APHRODITE observations (in red) during JJA and SON is comprised of the maximum 5-day mean rainfall (mm) taken from all 200 members of the model ensemble (i.e., 20 × 200 dots).

The model under and overestimates 5-day rainfall extremes compared to GPCC and CPC, respectively in JJA and SON. The extreme rainfall events with 50–100-year return periods are within the confidence intervals of APHRODITE, GPCC and CPC observations in the model's SMAM (shifted pre-monsoon season), while these events are overestimated in MAM.

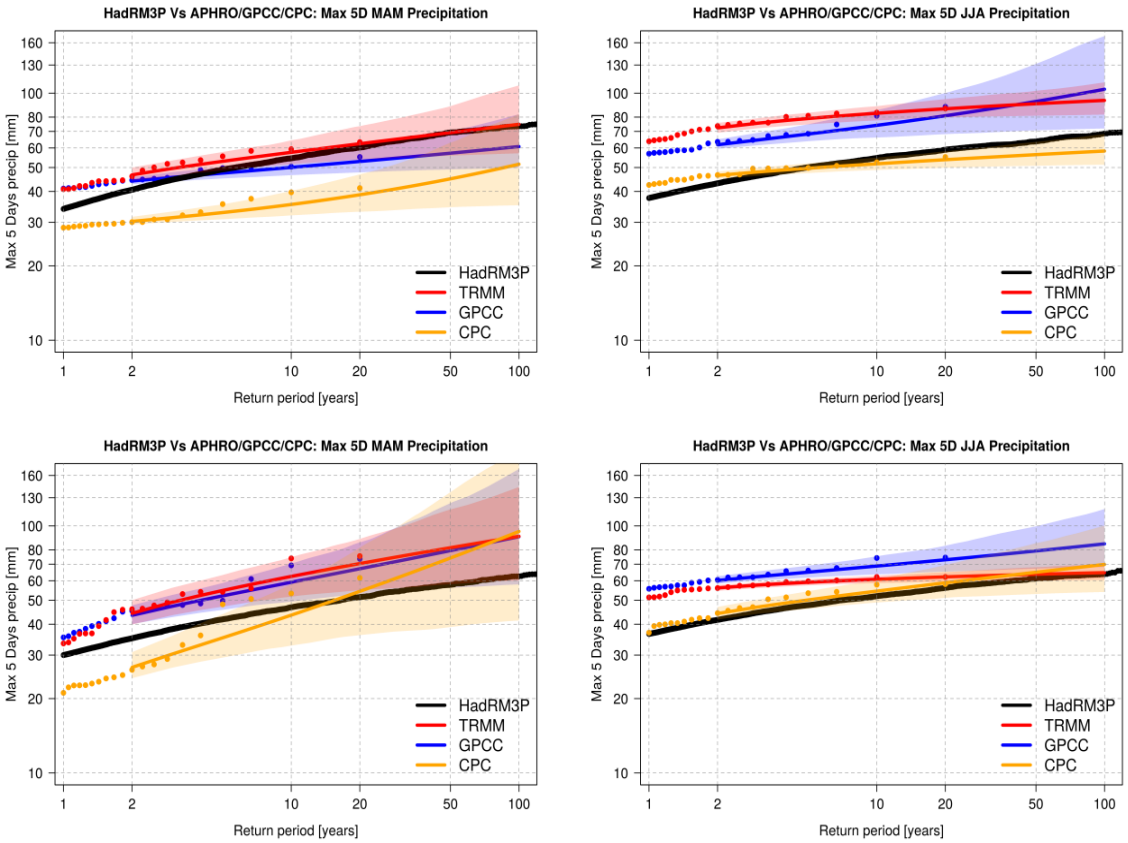


Figure 4.13: Same as Figure 4.10 but for the maximum 5-day mean rainfall events during MAM (left column) and JJA (right column) over the subregion 2 (top row) and subregion 4 (bottom row) of Bangladesh. The model-simulated extremes of 5-day mean rainfall events with return periods of 50–100 years are within the confidence intervals of at least one observation data set. MAM extremes are much better represented by the model and so a SMAM analysis is not required. The model underestimates the extremes during JJA when compared to APHRODITE and GPCC but lies within the confidence interval of CPC observations.

At local subregional scale, we focused on the pre-monsoon and monsoon seasons only over the two eastern subregions 2 and 4. These two subregions are the most vulnerable regions with high risk for economic and infrastructural damage due to extreme rainfall events. Interestingly, we find that the modelled pre-monsoon (MAM) extreme rainfall events are within the observational data bounds over both of these two subregions. However, the monsoon extreme rainfall events are underestimated in both subregions (Figure 4.13) when compared to GPCC and APHRODITE observations. Extreme

rainfall events with 50–100-year return periods are within the confidence interval of CPC observations. Model evaluation results for the more recent period of 1998–2013 that uses satellite TRMM data as a reference data for comparison; show a slight improvement for the pre-monsoon and monsoon extreme rainfall events, particularly for the subregion 2 (see Figure S4.6).

4.5. Conclusions

The weather@home RCM of HadRM3P is evaluated over the South Asia domain with particular focus on extreme temperature and rainfall events in Bangladesh. We find a substantial warm and wet bias in the pre-monsoon (MAM) season in the model, associated with too early an onset of the monsoon season, which is consistent with previous studies (Caesar et al., 2015; Fahad et al., 2017; Janes and Bhaskaran, 2012). To address this problem, a simple bias correction method is introduced; where the timing of pre-monsoon season is shifted backwards by 2 weeks in order minimize the bias while maintaining physical consistency between individual model simulations. In addition, there is no need to compromise on the ensemble size in contrast to other methods such as subsampling (Sippel et al., 2016).

The temporal shifting method to SMAM in the model provides some improvement particularly for alleviating mean seasonal temperature bias. However, this method has variable success for rainfall bias, which is worthy of further exploration. Therefore it is proposed as a potential bias correction method for future attribution studies looking at pre-monsoon extreme events over the study region. The mean monsoon rainfall events over the study area and over the subregions within Bangladesh are underestimated by the model. Using GEV theory to fit the extreme tail of the distribution, we find good an

agreement between modelled and observed extreme rainfall events during the monsoon season over the study region of Bangladesh, with somewhat underestimated extreme rainfall in the model in JJA over the sub-regions within the country. This study quantitatively assessed how realistically extreme events of 50–100-year return periods are simulated by the RCM, HadRM3P during pre-monsoon, monsoon as well as post-monsoon seasons over Bangladesh and also over subregions within this country.

We note that while limited availability of observation data with high spatiotemporal variability leads to considerable uncertainties in the observational rainfall record, the data are sufficient to identify regional and seasonal biases. Mean and extreme seasonal temperatures are well reproduced in HadRM3P except during the pre-monsoon period. We find a substantial warm bias, which is only marginally reduced with the proposed season shift bias correction method.

Overall, given that the timing and the magnitude of temperature and rainfall is reasonably well reproduced from a dynamic perspective, with biases mainly arising from deficiencies associated with the thermodynamic representation of convective processes, we deem HadRM3P fit for purpose over Bangladesh. We are confident that the identified biases will not compromise future attribution studies in the region and that the results presented here will provide useful guidance for such extreme event analyses.

Acknowledgements

We would like to thank our colleagues at the Oxford eResearch Centre: A. Bowery, S. Li, M. Rashid, and D. Wallom for their technical expertise. We would like to thank the Met Office Hadley Centre PRECIS team for their technical and scientific support for the development and application of weather@home. We acknowledge the use of the observation data sets of APHRODITE, GPCC, CPC and satellite data set of TRMM. Finally, we would like to thank all the volunteers who have donated their computing time to climateprediction.net and weather@home. Sarah N. Sparrow's time was supported by the EPSRC GCRF Institutional Sponsorship REBuILD project D4D00040.

Author contributions

Ruksana H. Rimi's contribution towards this work was performed as part of her DPhil research project. All results were analysed and plotted by Ruksana H. Rimi with advice from Myles R. Allen, Richard G. Jones, Karsten Haustein and Emily Barbour. The paper was written by Ruksana H. Rimi, with edits from all co-authors.

Conflict of Interests

The authors declare no potential conflict of interests.

ORCID

Ruksana H. Rimi: https://orcid.org/0000-0001-5344-1924

Supplement of

Evaluation of a large ensemble regional climate modelling system for extreme weather events analysis over Bangladesh

Ruksana H. Rimi et al.

Correspondence to: Ruksana H. Rimi (ruksana.rimi@ouce.ox.ac.uk)

Table S4.1: Basic information about the five observation datasets

Product Name	Product version	Spatial Resolution	Time Scale	Source/reference
APHRODITE	Monsoon Asia (MA) V1003R1	0.5°X 0.5°	1951-2007	Yatagai et al., 2012. Available at: http://journals.ametsoc.org/doi/pdf/10.1175/BAMS-D-11-00122.1
APHRODITE	Aphro Temp V1204R1	0.5°X 0.5°	1961-2007	Yasutomi et al., 2011. Available at: http://www.chikyu.ac.jp/precip/data/Yasutomi2011GER.pdf
CPC	CPC daily precipitation	0.5°X 0.5°	1979-2016	Available at: https://climexp.knmi.nl/NCEPData/prcp_GLB_daily.nc
GPCC	GPCC Full Data Daily Version 1	1° X 1°	1988-2013	Schamm et al., 2015. Available at: doi: 10.5676/DWD_GPCC/FD_D_V1_100
TRMM	3b42 Daily Version 7	0.25°X 0.25°	1998-2016	Available at: https://disc2.gesdisc.eosdis.nasa.gov/data/TRMM_L3/TRMT_3B42_Daily.7/

Description of weather@home model system:

The weather@home regional modelling system is part of the climateprediction.net and is able to generate very large ensembles of global and regional climate model simulations by harnessing spare CPU time on a large network of volunteers' personal computers. The climateprediction.net has become the largest climate modelling experiment to date by running climate models on volunteers' home computers. This distributed computing capacity is made possible by the Berkeley Open Infrastructure for Network Computing (BOINC; Anderson, 2004) open source infrastructure.

The weather@home system uses the Met Office Hadley Centre's regional climate model (RCM), HadRM3P, nested in the global model HadAM3P. Both HadRM3P and HadAM3P are based on the atmosphere component of the general circulation model HadCM3, a well-documented and widely used coupled ocean-atmosphere model (Gordon et al., 2000).

HadAM3P has 19 vertical levels, a regular latitude–longitude grid (1.25° latitude by 1.875° longitude) with regular poles (which approximates grid boxes of length ~150 km at mid-latitudes and ~200 km in the tropics), and operates using a 15 min timestep. HadRM3P shares the same vertical resolution, but has a 5 min timestep and a horizontal resolution of 50 km on a rotated lat-lon grid for extratropical domains, ensuring that each grid box in the region has approximately the same area (Jones et al., 2004; Massey et al., 2015). The global model HadAM3P acts as the driving

model and is run to generate the lateral boundary conditions (LBCs) for the RCM.

The coupling is strictly one way, meaning that there is no feedback from the regional model to the global model. The main variables of the LBCs (atmospheric pressure at the surface along with horizontal winds, temperature and humidity for all atmospheric layers) are relaxed across the buffer zone to values temporally interpolated from 6 hourly outputs from the global model. This relaxation technique is implemented across a four point buffer zone at each vertical level (Jones et al., 2004; Massey et al., 2015).

Sea surface temperatures (SSTs) and sea ice fraction (SIF) is prescribed using the Operational Sea Surface Temperature and Sea Ice Analysis (OSTIA) dataset (Donlon et al., 2012) as lower boundary condition. The radiative forcing follows the Coupled Model Intercomparison Project Phase 5 (CMIP5; Taylor *et al.*, 2012) protocol with prescribed greenhouse gases concentrations (CO_2, CH_4 and N_2O), ozone, halocarbons, sulphur emissions as well as solar incoming radiation and atmospheric optical depth from explosive volcanic eruptions. While solar and volcanic forcing is kept the same across all forcing scenarios, anthropogenic radiative forcing contributions and SSTs and SIF can be varied between different forcing scenarios.

This study uses an updated version of weather@home (weather@home 2), which includes a more recent land surface scheme, the Met Office Surface Exchange Scheme (MOSES 2, Essery and Clark, 2003). MOSES is a third generation land

surface model that can incorporate the direct physiological effect of CO_2 on photosynthesis and stomatal conductance (Sellers et al., 1997). MOSES 2 explicitly considers land surface heterogeneities within each grid cell through a tiling scheme (Essery and Clark, 2003).

The tiles allow consideration of each of the five vegetation types and four non-vegetated surface types and computation of surface fluxes for each surface type. The area-weighted average of the computed surface fluxes is returned to the atmospheric component of the model.

Therefore weather@home 2 provides a better representation of the land surface features than the earlier version. More details are provided in Massey et al. (2015). The model is configured to simulate one year of weather at a time which is send to the volunteers as one work unit. Initial conditions perturbation (Massey et al. 2015) is applied to each work unit to simulate a range of possible weather under the respective forcing scenario.

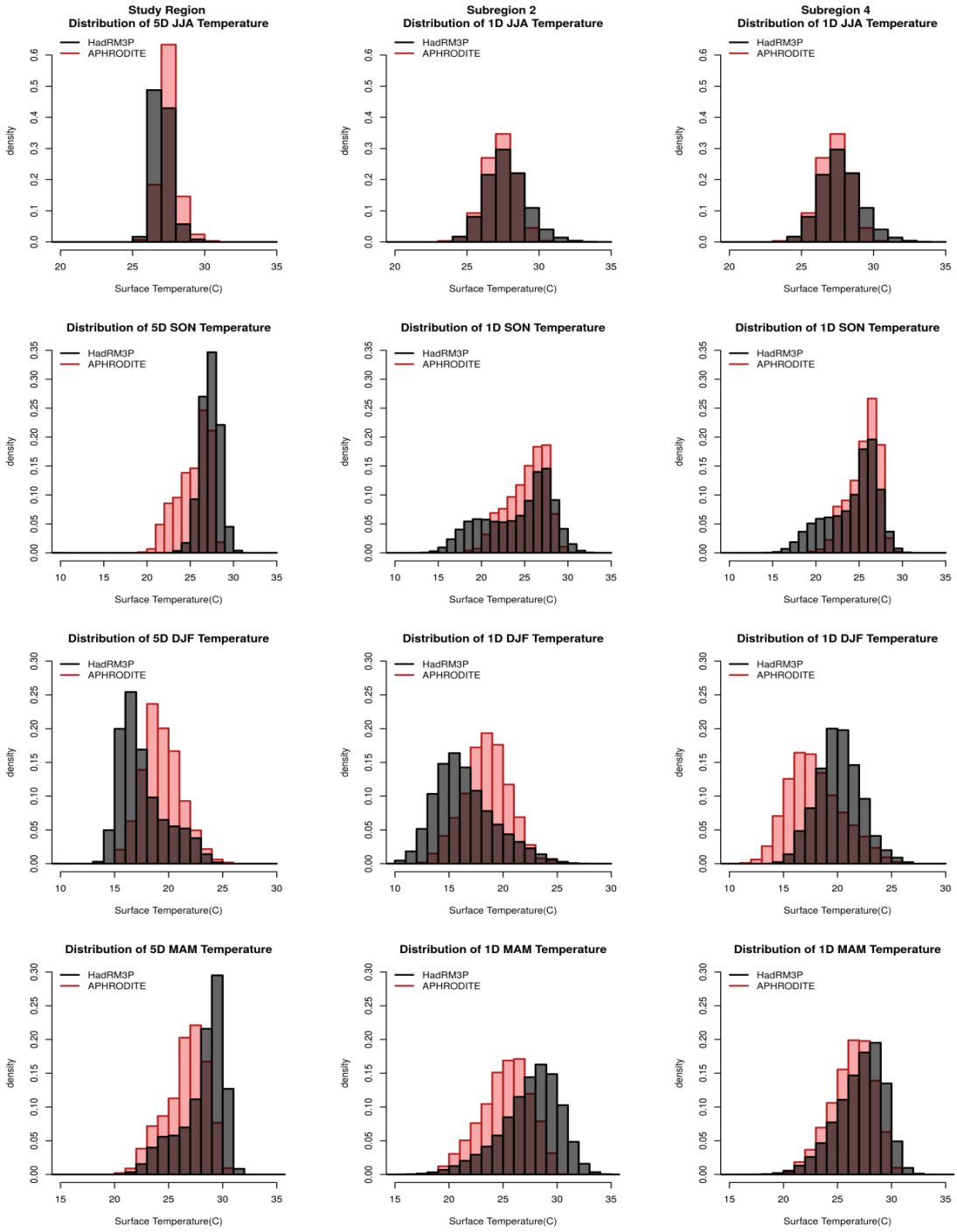


Figure S4.1: Histograms for 5 days mean surface temperature (°C) over the study region (left column) and daily surface temperature (°C) over subregion 3 (middle column) and subregion 4 (right column) during 1988–2007 in (a) monsoon (JJA), (b) post-monsoon (SON), (c) winter (DJF) and (d) pre-monsoon (MAM) season—model HadRM3P (black) versus APHRODITE (red). The model gives cold biases during winter and post-monsoon seasons. There exists minimum bias during monsoon and maximum hot bias during pre-monsoon summer season. The amounts of seasonal daily temperature biases vary between the two subregions 3 and 4 in Bangladesh.

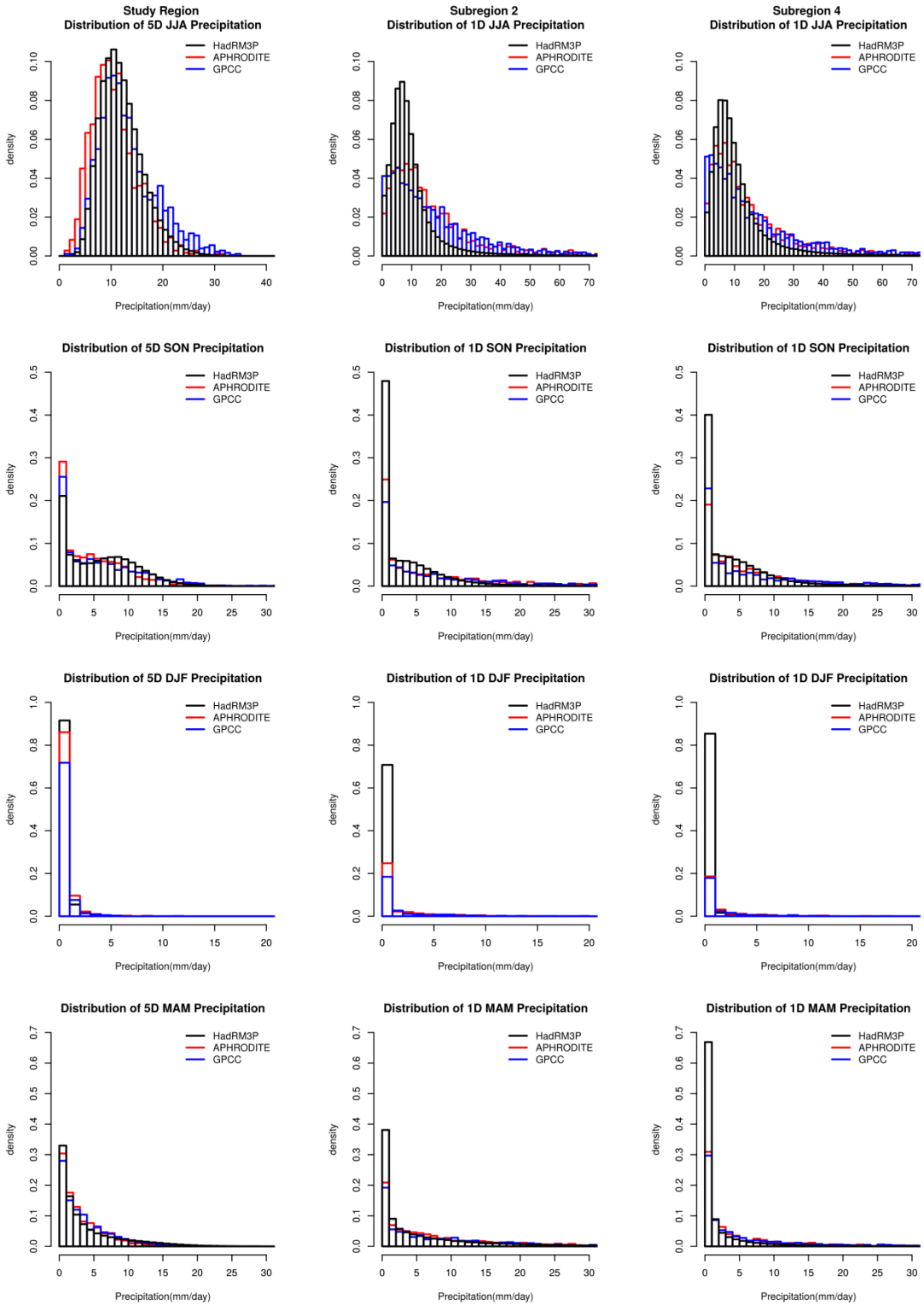


Figure S4. 2: Same as Figure S1 but for rainfall (mm/day)—model HadRM3P (black) versus APHRODITE (red) and GPCC (blue). The model tends to simulate high density events of 1 mm/day rainfall in all three seasons except in the monsoon season; when the rainfall is underestimated at the higher ends.

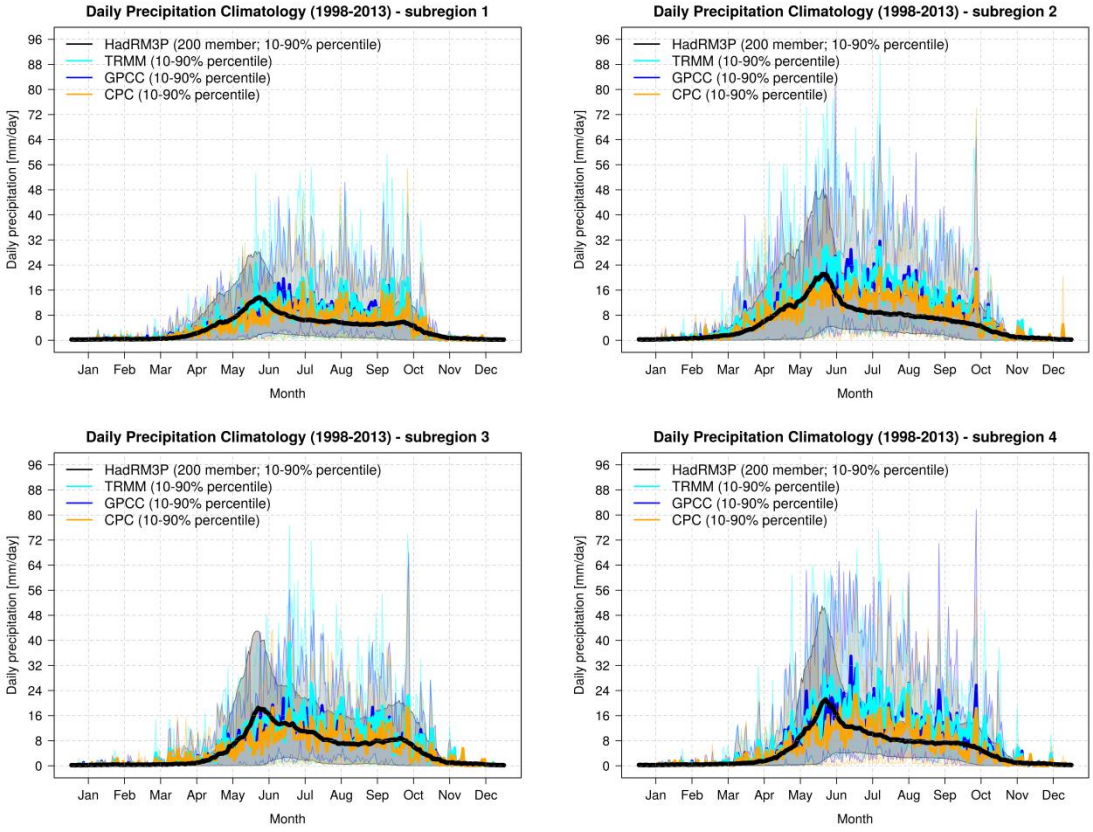


Figure S4.3: **Annual cycles of daily rainfall over the four subregions within Bangladesh during 1998–2013—model ensemble mean (black line), with range of 10–90th percentile (grey) versus TRMM (cyan), GPCC (blue) and CPC (orange). The amount of biases among these four subregions varies, and this variation is important to consider for local weather events. Subregions 2 and 4 experience the highest amounts of rainfall within Bangladesh, therefore looking at extremes can be useful in these two subregions.**

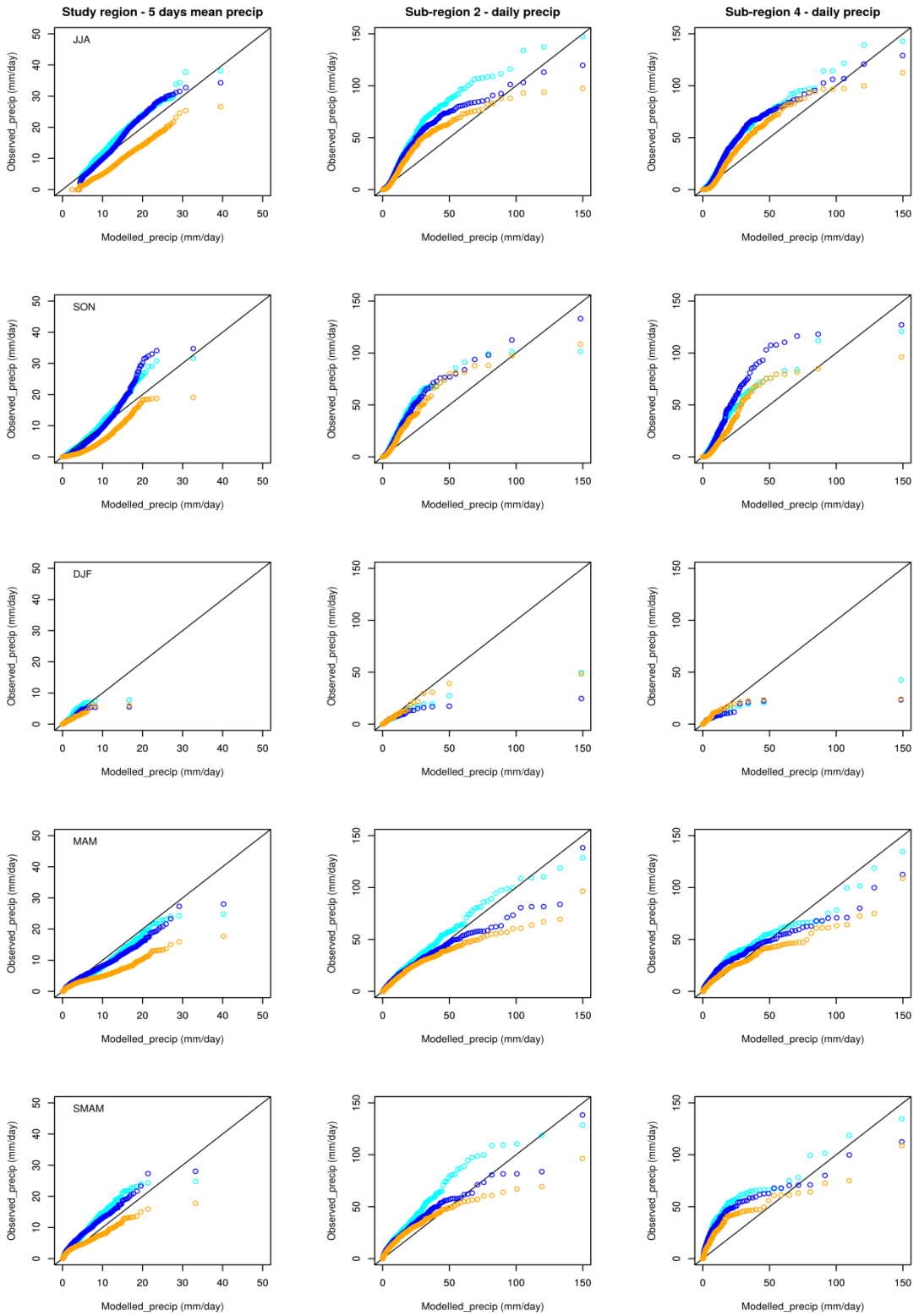


Figure S4.4 : Quantile–quantile plots for 5-day mean rainfall over Bangladesh (left column) and daily rainfall (mm/day) over subregions 3 and 4 (middle and right column) during 1998–2013—model HadRM3P versus TRMM (cyan), GPCC (blue) and CPC (orange). The wet biases in (d) MAM is largely resolved in the distributions in (e) shifted pre-monsoon (SMAM).

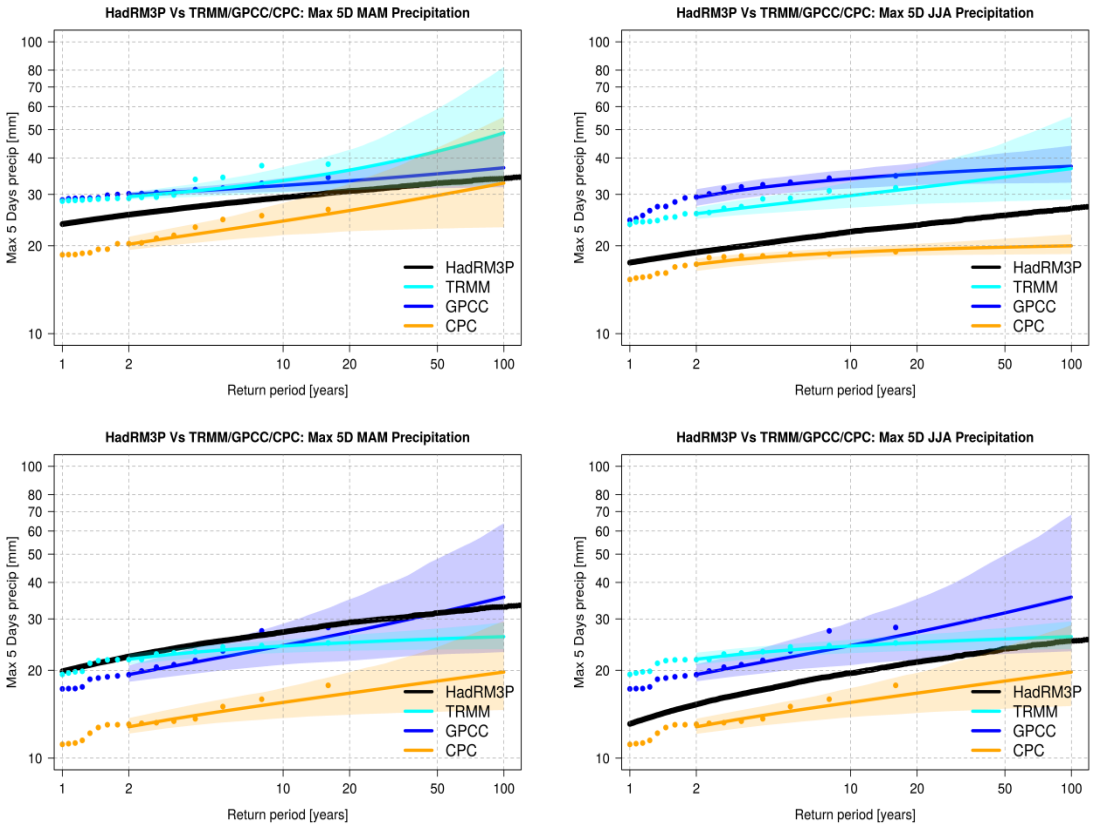


Figure S4.5: **Return time plots for GEV distributions fitted to maximum 5-day mean rainfall (mm) in wet seasons over the study region (shown in Figure 1, right panel) during 1998–2015—model HadRM3P (black), versus reference dataset of TRMM (cyan), GPCC (blue) and CPC (orange). The individual dots represent the maximum 5-day mean rainfall during a season in a year (i.e., total 16 dots per data sets); shaded polygons represent 2.5–97.5% range of the confidence interval and the solid lines represent the best fit lines within the confidence interval for events from 2 to 100 years of return period. The black line for the model is comprised of the maximum 5-day mean rainfall (mm) taken from all 200 members of the model ensemble (i.e., 20 × 200 dots).**

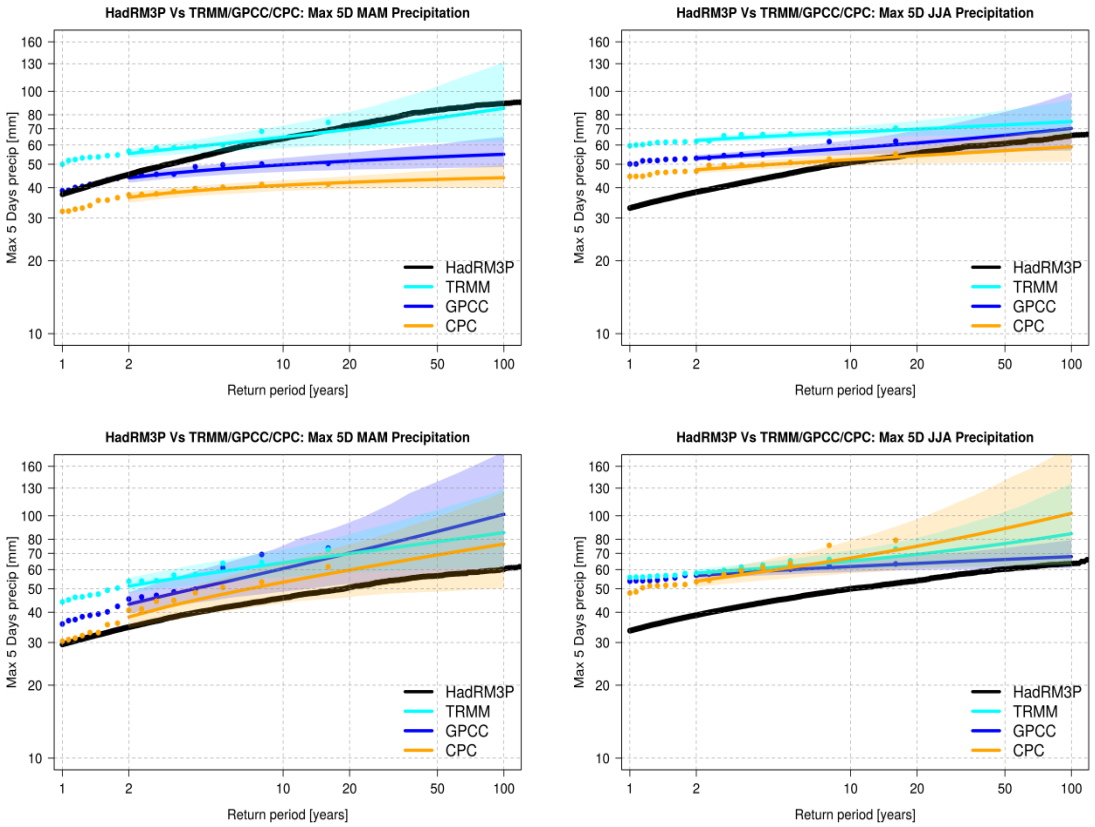


Figure S4.6 : Same as Figure S5 but for maximum 5-day mean rainfall events during MAM (left column) and JJA (right column) over subregion 2 (top row) and subregion 4 (bottom row). During MAM the model simulates the extreme rainfall events that are not highly overestimated and therefore a SMAM analysis is not required. During JJA, the model underestimates the maximum 5-day mean rainfall events of 2-16 years return periods but the extreme rainfall events of 50–100-year return period are within the confidence intervals of observations.

5. Risks of seasonal extreme rainfall events in Bangladesh under 1.5 and 2.0 degrees' warmer worlds – How anthropogenic aerosols change the story

Risks of seasonal extreme rainfall events in Bangladesh under 1.5 and 2.0 degrees' warmer worlds – How anthropogenic aerosols change the story

RUKSANA H. RIMI[1], KARSTEN HAUSTEIN[1], EMILY J. BARBOUR[1,2] ,

SARAH N. SPARROW[3], SIHAN LI[1,3], DAVID C.H. WALLOM[3] AND

MYLES R. ALLEN[1],

[1]Environmental Change Institute, School of Geography and the Environment, University of Oxford, Oxford, OX1 3QY, UK.

[2]Commonwealth Scientific and Industrial Research Organisation, Land and Water, Canberra, ACT 2601, Australia.

[3]Oxford e-Research Centre, Department of Engineering Science, University of Oxford, Oxford, OX1 3QG, UK.

Submitted to Journal of *Hydrology and Earth System Sciences (HESS)*

24 July, 2018;

Manuscript revised on 26 August, 2019

Available at https://www.hydrol-earth-syst-sci-discuss.net/hess-2018-400/

Short summary:

Extreme rainfall events are major concerns in Bangladesh because such events can cause flash floods and damage nearly harvestable crops in pre-monsoon season; whereas, in monsoon season, the impacts can range from widespread agricultural loss, huge property damage to loss of lives and livelihoods. This paper reveals the role of anthropogenic climate change drivers in changing the risks of extreme rainfall events during pre-monsoon and monsoon seasons at local sub-regional scale within Bangladesh.

Authorship Declaration

I, Ruksana H. Rimi, hereby declare that I conducted all of the analyses and writing for this paper with advice from Myles R. Allen, Karsten Haustein and Emily Barbour. The manuscript was finalized with edits from all co-authors including Sarah N. sparrow, and Sihan Li, and David C.H. Wallom.

Abstract.

Anthropogenic climate change is likely to increase risk (probability of occurrence of a hazard) of extreme weather events in the future. Previous studies have robustly shown how and where climate change has already changed the risks of weather extremes. However, developing countries have been somewhat underrepresented in these studies, despite high vulnerability and limited capacities to adapt. How additional global warming would affect the future risks of extreme rainfall events in Bangladesh needs to be addressed to limit adverse impacts. Our study focuses on understanding and quantifying the relative risks of extreme rainfall events in Bangladesh under the Paris Agreement temperature goals of 1.5°C and 2°C warming above pre-industrial levels. In particular, we investigate the influence of anthropogenic aerosols on these risks given their likely future reduction and resulting amplification of global warming. Using large ensemble regional climate model simulations from weather@home under different forcing scenarios, we compare the risks of rainfall events under pre-industrial (natural), current (actual), 1.5°C, and 2.0°C warmer and greenhouse gas (GHG)-only (with pre-industrial levels of anthropogenic aerosols) conditions. Both GHGs and anthropogenic aerosols influence changes in seasonal mean rainfall over this region. For extreme rainfall events, we find that the risk of a 1 in 100 year rainfall event has already increased significantly compared with pre-industrial levels across parts of Bangladesh, with additional increases likely for 1.5 and 2.0 degree warming (of up to 5.5 times higher, with an uncertainty range of 3.5 to 7.8 times). Climate change impacts on the probabilities of extreme rainfall events are found during both pre-monsoon and monsoon seasons, but the level of impacts are spatially variable across the country. Results also show that reduction in anthropogenic aerosols plays an important role in

determining the overall future climate change impacts; by exacerbating the effects of GHG induced global warming and thereby increasing the rainfall intensity. We highlight that the net aerosol effect varies from region to region within Bangladesh, which leads to different outcomes of aerosol reduction on extreme rainfall statistics, and must therefore be considered in future risk assessments. Whilst there is a substantial reduction in the impacts resulting from 1.5°C compared with 2°C warming, the difference is spatially and temporally variable, specifically with respect to seasonal extreme rainfall events.

5.1. Introduction

One of the major goals of the 2015 Paris Agreement of the United Nations Framework Convention on Climate Change (UNFCCC), on "Holding the increase in the global average temperature to well below 2°C above pre-industrial levels and to pursue efforts to limit the temperature increase to 1.5°C" (UNFCCC, 2015), needs strong support from research on the nature, benefits and feasibility of this challenging goal.

This Agreement calls for the quantification and comparison between the impacts of 1.5°C versus 2.0°C warmer global temperatures on different climate related aspects such as extreme weather events. While assessing both risks and vulnerabilities to incremental increases in global mean temperature, the discrimination of the impacts of different radiative forcing contributions as well as the quantification of spatially varying changes in risk are crucially important. For example, highly unusual heat extremes that are virtually absent in the present climate in South Asia, would affect

around 15% of land area of this region under 1.5°C and around 20% of land area under 2°C warming (The World Bank, 2012). The increase in heavy monsoon rainfall intensity for South Asia is projected to be 7% under 1.5°C and 10% under 2°C warming compared to pre-industrial conditions (Schleussner et al., 2016). Populations of this region largely depend on the stability of the monsoon, which provides water resources for agricultural production (The World Bank, 2012). It is projected that the years with above-normal monsoon rainfall will be more frequent (Endo et al., 2013; Kripalani et al., 2007).

The seasonality of rainfall will be amplified with more rainfall during the wet season (Fung et al., 2011; Turner and Annamalai, 2012). The number of extreme rainfall events are projected to increase as well (Endo et al., 2012; Kumar et al., 2011 in Vinke et al., 2017). As a consequence of additional global warming, parts of East Asia and India are likely to have more frequent daily extreme rainfall events in monsoon season (Chevuturi et al., 2018). Here we assess whether these generalized projections are also valid using a large ensemble regional climate model framework focusing on Bangladesh.

Bangladesh is potentially a hotspot of climate change impacts as it is vulnerable to a combination of increasing challenges from record-breaking temperatures, extreme rainfall events, more intense river floods, tropical cyclones, and rising sea levels (The World Bank, 2012). Bangladesh has a tropical monsoon climate, flat and low-lying topography, and unique geographical

location in the Ganges-Brahmaputra-Meghna Basin (Banglapedia, 2012; Rawlani and Sovacool, 2011). For these features, heavy rainfall events in the pre-monsoon (during Mar-Apr-May; MAM) and monsoon (during Jun-Jul-Aug-Sep; JJA) seasons are associated with a high risk of flooding and landslides almost every year. The frequencies of observed high-intensity rainfall events are increasing in the recent years (Murshed et al., 2011).

For example, in 2017, heavy rainfall across the upstream Meghalaya hills in India and in Bangladesh caused pre-monsoon floods in March in the northeastern parts of the country. Consequently, vast areas of Haors (local name for lowland wetlands) and low-lying areas were inundated and most of the nearly-harvestable 'Boro' paddy crop (a local high yielding variety of paddy) was damaged (Nirapad, 2017). In June 2017, at southeastern parts of Bangladesh heavy rainfall caused devastating floods and multiple landslides killing at least 156 people (Paul and Hussain, 2017). National Aeronautics and Space Administration (NASA)'s near-real time Integrated Multi-satellitE Retrievals for Global Precipitation Measurement, GPM (IMERG) data estimated the heaviest rainfall accumulation of more than 510 mm in only 3 days (12-14 June 2017 (Gutro, 2017).

Considering the unfolding change in risk of heavy rain in the region under present-day conditions how would a 1.5°C and a 2.0°C warmer world change the probability of extreme rainfall events in Bangladesh? If climate change is already playing a role, then similar events are likely to occur even more frequently as global warming continues in the future (Faust, 2017). Reliable information regarding the relative changes in future risks of extreme rainfall events can help local decision makers to address the problem,

develop appropriate adaptation strategies and allocate resources to minimize loss and damage associated with potential climate extremes.

According to global climate model (GCM) ensemble based study, by 2090, the north-western part of Bangladesh would experience ~9% and ~18% increase in the pre-monsoon and monsoon mean rainfall respectively (Kumar et al., 2014). Caesar et al., (2015) used the high resolution (25 km) regional climate model (RCM), HadRM3P that is nested in the global HadCM3 model and projected a large increase in the very heavy daily rainfall events (>99th percentile, i.e., >23.8mm/day) and a decrease in the light-moderate rainfall events (<75th percentile, i.e., <12.3mm/day) during monsoon season (Jun-Sep) over Bangladesh by 2099.

According to PRECIS (Providing REgional Climates for Impact Studies) model projection for 2080, the north-eastern Bangladesh would experience 0.42–75% more pre-monsoon rainfall compared to the baseline of 1971–2000 (Nowreen et al., 2015). While previous studies projected future changes in the seasonal mean or extreme rainfall events over a specific part or whole Bangladesh; none had the benefit of using very large model ensembles of high resolution RCM to examine exceptionally rare extreme rainfall events (e.g., events with 100 year of return period); explained whether or not anthropogenic climate change played a role in changing the probabilities of those projected future rainfall events; and explored how anthropogenic aerosols changed the overall climate change impacts on rainfall events.

The Fifth Phase Coupled Model Inter-comparison Project (CMIP5) models produced a broad range of temperature projections as a function of model sensitivity (van Vuuren et al., 2011). CMIP-style experiments are not ideal to provide with impact assessments specifically at 1.5°C or 2°C warming, because in these experiments, uncertainty increases with time and is dominated by responses and variability. While the UNFCCC in particular asking about the comparative risks associated with 1.5°C and 2°C warming, irrespective of what emission path is followed to achieve it. The Half a degree Additional warming, Prognosis and Projected Impacts (HAPPI) framework has been developed to address this call and provide with impact assessments specifically targeted for 1.5°C and 2.0°C warming (Mitchell et al., 2016b, 2017).

Hence the HAPPI framework has been developed, specifically targeted for 1.5°C and 2.0°C warming (Mitchell et al., 2016b). There are only a few studies using CMIP5 (e.g., Fahad et al., 2017), or PRECIS (e.g., Nowreen et al., 2015) simulations that investigated future changes in rainfall events over Bangladesh, but none of these have specifically addressed the warming targets of the Paris Agreement. The novelty of this study lies in meeting all these aforementioned challenges.

We considered anthropogenic aerosols in addition to greenhouse gases (GHGs) as a potential contributing factor in changing the risks of extreme rainfall events. Because aerosols can influence regional climate and change the risks of rainfall events by radiative forcing (Guo et al., 2013; Li et al., 2016b).

Furthermore, extreme rainfall events have higher sensitivity to aerosols removals, per degree of surface warming, in particular over the major aerosol emission regions like Asia (Samset et al., 2018). Therefore it is important to explore aerosol impacts while assessing the changes in the risks of extreme rainfall events under additional global warming scenarios of 1.5 and 2.0 degrees' of Paris Agreement.

Drawing on the large ensemble of regional climate model (RCM) runs generated with the weather@home system (Guillod et al., 2017; Massey et al., 2015) within the HAPPI experimental framework, we quantify changing rainfall risks for Bangladesh during MAM and JJAS. The risk of extreme rainfall events is evaluated for a counterfactual 'natural', current 'actual' and future 1.5 and 2.0 degrees warmer climate scenarios. The impact of anthropogenic aerosol emissions is quantified and discussed based on the GHG-only scenario.

We first introduce data and methods in Section 2, whilst a summary of model performance is presented in Section 3.1. We then assess percentage changes and standardized changes in the seasonal mean rainfall within five forcing scenarios (Natural, Actual, 1.5°C, 2.0°C and GHG-only) in Section 3.2. Finally, in Section 3.3 we detect the relative shifts in the probabilities of MAM and JJAS daily (and 5-day) rainfall extremes between the different forcing scenarios. The results are discussed in context of regional vulnerabilities and observed changes in Section 4.

5.2. Data and Methods

5.2.1. Observational data

The daily observational data sets that are used as a comparison against model results include: (i) Asian Precipitation Highly Resolved Observational Data Integration Towards Evaluation of Water Resources (APHRODITE) (Yatagai et al., 2012) and (ii) NOAA's Climate Prediction Center (CPC) global 0.5° analysis (Chen et al., 2008a).

APHRODITE is a high-resolution daily gridded rainfall dataset for Asia (V1901, available for 1998-2015); created primarily with data obtained from a rain-gauge-observation network.

CPC global daily rainfall dataset (available from 1979 to present) is constructed through a unified analysis of gauge-based daily rainfall over global land (Chen et al., 2008b).

Basic facts about these two observational data sets are presented in Table S1 in the supplementary information. Both model and observation data is re-gridded using bi-linear interpolation method to have similar and comparable grid structures.

5.2.2. Model setup and experimental design

The weather@home is part of the climateprediction.net programme (Stainforth et al., 2005) and is able to generate very large ensembles of climate model simulations by

harnessing spare CPU time on a network of volunteers' personal computers (Allen, 1999; Stott et al., 2004; Massey et al., 2015).

For this study, we use the high resolution (50 km) RCM, HadRM3P (over South Asia region) that is nested in the global atmosphere-only HadAM3P model of weather@home system and is driven by prescribed sea surface temperatures (SSTs) and radiative forcing (Massey et al. 2015; Guillod et al. 2017) to generate the required model ensembles with initial condition perturbations. The model includes a sulphur cycle (Jones et al., 2001) and uses the updated Met Office Surface Exchange Scheme version 2 (MOSES2; Essery et al., 2003). Recent ECLIPSE v5a global emissions dataset (Klimont et al., 2013) is used to prescribe the sulphur dioxide fields in the model. Information about the procedure of using this data in the model is given the supplementary material.

HAPPI experiments are designed to address research questions relating to 1.5°C and 2.0°C warming and as part of the experiments weather@home system is used to generate large model ensembles (Massey et al., 2015; Otto, 2017; Stainforth et al., 2005). Following the experimental set up of the HAPPI framework (for details see Mitchell et al., 2017), this study uses experiments of three decadal model ensembles:

1. Actual climate (denoted as 'ACT') model ensemble with 98 members per year representing the current decade (2006–2015) with observed SST data from the Operational Sea Surface Temperature and Sea Ice Analysis (OSTIA) dataset (Donlon et al., 2012; Stark et al., 2007) and present-day atmospheric GHG and aerosol concentration.

2. HAPPI 1.5 model ensemble (2091–2100) with 98 members per year representing 1.5°C warmer than pre-industrial (1861–1880) climatic conditions, and
3. HAPPI 2.0 model ensemble (2091–2100) with 98 members per year representing 2.0°C warmer than pre-industrial (1861–1880) climatic conditions.

For the HAPPI 1.5 model ensemble, the RCP 2.6 scenario is used to provide the model boundary conditions. In RCP 2.6 scenario, the mean global temperature reaches to ~1.55°C by 2100 (Mitchell et al., 2017). Since there is no analogous CMIP5 simulation available which results in ~2°C warmer temperatures relative to preindustrial levels, a weighted combination of RCP2.6 and RCP 4.5 is used to provide the model boundary conditions of SST and sea ice for the HAPPI 2.0 model ensemble. The global mean temperature response reaches to ~2.05°C by the end of century in the HAPPI 2.0 model ensemble (Mitchell et al., 2017). Following the RCP2.6 protocol, anthropogenic aerosol concentrations are approximately one-third of the current levels (IPCC, 2013c) in both HAPPI scenarios.

In addition, we use two model ensembles of hypothetical climate conditions:

4. Natural ('NAT') model ensemble with 98 members per year representing the current decade (2006–2015) climatic conditions, but here the modelled SST patterns of anthropogenic forcing (ΔSSTs) are removed from the OSTIA observed SSTs to simulate a counterfactual world. ΔSSTs are generated from the CMIP5 archive. In this case, HistoricalNat simulations are subtracted from the Historical simulations as described in Schaller et al. (2016), thereby generating a representation of human influences on the SSTs that can be

removed from the OSTIA SSTs. GHG and aerosol concentrations are set to pre-industrial levels.

5. 'GHG-only' model ensemble with 98 members per year representing the current decade (2006–2015) climatic conditions, but with anthropogenic aerosol concentrations reduced to pre-industrial levels to simulate a hypothetical climate, where impacts of aerosols are removed. The difference between ACT and GHG-only conditions simulates the net aerosol effect under current conditions assuming additive behaviour of different radiative ~~forces~~ forcing. The GHG-only model ensemble with anthropogenic aerosols reduction scenario in the HadRM3P model is satisfactorily representative when compared with the other GCMs (Haustein et al., in progress). Based on the very limited sample of CMIP5 aerosol only (AA) experiments, we found that the resulting ΔSST patterns are reasonably similar compared with ΔSSTs from ACT minus GHG-only (not shown).

5.2.3. Methods

To understand how seasonal mean rainfall changes from one climate condition to another, we looked at percent change (PC) and standardized precipitation index (SPI) change between different two forcing scenarios (from pre-industrial NAT to current ACT, ACT to HAPPI 1.5, HAPPI 1.5 to 2.0 and from ACT to GHG-only). PC and SPI analyses are done for rainfall changes over the central parts of South Asia and then over Bangladesh. For brevity, the supplementary text includes the details of the calculation methods for PC and SPI changes.

In Bangladesh, any MAM extreme rainfall events are known to cause flash floods and substantial crop damage (Ahmed et al., 2017). Bangladesh receives more than 75% of the annual total rainfall during JJAS (Shahid, 2010a). An extreme rainfall event in this period can therefore cause wide-spread flooding and landslide eventually leading to loss of lives and livelihoods. A high impact post-monsoon (Oct-Nov; ON) rainfall event may be associated with the coastal floods that occur due to storm surges or tidal effects along the northern part of Bay of Bengal (Hossain, 1998).

Considering meteorological hazards and potential impacts, MAM and JJAS extreme rainfall events are analyzed in this study while, ON rainfall events are excluded. Winter (during Dec-Jan-Feb; DJF) season is also excluded because little or no rain occurs during DJF and we are interested in wet extremes.

We use sub-regions 1-4 located at north-west (88°-90°E, 24°-26°N), north-east (90.5°-92.5°E, 24°-25.5°N), south-west (89°-91°E, 21.5°-23.5°N) and south-east (91°-93°E, 20.5°-24°N) respectively. The two eastern sub-regions 2 and 4 are the rainier parts of the country compared to the other two western sub-regions of 1and 3.

MAM and JJAS extreme rainfall events with up to 100 years of return periods are adequately well captured by the HadRM3P model over these same 4 sub-regions in Bangladesh when compared to high resolution gridded observation datasets (Rimi et al., 2019a). Such pre-evaluated model simulations provide confidence in analyzing comparative risks of extreme rainfall events under different forcing scenarios. The model is therefore considered to be fit for assessing climate change impacts on extreme rainfall events in Bangladesh.

In Bangladesh 1- to 10-day high impact rainfall events can trigger flooding and landslides. For example, at north-east Bangladesh (sub-region 2), more than 150 mm MAM rainfall over a 6-day period can lead to an early flash flood (Ahmed et al., 2017). In contrast, at south-east Bangladesh (sub-region 4), more than 350 mm JJAS rainfall over a 3-day period is enough to cause a landslide (Ali et al., 2014). For a wide-spread river flooding e.g., the Brahmaputra River Basin flooding in August 2017, 10-day extreme rainfall event is considered (Philip et al., 2018).

Considering such variations in rainfall magnitudes causing different hazards, we focused on daily and 5-day rainfall events to analyze the potential risks. The seasonal cycles of presented here are based on 5-day rainfall, which is used to represent the timescale responsible for river flooding as opposed to daily extremes that cause flash floods primarily in the pre-monsoon season.

"Return time" of an event, also known as the "return period" is the likelihood of an event occurring, defined by a particular variable exceeding a certain threshold during a given time interval. If variable X is equal to or greater than an event of magnitude x_T, occurs once in T years, then the probability of occurrence $P(X \geq x)$ in a given year of the variable is (Wilks, 2011):

$$\boldsymbol{P(X \geq x = \frac{1}{T})} \ \textbf{Or,} \ \boldsymbol{T = \frac{1}{1-P(x \geq x_T)}}$$

A "1 in 10 year event" is an event with a 10% chance of occurring. On the contrary, the rarest event is a "1 in 1000 year event", with a 0.1% chance of occurring in a given year. The rainfall amounts associated with the 50- or 100-year return periods are extracted from the 98th and 99th percentiles, respectively, of a fitted distribution (i.e., $[1–0.98^{-year}]^{-1}$ = 50 years and $[1–0.99^{-year}]^{-1}$ =100 years) (Wilks, 1993). The uncertainty of the return

period is calculated using bootstrapping method. The time series of each ensemble is resampled a 1000 times using bootstrapping to derive 5 to 95% confidence intervals for return periods. We note that structural model uncertainty (such as parameter sensitivity) is not included in our uncertainty estimate.

Return time plots are used to explore the relative risks of rare events (like those with probabilities of <= 1 in 100 years). To construct the return time plots for MAM and JJAS daily (and 5-day) rainfall events, we use 98 plausible model realizations for the 10-year period of each model ensemble. For each year, three (MAM) and four (JJAS) months of data are used for pre-monsoon and monsoon season, respectively. The model uses a 360-day calendar with all 12 months spanning for 30 days. Therefore, we have 3x30x10x98 = 88,200 and 4x30x10x98 = 117,600 simulated values to calculate the return periods of MAM and JJAS rainfall events, respectively.

Such large sample size allows us to estimate a range of physically plausible climate conditions with focus on the tails of the distribution, which can be robustly determined. We consider all days of a season for calculating the return periods or rainfall events. In this way, we can look at low intensity rainfall events with minimum return period of 1 year, and also high intensity rainfall events with up to 98x10 = 980 years return period. However, we focused on rainfall events with high return periods that are relevant for impacts and adaptation planning (i.e., 10-100 year events).

To add a qualitative representation of the year-to-year natural variability from the ACT model ensemble, we use two wettest and two driest years during the decade of 2006-2015. The spatiotemporal average for the corresponding sub-region and season over the

10-year simulation period has been used to identify the two wettest and driest years. ACT model ensemble has the same forcings in each year for the historical period of 2006-2015; the only variability playing a role in changing rainfall intensity is therefore the natural variability of SSTs.

For this reason, these two wettest and driest years of ACT model ensemble approximately indicate how much natural SST variation can contribute to changing rainfall intensities. By comparing these two subsampled model ensembles with the other ensembles of different forcing scenarios, we can estimate the signal-to-noise ratio in the return period plots. The supplementary material of Table S2 lists the wettest and driest years for MAM and JJAS over the four different sub-regions.

In order to examine robustness of the return time plots based on weather@home's RCM, HadRM3P model outputs; we compare similar results based on decadal simulations from additional four atmospheric general circulation models (AGCMs) from the HAPPI Tier-1 experiments (Mitchell et al., 2017).

All forcings scenarios are available in the four AGCM simulations to do the comparison except for GHG-only scenario. These model ensembles are available with ≥100 members per year with initial condition perturbations however; we have used 98 members per year to compare with HadRM3P results. The basic information about these four AGCMs is given at Supplementary Table S3, while more details and evaluation of these models is available in Chevuturi et al., (2018).

In order to quantify changes in the probability of occurrence of extreme rainfall event, we use Risk Ratio (RR), which is calculated as $RR = P_f / P_{cf}$ (NAS, 2016). Here P_f denotes the probability of the event in factual climate including climate change (ACT, HAPPI 1.5 and HAPPI 2.0) and P_{cf} denotes the probability of an event of the same magnitude in a counterfactual climate without anthropogenic climate change (NAT).

But, in case of RR for GHG-only scenario, it is calculated with regard to ACT instead of NAT. We quantified the changes in the RRs for four event thresholds during MAM and JJAS with return period of 10, 20, 50 and 100 year over the four sub-regions of Bangladesh.

In case of the model results, we have large enough an ensemble to calculate the probabilities of occurrence (P) of the event in question explicitly by means of the different forcing scenarios. For example, suppose a 200 mm/day rainfall event has a P_{actual} of 50 years and a $P_{natural}$ of 100 years. The resulting change of probability of that event would simply be a doubling (RR= 2) due to the change in forcing.

To calculate the upper and lower limits of the uncertainty of RR we have used the following formula (based on error propagation model for independent contributors):
Upper limit of RR uncertainty = $\sqrt{(a^2 + c^2)}$; and
Lower limit of RR uncertainty = $\sqrt{(b^2 + d^2)}$
Where, a = upper limit of uncertainty of P_{ACT}, b = lower limit of uncertainty of P_{ACT},
c = upper limit of uncertainty of P_{NAT}, d = lower limit of uncertainty of $P_{NAT.}$

5.3. Results and Discussion

5.3.1. Model Evaluation

In Figure 5.1, seasonal cycles of 5-day rainfall as in the simulations of model ensembles under five different forcing scenarios (ACT, NAT, GHG-only, HAPPI 1.5 and HAPPI 2.0) and two observations (APHRODITE and CPC) are shown.

The coloured lines represent the ensemble means, with light-coloured shading representing the 10-90% percentile ranges (only shown for ACT model ensemble and the observations). The seasonal cycles of 5-day rainfall from the different model ensembles are adequately representative of the observed seasonal cycles. Most of the observed rainfall is found to be within the 10-90% confidence intervals of the model data. We find an early monsoon onset in the model simulations, which is also reported in previous studies (e.g., in Caesar et al., 2015; Fahad et al., 2017; Janes and Bhaskaran, 2012).

However, JJAS rainfall is underestimated by 25-50% depending on the observational dataset and sub-regions. This bias is higher (up to 50% dry bias) in the wetter sub-regions of 2 and 4 (Figs. 5.1b & d) and lower (up to 30% dry bias) in the drier sub-regions of 1 and 3 (Figs. 5.1a & c). Underestimation of JJAS rainfall is reported in other model based studies over Indian monsoon region (Goswami et al., 2014; Kumar and Dimri, 2019; Saha et al., 2014) and specifically in Bangladesh (Caesar and Janes, 2018; Islam, 2009; Macadam and Janes, 2017).

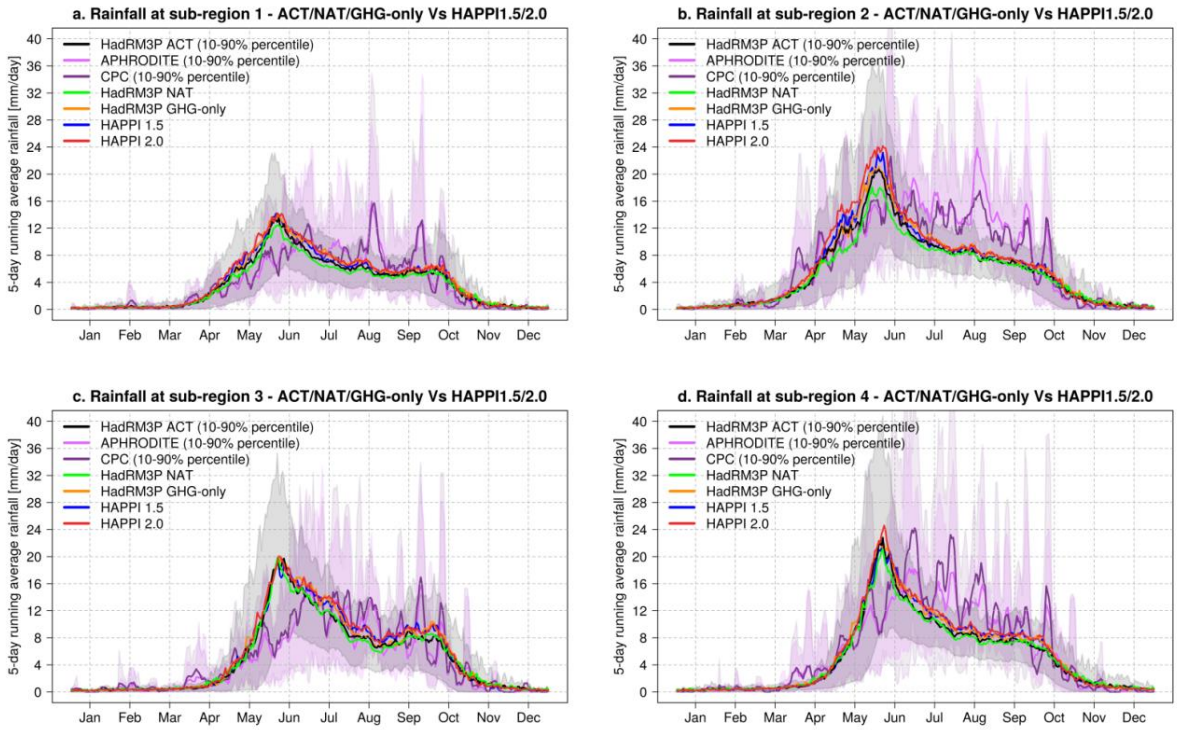


Figure 5.1: Seasonal cycles of five day mean rainfall under different forcing scenarios over the four sub-regions of Bangladesh. The ACT (black), NAT (green) and GHG-only (orange), HAPPI 1.5 (blue) and 2.0 (red) ensembles are compared with the observations from APHRODITE (dark purple) and CPC (dark purple). The model adequately captures the seasonal cycle of rainfall compared to observation but underestimates monsoon rainfall. Only over sub-region 2, rainfall is clearly shifting from NAT to ACT, from ACT to GHG-only, from ACT to HAPPI 1.5 and from HAPPI 1.5 to 2.0 forcing scenarios.

The bias is apparently present in all model scenarios used in this study; hence it is unlikely to affect the comparison between model scenarios. We also note that the signal of the change due to the changing climate is relatively small in comparison to the total rainfall. Therefore, the model is considered fit for purpose in assessing the potential impacts of climate change on extreme rainfall events. The differences between the forcing scenarios throughout the seasonal rainfall cycle are discussed below.

5.3.2. Impact of Climate Change and Aerosol Reduction on Seasonal Mean Rainfall

Our results suggest that changes in mean rainfall due to global warming are significant for both MAM and JJAS, and that aerosols play an important role in determining the magnitude of future changes (Figs. 5.2 & 5.3).

Based on PC, these changes are particularly evident during MAM, yet a smaller PC during JJAS can still have a significant impact given the magnitude of rainfall. Relative changes between pairs of forcing scenarios show large spatial variability over Bangladesh and the wider central South Asia region, although they suggest a general wetting trend across Bangladesh for both 1.5°C and 2.0°C warmer worlds.

During MAM, results show a non-linear response to temperature change in the PC over the eastern part of South Asia (Figs. 5.2a, b, & c) that is likely to be caused at least in part by the response for aerosols in Fig. 5.2d. The present-day ACT PC relative to NAT indicates that mean MAM rainfall is reduced by 15-30% over the eastern parts of South Asia and increased by 15-25% over the northern parts Bangladesh (Fig. 5.2a). Figure 5.2d shows the spatial distribution of the "omitted" aerosol induced rainfall over the South Asia region. Once aerosol levels drop to one-third of its current values (following the RCP2.6 protocol, IPCC, 2013), an increase of up to 20% in MAM rainfall is very likely to happen over most parts of South Asia region. Associated with this increased rainfall, PC relative to ACT in HAPPI 1.5 increases up to 20% over South Asia (Fig. 5.2b), with Bangladesh being the region where the aerosol effect dominates the total change (Figs. 5.2f & h).

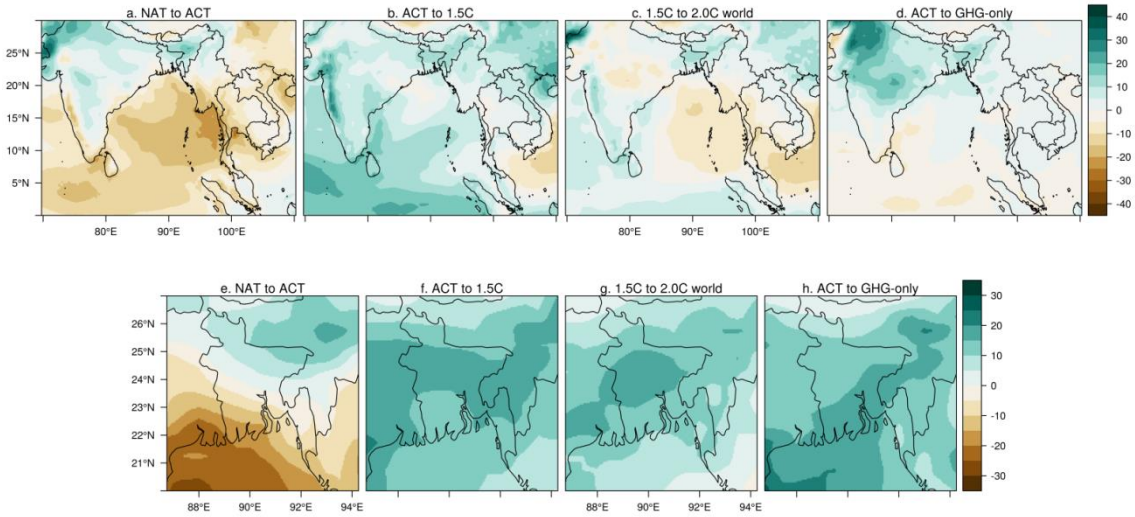


Figure 5.2: Percentage change (PC) in MAM mean rainfall between different forcing scenarios. The top row (panels a-d) shows the regional PC over central parts of the South Asia. a. ACT rainfall PC relative to NAT over SA b. ACT rainfall PC relative to HAPPI 1.5°C over SA c. HAPPI 1.5°C rainfall PC relative to HAPPI 2.0°C over SA d. ACT rainfall PC relative to GHG-only. Bottom row (panels e-h) shows PC in the same way but over Bangladesh. The four boxes (1-4) on top of the panel e represent the four sub-regions of Bangladesh.

Across Bangladesh, our results indicate that MAM rainfall increases approximately linearly with temperature, suggesting a relevant role for thermodynamic effects and perhaps a smaller role for dynamic changes as far as our HadRM3P model results are concerned. By linear response, we meant steady and gradual increase in the climate change impact on rainfall from one forcing scenario to another due the warming effects starting from NAT to ACT, ACT to HAPPI 1.5 and HAPPI 1.5 to HAPPI 2.0.

The additional warming effects in HAPPI 2.0 increase the mean MAM rainfall by an extra 10-20% over Bangladesh (Fig. 5.2g), in contrast to other parts of Asia. We note that our conjectures are speculative at this point, yet likely based on established research into monsoon dynamics (e.g., Bollasina et al. 2011).

Using other RCM projections (based on RCP8.5), Fahad et al. (2017) pointed out that MAM mean rainfall may increase by up to 20% relative to their baseline period (1971–2000) over the eastern mountainous region of Bangladesh, in line with our results for 1.5 and 2.0°C warming. However, the fact that the northern parts of India show very non-linear behaviour with regard to rainfall PC in response to the combined GHG and aerosol-related radiative forcing (Figs. 5.2a-d) is indicative of circulatory, dynamic shifts with stronger warming.

The PC of mean JJAS rainfall (Fig. 5.3a) in ACT relative to NAT indicates a weakening monsoon over central India and strengthening of the monsoon over Bangladesh and north-east India (10-15% increase). Evidence for reduced JJAS rainfall amounts over the last few decades in South Asia region is also found in the observational records (Bollasina et al., 2011; Srivastava et al., 2010; Turner and Annamalai, 2012; Wang et al., 2012).

In contrast, the CMIP5 models simulate about 2.3% increase in rainfall per degree of warming for the Indian summer monsoon (Menon et al., 2013) due to an increase in moisture availability in a warmer world. These conflicting results can be attributed to an underestimated aerosol effect in many CMIP5 models. Subsampling those models that include indirect aerosol effects helps to resolve the discrepancy (Bollasina et al., 2011; Turner and Annamalai, 2012).

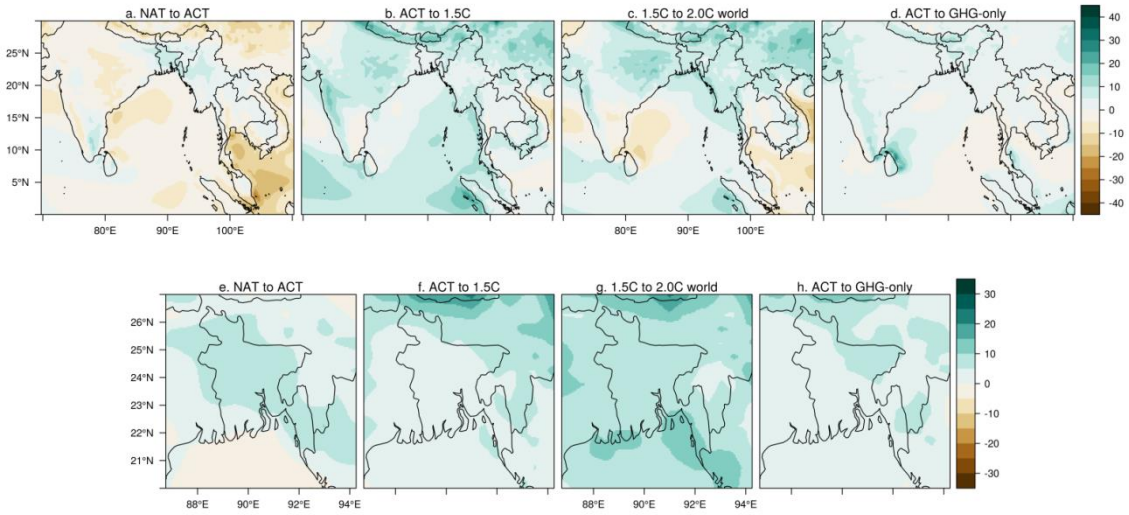


Figure 5.3: **Same as Fig. 5.2, but for JJAS rainfall PC. This figure shows that the apparently non-linear response between panels of a, b, and c (or, e, f, g) can be explained by the response for GHG-only (anthropogenic aerosols reduced to pre-industrial levels) in the panel d (or, h).**

The most important change in the PC occurs in HAPPI1.5 relative to ACT (Fig. 5.3b). Comparing HAPPI 1.5 and 2.0, we find an additional increase in mean JJAS rainfall but of lower magnitude (a further 10 to 20% increase; Fig. 5.3c). We find a very strong drying tendency during JJAS due to anthropogenic aerosols over most parts of South Asia (Fig. 5.3a). Correspondingly, the "committed" rainfall increase, which will be realised once aerosol emissions are reduced (Fig. 5.3d), is in the order of 15-30%.

This means that the observed drying is entirely caused by the aerosols that have overcompensated, the GHG induced rainfall increase. In Bangladesh (Figs. 5.3e-h), the aerosol effect is less strong and GHG induced intensification of summer monsoon rainfalls have already increased the risk of more intense rain. The Standardized Precipitation Index (SPI) analysis for the pre-monsoon and monsoon seasons (Supplementary Figs. 5S1 & 2) corroborates our results from the PC analysis.

In addition to PC and SPI analyses, we looked at the absolute rainfall (Figs. 5.4 & 5.5) for all five forcing scenarios during MAM and JJAS (median, as well as the 25-75th percentiles of seasonal mean rainfall) to explain the variability in the mean of absolute rainfall relative to the change between scenarios over the four sub-regions in Bangladesh (for locations of the sub-regions, see boxes in Figs. 5.2e & 5.3e). Changes in mean absolute rainfall are much more pronounced over sub-regions 1 and 2, where both MAM and JJAS rainfall exhibit clear shifts from one forcing to another forcing scenario (Fig.5. 4).

On the other hand, over sub-regions 3 and 4, only JJAS rainfall exhibited a robust shift (Fig. 5.5 b & d). The absolute aerosol effect is strongest in summer during JJAS, yet the relative change is smaller which is in line with lower rainfall PC as discussed above. Most importantly, aerosols play a dominant role in all sub-regions and seasons, except for MAM rainfall over sub-region 3 and 4. Despite more effective aerosol removal from the atmosphere by means of wet deposition during JJAS, high regional emission rates prevent drastic reductions of the aerosol optical depth. Consequently, direct and indirect aerosol effects, accompanied by feedbacks such as reduced lapse rate, reduced boundary layer turbulence, or a modified land-sea circulation, remain to be a potent driver for changing monsoonal rainfall amounts. For future warming scenarios of HAPPI 1.5 and HAPPI 2.0 compared to ACT, we find robust linear increase in (absolute) rainfall in almost all sub-regions and seasons. We notice a persistent change with increase in absolute mean rainfall from ACT to HAPPI 1.5 and HAPPI 1.5 to HAPPI 2.0. Conversely, we find no clear shifts between NAT, ACT and HAPPI 1.5 during MAM over sub-region 3 and 4 (Figs. 5.5a & c).

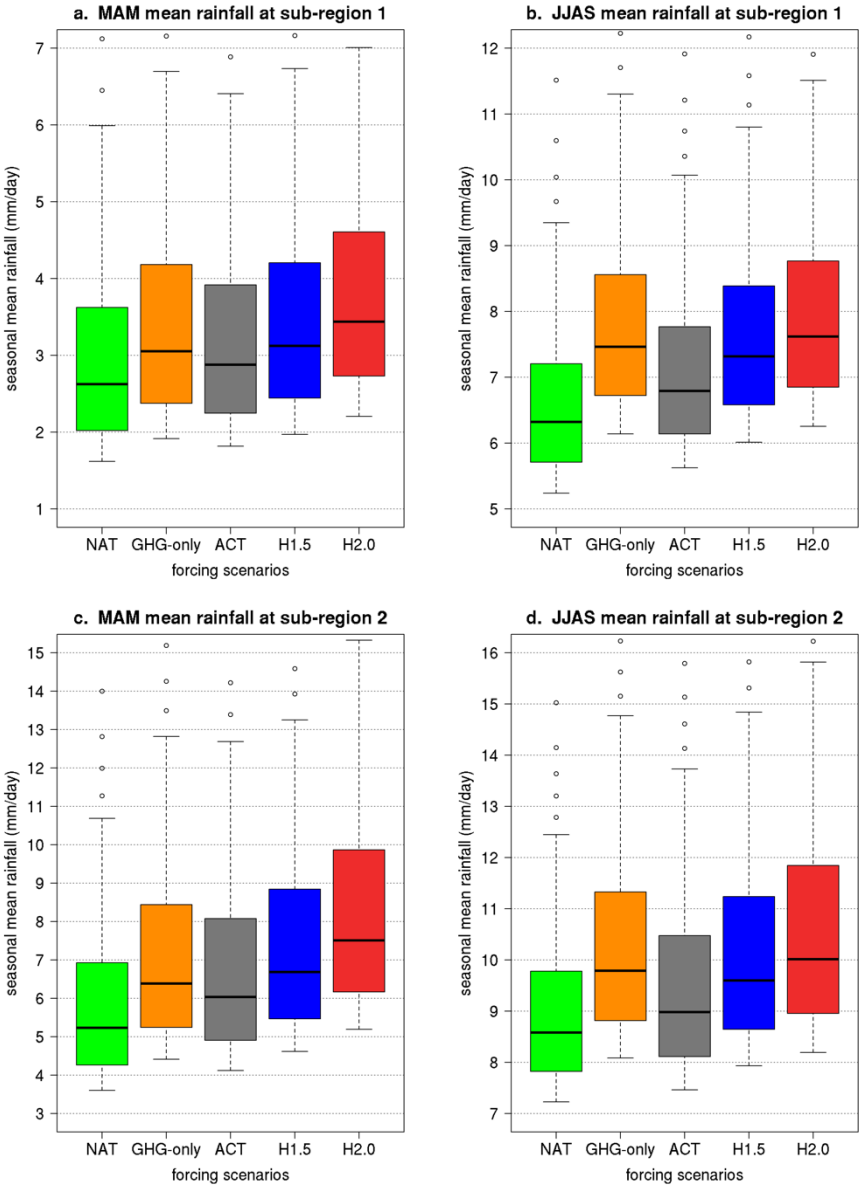


Figure 5.4: **Seasonal mean rainfall in MAM (left column) and JJAS (right column) over the sub-regions 1 and 2 (top and bottom row) of Bangladesh. Green, orange, grey, blue and red colours represent NAT, GHG-only, ACT, HAPPI 1.5 and HAPPI 2.0 ensembles respectively. Each panel has different y-scale range to clearly indicate the details of changes in the median values between different model ensembles. The horizontal black line in each box indicates the median value, the bottom and top limits of the box represents the 25th and 75th percentiles respectively. The figure shows that aerosol impacts over both sub-regions 1 and 2 are larger in MAM dry season than that in JJAS wet season.**

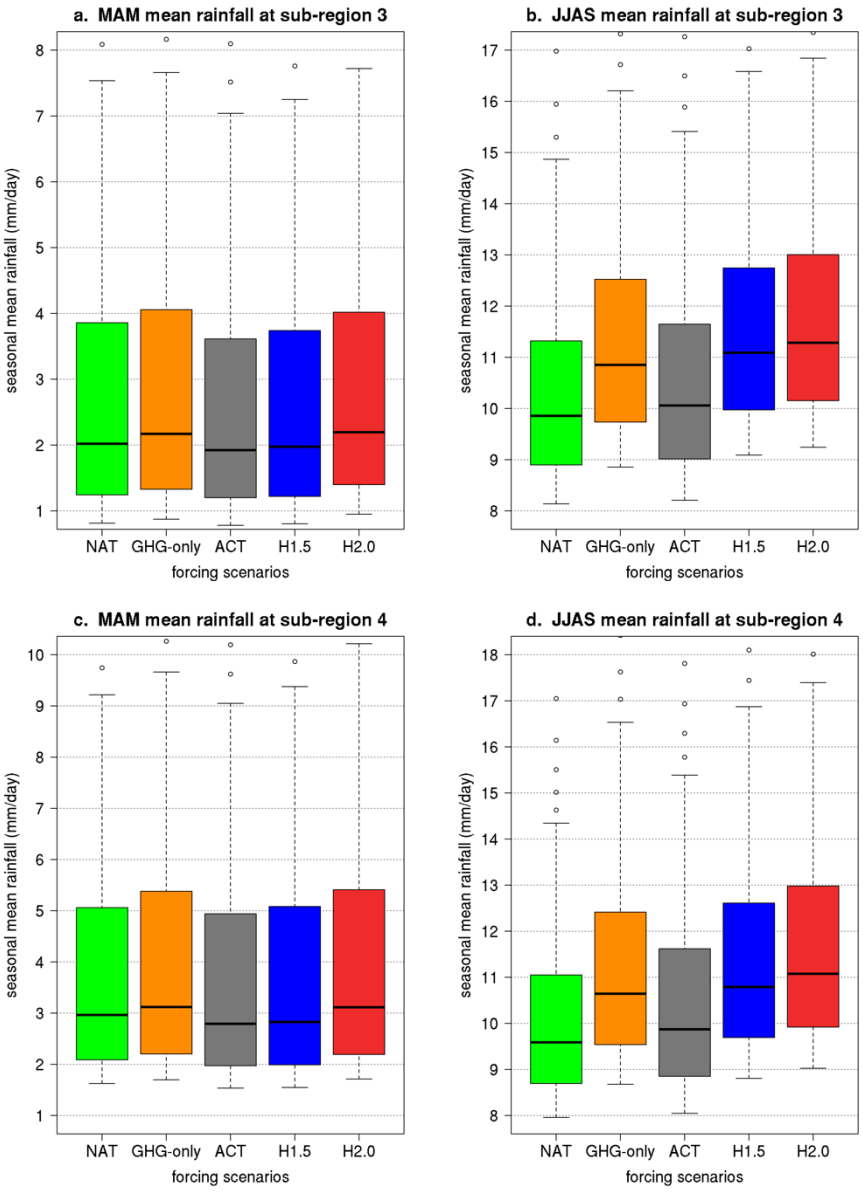


Figure 5.5: Same as Fig. 5.4, but for sub-regions 3 and 4. During MAM over both sub-regions 3 and 4, aerosol effects repress the mean rainfall change between NAT and ACT (i.e., ACT rainfall is lower than NAT). On the other hand, during JJAS over both sub-regions 3 and 4, with lesser aerosol masking effects, ACT has higher mean rainfall than NAT and GHG-only would have noticeably much higher mean rainfall.

While aerosol effects are consistent with those in other regions, the GHG induced rainfall is hampered, likely due to dynamic changes such as a delayed onset of the monsoon in response to warming (Bollasina et al., 2011; Zhao et al., 2019).

The proximity to the Indian Ocean may also be a contributing factor. Even though the atmosphere can hold more moisture, the slower ocean warming stabilises the atmosphere over sea in the same way aerosols stabilise the atmosphere over land. Impact of climate change and aerosol reduction on seasonal mean rainfall (as in PC, SPI and absolute) is in agreement with the findings in the seasonal cycles (Fig. 5.1) presented before. As shown in Fig. 5.1, the monsoon onset in sub-region 3 and 4 (Figs. 5.1c & d) does not change notably under different forcing scenarios as far as 5-day rainfall is concerned.

Otherwise, the aerosol and GHG induced response is consistent with the conclusions based on the spatial maps across the four sub-regions. Sub-regions 1 and 2 show considerable changes in rainfall strength during MAM, with an earlier onset in the HAPPI 2.0 scenario over sub-region 2. The most pronounced change is simulated at the peak of monsoon season, in early June over sub-region 2, with an associated increase in magnitude of almost one-third between NAT and HAPPI 2.0. It is noteworthy that this increase in rainfall is very linear with progressively warmer climate conditions (Fig. 5.1b).

5.3.3. Extreme Rainfall Events

An analysis of changes in extreme rainfall events suggests that Bangladesh is likely to experience significantly higher magnitude of 1 and 5-day rainfall events (Figs. 5.6-5.9 and 5S3-5S6) during both pre-monsoon and monsoon seasons across all sub-regions for a 1.5°C change. The only exceptions included MAM rainfall events over sub-region 4 (Fig. 5.7b) and JJAS rainfall events over sub-region 3 (Fig. 5.9a).

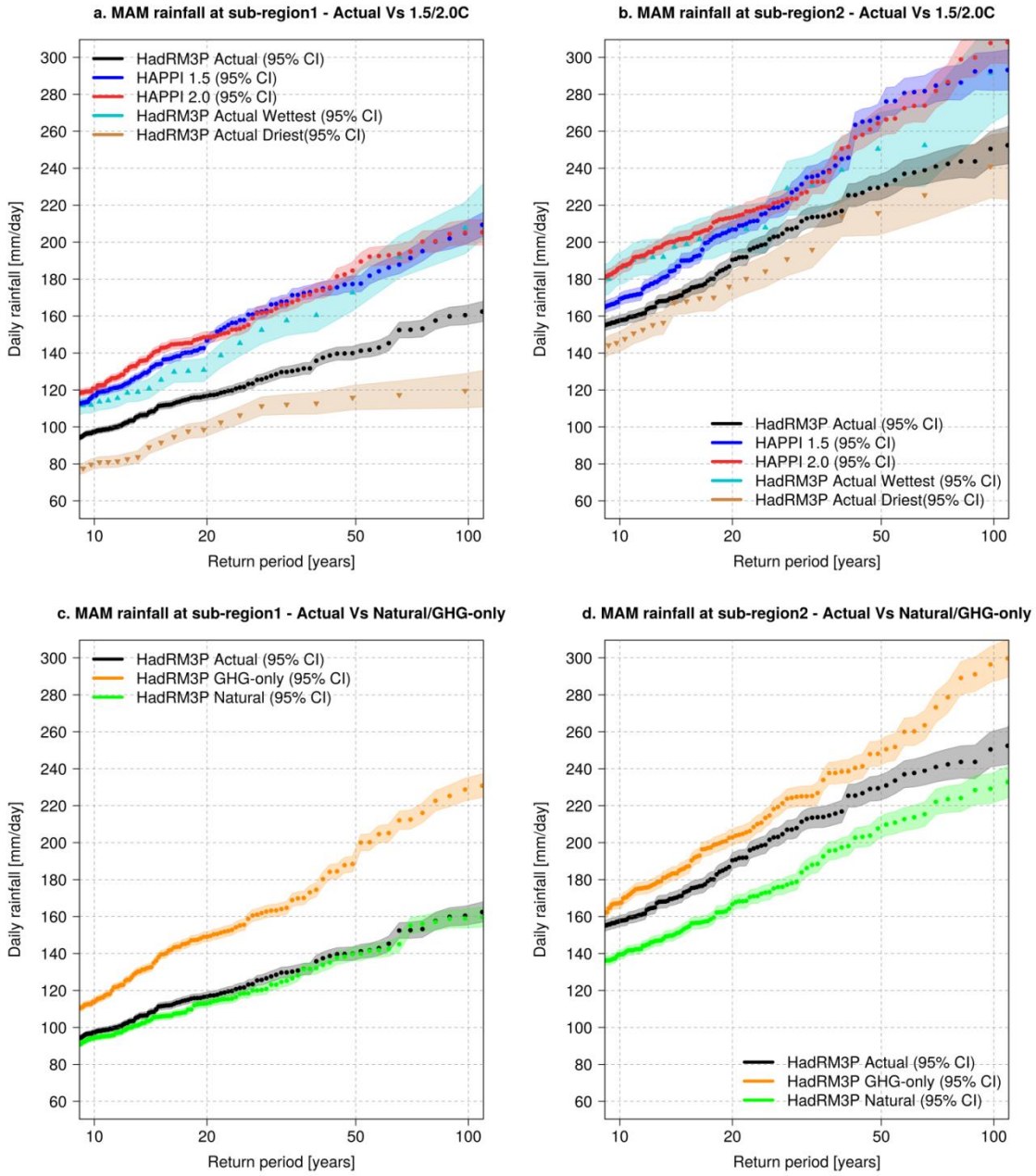


Figure 5.6: **Return time plots for MAM daily rainfall under different forcing scenarios over the sub-regions 1 and 2 of Bangladesh. The ACT (black), ACT highest (sky-blue), ACT lowest (grey), NAT (green) and GHG-only (orange) ensembles are compared with the HAPPI 1.5 (blue) and HAPPI 2.0 (red) ensembles. Anthropogenic warming effects have not strongly influenced the present-day risks of extreme MAM rainfall over sub-region 1 (Fig. 5.6a). With a 1.5 or 2.0 degrees' world, this sub-region might see extreme rainfall events with four-fold higher risks.**

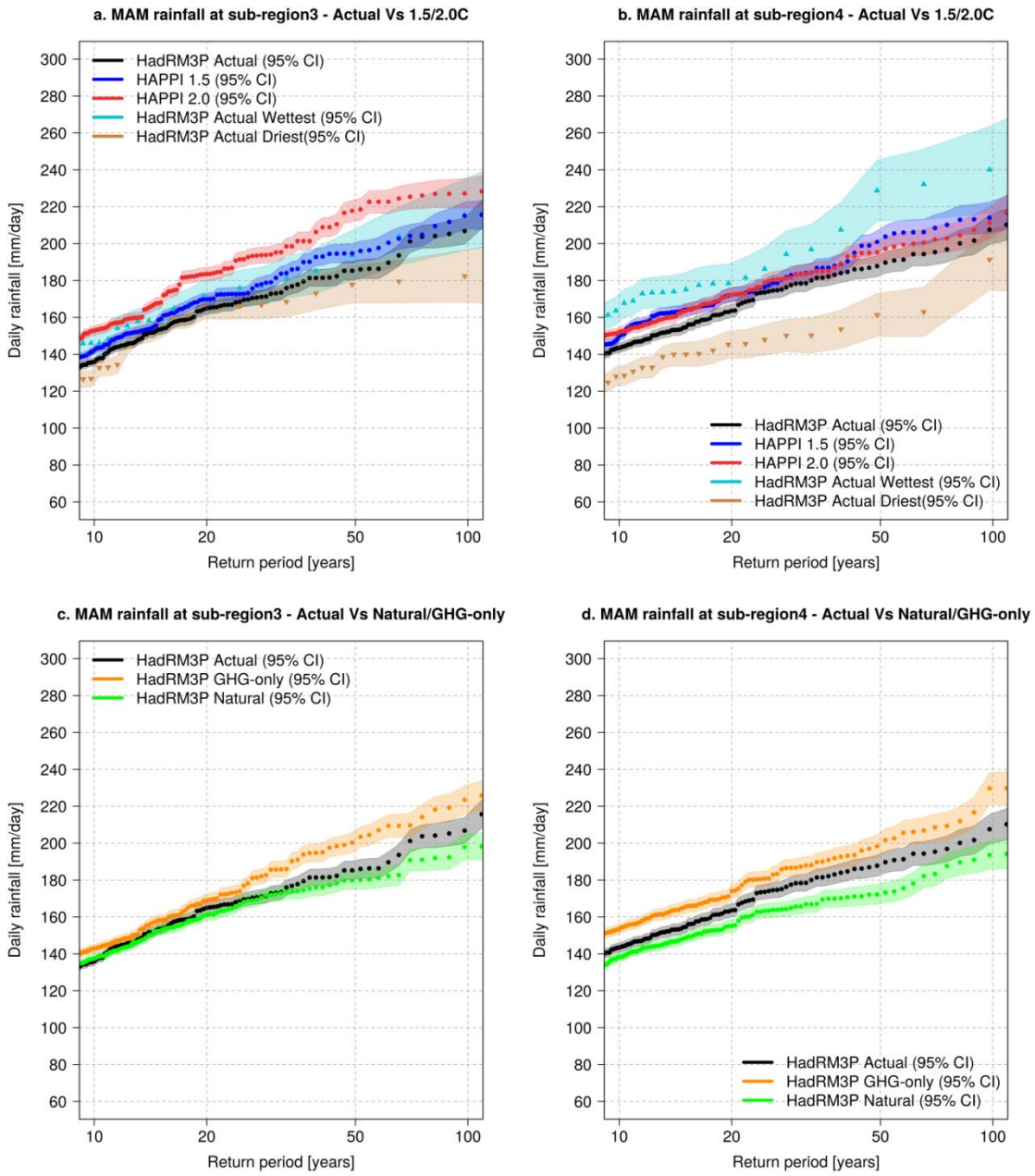


Figure 5.7: Same as Fig 5.6, but showing return time plots for MAM daily rainfall under different forcing scenarios over the sub-regions 3 and 4 of Bangladesh.

In contrast, changes between HAPPI 1.5 and HAPPI 2.0 are only significant in JJAS over sub-regions 1 and 2 (Figs. 5.8a & b). Overall, the signal-to-noise ratio is higher across all sub-regions, during JJAS compared to that during MAM. During MAM, the highest and lowest signal-to-noise ratio is over sub-region 1 and 3, respectively (Figs. 5.6a & 5.7a).

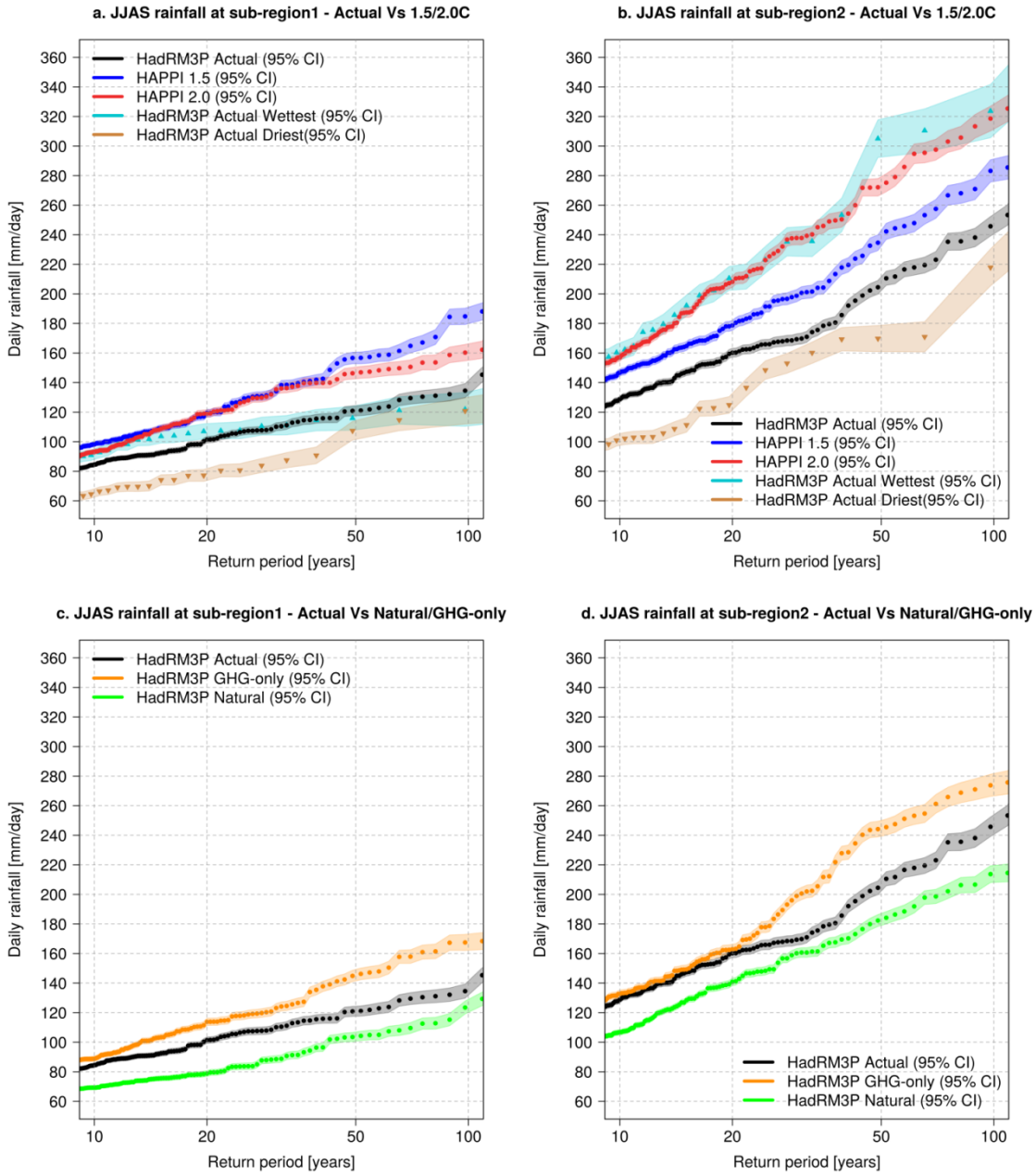


Figure 5.8: **Return time plots for daily rainfall during monsoon (JJAS) season in different forcing scenarios over the sub-regions of 1 and 2 of Bangladesh. The HadRM3P ACT (black), ACT highest (upper grey with upward triangles), ACT lowest (lower grey with downward triangles), NAT (green) and GHG-only (orange) ensembles are compared with the HAPPI 1.5 (blue) and 2.0 (red) ensembles. The most significant changes in the risks of extreme monsoon rainfall take place in the sub-region2, which is already the wettest part of Bangladesh.**

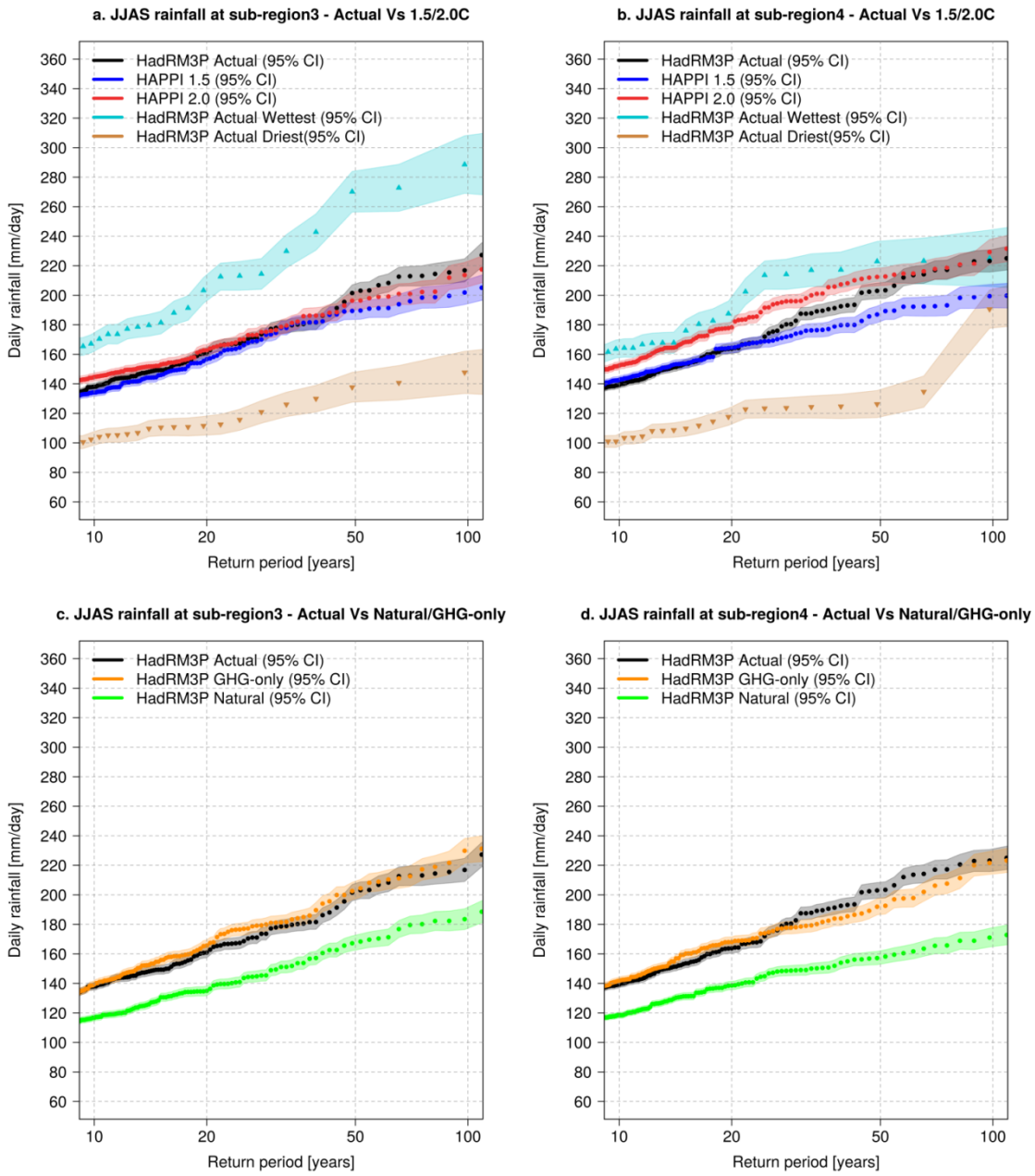


Figure 5.9: Same as Fig 5.8, but showing return time plots for daily rainfall during monsoon (JJAS) season in different forcing scenarios over the sub-regions of 3 and 4 of Bangladesh.

On the other hand, during JJAS, we find the highest and lowest signal-to-noise ratio is over sub-region 3 and 1, respectively (Figs. 5.9a & 5.8a). The lower the ratio, the more difficult it is to establish causality as natural variability due to ENSO or circulation

anomalies is higher. The most linear rainfall response to warming is simulated in sub-region 2 in MAM and JJAS (Figs. 5.6b & 5.8b), with aerosols masking approximately 50% of the increased risk with regard to 1-in-100-year NAT return time. Hence future rainfall in sub-region 2 continues to increase, with accelerated pace once aerosol levels drop significantly. Sub-region 1 is likely to receive more extreme rainfall as well with continued warming, with strong increases once aerosol levels drop. Sub-regions 1 and 2 are equally sensitive to aerosols, yet dynamic feedback processes might partially counter the thermodynamic increase in rainfall risk with continued warming.

Figures 5.10 and 5.11 give simple illustration for the change in risk ratios, which remarkably vary with seasons (pre-monsoon and monsoon) as well as locations (sub-regions of 1-4) and also indicate how aerosols impact risk ratios. Supplementary material of Table S4 and S5 present the risk ratios with associated uncertainty ranges for MAM and JJAS rainfall over four sub-regions, respectively. Figure 5.10 demonstrates that there is noticeable masking effect of aerosols during MAM that repress the change between NAT and ACT worlds at sub-region 1.

Hence, present-day risk for MAM rainfall event has not changed (see RR for ACT/NAT in Fig. 5.10a). But then the risk of extreme rainfall event with respect to 1-in-100-year NAT return time increase by a factor of 4 (with uncertainty range 2.0-7.0) in a 1.5°C world (see RR for HAPP1.5/NAT in Fig. 5.10a). In contrast, the aerosol masking effect during MAM is minimal at sub-region 2; leading to a robust change between NAT and ACT worlds (see RR for ACT/NAT in Fig. 5.10b).

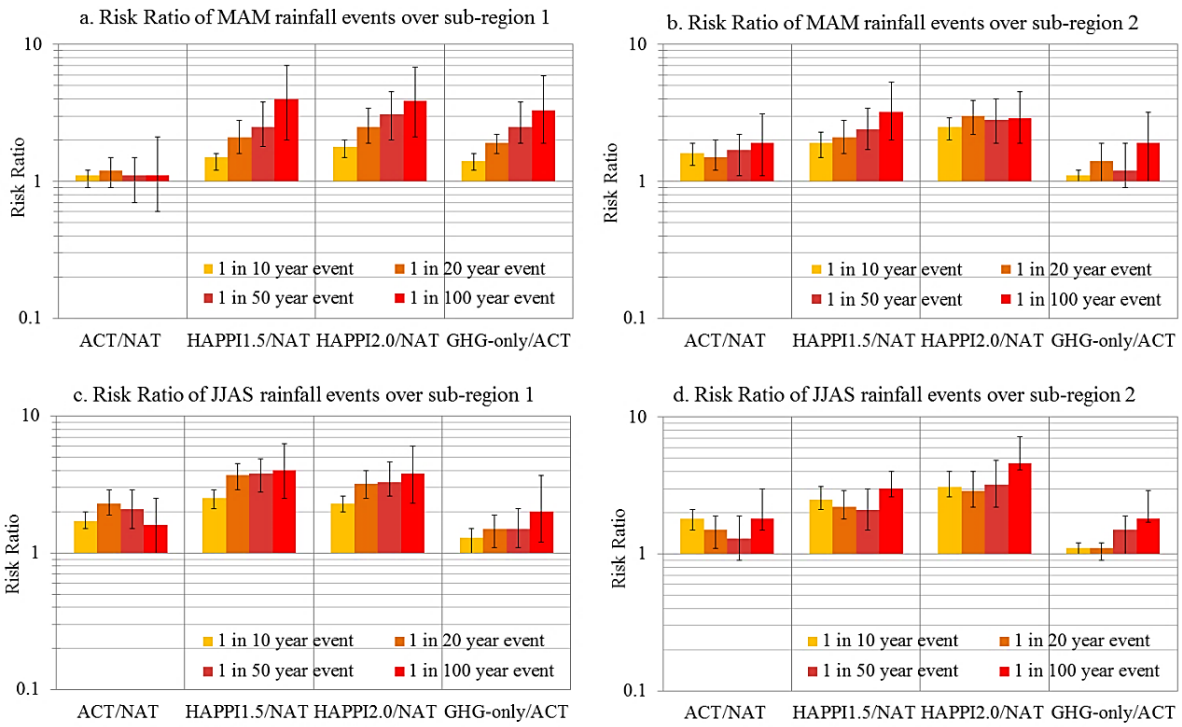


Figure 5.10: The risk ratios of four specific rainfall events with return periods of 10, 20, 50, and 100 years between ACT/NAT, HAPPI 1.5/NAT, HAPPI 2.0/NAT and GHG-only /ACT over the two northern sub-regions 1 and 2 during MAM (top two panels of a. & b.) and JJAS (bottom two panels of c. & d.). The error bars indicate the associated uncertainty range with 95% confidence level for individual event.

We find persistent increase in the RRs for JJAS extreme rainfall events at the sub-regions 2 and 4. At sub-region 2, risk of JJAS extreme rainfall event with respect to 1-in-100-year NAT return time increases 3-fold (with uncertainty range 1-4) in a 1.5°C world and then 4.6-fold (with uncertainty range 2.9-7.2) in a 2.0°C world (see RRs for HAPP1.5/NAT and HAPP2.0/NAT in Fig. 5.10d).

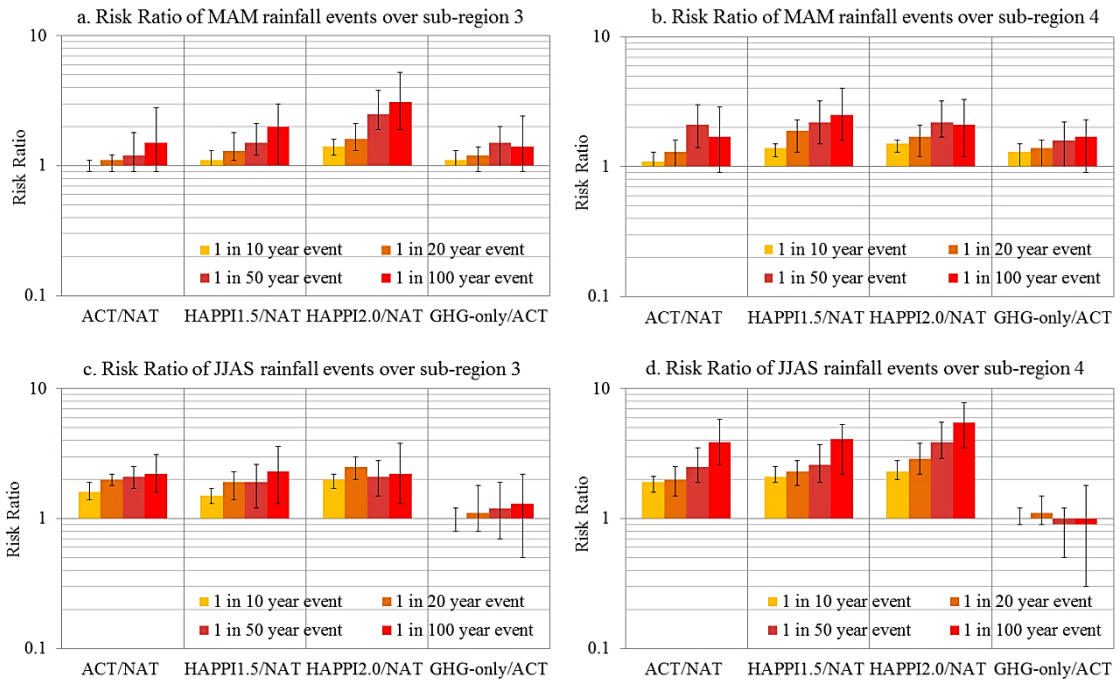


Figure 5.11: Same as Fig 5.10, but for MAM and JJAS risk ratios over the two southern sub-regions 3 and 4.

At sub-region 4 (Fig. 5.11d), where current risks of JJAS extreme rainfall events are already increased 3.9 times (with uncertainty range 2.6-5.8) with respect to 1-in-100-year NAT return time; the risk for similar event increases 4.1 times (with uncertainty range 2.2-5.3) in a 1.5°C world and 5.5 times in a 2.0°C world (with uncertainty range 3.5-7.8).

5.4. Conclusions

Results of the weather@home HadRM3P South Asia regional model suggest that both, 1.5°C and 2.0°C warming are projected to increase seasonal mean and extreme rainfall probabilities during the pre-monsoon and monsoon seasons across Bangladesh. The magnitude of change exceeds the current internal year-to-year variability in the associated sub-regions 1 and 2 during both pre-monsoon and monsoon seasons. These

increases are likely to be amplified by a reduction in aerosols, consistent with previous findings (e.g., Samset et al., 2018).

We find that there are large spatial variations in the patterns of changes in the relative risks of extreme rainfall in Bangladesh. Sub-regions 1 and 2 shows an enhanced susceptibility to aerosols during the pre-monsoon season; whereas, sub-regions 3 and 4 show a smaller aerosol sensitivity during the monsoon season. Aerosols have reduced the absolute daily rainfall amount by up to 1mm (~ 5-10%) during the monsoon season in sub-region 1 and 2, comparable to the simulated rainfall change in a future 2.0°C warming scenario. This is in line with a growing array of research that has shown that anthropogenic aerosols play a substantial role in modulating the strength of the monsoon in South Asia (Bollasina et al., 2011, 2013; Lau and Kim, 2010; Ramanathan et al., 2005).

As far as other regions in South Asia are concerned, our results imply that the present-day decline in the mean monsoon seasonal rainfall can be explained by the existing atmospheric aerosols impacts, which offsets the GHG-induced global warming effects. Future aerosol removal from the atmosphere will unmask the GHG induced rainfall increase with surprisingly fast changes in risk due to the non-linear nature of the imposed external forcing contributions (e.g., over sub-region 1 in pre-monsoon season). For that reason we emphasize that the impacts of aerosol reductions on the changing risks of extreme rainfall events should be considered for future risk assessments.

Considering the importance of the climate change impacts found in sub-region 1 and 2 for MAM and JJAS rainfall extremes, Figs. 5.12 and 5.13 demonstrate how robust the HadRM3P results are compared to four other HAPPI AGCMs of MIROC5, ETH_CAM4, CanAM4 and NorESM1 models. Similar comparisons for other sub-regions and seasons are presented at the supplementary material for brevity (in Figs. S7 - S12).

For MAM rainfall extremes over sub-region 1, HadRM3P, MIROC5 and NorESM1 models suggest increasing risks but ETH_CAM4 and CanAM4 models show increasing risks only for a 2.0°C warmer climate condition. MIROC5 model shows a linear progression of MAM rainfall risks, increasing from NAT to Act and then from ACT to 1.5° and 2.0°C warmer conditions (Fig. 5.12b). In contrast, HadRM3P model shows a non-linear change in the MAM rainfall risks with nearly no increase between NAT and ACT but then a drastic increase in warmer scenarios (Fig. 5.12a).

Since the other HAPPI AGCMs do not provide a GHG-only scenario, we can only infer causality of potential non-linear changes between the warming scenarios from HadRM3P model in this case. For JJAS rainfall extremes over sub-region2, all five models suggest increasing risks in warmer conditions (see Figs. 5.13a-e). However intensities of rainfall events vary within different models.

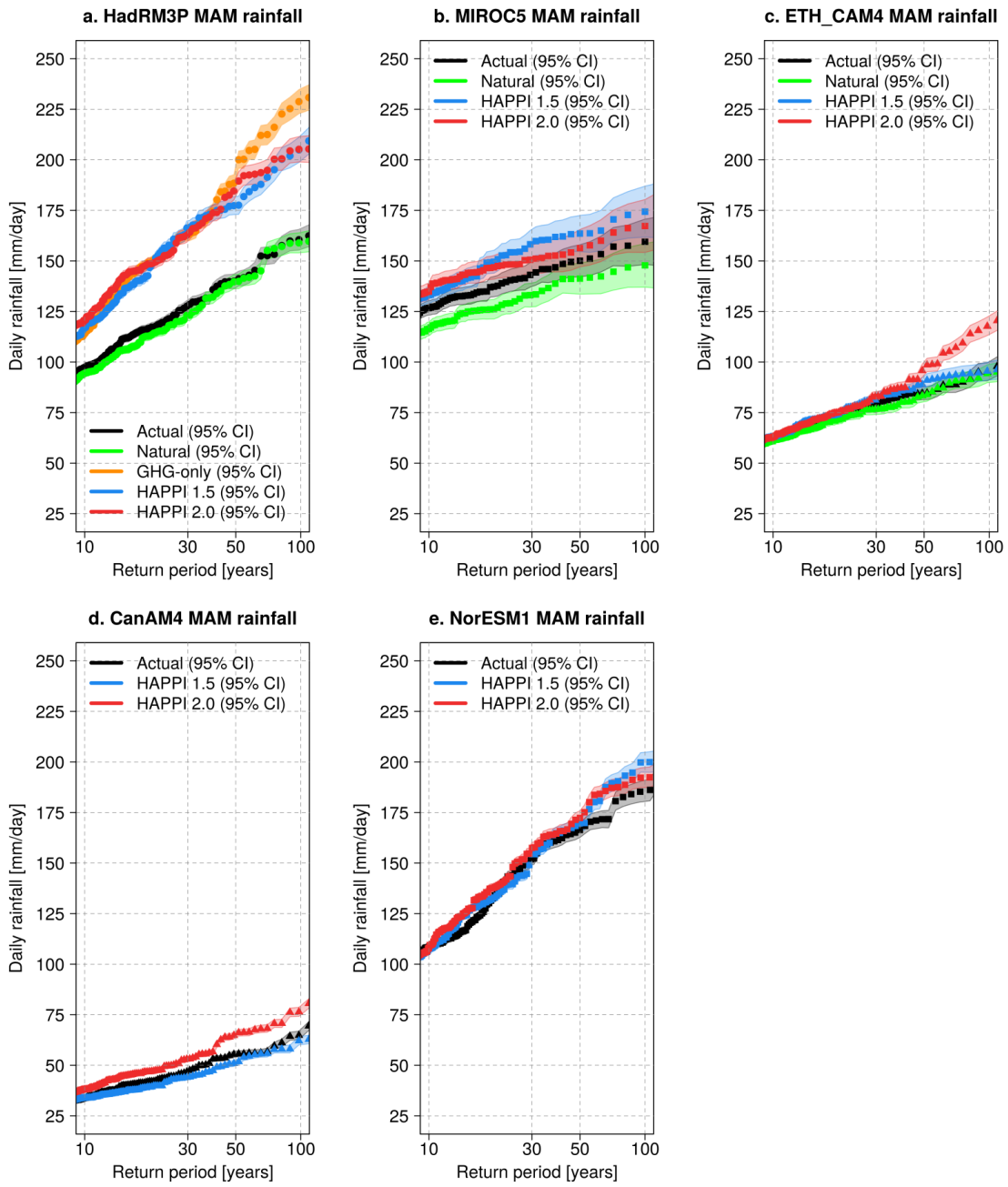


Figure 5.12: Comparative return periods (10-100 year events) of MAM daily rainfall (mm/day) over sub-region 1 during 1986-2015 as per (a) HadRM3P, (b) MIROC5, (c) ETH_CAM4, (d) CanAM4 and (e) NorESM1 models. ACT, NAT, GHG-only, plus 1.5°C and 2.0°C model ensembles are shown in black, green, orange, blue and red colours respectively.

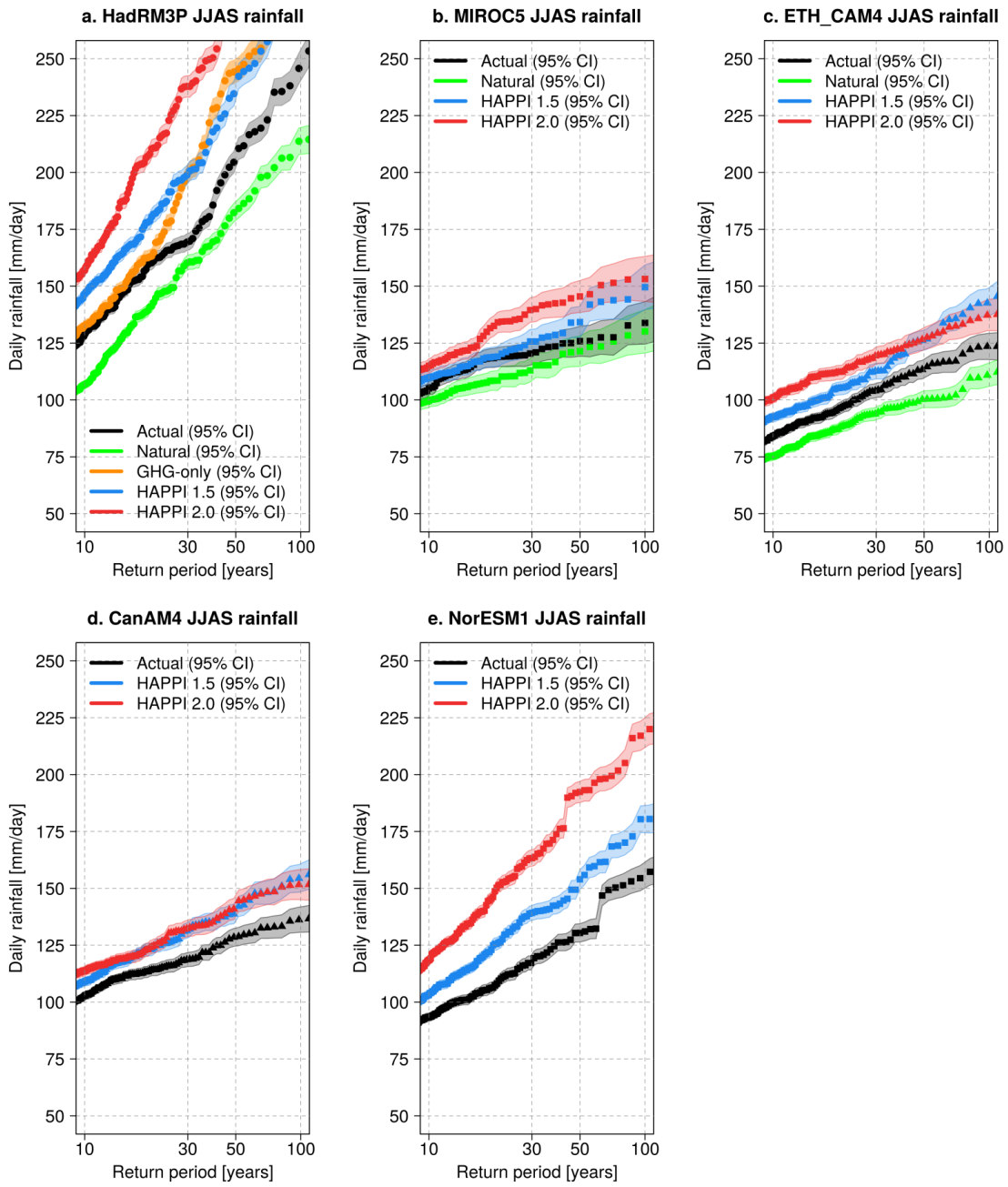


Figure 5.13: Comparative return periods (10-100 year events) of JJAS daily rainfall (mm/day) over sub-region 2 during 1986-2015 as per (a) HadRM3P, (b) MIROC5, (c) ETH_CAM4, (d) CanAM4 and (e) NorESM1 models. ACT, NAT, GHG-only, plus 1.5°C and 2.0°C model ensembles are shown in black, green, orange, blue and red colours respectively.

For JJAS rainfall extremes over sub-region 2, HadRM3P model results show better agreement with NorESM1 model in terms of both increasing risks and rainfall

intensities (compare Figs. 5.13a &e); probably because this model includes updated module for aerosols (Kirkevåg et al., 2013).

This study for the first time presents a multi-model assessment of both current and future changes in the risks of seasonal extreme rainfall events, considering anthropogenic climate change drivers of GHGs and aerosols, at sub-regional local scales in Bangladesh. These projected changes have important implications for agricultural yields and associated economic losses, particularly during the pre-monsoon season.

For example, at north-east Bangladesh, in 2017, pre-monsoon extreme rainfall caused the earliest flash flood since 2000. Consequent damage of nearly harvestable rice crop in turn, caused the highest price hike in the following year. Anthropogenic climate change drivers are found to make this extreme rainfall event twice as likely (Rimi et al., 2019b).

In contrast, during the monsoon season, property damage is more likely to occur when large inhabited areas are inundated on a regular basis. Finding of this study implies that policy-makers and relevant stakeholders not only need to take distinctively different regional responses in extreme rainfall into account, but also the non-linearity in the response.

Relying on observed changes can be deeply misleading, creating an unwarranted sense of security. Our study highlights that preparedness for more frequent extremes is key in the northern part of Bangladesh during both the pre-monsoon and the monsoon season.

While additional regional model experiments are needed to confirm the weather@home model results, our analysis of available data from other HAPPI GCMs point in the same direction for seasonal extreme rainfall events in Bangladesh. Similar findings are also reported for the larger South Asia region (e.g., Chevuturi et al., 2018; Lee et al., 2018). However, since they do not allow for a quantification of the aerosol effect, we call for more nuanced experiments in that regard in the future.

Data/Code availability

Observation data set of APHORODITE is available for download at http://aphrodite.st.hirosaki-u.ac.jp/products.html and CPC can be downloaded from https://climexp.knmi.nl/select.cgi?id=someone@somewhere&field=prcp_cpc_daily.
The additional four HAPPI AGCM simulation data can be accessed at http://portal.nersc.gov/c20c/data/. Analysis codes in R programming language can be made available upon request from the corresponding author.

Supplement

The supplement related to this article is available online at: [a web link will be provided once accepted for publication]

Author contributions

Ruksana H. Rimi's contribution towards this work was performed as part of her DPhil research project. Sihan Li and Sarah N. Sparrow prepared and distributed the computational simulations to generate the data used in the study onto the weather@home system. David C.H. Wallom manages operation of the

weather@home/climateprediction.net infrastructure which was used to generate the data. Karsten Haustein generated and extracted the weather@home HadRM3P model data. Md. Zahidul Abedin contributed to the discussion about social implications of the results. All results were analysed and plotted by Ruksana H. Rimi with advice from Myles R. Allen, Karsten Haustein, and Emily Barbour. The paper was written by Ruksana H. Rimi, with edits from all co-authors.

Competing interests

The authors declare that they have no conflict of interests.

Acknowledgments

We would like to thank the Met Office Hadley Centre PRECIS team for their technical and scientific support for the development and application of weather@home. We would like to thank our colleagues at the Oxford eResearch Centre for their technical expertise. We acknowledge the use of the observation datasets of APHRODITE and CPC. We would like to thank the HAPPI project team and the different modeling centers, who contributed to simulations. Finally, we would like to thank all the volunteers who have donated their computing time to climateprediction.net and weather@home.

Supplement of

"Risks of seasonal extreme rainfall events in Bangladesh under 1.5 and 2.0 degrees' warmer worlds – How anthropogenic aerosols change the story"

Ruksana H. Rimi et al.

Correspondence to: Ruksana H. Rimi (ruksana.rimi@ouce.ox.ac.uk)

Table S5.1: Basic information about the two observation data sets

Product Name	Product version	Spatial Resolution	Time Scale	Source/reference
APHRODITE	Monsoon Asia (MA) V1901	0.5°X 0.5°	1998-2015	Yatagai et al., 2012. Available at: http://journals.ametsoc.org/doi/pdf/10.1175/BAMS-D-11-00122.1
CPC	CPC daily rainfall	0.5°X 0.5°	1979-2016	Chen, M. and Xie, P. 2008. Available at: ftp://ftp.cpc.ncep.noaa.gov/precip/CPC_UNI_PRCP/GAUGE_CONUS/DOCU/Chen_et_al_2008_Daily_Gauge_Anal.pdf

Table S5.2: As per actual climate model ensemble during 2006-2015 - the wettest and driest two years over the four sub-regions.

	pre-monsoon season (MAM)		monsoon season (JJAS)	
Sub-regions	Wettest years	Driest years	Wettest years	Driest years
Sub-region 1 (north-west region)	2008, 2011	2009, 2014	2008, 2009	2013, 2014
Sub-region 2 (north-east region)	2008, 2015	2009, 2014	2008, 2012	2006, 2013
Sub-region 3 (south-west region)	2008, 2012	2009, 2014	2008, 2014	2011, 2013
Sub-region 4 (south-east region)	2008, 2015	2009, 2013	2008, 2014	2011, 2013

Table S5.3: Basic information about the four HAPPI AGCMs used in this study (adapted from Chevuturi et al., 2018)

Model Name	Organization	Spatial Resolution	Available Ensemble Members	Reference
Community Atmosphere Model 4-2 (ETH_CAM4)	ETH, Federal Institute of Technology; Zurich, Switzerland.	2° × 2° (96 ×144)	501	Neale et al., (2013)
Canadian Fourth generation atmospheric global climate model (CanAM4)	Canadian Centre for Climate Modelling and Analysis; Victoria, Canada.	T42 (64 ×128)	100	von Salzen et al., (2013)
Model for interdisciplinary research on climate 5 (MIROC5)	Atmosphere and Ocean Research Institute (AORId), University of Tokyo; Chiba, Japan. National Institute for Environmental Studies (NIES); Ibaraki, Japan. Japan Agency for Marine-Earth Science and Technology (JAMSTEC); Kanagawa, Japan.	150 × 150 km (128× 256)	100	Watanabe et al., (2010) Shiogama et al., (2014)
Norwegian earth system model 1 (NorESM1)	NorESM Climate modelling Consortium (NCC), Norway.	1.25×0.94∘ (192× 288)	125	Bentsen et al., (2013); Iversen et al.(2013); Kirkevåg et al. (2013)

Table S5.4: The risk ratios with associated uncertainty ranges (in brackets) for four MAM rainfall events.

Return periods	**Sub-region 1 (north-west region) – pre-monsoon season**			
	ACT/NAT	HAPPI1.5/NAT	HAPPI2.0/NAT	GHG/ACT
10 years	1.1	1.5	1.8	1.4
	(0.9-1.2)	(1.2-1.6)	(1.5-2.0)	(1.2-1.6)
20 years	1.2	2.1	2.5	1.9
	(0.9-1.5)	(1.6-2.8)	(1.9-3.4)	(1.6-2.2)
50 years	1.1	2.5	3.1	2.5
	(0.7-1.5)	(1.8-3.8)	(2.0-4.5)	(1.9-3.8)
100 years	1.1	**4**	**3.9**	**3.3**
	(0.6-2.1)	**(2.0-7.0)**	**(2.1-6.8)**	**(1.9-5.9)**
Return periods	**Sub-region 2 (north-east region) – pre-monsoon season**			
	ACT/NAT	ACT/NAT	ACT/NAT	ACT/NAT
10 years	1.6	1.9	2.5	1.1
	(1.3-1.9)	(1.5-2.3)	(2.0-2.9)	(1.0-1.2)
20 years	1.5	2.1	3	1.4
	(1.2-2.0)	(1.6-2.8)	(2.2-3.9)	(1.0-1.9)
50 years	1.7	2.4	2.8	1.2
	(1.1-2.2)	(1.7-3.4)	(1.9-4.0)	(0.9-1.9)
100 years	1.9	**3.2**	**2.9**	1.9
	(1.1-3.1)	**(2.0-5.3)**	**(1.9-4.5)**	(1.0-3.2)

Return periods	**Sub-region 3 (south-west region) – pre-monsoon season**			
10 years	ACT/NAT	HAPPI1.5/NAT	HAPPI2.0/NAT	GHG/ACT
	1	1.1	1.4	1.1
	(0.9-1.1)	(1.0-1.3)	(1.2-1.6)	(1.0-1.3)
20 years	1.1	1.3	1.6	1.2
	(0.9-1.2)	(1.1-1.8)	(1.3-2.1)	(0.9-1.4)
50 years	1.2	1.5	2.5	1.5
	(0.9-1.8)	(1.2-2.1)	(1.9-3.8)	(1.0-2.0)
100 years	1.5	2	**3.1**	1.5
	(0.9-2.8)	(1.0-3.0)	**(1.9-5.2)**	(0.9-2.4)
Return periods	**Sub-region 4 (south-east region) – pre-monsoon season**			
	ACT/NAT	HAPPI1.5/NAT	HAPPI2.0/NAT	GHG/ACT
10 years	1.1	1.4	1.5	1.3
	(1.0-1.3)	(1.2-1.5)	(1.3-1.6)	(1.0-1.5)
20 years	1.3	1.9	1.7	1.4
	(1.0-1.6)	(1.3-2.3)	(1.2-2.1)	(1.0-1.6)
50 years	2.1	2.2	2.2	1.6
	(1.4-3.0)	(1.5-3.2)	(1.6-3.2)	(1.0-2.2)
100 years	1.7	**2.5**	2.1	1.7
	(0.9-2.9)	**(1.6-4.0)**	(1.2-3.3)	(0.9-2.3)

Table S5.5: The risk ratios with associated uncertainty ranges (in brackets) for four JJAS rainfall events.

Return periods	**Sub-region 1 (north-west region) – monsoon season**			
	ACT/NAT	HAPPI1.5/NAT	HAPPI2.0/NAT	GHG/ACT
10 years	1.7	2.5	2.3	1.3
	(1.5-2.0)	(2.1-2.9)	(2.0-2.6)	(1.0-1.5)
20 years	2.3	**3.7**	**3.2**	1.5
	(1.9-2.9)	**(2.9-4.5)**	**(2.5-4.0)**	(1.1-1.9)
50 years	2.1	**3.8**	**3.3**	1.5
	(1.5-2.9)	**(2.8-4.9)**	**(2.6-4.6)**	(1.1-2.1)
100 years	1.6	**4**	**3.8**	2
	(1.0-2.5)	**(2.5-6.3)**	**(2.3-6.0)**	(1.2-3.7)
Return periods	**Sub-region 2 (north-east region) – monsoon season**			
	ACT/NAT	ACT/NAT	ACT/NAT	ACT/NAT
10 years	1.8	1.8	1.8	1.8
	(1.5-2.1)	(1.5-2.1)	(1.5-2.1)	(1.5-2.1)
20 years	1.5	1.5	1.5	1.5
	(1.1-1.9)	(1.1-1.9)	(1.1-1.9)	(1.1-1.9)
50 years	1.3	1.3	1.3	1.3
	(0.9-1.9)	(0.9-1.9)	(0.9-1.9)	(0.9-1.9)
100 years	1.8	1.8	1.8	1.8
	(1.0-3.0)	(1.0-3.0)	(1.0-3.0)	(1.0-3.0)

Return periods	**Sub-region 3 (south-west region) – monsoon season**			
	ACT/NAT	HAPPI1.5/NAT	HAPPI2.0/NAT	GHG/ACT
10 years	1.6	1.5	2	1
	(1.4-1.9)	(1.3-1.7)	(1.7-2.2)	(0.8-1.2)
20 years	2	1.9	2.5	1.1
	(1.8-2.2)	(1.4-2.3)	(2.0-3.0)	(0.8-1.8)
50 years	2.1	1.9	2.1	1.2
	(1.7-2.5)	(1.2-2.6)	(1.5-2.8)	(0.7-1.9)
100 years	2.2	2.3	2.2	1.3
	(1.6-3.1)	(1.3-3.6)	(1.3-3.8)	(0.5-2.2)
Return periods	**Sub-region 4 (south-east region) – monsoon season**			
	ACT/NAT	HAPPI1.5/NAT	HAPPI2.0/NAT	GHG/ACT
10 years	1.9	2.1	2.3	1
	(1.6-2.1)	(1.9-2.5)	(2.0-2.8)	(0.9-1.2)
20 years	2	2.3	**2.9**	1.1
	(1.5-2.5)	(1.8-2.8)	**(2.2-3.8)**	(0.9-1.5)
50 years	2.5	2.6	**3.9**	0.9
	(1.9-3.5)	(1.9-3.7)	**(2.9-5.5)**	(0.5-1.2)
100 years	**3.9**	**4.1**	**5.5**	0.9
	(2.6-5.8)	**(2.2-5.3)**	**(3.5-7.8)**	(0.3-1.8)

Supplementary Figures:

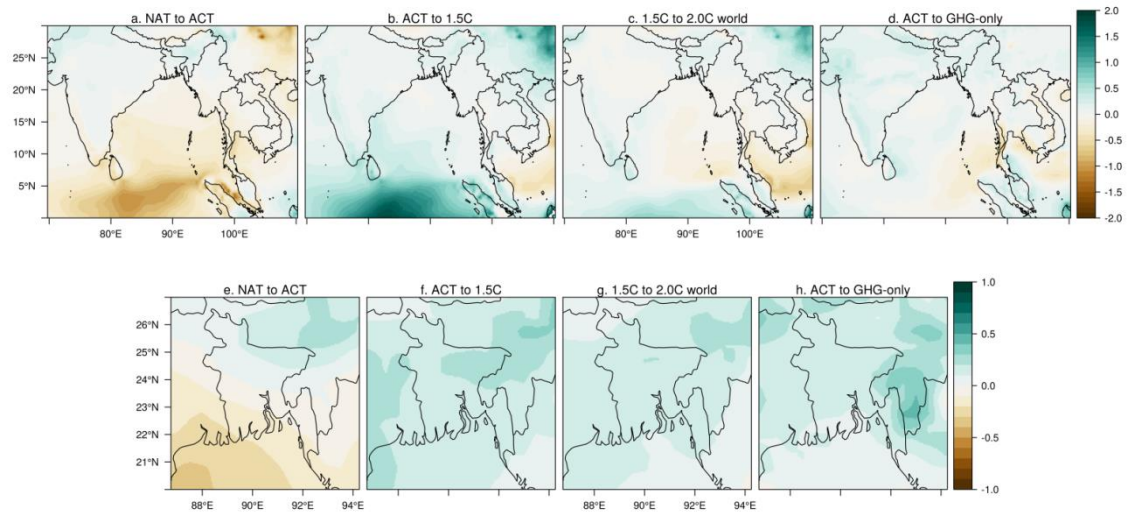


Figure S5.1: Relative change in SPI of MAM mean rainfall between different forcing scenarios. The top row (panels a-d) shows the regional SPI changes over central parts of the South Asia (SA) while, bottom row (panels e-h) shows the SPI changes over Bangladesh. The four boxes (1-4) on top of the panel e represent the four sub-regions of Bangladesh. a. ACT rainfall SPI relative to NAT over SA b. ACT rainfall SPI relative to HAPPI1.5 over SA c. HAPPI1.5 rainfall SPI relative to HAPPI 2.0 over SA d. ACT rainfall SPI relative to GHG-only over SA.

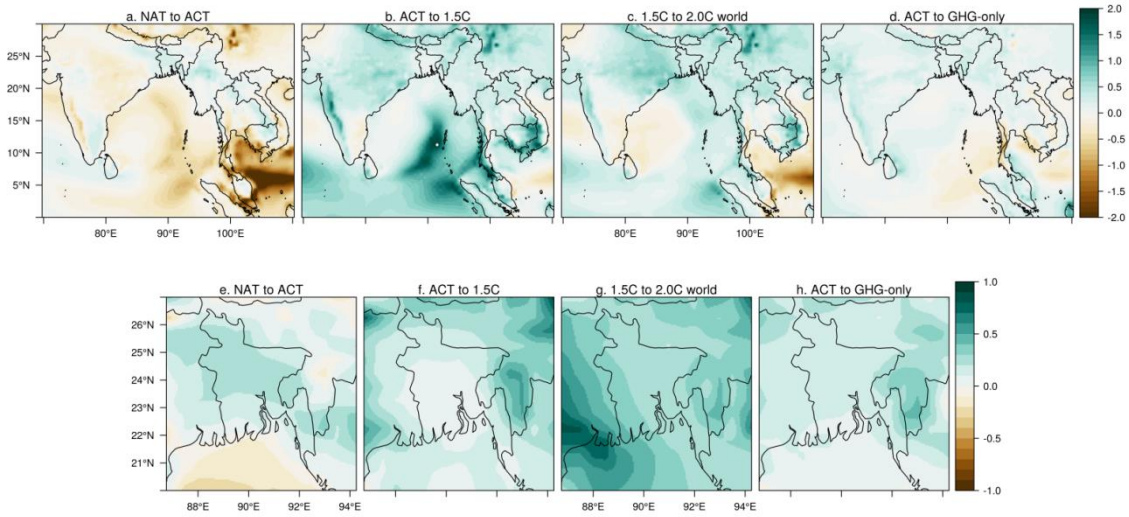


Figure S5.2: Same as Fig. S1, but for SPI changes in JJAS mean rainfall. This figure shows that the apparently non-linear response between panels of a, b, and c (or, e, f, g) can be explained by the response for aerosols in the panel d (or, h).

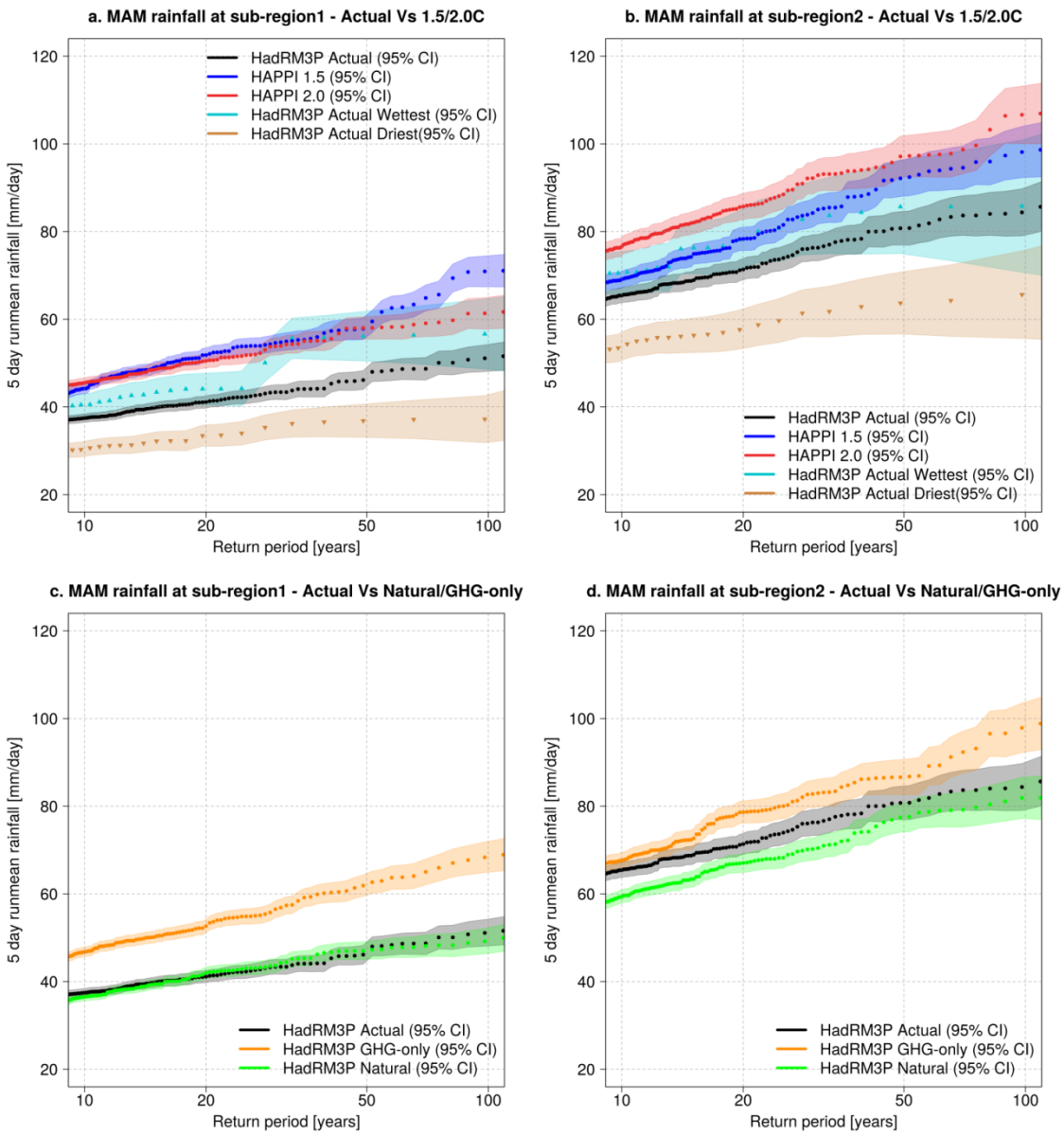


Figure S5.3: Return time plots for MAM five day mean rainfall under different forcing scenarios over the sub-regions 1 and 2 of Bangladesh. The ACT (black), ACT highest (sky-blue), ACT lowest (grey), NAT (green) and GHG-only (orange) ensembles are compared with the HAPPI 1.5 (blue) and HAPPI 2.0 (red) ensembles.

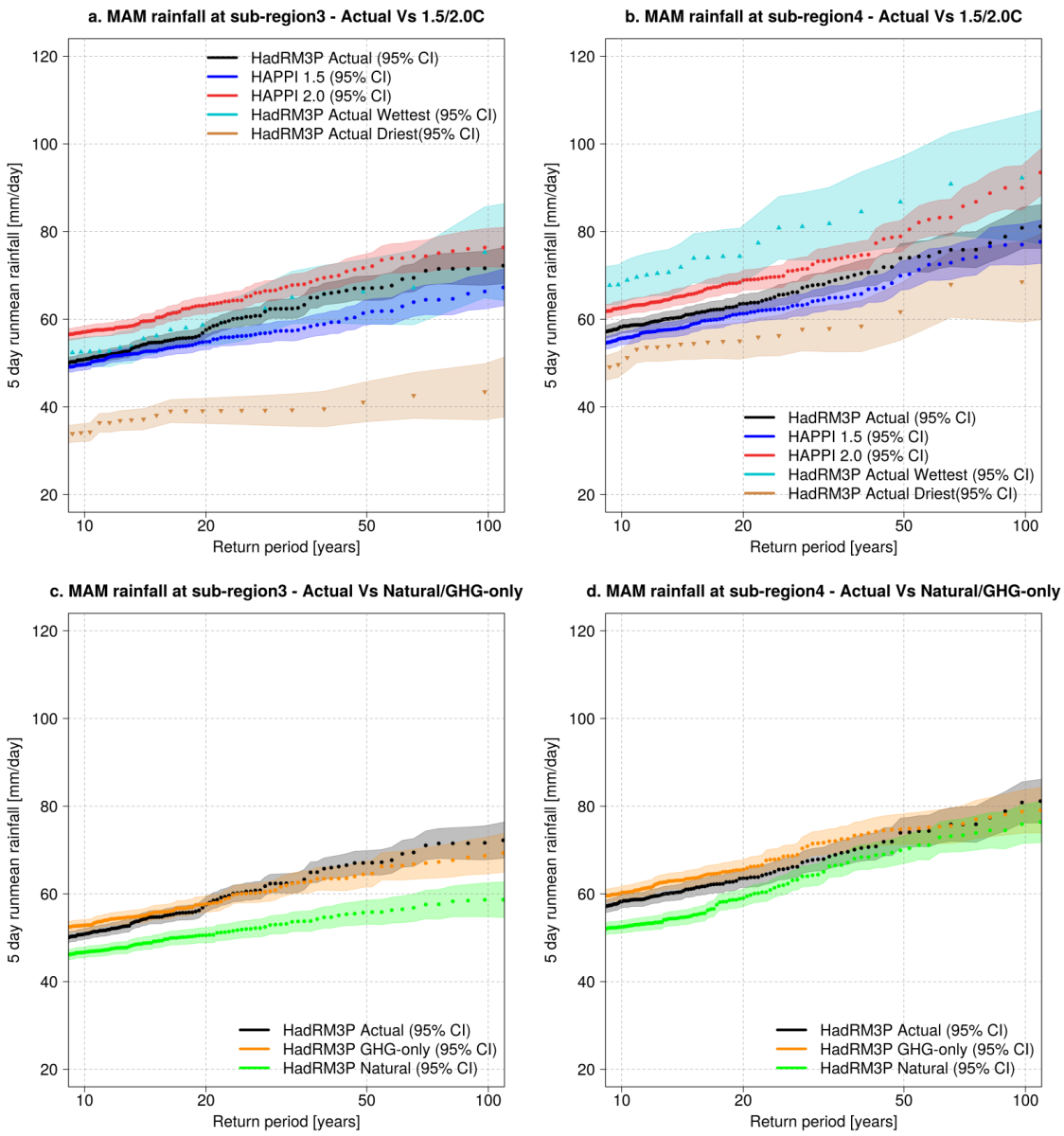


Figure S5.4: Same as Fig. S3, but for return time plots for MAM five day mean rainfall under different forcing scenarios over the sub-regions 3 and 4 of Bangladesh.

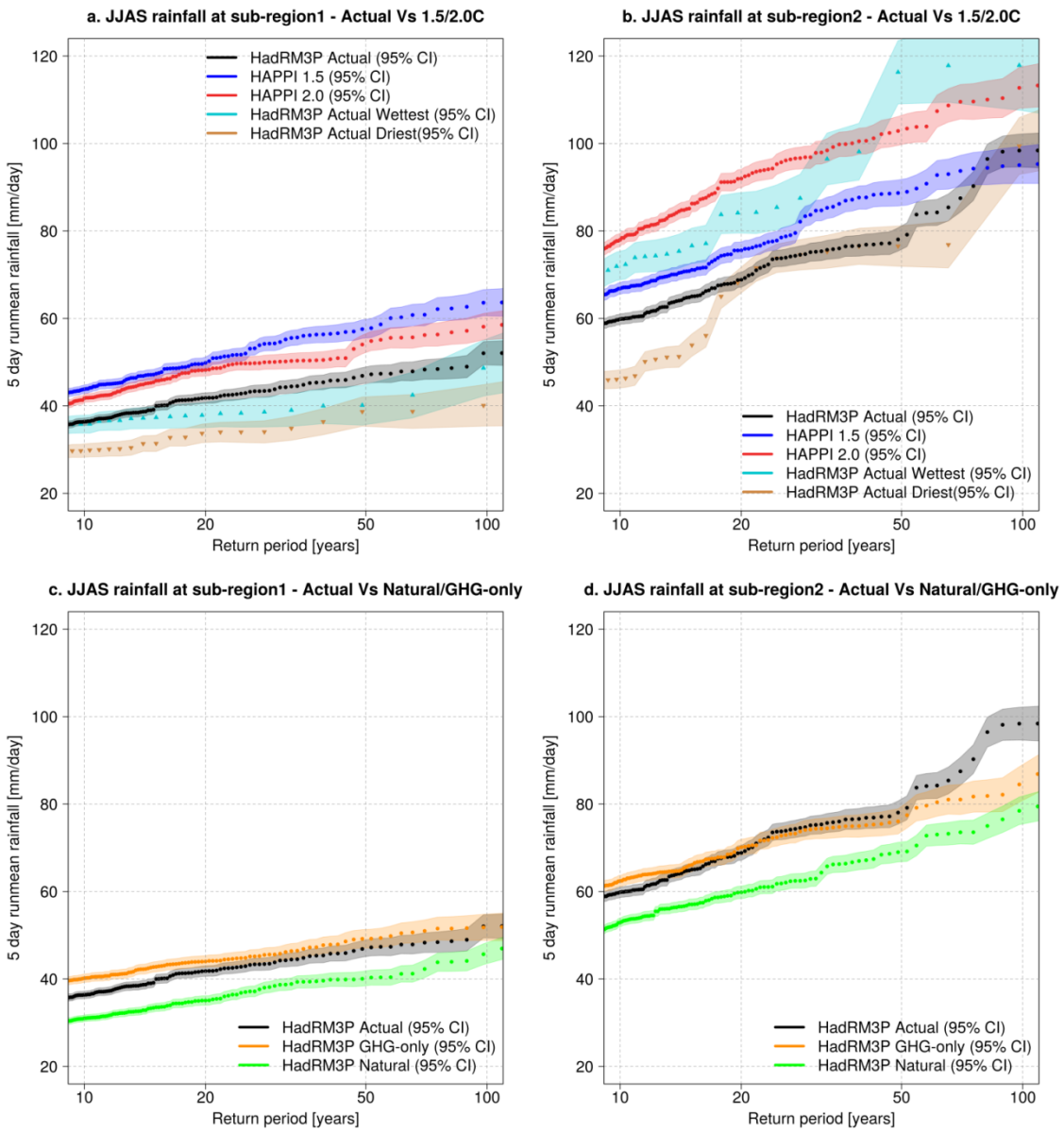


Figure S5.5: Return time plots for JJAS five day mean rainfall different forcing scenarios over the sub-regions 1 and 2 of Bangladesh. The ACT (black), ACT highest (sky-blue), ACT lowest (grey), NAT (green) and GHG-only (orange) ensembles are compared with the HAPPI 1.5 (blue) and HAPPI2.0 (red) ensembles. The risks of extreme rainfall events are evidently increasing between different forcing scenarios over sub-region 2.

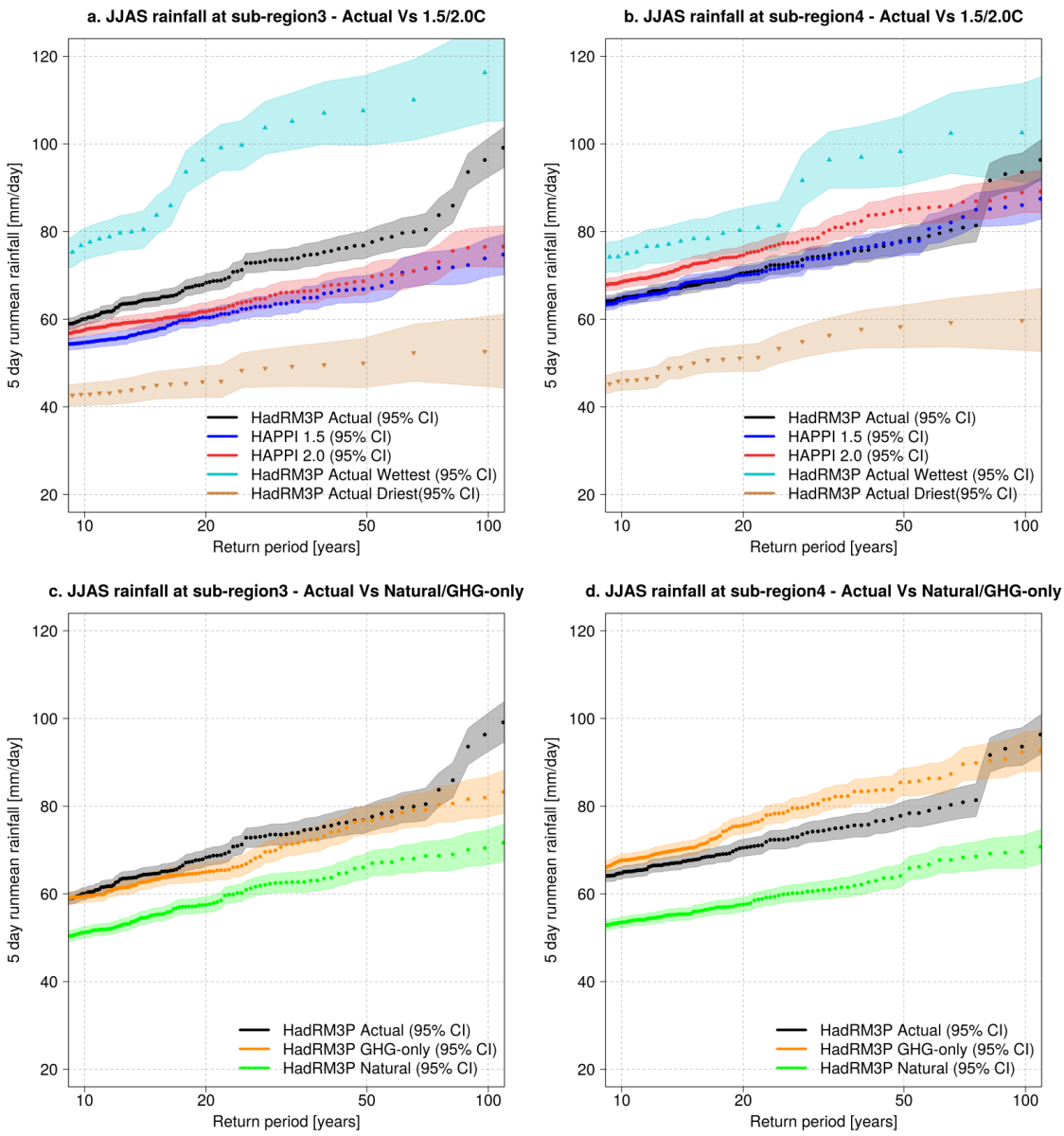


Figure S5.6: Same as Fig. S5, but for return time plots for JJAS five day mean rainfall under different forcing scenarios over the sub-regions 3 and 4 of Bangladesh.

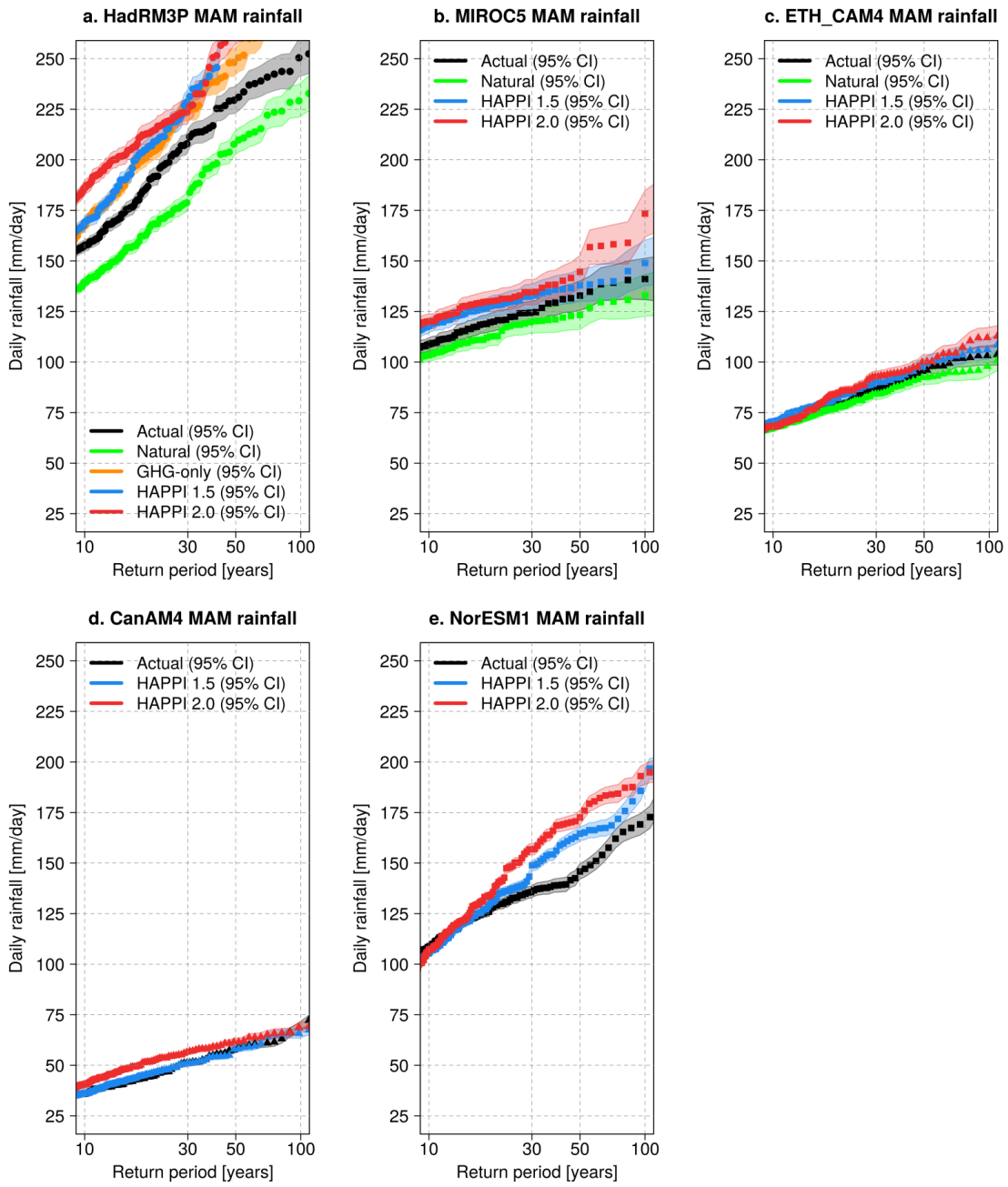


Figure S5.7: Comparative return periods (10-100 year events) of MAM daily rainfall (mm/day) over sub-region 2 during 1986-2015 as per (a) HadRM3P, (b) MIROC5, (c) ETH_CAM4, (d) CanAM4 and (e) NorESM1 models. ACT, NAT, GHG-only, plus 1.5°C and 2.0°C model ensembles are shown in black, green, orange, blue and red colours respectively.

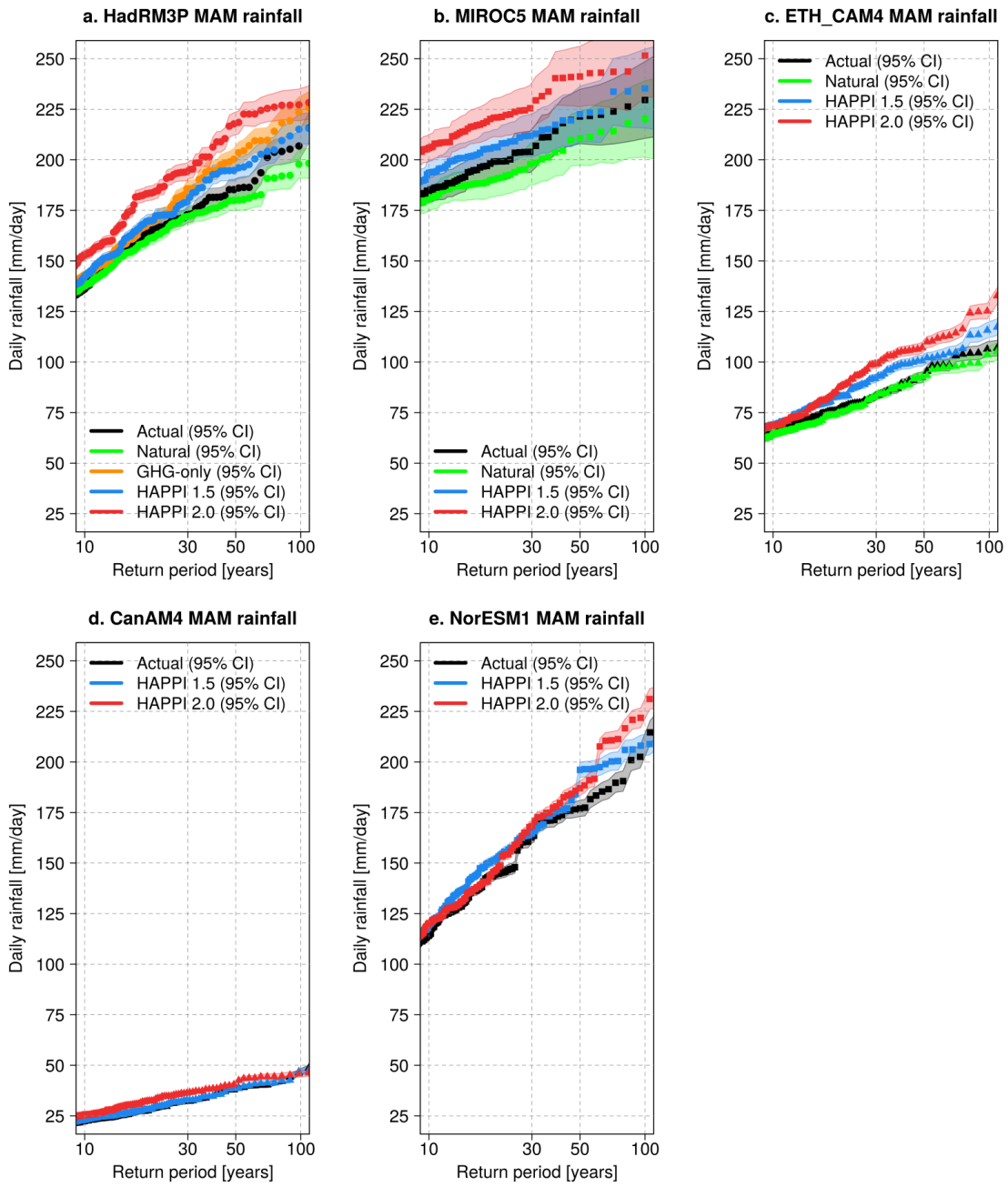


Figure S5.8: Same as Figure S7 but for sub-region 3.

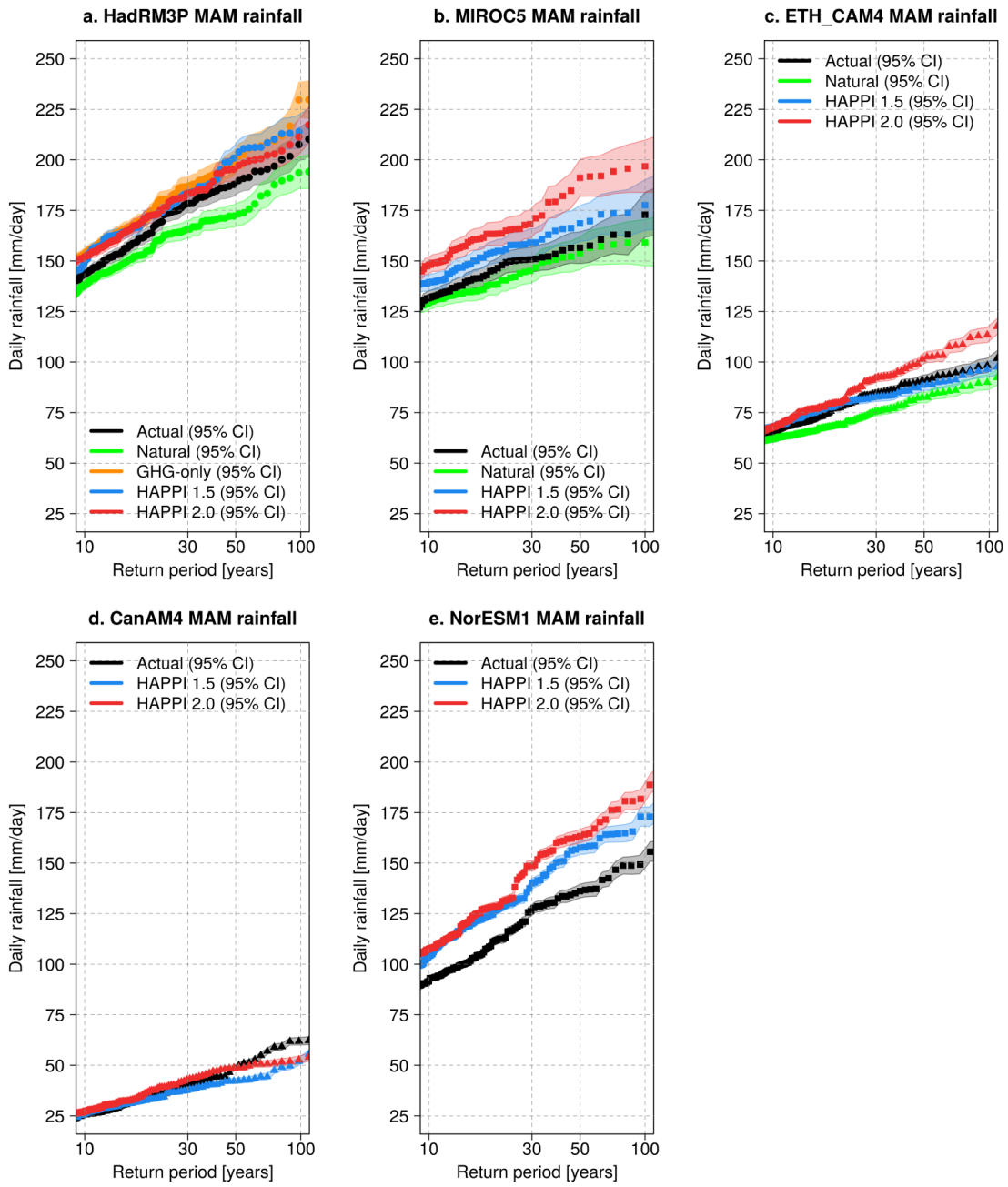


Figure S5. 9: Same as Figure S7 but for sub-region 4.

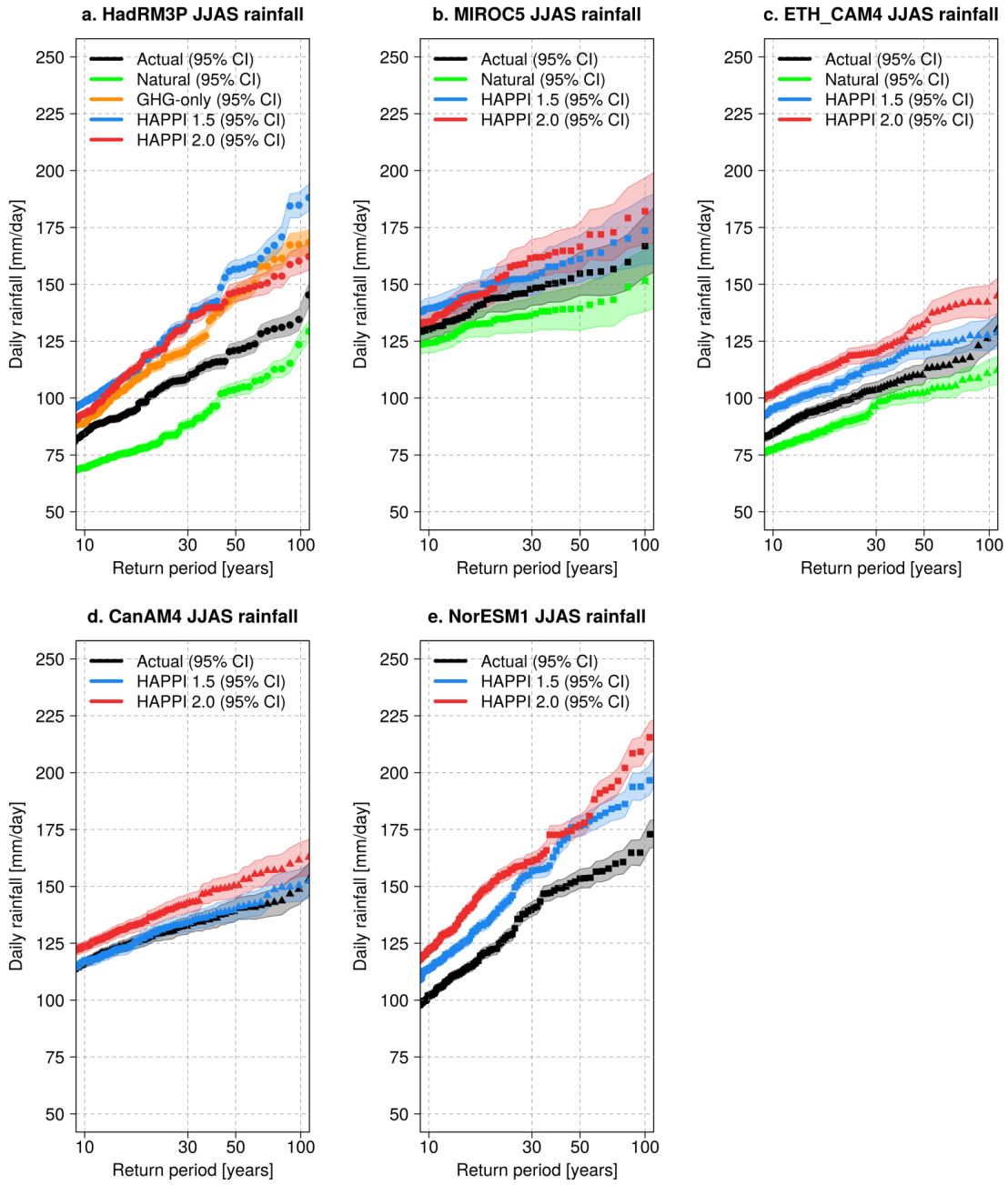


Figure S5.10: Comparative return periods (10-100 year events) of JJAS daily rainfall (mm/day) over sub-region 1 during 1986-2015 as per (a) HadRM3P, (b) MIROC5, (c) ETH_CAM4, (d) CanAM4 and (e) NorESM1 models. ACT, NAT, GHG-only, plus 1.5ºC and 2.0ºC model ensembles are shown in black, green, orange, blue and red colours respectively.

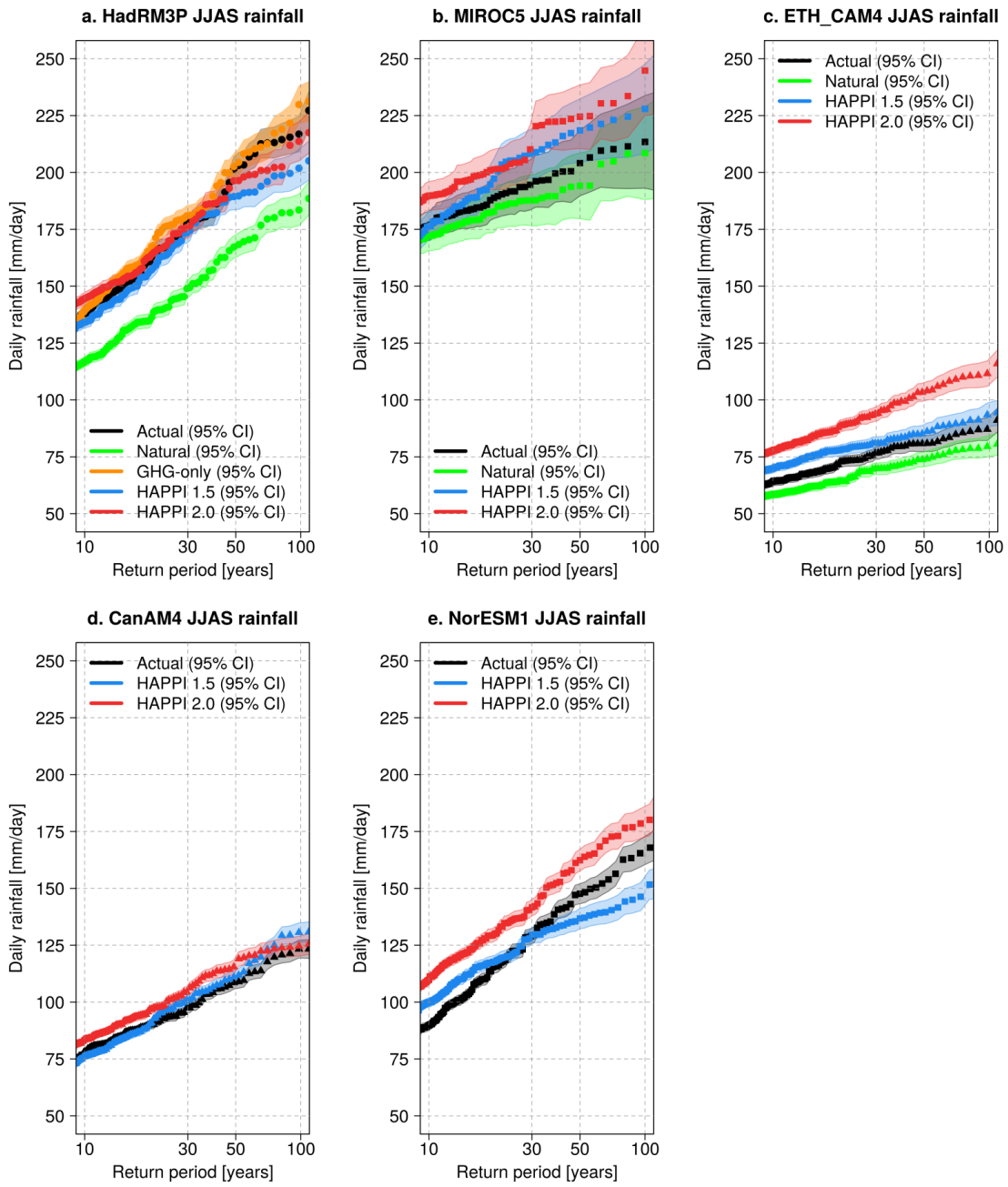


Figure S5.11: Same as Figure S9 but for sub-region 3.

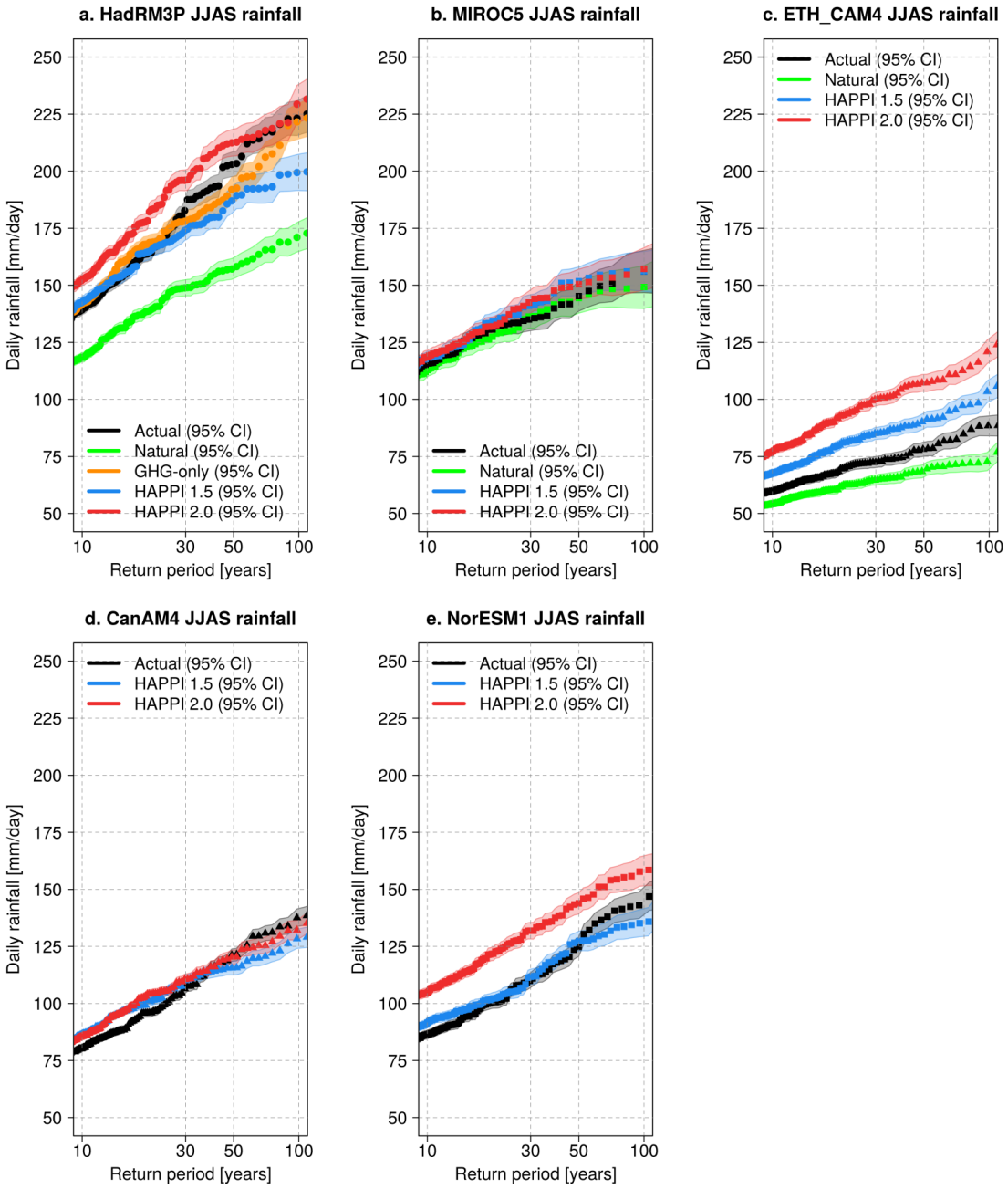


Figure S5.12: Same as Figure S9 but for sub-region 4.

Supplementary Text

Prescribed fields of Sulphur dioxide (SO_2) emission data in the model

A major source of uncertainty in climate model studies is the representation of SO_2 emissions. The climate models in general use historical data from the Coupled Model Intercomparison Project Phase 5 (CMIP5) and representative concentration pathway (RCP) data. But the problem is that after 2005, the contribution from observational data stops.

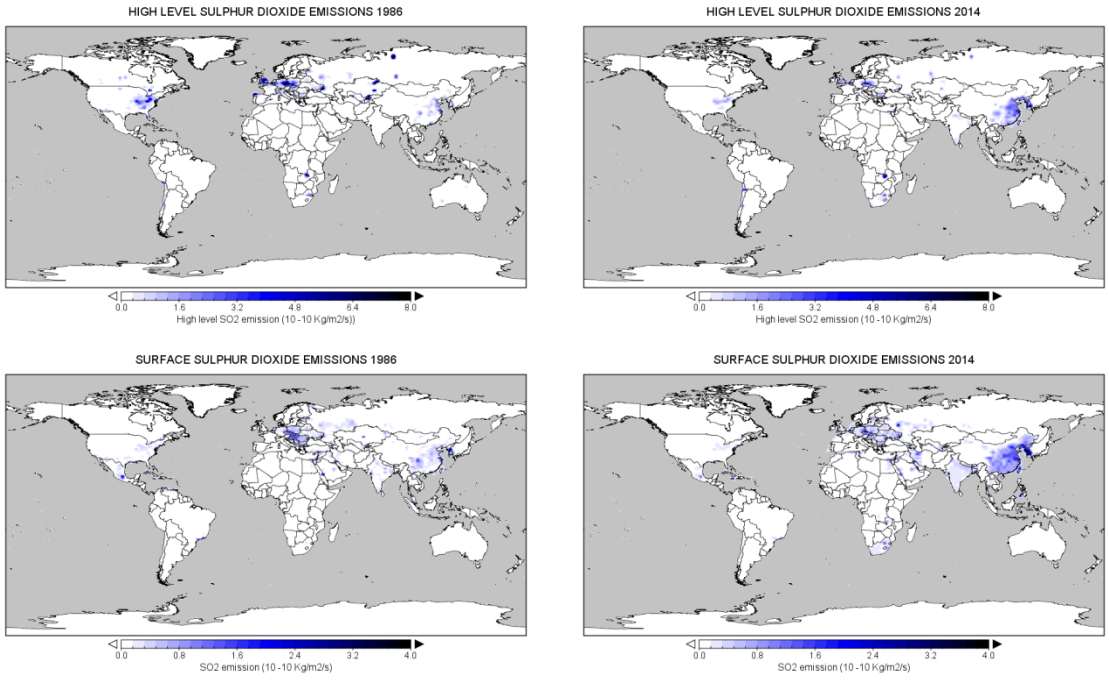


Figure S5.13: Prescribed field of high level and surface SO_2 emissions in the model in 1986 (top panel) and 2014 (bottom panel).

To overcome this problem, a more recent SO_2 emission data from the ECLIPSE v5a (Klimont et al., 2013) global emissions dataset is used to prescribe the fields in the model used in weather@home. Five yearly data estimates and projections are taken from the ECLIPSE dataset

and interpolated using conservative method both spatially onto an N96 global grid (1.875° longitude x 1.25° latitude) and temporally into monthly emissions data.

SO_2 emissions need to be expressed as kg/m2/s of S in the models. Hence the surface and high level emissions fields are rescaled from kt/yr and divided by unit area of each grid cell. An additional division by 2 is required to account for the difference in molar mass between SO_2 and S. More details of the method for the unit conversion of SO_2 data can be made available on request from Sarah Sparrow.

Figure S13 shows the prescribed SO_2 fields in the model in two different years of 1986 and 2014 and indicates how the distribution of SO_2 emissions changes in both spatial and temporal scales. Such variability of the SO_2 emissions in the model is prerequisite for having meaningful propagation of aerosol impacts on rainfall events at regional scales.

Analytic methods:

1. **Percentage Change (PC)** in seasonal mean rainfall is calculated for one forcing scenario relative to another forcing scenario to indicate the magnitude of change between the scenarios across the study region. This approach enables the identification of areas at risk of becoming wetter or drier. For instance, the PC for ACT relative to NAT in monsoon (JJAS) season is calculated as:

$$PC_{\text{ACT relative to NAT}} = \left[\frac{\text{JJAS rainfall in ACT} - \text{JJAS rainfall in NAT}}{\text{Mean JJAS rainfall in ACT}}\right] \times 100$$

   The multi-year monthly means of JJAS months for each decadal model ensemble is used to calculate the PC in all cases. The PC for pre-monsoon (MAM) season is calculated using the same approach.

2. The **Standardized Precipitation Index (SPI)** (Mckee et al., 1993; McKee et al., 1995) is a simple, flexible index which is powerful to effectively analyse both wet and dry periods. SPI is widely used for assessing wetting/drying effects (e.g., Du et al., 2013; Li et al., 2015, 2008; Mahfouz et al., 2016). Rainfall data is the only required input parameter to calculate the SPI and this can be computed for multiple timescales from 1 to 24 months (WMO, 2012).

   For example, SPI for monsoon rainfall during JJAS months in GHG only climate model ensemble (denoted as GHG-only) relative to actual climate model ensemble (denoted as ACT) is calculated by the following equation:

$$\text{SPI}_{\text{GHG-only relative to Act}} = \frac{\text{JJAS rainfall in GHG-only - JJAS rainfall in ACT}}{\text{Standard deviation of JJAS rainfall in ACT}}$$

   The multi-year monthly means of JJAS months for each model ensemble is used to calculate the SPI in all cases. An SPI index value greater than 2.0 indicates areas are extremely wet, 1.5 to 1.99 indicates very wet; 1.0 to 1.49 moderately wet; -0.99 to 0.99 near normal; -1.0 to -1.49 moderately dry; -1.5 to -1.99 severely dry; and -2 and less indicate areas to be extremely dry (WMO, 2012).

6. Risks of pre-monsoon extreme rainfall events of Bangladesh: Is anthropogenic climate change playing a role?

Risks of pre-monsoon extreme rainfall events of Bangladesh: Is anthropogenic climate change playing a role?

RUKSANA H. RIMI[1], KARSTEN HAUSTEIN[1], EMILY J. BARBOUR[1], AND MYLES R. ALLEN[1]

[1]Environmental Change Institute, School of Geography and the Environment, University of Oxford, Oxford, OX1 3QY, United Kingdom.

[2]CSIRO Land and Water, Canberra, ACT 2601, Australia.

Submitted to *Bulletin of the American Meteorological Society (BAMS) Special Report on Explaining Extreme Events (EEE) of 2017 from a Climate Perspective*

May 24, 2018

First published accepted manuscript online

December 05, 2018

Available at http://www.ametsoc.net/eee/2017a/ch13_EEEof2017_Rimi.pdf

Authorship Declaration

I, Ruksana H. Rimi, hereby declare that I conducted all of the analyses and writing for this paper with advice from Myles R. Allen, Karsten Haustein and Emily Barbour. The manuscript was finalized with edits from all co-authors.

Main Findings

Anthropogenic climate change doubled the likelihood of the 2017 pre-monsoon extreme 6-day rainfall event at northeast Bangladesh. The magnitude of this contribution is sensitive to the climatological period in use.

6.1. Introduction

Northeastern Bangladesh (NEB; 90.5°–92.5°E, 24°–25.5°N) has unique low-land areas known as haors. The "Boro" paddy (rice) crop is cultivated in these haors in dry winter season (December–February) and harvested during April–May. Boro accounted for ~55% of national rice production per annum during 2011–16 and NEB contributed to ~15% of the total Boro rice production over this period (FAO, 2017).

NEB receives highest annual mean rainfall of >4,300 mm, in contrast to western Bangladesh, which receives 1,400 mm (Shahid, 2010a). Topographic uplifting of the south-westerly flow by the Meghalaya Plateau and other surrounding mountains triggers heavy convective rainfall at NEB in the pre-monsoon season season (Murata et al., 2008; Murata et al., 2011; Sanderson and Ahmed, 1979; Shahid, 2010).

Pre-monsoon rainfall during March–April facilitates growth of Boro but events >150 mm of total 6-day rainfall can cause early flash floods and damage crops. On 27 March 2017, extreme rainfall over NEB triggered the earliest flash flood since 2000 (Ahmed et al., 2017). Subsequently, ~850,000 households were affected and ~220,000 ha of nearly harvestable Boro were damaged. Crop failure in 2017 contributed to a record 30% rice price hike compared to 2016 (FAO, 2017).

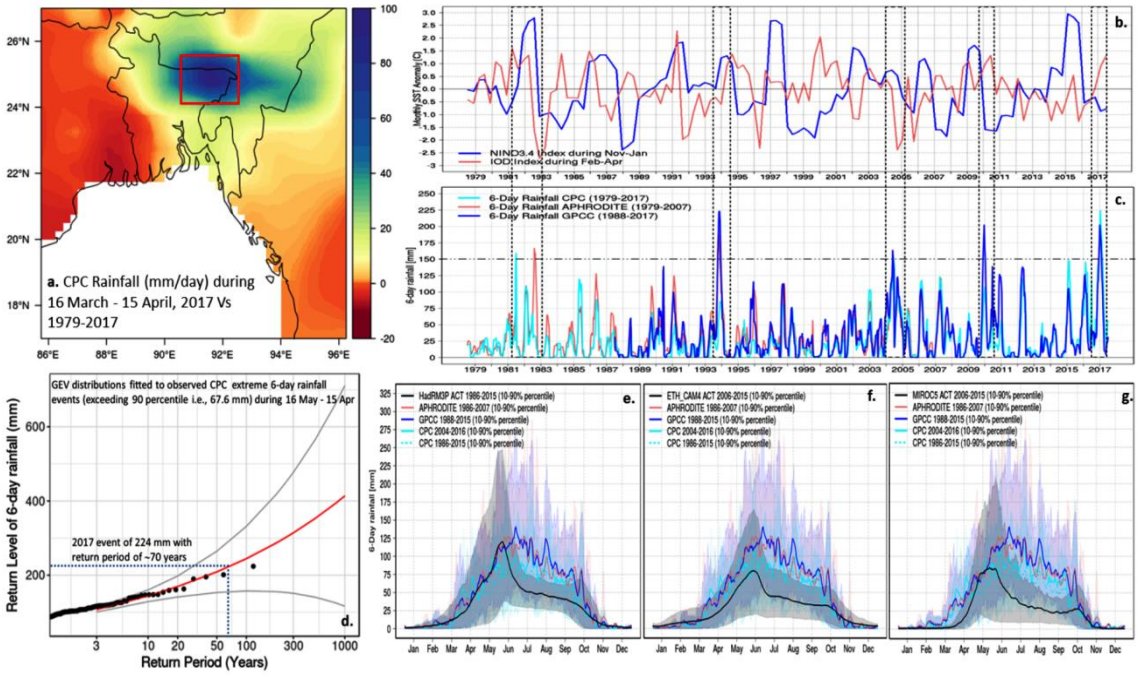


Figure 6.1: (a) Spatial distribution of CPC rainfall (mm day–1) over Bangladesh during 16 March–15 April 2017 relative to climatology (1979–2017). The red box indicates the study area of NEB. (b) Niño-3.4 (November–January) and IOD (February–April) indices during 1979–2017. The horizontal dashed black line in (c) indicates the threshold value for heaviest rainfall events. The vertical dashed black rectangles in (b) and (c) indicate the association between the heaviest rainfall events and IOD (Niño-3.4). (d) Return level plot of GP distribution fitted to CPC observed extreme 6-day rainfall events exceeding a 90th percentile threshold. (e)–(g) Annual cycles of 6-day rainfall over NEB as in models and observations (HadRM3P, ETH_CAM4 and MIROC5, respectively), with CPC (1979–2017 and 2004–16), GPCC (1988–2017), and APHRODITE (1979–2007).

Analysing NOAA's Climate Prediction Center (CPC) observation data, we find that during 16 March–15 April 2017, 6-day total rainfall over NEB amounted to 225 mm (i.e., 33.33% higher than the flash flood triggering threshold of 150 mm). The highest positive rainfall anomaly (up to 100 mm day–1; relative to 1979–2017) during 16 March–15 April 2017 is found at NEB (see red box in Fig. 6.1a). To determine how rare this event is, we apply a generalized Pareto (GP) distribution fit to CPC data exceeding 90th percentile values, and find a return time of ~70 years (Fig. 6.1d).

Most of the attribution studies are done for mid-latitude extreme events of the developed countries while very few of them focus on the tropical region(Marthews et al., 2015; Otto et al., 2015a; Otto, 2017) or developing countries, even though these countries experience extreme events and have the least capacity to adapt with the consequent impacts (IPCC, 2013b).

To understand the drivers behind the 2017 floods, here we investigate the probabilities of extreme 6-day rainfall during pre-monsoon season in Bangladesh and analyse whether or not anthropogenic climate change has changed the odds of such events occurring (Allen, 1999). We utilize the very large weather@home regional climate model (RCM) ensemble based on HadRM3P.

We also investigate the potential contribution of radiative cooling from anthropogenic aerosols as their presence can counterbalance the greenhouse gas (GHG) induced intensification of the hydrological cycle (Li et al., 2016a). Niño-3.4 and Indian Ocean dipole (IOD) indices are used to quantify the role of two key climate modes. Additionally, two global climate models (GCMs) of MIROC5 and ETH_CAM4 are used to test the robustness of our results.

6.2. Data and methods

We use daily rainfall data from Asian Precipitation Highly Resolved Observational Data Integration toward Evaluation of Water Resources (APHRODITE) covering 1979–2007 (Yatagai et al., 2012), CPC global 0.5° analysis of daily rain gauge measurements covering 1979–2017 (Chen et al., 2008a), and Global Rainfall

Climatology Centre (GPCC) daily rainfall data covering 1988–2017 (Schamm et al., 2015).

The higher-resolution (50 km) weather@home HadRM3P RCM is nested in the global atmosphere-only HadAM3P model [an atmospheric general circulation model (AGCM)] and is driven by prescribed SSTs and sea ice concentration (SIC) (Guillod et al., 2017; Massey et al., 2015) and radiative forcing.

Following Schaller et al. (Schaller et al., 2016), we use 75,000 (30 × 2500) simulations for "Actual March 2017" under factual conditions with observed 2017 GHG concentrations, OSTIA SSTs, and SIC (Donlon et al., 2012) and 15,7500 (30 × 5250) simulations for "Natural March 2017" under conditions that might have been in a counterfactual world without past GHG emissions and other pollutants.

We also use 2,160,000 (360 × 30 × 200) simulations for each of the Actual, Natural, and GHG-only climatology over the 30 years (1986–2015) of reference period. Here the GHG-only scenario has current levels of GHGs but the anthropogenic aerosols are set to pre-industrial levels.

In addition, we use smaller ensembles from two GCMs, with 1500 (30 × 50) simulations from MIROC5 and 15,000 (30 × 500) simulations from ETH_CAM4 representing Actual and Natural March during a 10-yr (2006–15) period [see Mitchell et al. 2017 for more details]. All model and observation data are re-gridded using bilinear interpolation method and then area-averaged rainfall statistics over NEB are analyzed.

We use the Niño-3.4 index (Rayner et al., 2003) to determine the lagged correlation with March rainfall over NEB, and with the IOD index (Huang et al., 2017). We quantified the change in the occurrence probability of rainfall event, the risk ratio (RR), as

$$\mathbf{RR} = \boldsymbol{P_f / P_{cf}} \qquad \textit{(6.1)}$$

Where, the probability of the event in the factual climate is denoted by P_f and the probability of the same event in a counterfactual climate without anthropogenic climate change is denoted by P_{cf} (National Academies of Sciences, Engineering, 2016). An exception to this is the GHG-only scenario, where RR is calculated using P_{cf} = actual climate instead of natural climate.

As far as the HadRM3P's performance with regard to APHRODITE, GPCC, and CPC is concerned, the model reproduces the annual rainfall cycle with satisfactory agreement. However, monsoon rainfall is underestimated in HadRM3P by ~30% (Fig. 6.1e) with an early onset. We are using model data for March rather than mid-March to mid-April to remove this bias. MIROC5 is biased dry (Fig. 6.1g) in March (~50%), whereas ETH-CAM4 (Fig. 6.1f) is biased extremely dry (~40% in March and ~25%–50% throughout the monsoon season).

6.3. Results and discussion

Figure 6.2 illustrates how the return periods of March extreme 6-day rainfall events have changed from natural counterfactual climate to actual climate scenarios. The likelihood of extreme 6-day rainfall event under 2017 SST conditions in March has increased by ~20% (Fig. 6.2a) in HadRM3P compared to natural conditions.

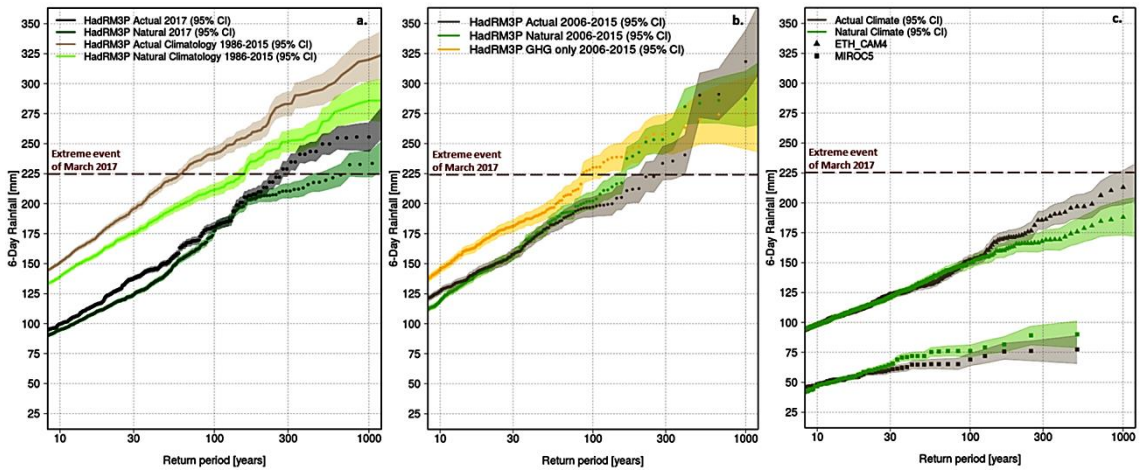


Figure 6.2: Return periods for 6-day rainfall events in March over NEB showing (a) HadRM3P Actual 2017 (black) and Natural 2017 (dark green) vs Actual climatology 1986–2015 (gray) and Natural climatology 1986–2015 (light green) ensembles. (b) Actual climatology 2006–15 (gray), Natural climatology 2006–15 (light green), and GHG-only climatology 2006–15 (yellow). (c) Actual climatology 2006–15 (gray) and Natural climatology 2006–15 (light green) but as in MIROC5 (squares) and ETH_CAM4 (triangles) model ensembles. Each dot, triangle, or square represents one simulation of the HadRM3P, MIROC5, or ETH_CAM4 model, respectively, and the shaded polygon shows 95% confidence intervals. The horizontal dashed deep brown line in each panel indicates the extreme event of March 2017.

We find RR of ~2 (100% increase) for the 1986–2015 climatology period (Fig. 6.2a), but then unaltered risks for the shorter 2006–15 period (for events < 200 mm; Fig. 6.2b). This suggests that there are interesting nonlinear dynamic feedbacks at play, which depend on the state of the climate (i.e., ENSO or IOD variability). For March and the preceding winter (DJF 2016/17), very weak La Niña conditions were present (see Fig. S6.2c in the supplemental material). While not conclusive, HadRM3P results indicate that La Niña made drier conditions more likely over NEB (Fig. S6.1c). Such feedback arises from global teleconnections, which can be detected in the upper-level zonal wind anomaly fields, in HadRM3P and reanalysis (not shown).

In general, we find a moderate correlation (r = 0.4 to 0.6; no lag) between Niño-3.4 and NEB rainfall in March (Fig. S6.2g). Regarding the interplay between ENSO and IOD itself, we argue that ENSO leads most IOD changes as notable particularly during strong El Niño events (Figs. 6.1 b, c) because correlation between Niño-3.4 during November to January and IOD during February and March (r = 0.467; 4 months' lead time; p = 0.0081 at 95% confidence level) is significant.

While positive IOD events tend to weaken the El Niño impact on the rainfall (e.g., Behera and Ratnam 2018), we obtain mixed results for the five heavy rainfall events (vertical dashed rectangles through Figs. 6.1b and 6.1c) exceeding the 150-mm threshold. Only two out of five events were associated with positive IOD and El Niño conditions. March 2017 is drier not only from an ENSO but also from an IOD point of view. Since March is in the beginning of the pre-monsoon season, small changes can cause drastically different outcomes. Matsumoto (1997) and Ashfaq et al. (2009) identified an early onset of the rainy days at NEB on 8 April and 21 May, respectively. We speculate that the current warming has shifted the pre-monsoon heavy rain's onset to even an earlier start.

We notice a decreasing risk for the extreme rainfall event of March 2017 (225 mm) from Natural to Actual climate but then an increasing risk from natural to GHG-only climate conditions during 2006–15. This result demonstrates a considerable contribution of the anthropogenic aerosols for March 2006–15 (Fig. 6.2b); however, this is not the same for 1986–2015 (not shown). MIROC5 and ETH_CAM4 simulate much smaller changes in risk, with ETH_CAM4 even suggesting a drying trend, but none of these GCMs captured the observed extreme event of 2017 (Fig. 6.2c).

6.4. Conclusions

Based on the results from HadRM3P model only (for 1986–2015), we conclude that anthropogenic climate change doubled the likelihood of extreme pre-monsoon rainfall (~100% more likely) over NEB. Interestingly, the attribution signal in March is sensitive to the chosen climatology period. Natural ENSO and IOD variability influence inter-annual changes in rainfall risks, yet both indices made the 2017 rainfall event less likely.

The anthropogenic aerosol cooling effect is noticeably observed during the recent decade (2006–15). How the interplay between the two competing forces of GHGs and the anthropogenic aerosols influences the risks of extreme rainfall events should be explored more.

For the first time, this study presents attribution assessment for pre-monsoon extreme rainfall event for Bangladesh. Understanding the physical mechanisms behind such event and using a multi-model approach to incorporate associated uncertainties can be useful for further studies.

Acknowledgments

This paper was supported in part by the UKIERI-DST project. We thank our colleagues at the Oxford e-Research Centre for their technical expertise, the Met Office Hadley Centre PRECIS team for their technical and scientific support for the development and application of weather@home, and all the volunteers who have donated their computing time to weather@home.

Risks of extreme rainfall events of Bangladesh: Is anthropogenic climate change playing a role?

Ruksana H. Rimi[1], Karsten Haustein[1], Emily J. Barbour[1,2], and Myles R. Allen[1]

[1] Environmental Change Institute, School of Geography and the Environment, University of Oxford, Oxford, OX1 3QY, UK

[2] CSIRO Land and Water, Canberra, ACT 2601, Australia

Supplementary Materials

Supplementary text:

1) Using Bayesian estimation method the generalized Pareto (GP) distribution is fitted to extreme 6-day rainfall events that exceeded the 90th per-centile, giving data points over threshold (POT) during 16 March–15 April during 1979–2017.

2) Following Black et al. (2016), the ENSO composite is calculated based on 4 years for each ENSO mode (El Niño, neutral, and La Niña). The monthly rainfall anomaly in response to ENSO for March (post-ENSO) is compared between the model and observations (GPCC, CPC).

3) The intensity of the dipole mode index (IDMI) is represented by anomalous SST gradient between the western equatorial Indian Ocean and the southeastern equatorial Indian Ocean. When the SST anomaly is positive (negative), the phenomenon is referred to as the positive (negative) IOD.

4) Positive (negative) values of Niño-3.4 index correspond to El Niño (La Niña) conditions, whereas a positive IOD (pIOD) indicates warmer than nor-mal water in the tropical western Indian Ocean and cooler than normal water in the tropical eastern Indian Ocean.

5) We use Goddard Institute for Space Studies (GISS) surface temperature analysis data for land (Hansen et al. 2010) and ERSSTv5 data for ocean to have mean temperature (°C) anomaly pattern averaged over a season (DJF, MAM, JJA, and SON) or month (March and June) of 2017 relative to base period of 1986–2015.

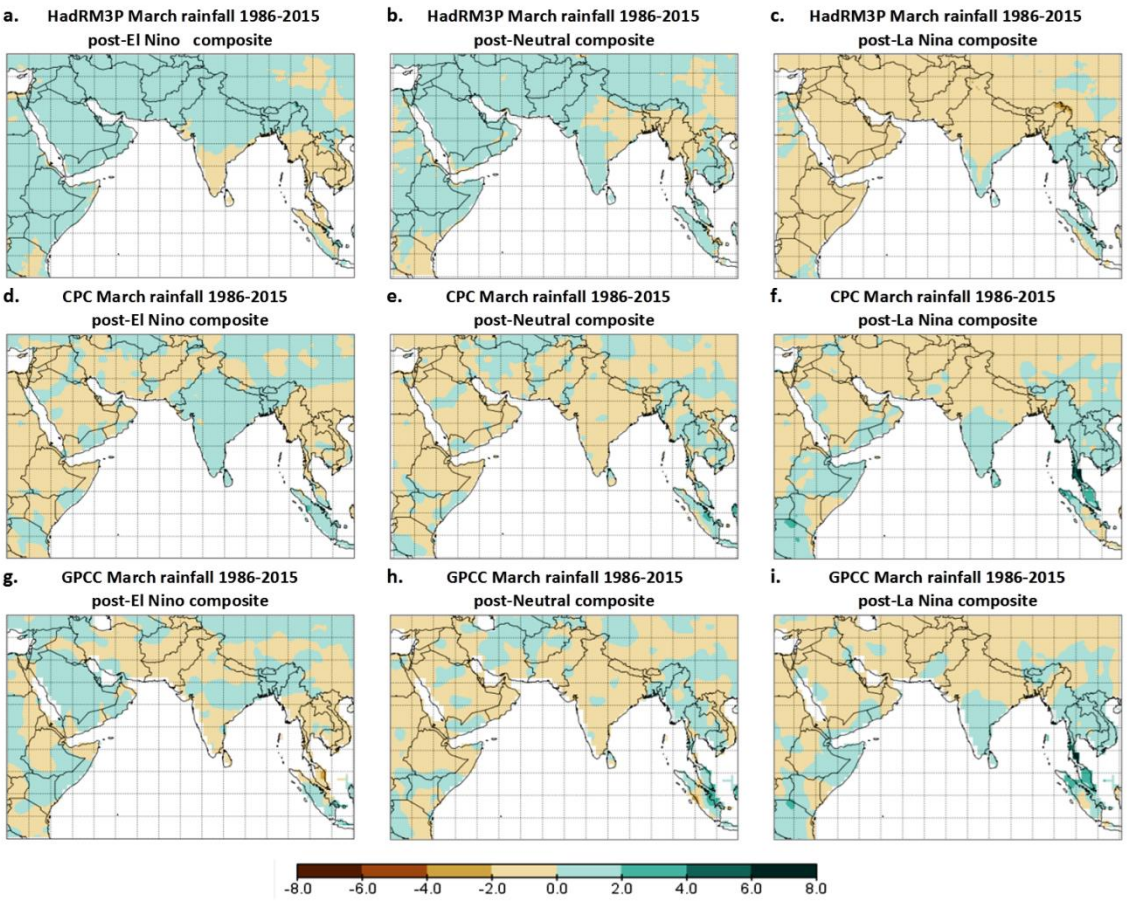


Figure S6.1: ENSO response in March rainfall anomalies during (left) post–El Niño, (middle) post-neutral and (right) post–La Niña conditions in (top) HadRM3P, (middle) CPC, and (bottom) GPCC in each composite.

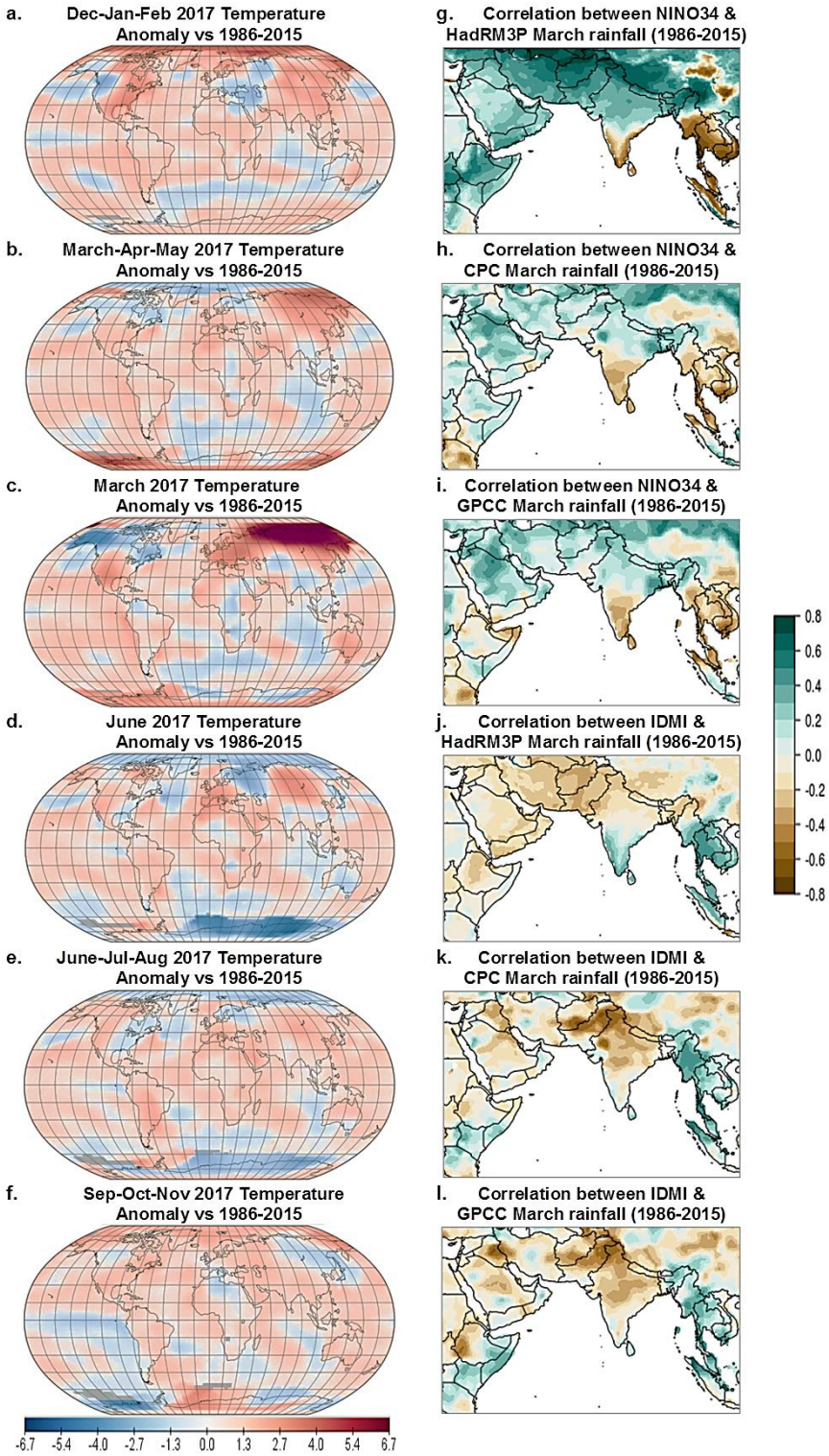


Figure S6.2: The left column shows global mean temperature (°C) anomaly averaged over a season [DJF, MAM, JJA, and SON in (a), (b), (e), and (f), respectively] and the months of (c) March and (d) June of 2017 relative to base climatological period of 1986–2015. Any gray areas in the maps signify missing data. The right column shows (g)–(i) Niño-3.4 and (j)–(l) IDMI regression with HadRM3P, CPC and GPCC rainfall in March during 1986–2015.

6.5. Additional notes of clarification

6.5.1. Reason behind no bias correction

While assessing contribution of anthropogenic climate change in altering the probability of occurrences of extreme weather events, attribution studies generally consider specific single event as observed or, classes of events that are similar to the event that has been observed (National Academies of Sciences, Engineering, 2016). We are considering the 2017 event as a class and not a single entity and so we are not looking at the specific dates when it actually happened (March 29 - April 03).

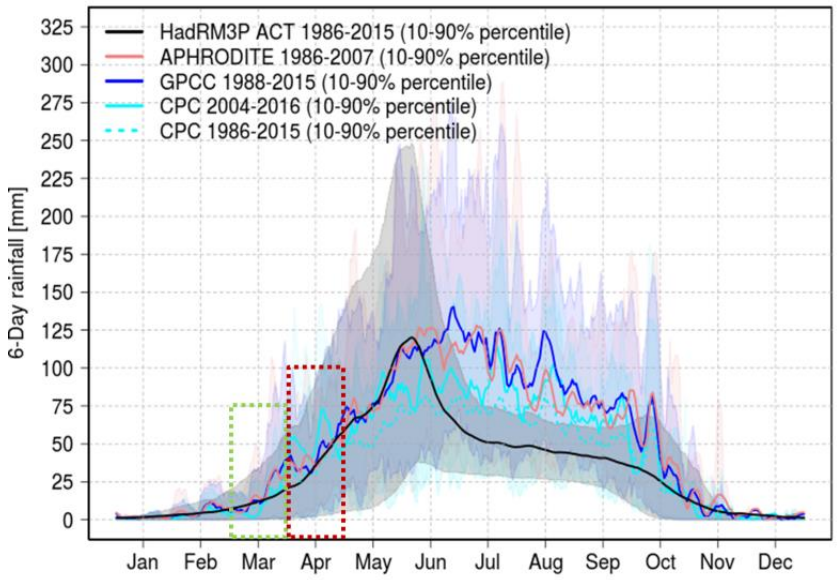


Figure 6.3: Annual cycles of 6-day rainfall over NEB as in HadRM3P model and observations of CPC (1979–2017 and 2004–2016 in dotted and solid sky-blue coloured lines respectively), GPCC (1988–2017 in blue), and APHRODITE (1979–2007 in pink). The green and red dotted rectangles indicate that in March model bias is very small but it is comparatively large in April.

For model data analysis, we use the entire month of March as this is the period that corresponds to the pre-monsoon season in the model. We account for the event specific characteristic by analysing 6-day running totals during March.

This corresponds to the very bias correction method introduced in Chapter 3 (in section 3.4.2), where we propose to shift the model data by 14 days to remove the timing bias with regard to the monsoon onset in HadRM3P. In an unbiased model setup, we would use 16 March to 15 April instead of March to represent the climatological conditions.

As far as the bias in the model simulated rainfall magnitude is concerned, we do not have sufficient confidence in one observational product over another to determine which one should be used for a quantitative bias correction (using methods such as quantile-quantile mapping).

Also, arguably more importantly, none of the standard bias correction methods can tell us anything about the potential biases of the model related to dynamic changes in response to the warming. All model scenarios have to be bias-corrected in the same way, which generally has little effect on the estimated risk ratio. Bias correction would be required if rainfall thresholds were considered, something which has not been done for this reason.

6.5.2. Observational uncertainties

We compared three observational data sets of CPC, GPCC and APHRODITE in Fig. 5.1(c) and found discrepancies in the rainfall magnitudes. Those disagreements exist possibly due to differences in the data acquisition methods, lack of coverage of available all meteorological stations or, absence of stations particularly in high mountain regions.

Comparison between datasets is limited by differing temporal coverage, with APHRODITE daily data available for 45 years (1963-2007); CPC for 32 years (1979-2017); and GPCC for 30 years (1988-2017).

We additionally look at the Integrated Multi-satellitE Retrievals for GPM (IMERG) data for 6-day rainfall events over north-east Bangladesh during 16 March – 15 April (2014-2017) and find that the magnitude of the 2017 event is 225 mm. Due to its very short length of record, we do not use this data to assess return period of the 2017 event.

We ultimately use CPC daily data to analyse the 2017 event's characteristics (e.g., event's magnitude compared to hazard threshold, anomaly from climatology, and return period). The magnitude of 2017 rainfall event is same in CPC data as it is in the IMERG data.

While IMERG appears to be the most reliable observational data set, it is beyond the scope of this study to determine the actual degree of robustness attached to any single satellite-based product. Hence the hesitation to bias correct the model in light of this systematic uncertainty. In fact, we argue that bias correction may introduce a false sense of precision in this case.

6.5.3. Does GPCC observation change the attribution statement?

As per GPCC observations, the 6-day rainfall event of 2017 at northeast Bangladesh equals to 200 mm, which is 25% higher than the flash flood triggering threshold (150 mm). By fitting Generalized Pareto distributions to GPCC extreme 6-day rainfall

events during 16 March – 15 April that exceeded 90 percentiles during 1988-2017, we estimate that the 2017 event of 200 mm has a return period of ~27 years.

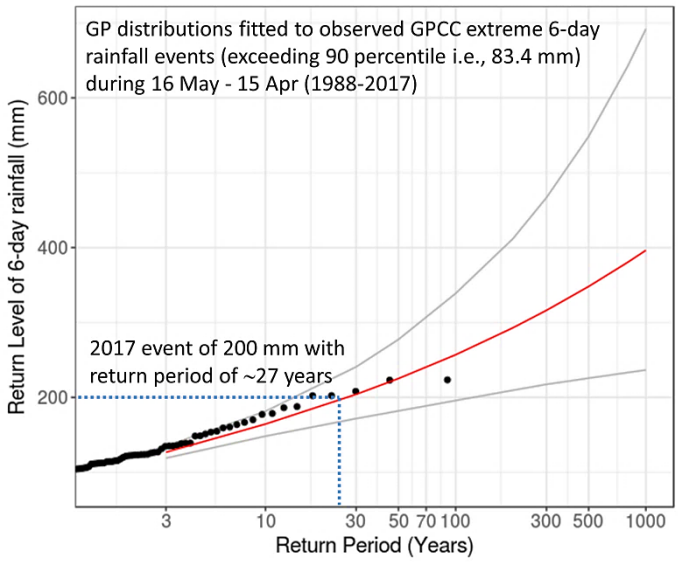


Figure 6.4: Return level plot of GP distribution fitted to GPCC observed extreme 6-day rainfall events exceeding a 90th percentile threshold.

While, using the same estimation method, CPC observation data based return period is ~70 years. We argue that, relatively short record length of GPCC data makes it difficult to assess the event's rareness.

Figure 5.2 indicates that the likelihood of 200 mm has nearly doubled from natural to actual climate conditions according to HadRM3P model climatology runs (1986-2015). The two other GCMs of MIROC5 and ETH_CAM4 still cannot capture the GPCC observed event magnitude. The model results based on GPCC based event threshold compare favourably with those calculated using the CPC. In both cases, we find an increase in the likelihood of the 2017 event by a factor of ~2 (based on the climatology model runs) and the model results are sensitive to the climatological period in use.

6.5.4. Concluding remark

The uncertainty that exists between different observation datasets, meaning bias correction to one particular dataset may not necessarily improve the accuracy of the model. Long-term reliable record of observations is crucial for extreme event characterization. The attribution statement would be the same for the two different observed event thresholds from GPCC and CPC.

Confidence in attribution statements can be limited by observational as well as model uncertainties. Observational uncertainties in this study are addressed by using available multiple sources of observation data set. Potential future improvements in observation data set with best estimates of real events over longer term can help in model evaluation by providing better ground-truth.

Use of multiple realisations of the 2017 event within the model helps to consider some elements of uncertainty. Additional two model ensembles from the GCMs are used to assess the robustness of the attribution result and to capture further uncertainties within different models. Addressing physical mechanisms might help better understand the underlying causes of the model limitations and thereby might contribute to resolve some of these model uncertainties.

7. Conclusion

7.1. Synthesis of thesis findings

Human influence on global climate is changing the risks of experiencing some classes of extreme weather events. For public, scientists and policy-makers, it is important to know to what extent human-induced climate change played (or did not play) a role behind changing those risks. Probabilistic event attribution (PEA) can provide scientific information regarding this association and reveal whether and to what extent external drivers of climate change have influenced the probability of those events.

The regional climate modelling system of the weather@home system has been successfully used for this purpose. To date, most of the PEA based studies have focused on extreme events of mid-latitudes and predominantly events that have occurred in the developed countries. Developing countries located at the tropical monsoon regions are underrepresented in this field of research, despite that fact that these countries are highly climate vulnerable, often experience extreme weather events that cause severe damages and have the least capacity to adapt.

Bangladesh, a South Asian country with tropical monsoon climate, is a hotspot of climate change impacts as it is vulnerable to a combination of increasing challenges from record-breaking temperatures, extreme rainfall events, more intense river floods, tropical cyclones, and rising sea levels (The World Bank, 2012). The unique geographical location of Bangladesh in the Ganges-Brahmaputra-Meghna Basin, and the flat and low-lying topography particularly exposes this country to high risks of flooding and landslides caused by heavy rainfall events in the pre-monsoon and monsoon seasons (Rawlani and Sovacool, 2011; Banglapedia, 2012).

Observation based studies indicate that the frequency of high-intensity rainfall events may have already increased (e.g., Murshed et al., 2011), with significant repercussions for agriculture, health, ecosystems and economic development (Dasgupta et al., 2011; Sarraf et al., 2011).

Public, media and the government of Bangladesh have huge interest in recognizing and quantifying the possible role of climate change, but attribution studies for localised events in Bangladesh are sorely missing. This thesis attempts to fill this gap by addressing the meteorological hazard aspects of extreme events at the sub-regional scale within Bangladesh, aided by the HadAM3P-HadRM3P model set-up of weather@home.

Prior to this PEA assessment, a process-based evaluation is carried out to investigate the model responses to internal modes of natural variability relevant for South Asian monsoon climate, including El Niño Southern Oscillation (ENSO) and Indian Ocean Dipole (IOD); and a performance-based evaluation is done to evaluate the skill of the model to reproduce the observed distribution of extremes at sub-regional local scales in Bangladesh (in chapter 3 and 4, respectively).

This final chapter of the thesis synthesizes the main findings of the two model evaluation chapters followed by key results from the two chapters presenting PEA based studies. The broader relevance and applicability of these results and potential avenues for future research activities are briefly discussed before making the concluding remarks of this thesis.

7.1.1. Model evaluation results

7.1.1.1. Process-based model evaluation

A process-based model evaluation presented in **chapter 3** look at the model's capability to simulate the key features of monsoon climate system of South Asia and the model's response to observed variations in sea surface temperatures (SSTs); considering the two important natural modes of El Niño Southern Oscillation (ENSO) and Indian Ocean Dipole (IOD).

Findings of this chapter suggests that the mean state of the monsoon climate system including the key features like the complete reversal of the wind circulation between the two seasons of winter and summer is well captured by the model. The wet and dry conditions of the two seasons are also representative of the observed ones; however, the monsoon rainfall is systematically under-estimated by the model. The MSLP gradients that drive the monsoon weather patterns over the lands are approximately captured by the model over the Indian Ocean.

Due to the contested relationship between ENSO and IOD, a simple lead-lag correlation analysis is done, which reveals that a noticeable IOD signal is only observed in the post-monsoon season (SON), without an identifiable signal during the rest of the year. There is a strong significant negative correlation between rainfall anomaly and ENSO whereas; the correlation with IOD is weakly positive (non-significant). The comparisons made between the model outputs and observations indicates that the model performs adequately well in capturing the teleconnections from ENSO but not IOD over South Asia and Bangladesh.

7.1.1.2. Performance-based model evaluation

Chapter 4 presents a paper published in the International Journal of Climatology that documents the results from performance-based evaluation of the regional climate model (RCM) of the weather@home system particularly for extreme events in Bangladesh.

The findings from this model evaluation paper suggest that there are substantial spatial and temporal variations in rainfall and temperature biases compared with observations. These are highest in the pre-monsoon, which are largely caused by timing issues in the model. Modelled mean monsoon and post-monsoon temperatures are in good agreement with observations, whereas, there is a dry bias in the modelled mean monsoon rainfall. The rainfall bias varies both spatially and with the dataset used for comparison.

Despite of these biases in the mean climate variables, the model simulated temperature and rainfall extremes in summer monsoon over Bangladesh are approximately representative of the observed ones (when compared to APHRODITE). At the wettest parts of north-east Bangladesh, rainfall extremes are underestimated compared to GPCC and APHRODITE but are within the range of CPC observations. Therefore, the South Asia regional climate modelling experiments of weather@home system can potentially offer a tool for assessing the changing risks of extreme weather events in Bangladesh.

7.1.2. Results from PEA-based studies

7.1.2.1. Present and future risks of seasonal extreme events

Chapter 5 presents a paper (under review at the journal of Hydrology and Earth System Sciences) that quantifies the risks of seasonal extreme rainfall events at sub-regional scales in Bangladesh under current climate and future climate scenarios of the Paris Agreement temperature targets of 1.5°C and 2°C warming. Findings of this paper suggest that both a 1.5°C and 2.0°C warmer world is poised to experience increased seasonal mean and, to a lesser extent, increased extreme rainfall during the pre-monsoon and monsoon seasons across Bangladesh.

According to this paper's analysis, the risk of a 1 in 100 year rainfall event under current climate conditions has already increased significantly compared with pre-industrial levels in parts of Bangladesh. This paper highlights that reduction in the anthropogenic aerosols (due to their effectiveness in suppressing rainfall as outlined in the paper) play an important role in determining the overall future climate change impacts; by exacerbating the effects of GHG induced global warming and thereby increasing the rainfall intensity.

Substantial reduction in the impacts resulting from 1.5°C compared with 2°C warming is reported in this study; however the difference is spatially and temporally variable, specifically with respect to seasonal extreme rainfall events.

In order to test the robustness of the HadRM3P model results for extreme rainfall events, available four atmosphere only global circulation model (AGCM) simulations from the HAPPI Tier1 experiment are analysed. This enabled for the first time, a multi-model assessment of risks of seasonal extreme rainfall events at sub-regional local scales in Bangladesh considering anthropogenic climate change drivers of GHGs and aerosols. Findings of this study highlight that policy-makers need to consider both current and future changes in the risks in the face of changeable GHG and aerosol impacts in this region.

7.1.2.2. Extreme event attribution of 2017

The paper presented in **Chapter 6** is the first event attribution study published in the Bulletin of the American Meteorological Society (BAMS) for an extreme event that occurred in Bangladesh. Findings of this paper suggest that in Bangladesh the inter-annual changes in the risks of rainfall is influenced by the natural variability modes of ENSO and IOD. However, this extreme rainfall event of 2017 would have been less likely given the particular ENSO and IOD state in 2017.

Based on very large model ensembles generated by the regional climate model of weather@home system for South Asia region, this paper concluded that anthropogenic climate change doubled the likelihood of the 2017 pre-monsoon extreme 6-day rainfall event at northeast Bangladesh.

7.2. Broader relevance and applicability

7.2.1. Contribution towards climate modelling for studying extremes

Chapter 4 uses a novel model evaluation approach that compares the observations with model data after applying a Generalized Extreme Value (GEV) theory. While previous RCM evaluation studies for the South Asia region and Bangladesh mainly focused on climatological means and variabilities, the performance of the RCM in this paper is evaluated for extreme events with up to 100-year return period by using GEV fitted distributions of model and observation data.

This enables to test the model's ability to capture extreme events of such rare return periods, even though the actual length of the observational record is less than 30 years (APHRODITE dataset). In general, a long-term (at least 50-100 years of length) observation data is required to characterize an observed event as extreme and to do the necessary model evaluation before any attribution study. This GEV approach helps to rectify the problem and is therefore recommended to be used for other regions where there is a lack of long-term observations.

7.2.2. Better resilience and adaptation

By definition, adaptation is a process of adjusting to new conditions, stresses and natural hazards that result from climate change (Allwood J. M. et al., 2014). But in practice, adaptation projects are mainly designed around existing climate condition, due to the large adaptation deficit – the gap between the (in)ability to cope with climate

variability and what needs to be the baseline in order to adapt to climate change. This raises questions about whether there is a difference between adapting to current climate and adapting to future climate changes, and whether focusing on current climate characteristics can undermine adaptation to future climate change (James and Schipper, personal communication).

Chapter 5 results help open this for discussion. Analysis of relative risks of seasonal extreme rainfall events in Bangladesh suggests that what is currently seen as a drying climate is in fact likely to be masked by large aerosol content, meaning that a wetter climate is hiding under the air pollution. It is argued that in future likely air pollution abatement through large scale clean and green energy use; subsequent removal of anthropogenic aerosols will unmask the GHG warming effects causing unexpectedly fast and severe changes in the risks of extreme rainfall events. As a consequent, adaptation strategies being implemented to address less rainfall will prove to be maladaptive for the resulting much wetter climate (Rimi et al., forthcoming).

This thesis in its **chapter 5** also highlights that the drier regions of western Bangladesh exhibit greater masking effects from the aerosols during the pre-monsoon season, while wetter regions of eastern Bangladesh are associated with a smaller aerosol effects during the monsoon season. Such seasonal as well as spatial variation in the aerosol sensitivity means that the policy-makers and relevant stakeholders needs to consider the regionally distinct patterns of the changes in the risks of extreme rainfall events and the non-linearity in the response particularly due to aerosol impacts.

PEA assessments in general can contribute to promote public awareness about the costs of the extreme events; call for urgent actions to reduce emissions, scientifically support claims for additional adaptation funds, or design more resilient structures for future climate conditions.

For example, risk assessments for future warming scenarios for extreme rainfall events (as presented in **chapter 5**) can be used to define the high-risk scenario for the worst possible flooding events in Bangladesh. This high-risk scenario information can be very useful in updating the flood management schemes to prepare and reduce the impacts from anticipated future extreme events. Policy-makers can effectively plan for better adaptation if they consider the estimated changes in the risks of extreme events.

7.2.3. Contribution to loss and damage

PEA results can be highly relevant in investigating the influence of climate change on loss and damage (L&D) from extreme events (James et al., 2014). Quantification of the risks of extreme events, and investigation on the different important external drivers of change can be useful in better understanding of L&D (James et al., 2019). Consequently attribution results of **chapter 5 and 6** have potential to contribute to the ongoing L&D debates done by Bangladesh in the international climate change negotiations.

Considering the changeable impacts of GHGs and anthropogenic aerosols on present and future risks of extreme rainfall events (as presented in **chapter 5**), L&D can be interpreted in terms of the drivers along three dimensions. Firstly, emissions of GHGs and aerosols (such as sulphate and black carbon) and albedo changes from land surface

changes perturb the radiative balance of the earth-atmosphere system and cause radiative forcing. Secondly, these emissions and changes in albedo from land use changes can be spatially distributed to specific regions, nations, and economic sectors. Thirdly, the time dimensions of these changes can be different ranging from an early deforestation and coal burning to late emissions from more modern sectors like aviation and technologies that use halogenated gases (James et al., 2019).

Quantification of the contributions of different climate change drivers by regions (e.g., den Elzen *et al.*, 2005), nations (e.g., Matthews, 2016; Skeie *et al.*, 2017), sectors (e.g., Fuglestvedt *et al.*, 2008) and even companies (Heede, 2014) has been done already. Similar research approach can help to quantify the contributions of the GHG and aerosol emissions by specific region, nation, sector or companies while claiming for L&D.

7.3. Potential future research avenues

This thesis has contributed three new research papers to the scientific literature using weather@home RCM outputs and additional HAPPI AGCMs for the complex tropical monsoon region of South Asia and extreme weather events of Bangladesh. The three research papers presented provide: (i) a novel model evaluation approach that can be applied elsewhere to overcome limited availability of reference observation data. By fitting GEV distributions to available short length observation data, model simulated rare events of 100 year return period are evaluated. (ii) a multi-model risk analysis for both present and future pre-monsoon and monsoon seasonal extreme rainfall events in Bangladesh revealing how the interplay between GHGs and anthropogenic aerosols can influence the risks and (iii) the first attribution study for an extreme pre-monsoon

rainfall event at north-east Bangladesh, providing insight into how anthropogenic climate change in playing a role in changing likelihoods of extreme weather events in this country.

However, significant challenges remain in our understanding of extreme weather events in complex tropic monsoon regions, as well as the effectiveness of climate models in representing these events. Known model biases exist within RCMs for this region due to the difficulty in representing the underlying complex physics of tropical monsoons (such as convective schemes, topography, and land-surface processes), as well as the lateral boundary conditions and possible biases inherited from the global model (Alves and Marengo, 2010).

These biases have the potential to impact upon model performance, and consequently the confidence of attribution analyses. For instance, climate models cannot attribute heatwave of 2016 in India because both increased anthropogenic aerosols and irrigation have offset the effect of greenhouse gases and the models do not represent these processes well (Van Oldenborgh et al., 2018).

It is recommended that future research explores methods for reducing both model and observation uncertainty. This may include:

(7.3.1.) exploration of different model spatial resolutions;

(7.3.2.) modifying model parameterisation;

(7.3.3.) advanced correction techniques;

(7.3.4.) multi-model studies for attribution analysis;

(7.3.5.) aerosol-only forcings scenario;

(7.3.6.) fixed versus variable SSTs;

(7.3.7.) Physical mechanisms;

(7.3.8.) improved observational data; and

(7.3.9.) extended attribution studies for impact assessments.

Attribution studies can also be extended beyond climate variables to provide broader insights into the complex dynamics between multiple drivers and implications for social, economic, and ecological impact. These are discussed in more detail as follows.

7.3.1. Spatial resolution and domain size

Bhaskaran *et al.,* (2012) use the RCM, HadRM3P with horizontal resolution of 25 and 50 km over the South Asia monsoon region and looked at rainfall characteristics over three different sized domains to assess the sensitivity of the sub-domain hydrological cycle to the model domain size. This study reports that over the smaller domains model simulations produce higher number of moderate rainfall days relative to the corresponding larger domain simulations because the smaller domains may favour more frequent moderate uplifting. The results remained largely insensitive to the horizontal resolution of the model.

Caesar *et al.,* (2015) used the 17 members perturbed physics ensemble and flux corrected versions of HadCM3 for their boundary conditions for the RCM, HadRM3P with horizontal resolution of 25 km over Bangladesh. In this study, the RCM is found to simulate an early onset and dry bias in the monsoon rainfall.

This thesis uses the RCM, HadRM3P with spatial resolution of 50 km and uses the model simulations for analysing extreme events in Bangladesh. According to **chapter 4** model evaluation results, the model shows an early onset and dry bias in the monsoon season, and a wet and hot bias in the pre-monsoon season. Despite of these biases, the model captures the observed extreme events satisfactorily when compared against observations. Whether using higher spatial resolution than 50/25km in this RCM improve the model's performance in simulating pre-monsoon and monsoon rainfall still needs to be examined.

7.3.2. Convection parameterisation at a coarse grid scale

Models with coarse resolutions (of 25/50 km) provide inadequate representation of atmospheric convection, a process which occurs on a spatial scale of a few kilometres. For this type of fine-scale atmospheric process, the models do not allow convection to be well simulated on the explicit model grid due to its coarser resolution (National Academies of Sciences, Engineering, 2016). In perturbed physics experiments, model performance in such coarser resolution models can potentially be improved by changing parameters across a range of plausible values.

The models of the weather@home system described in **chapter 2** use standard, or default, model parameters (standard physics). This means that there are no changes in the schemes which parameterise sub-grid scale processes in the models. A perturbed physics ensemble (PPE) experiment may be useful to address the warm and dry biases found in the pre-monsoon season.

There is a possibility of reducing temperature and rainfall biases in the model outputs by using a PPE experiment with the weather@home regional model set. For example, Li et al., (2018) evaluated weather@home RCM, HadRM3P for the western United States and demonstrated that different parameter combinations is useful to produce model variants performing better than the standard version and suggested that a PPE experiment can help to produce model variants that are capable to simulate the orographic enhancement more realistically than the standard version.

7.3.3. Advanced correction techniques

Bellprat *et al.*, (2019) argued that recent attribution studies did not properly account for model errors in simulating the probabilities of extreme event occurrences and suggested that advanced correction techniques from the weather forecasting field needs to be applied to correct model errors and to provide trust-worthy assessments of climate change impacts. The possibility of using these advanced techniques can motivate another dimension in the future studies.

7.3.4. Multi-model studies for attribution analysis

Attribution statements are sensitive to the way the extreme event under consideration is characterized and the context within which the attribution questions are posed. Use of scientifically appropriate multiple methods as well as multiple ensembles from different models can help distinguishing the robust results from those that are sensitive to how the question is posed and the approach taken (National Academies of Sciences, Engineering, 2016). Attribution studies have usually relied on single model ensembles

however; recently multi-model and multi-method applications are becoming the new common approach.

Although this DPhil research project is primarily based on weather@home model outputs, addition of other models is found beneficial in assessing the model uncertainties and testing the robustness of the results from the single model experiments.

In **chapter 5**, a multi-model assessment for Bangladesh is done to show robust results of increasing probabilities of extreme rainfall events, but multi-method applications are yet to be done. A multi-model ensemble-based experiment using different models can provide more rigorous analyses of extreme events and agreements between model results builds a stronger case for motivating policy-makers and stakeholders.

7.3.5. Aerosol-only forcings scenario

In the tropical monsoon climate of South Asia, climate risk assessments can be benefitted by better understanding the influence of different aerosol emissions trajectories on the regional climate dynamics (Singh et al., 2018). Therefore, experiments exploring a true "Anthropogenic-Aerosols-Only" scenario in addition to the herein used "GHG-only" can be one future avenue for research to understand the interactions between these two forcing components.

7.3.6. Use of Fixed versus variable SSTs

Hirons *et al.*, (2018) shows that atmosphere-only model simulations tend to overestimate the frequency, intensity, and persistence of extreme tropical rainfall relative to the coupled model, likely due to excessive SST-forced rainfall variability. This implies that atmosphere-only attribution and time-slice experiments may overestimate the strength and duration of rainfall extremes.

Attribution studies based on atmosphere-only climate models can to some extent undermine the estimation of the associated uncertainties for using prescribed SSTs or, fixed natural SST. Risser *et al.*, (2017) demonstrated that the SST influence is of greater significance over tropical regions than the mid-latitude regions, and suggested the consideration of ocean coupling in attribution studies.

However, it is important to note that this applies to extreme temperature and rainfall related events but possibly not applicable for some events like tropical cyclones. The possible use of ocean coupling or, improved methods for incorporating SST variations may provide motivation for one of the future research avenues for having higher confidence in attribution studies for the tropical region like South Asia.

7.3.7. Physical mechanisms

As highlighted in **chapter 3,** no fundamental obstacle is found to apply weather@home's model in simulating the rainfall response to SST anomalies in attribution and prediction studies; however a more thorough investigation of the

physical mechanisms behind these relationships is necessary. Findings of this chapter present another future research opportunity that can address - how physical mechanisms play their role behind the teleconnections over this complex tropical monsoon region and how these processes can change in a warmer world.

7.3.8. Use of improved observational data

There exist considerable dissimilarities among different sources of observation data sets with limited means by which their accuracy and reliability can be determined. This limits the capacity for identifying uncertainty in the model evaluation results as well as in the extreme event analyses.

Access to reliable high resolution gridded long-term records of daily climate variables is essential for undertaking a systematic climate model evaluation with greater confidence. Therefore, potential improvements in the observation data sets by adding longer records, increased spatial coverage and additional meta data can provide motivations for further model evaluation studies and better assessment of the exceptionality of any observed event.

For instance, in **chapter 5**, model evaluation using older version of APHRODITE (1998-2007) and recent version of CPC (2006-2015) results in high model biases and large discrepancy between these two observations. But using the updated version of APHRODITE (2006-2015; the updated version become available later during this paper's review process) is found to be beneficial because the amount of model bias and discrepancy between two observations both reduced noticeably.

7.3.9. Extended attribution studies for impact assessments

Extended PEA based studies look beyond climatic variables and address for example, impacts on river flow for assessing flood risks (Philip *et al.*, 2019); droughts (Marthews *et al.*, 2015); ecosystem (Sippel and Otto, 2014); infrastructure (Pall et al., 2011b); human mortality during heat waves (Mitchell *et al.*, 2016); and monetary losses (Schaller *et al.*, 2016). In the South Asia region and particularly in Bangladesh, similar research approaches can potentially be taken to study the impacts on agriculture for food security and migration for climate-driven displacement due to extreme weather events.

7.4. Concluding remarks

The main aim of this thesis is to make PEA assessments of extreme weather events occurring in Bangladesh using the weather@home's high resolution RCM simulations. An attribution statement can be provided with confidence only when climate models in use perform satisfactorily against the observations. This evaluation step is vital for any attribution assessments that quantify the human impacts on extreme weather events.

Therefore, first the model outputs from weather@home system for the complex tropical monsoon climate of South Asia region focusing on Bangladesh are evaluated by a combination of both process-based and performance-based model evaluation approaches in this thesis.

Findings from these two model evaluation approaches suggest that the high resolution regional modelling system of weather@home of South Asia region performs well in capturing important teleconnections of this region and in simulating the extreme events in Bangladesh.

The results of two PEA based studies suggest that the risks of extreme rainfall events are increasing due to anthropogenic climate change drivers in Bangladesh. With additional global warming effects, particularly under the Paris Agreement temperature goals of 1.5°C and 2.0°C, the climate change impacts on the risks are projected to intensify. Based on these findings, this thesis concludes that the risks of extreme rainfall events in Bangladesh are increasing due to anthropogenic climate change, which implies serious detrimental impacts for agriculture and economy of this country that need to be addressed in a loss and damage context.

It is hoped that outputs of this thesis will motivate future research work to conduct further climate modelling experiments for studying extreme weather events to provide reliable climate information to contribute to better adaptation policies in this region. There is much more work to be done, but this thesis has for the first time evaluated and successfully used the weather@home regional climate modelling system for analysing extreme weather events in Bangladesh at sub-regional local scales and therefore has made an important pioneering contribution to show the way forward.

8. Bibliography

Agilan, V. and Umamahesh, N. V.: El Niño Southern Oscillation cycle indicator for modeling extreme rainfall intensity over India, Ecol. Indic., 84, 450–458, doi:10.1016/j.ecolind.2017.09.012, 2018.

Agrawala, S., Ota, T., Ahmed, A. U., Smith, J. and van Aalst, M.: Development and Climate Change in Bangladesh: focus on coastal flooding and the Sundarbans, Paris., 2003.

Ahmed, A. U. and Mirza, M. M. Q.: Review of causes and dimensions of floods with particular reference to flood'98: national perspectives, in Perspectives on flood, edited by Q. K. Ahmad, A. K. A. Chowdhury, S. H. Imam, and M. Sarker, pp. 67–84, University Press Limited, Dhaka., 2000.

Ahmed, M. R., Rahaman, K. R., Kok, A. and Hassan, Q. K.: Remote sensing-based quantification of the impact of flash flooding on the rice production: A case study over Northeastern Bangladesh, Sensors (Switzerland), 17(10), doi:10.3390/s17102347, 2017.

Ahmed, R.: Rainfall: in Banglapedia - the National Encyclopedia of Bangladesh, Dhaka, Bangladesh. [online] Available from: http://en.banglapedia.org/index.php?title=Rainfall, 2012.

Ali, R. M. E., Tunbridge, L. W., Bhasin, R. K., Akter, S., Khan, M. M. H. and Uddin, M. Z.: Landslides susceptibility of chittagong city, bangladesh and development of landslides early warning system, in Landslide Science for a Safer Geoenvironment, vol. 1, pp. 423–429., 2014.

Allan, R. J., Chambers, D., Drosdowsky, W., Hendon, H., Latif, M., Nicholls, N., Smith, I., Stone, R. and Tourr, Y.: Is there an Indian Ocean Dipole independent of the El Niño-Southern Oscillations?, CLIVAR Exch., 6(3), 18–22, 2001.

Allen, M.: Do-it-yourself climate prediction, Nature, 401(6754), 642, doi:10.1038/44266, 1999.

Allen, M.: Liability for climate change, Nature, 421(6926), 891–92, 2003.

Allwood J. M., Bosetti, V., Dubash, N. K., Gómez-Echeverri, L. and Stechow, C. von: Glossary, in Glossary. In: Climate Change 2014: Mitigation of Climate Change. Contribution of Working Group III to the Fifth Assessment Report of the Intergovernmental Panel on Climate Change, edited by O. Edenhofer, R. Pichs-Madruga, Y. Sokona, E. Farahani, S. Kadner, K. Seyboth, A. Adler, I. Baum, S. Brunner, P. Eickemeier, B. Kriemann, J. Savolainen, S. Schlömer, C. von Stechow, T. Zwickel, and J. C. Minx, pp. 1247–1280, Cam-bridge University Press, Cambridge, United Kingdom and New York, NY, USA. [online] Available from: https://www.ipcc.ch/site/assets/uploads/2018/02/ipcc_wg3_ar5_annex-i.pdf, 2014.

Alves, L. M. and Marengo, J.: Assessment of regional seasonal predictability using the PRECIS regional climate modeling system over South America, Theor. Appl. Climatol., 100(3), 337–350, doi:10.1007/s00704-009-0165-2, 2010.

Andermann, C., Bonnet, S. and Gloaguen, R.: Evaluation of precipitation data sets along the Himalayan front, Geochemistry, Geophys. Geosystems, 12(7), doi:10.1029/2011GC003513, 2011.

Anderson, D. P.: BOINC: A system for public-resource computing and storage, Pittsburgh, P.A., 2004.

Añel, J. A., López-Moreno, J. I., Otto, F., Vicente-Serrano, S., Schaller, N., Massey, N., Buisán, S. T. and Allen, M. R.: The extreme snow accumulation in the western Spanish Pyrenees during winter and spring 2013 [in "Explaining Extreme Events of 2013 from a Climate Perspective"], Bull. Am. Meteorol. Soc., 95(9), S73–S76, 2014.

Anja, M.-C., Becker, A., Finger, P., Schneider, U. and Ziese, M.: GPCC Climatology Version 2018 at 0.5°: Monthly Land-Surface Precipitation Climatology for Every Month and the Total Year from Rain-Gauges built on GTS-based and Historical Data, Glob. Precip. Climatol. Cent. (GPCC, http//gpcc.dwd.de/) Dtsch. Wetterd., doi:10.5676/DWD_GPCC/CLIM_M_V2018_050, 2018.

Annamalai, H., Murtugudde, R., Potemra, J., Xie, S. P., Liu, P. and Wang, B.: Coupled dynamics over the Indian Ocean: Spring initiation of the Zonal Mode, Deep. Res. Part II Top. Stud. Oceanogr., 50(12–13), 2305–2330, doi:10.1016/S0967-0645(03)00058-4, 2003.

Ashfaq Moetasim, Ying Shi, Tung, W., Trapp, R. J., Gao, X., Pal, J. S. and Diffenbaugh, N. S.: Suppression of South Asian summer monsoon precipitation in the 21st century, Geophys. Res. Lett., 36(L01704), doi:10.1029/2008GL036500, 2009.

Ashok, K., Guan, Z., Saji, N. H. and Yamagata, T.: Individual and Combined Influences of ENSO and the Indian Ocean Dipole on the Indian Summer Monsoon, Am. Meterological Soc., 17, 3141–3155, doi:10.1175/1520-0442(2004)017<3141:IACIOE>2.0.CO;2, 2004.

Bajracharya, S. R., Palash, W., Shrestha, M. S., Khadgi, V. R., Duo, C., Das, P. J. and Dorji, C.: Systematic evaluation of satellite-based rainfall products over the brahmaputra basin for hydrological applications, Adv. Meteorol., 2015, doi:10.1155/2015/398687, 2015.

Banglapedia: River and Drainage system, Banglapedia- Natl. Encycl. Bangladesh [online] Available from: http://en.banglapedia.org/index.php?title=River_and_Drainage_System, 2012.

Baquero-Bernal, A., Latif, M. and Legutke, S.: On dipolelike variability of sea surface temperature in the tropical Indian Ocean, J. Clim., 15(11), 1358–1368, doi:10.1175/1520-0442(2002)015<1358:ODVOSS>2.0.CO;2, 2002.

BARC: Generalized map of avearge rainfall Bangladesh from Bangladesh Agricultural Research Council(BARC), UNDP, FAO GIS Project, Dhaka, Bangladesh. [online] Available from: http://maps.barcapps.gov.bd/index.php?t=climate, 2014.

Bari, S. H., Rahman, M. T. U., Hoque, M. A. and Hussain, M. M.: Analysis of seasonal and annual rainfall trends in the northern region of Bangladesh, Atmos. Res., 176–177, 148–158, doi:10.1016/j.atmosres.2016.02.008, 2016.

Basak, J. K.: Dynamics of Labour Force for Human Resource Management: A Local Economy Perspective in Bangladesh, J. Hum. Resour. Manag., 2(6), 1, doi:10.11648/j.jhrm.s.2014020601.11, 2014.

Behera, S. K. and Ratnam, J. V.: Quasi-asymmetric response of the Indian summer monsoon rainfall to opposite phases of the IOD, Sci. Rep., 8(1), doi:10.1038/s41598-017-18396-6, 2018.

Bellprat, O., Guemas, V., Doblas-Reyes, F. and Donat, M. G.: Towards reliable extreme weather and climate event attribution, Nat. Commun., 10(1), 1732, doi:10.1038/s41467-019-09729-2, 2019.

Bentsen, M., Bethke, I., Debernard, J., Iversen, T., Kirkevag, A., Seland, Ø., Drange, H., Roelandt, C., Seierstad, I., Hoose, C. and Kristjansson, J.: The Norwegian Earth System Model, NorESM1-M- Part 1: Description and basic evaluation of the physical climate, Geosci. Model Dev., 6, 687–720, doi:10 .5194/gmd-6-687-2013, 2013.

Bhaskaran, B., Jones, R. and Murphy, J.: Simulations of the Indian summer monsoon using a nested regional climate model: Domain size experiments, Clim. Dyn., 12(9), 573–587, doi:10.1007/s003820050129, 1996.

Bhaskaran, B., Ramachandran, A., Jones, R. and Moufouma-Okia, W.: Regional climate model applications on sub-regional scales over the Indian monsoon region: The role of domain size on downscaling uncertainty, J. Geophys. Res. Atmos., 117(10), doi:10.1029/2012JD017956, 2012.

Black, M. T. and Karoly, D. J.: 23. Southern Australia's warmest October on record: The role of ENSO and climate change, Bull. Am. Meteorol. Soc., 97(12), S118–S121, doi:10.1175/BAMS-D-16-0124.1, 2016.

Black, M. T., Karoly, D. J., Rosier, S. M., Dean, S. M., King, A. D., Massey, N. R., Sparrow, S. N., Bowery, A., Wallom, D., Jones, R. G., Otto, F. E. L. and Allen, M. R.: The weather@home regional climate modelling project for Australia and New Zealand, Geosci. Model Dev., 9(9), 3161–3176, doi:10.5194/gmd-9-3161-2016, 2016.

Blake, E. S. and Gibney, E. J.: The deadliest, costliest and most intense United States

tropical cyclones from 1851 to 2010 (and other frequently requested hurricane facts), NOAA Tech. Memo. NWS NHC -6, 1–49 [online] Available from: https://www.nhc.noaa.gov/pdf/nws-nhc-6.pdf, 2011.

Bollasina, M. A., Ming, Y. and Ramaswamy, V.: Anthropogenic aerosols and the weakening of the south asian summer monsoon, Science (80-.)., 334(6055), 502–505, doi:10.1126/science.1204994, 2011.

Bollasina, M. A., Ming, Y. and Ramaswamy, V.: Earlier onset of the Indian monsoon in the late twentieth century: The role of anthropogenic aerosols, Geophys. Res. Lett., 40(14), 3715–3720, doi:10.1002/grl.50719, 2013.

Bothale, R. V. and Katpatal, Y. B.: Trends and Anomalies in Extreme Climate Indices and Influence of El Niño and La Niña over Pranhita Catchment in Godavari Basin, India, J. Hydrol. Eng., 21(2), 05015023, doi:10.1061/(ASCE)HE.1943-5584.0001283, 2016.

Caesar, J. and Janes, T.: Regional climate change over South Asia, in Ecosystem Services for Well-Being in Deltas: Integrated Assessment for Policy Analysis, pp. 207–221., 2018.

Caesar, J., Janes, T., Lindsay, A. and Bhaskaran, B.: Temperature and precipitation projections over Bangladesh and the upstream Ganges, Brahmaputra and Meghna systems, Environ. Sci. Process. Impacts, 17(6), 1047–1056, doi:10.1039/C4EM00650J, 2015.

Cai, W., Borlace, S., Lengaigne, M., van Rensch, P., Collins, M., Vecchi, G., Timmermann, A., Santoso, A., McPhaden, M. J., Wu, L., England, M. H., Wang, G., Guilyardi, E. and Jin, F.-F.: Increasing frequency of extreme El Niño events due to greenhouse warming, Nat. Clim. Chang., 4, 111 [online]

Available from: https://doi.org/10.1038/nclimate2100, 2014.

Cai, W., Santoso, A., Wang, G., Yeh, S.-W., An, S.-I., Cobb, K. M., Collins, M., Guilyardi, E., Jin, F.-F., Kug, J.-S., Lengaigne, M., McPhaden, M. J., Takahashi, K., Timmermann, A., Vecchi, G., Watanabe, M. and Wu, L.: ENSO and greenhouse warming, Nat. Clim. Chang., 5, 849 [online] Available from: https://doi.org/10.1038/nclimate2743, 2015.

Cattiaux, J. and Yiou, P.: Contribution of atmospheric circulation to remarkable European temperatures of 2011, Bull. Am. Meteorol. Soc., 93(7), 1054–1057, 2012.

Chen, M. and Xie, P.: CPC Unified Gauge-based Analysis of Global Daily Precipitation, 2008 West. Pacific Geophys. Meet., doi:10.1016/j.jpowsour.2010.07.060, 2008.

Chen, M., Shi, W., Xie, P., Silva, V. B. S., Kousky, V. E., Higgins, R. W. and Janowiak, J. E.: Assessing objective techniques for gauge-based analyses of global daily precipitation, J. Geophys. Res. Atmos., 113(4), doi:10.1029/2007JD009132, 2008a.

Chen, M., Xie, P. and NOAA Climate Prediction Center(CPC): CPC Gauge-Based Analysis of Global Daily Precipitation, in Western Pacific Geophysics Meeting, Cairns, Australia, 29 July - 1 August, 2008. [online] Available from: ftp://ftp.cpc.ncep.noaa.gov/precip/CPC_UNI_PRCP/GAUGE_GLB/DOCU/Chen_et_al_2008_Daily_Gauge_Anal.pdf, 2008b.

Chevuturi, A., Klingaman, N. P., Turner, A. G. and Hannah, S.: Projected Changes in the Asian-Australian Monsoon Region in 1.5°C and 2.0°C Global-Warming Scenarios, Earth's Futur., 6(3), 339–358, doi:10.1002/2017EF000734, 2018.

Christian Aid: Counting The Cost: A Year of Climate Breakdown. [online] Available from: https://mediacentre.christianaid.org.uk/download/?id=4170&pn=21e38f435ea050ce63ac6b7e52c58d72-pdf, 2018.

Christidis, N., Stott, P. A., Scaife, A. A., Arribas, A., Jones, G. S., Copsey, D., Knight, J. R. and Tennant, W. J.: A new HADGEM3-a-based system for attribution of weather- and climate-related extreme events, J. Clim., 26(9), 2756–2783, doi:10.1175/JCLI-D-12-00169.1, 2013.

Christidis, N., Manomaiphiboon, K., Ciavarella, A. and Stott, P. A.: The Hot and Dry April of 2016 in Thailand, in Bulletin of the American Meteorological Society, vol. 98, pp. S128–S132., 2017.

Coles, S., Bawa, J., Trenner, L. and Dorazio, P.: An Introduction to Statistical Modeling of Extreme Values, Springer, London, UK., 2001.

Collins, M., Booth, B. B. B., Harris, G. R., Murphy, J. M., Sexton, D. M. H. and Webb, M. J.: Towards quantifying uncertainty in transient climate change, Clim. Dyn., 27(2–3), 127–147, doi:10.1007/s00382-006-0121-0, 2006.

Collins, M., Booth, B. B. B., Bhaskaran, B., Harris, G. R., Murphy, J. M., Sexton, D. M. H. and Webb, M. J.: Climate model errors, feedbacks and forcings: a comparison of perturbed physics and multi-model ensembles, Clim. Dyn., 36(9–10), 1737–1766, doi:10.1007/s00382-010-0808-0, 2011.

Cox, P. M.: Description of the TRIFFID dynamic global vegetation model, Hadley Centre Technical Note 24, Hadley Centre, Met Office, Bracknell, UK., [online] Available from: https://digital.nmla.metoffice.gov.uk/file/sdb%253AdigitalFile%25%0A7Cdaf

e8eae-e394-480f-885f-6963f0044ab6/, 2001.

Creese, A. and Washington, R.: A process-based assessment of CMIP5 rainfall in the Congo basin: The September-November rainy season, J. Clim., 31(18), 7417–7439, doi:10.1175/JCLI-D-17-0818.1, 2018.

Dasgupta, S., Huq, M., Khan, Z. H., Masud, M. S., Ahmed, M. M. Z., Mukherjee, N. and Pandey, K.: Climate proofing infrastructure in bangladesh: The incremental cost of limiting future flood damage, Washington, DC., 2011.

Dee, D. P., Uppala, S. M., Simmons, A. J., Berrisford, P., Poli, P., Kobayashi, S., Andrae, U., Balmaseda, M. A., Balsamo, G., Bauer, P., Bechtold, P., Beljaars, A. C. M., van de Berg, L., Bidlot, J., Bormann, N., Delsol, C., Dragani, R., Fuentes, M., Geer, A. J., Haimberger, L., Healy, S. B., Hersbach, H., Hólm, E. V., Isaksen, L., Kållberg, P., Köhler, M., Matricardi, M., Mcnally, A. P., Monge-Sanz, B. M., Morcrette, J. J., Park, B. K., Peubey, C., de Rosnay, P., Tavolato, C., Thépaut, J. N. and Vitart, F.: The ERA-Interim reanalysis: Configuration and performance of the data assimilation system, Q. J. R. Meteorol. Soc., 137(656), 553–597, doi:10.1002/qj.828, 2011.

Dittus, A. J., Karoly, D. J., Donat, M. G., Lewis, S. C. and Alexander, L. V.: Understanding the role of sea surface temperature-forcing for variability in global temperature and precipitation extremes, Weather Clim. Extrem., 21, 1–9, doi:10.1016/j.wace.2018.06.002, 2018.

Dommenget, D. and Latif, M.: A cautionary note on the interpretation of EOFs, J. Clim., 15(2), 216–225, doi:10.1175/1520-0442(2002)015<0216:ACNOTI>2.0.CO;2, 2002.

Donlon, C. J., Martin, M., Stark, J., Roberts-Jones, J., Fiedler, E. and Wimmer, W.: The Operational Sea Surface Temperature and Sea Ice Analysis (OSTIA) system, Remote Sens. Environ., 116, 140–158, doi:10.1016/j.rse.2010.10.017, 2012.

Du, J., Fang, J., Xu, W. and Shi, P.: Analysis of dry/wet conditions using the standardized precipitation index and its potential usefulness for drought/flood monitoring in Hunan Province, China, Stoch. Environ. Res. Risk Assess., 27(2), 377–387, doi:10.1007/s00477-012-0589-6, 2013.

Eckstein, D., Künzel, V. and Schäfer, L.: Global Climate Risk Index 2018. Who Suffers Most From Extreme Weather Events? Weather-related Loss Events in 2016 and 1997 to 2016., Bonn, Germany. [online] Available from: https://germanwatch.org/sites/germanwatch.org/files/publication/20432.pdf, 2018.

Eckstein, K., Dorsch, L. and Fischer, L.: Global Climate Risk Index 2016, Bonn, Germany. [online] Available from: http://germanwatch.org/en/download/13503.pdf, 2015.

Efron, B.: Bootstrap Methods: Another Look at the Jackknife, Ann. Stat., 7(1), 1–26, doi:10.1214/aos/1176344552, 1979.

Efron, B. and Gong, G.: A leisurely look at the bootstrap, the jackknife, and cross-validation, Am. Stat., 37(1), 36–48, doi:10.1080/00031305.1983.10483087, 1983.

Efron, B. and Tibshirani, R. J.: An introduction to the bootstrap, Chapman and Hall., 1993.

den Elzen, M., Fuglestvedt, J., Höhne, N., Trudinger, C., Lowe, J., Matthews, B., Romstad, B., de Campos, C. P. and Andronova, N.: Analysing countries'

contribution to climate change: Scientific and policy-related choices, Environ. Sci. Policy, 8(6), 614–636, doi:10.1016/j.envsci.2005.06.007, 2005.

Endo, H., Kitoh, A., Ose, T., Mizuta, R. and Kusunoki, S.: Erratum: Future changes and uncertainties in Asian precipitation simulated by multiphysics and multi-sea surface temperature ensemble experiments with high-resolution Meteorological

Research Institute atmospheric general circulation models (MRI-AGCMs) (Jo, J. Geophys. Res. Atmos., 118(5), 2303, doi:10.1002/jgrd.50267, 2013.

Essery, R. and Clark, D. B.: Developments in the MOSES 2 land-surface model for PILPS 2e, Glob. Planet. Change, 38(1–2), 161–164, doi:10.1016/S0921-8181(03)00026-2, 2003.

Essery, R. L. H., Best, M. J., Betts, R. A., Cox, P. M. and Taylor, C. M.: Explicit representation of subgrid heterogeneity in a GCM land surface scheme, J. Hydrometeorol., 4(3), 530–543, doi:10.1175/1525-7541(2003)004<0530:EROSHI>2.0.CO;2, 2003.

Fahad, M. G. R., Saiful Islam, A. K. M., Nazari, R., Alfi Hasan, M., Tarekul Islam, G. M. and Bala, S. K.: Regional changes of precipitation and temperature over Bangladesh using bias-corrected multi-model ensemble projections considering high-emission pathways, Int. J. Climatol., doi:10.1002/joc.5284, 2017.

FAO: Bangladesh: Severe floods in 2017 affected large numbers of people and caused damage to the agriculture sector. [online] Available from: http://www.fao.org/3/a-i7876e.pdf, 2017.

Faust, E.: Rapid attribution: Is climate change involved in an extreme weather event?, [online] Available from: https://www.munichre.com/topics-online/en/2017/topics-geo/rapid-attribution, 2017.

Flato, G., Marotzke, J., Abiodun, B., Braconnot, P., Chou, S. C., Collins, W., Cox, P., Driouech, F., Emori, S., Eyring, V., Forest, C., Gleckler, P., Guilyardi, E., Jakob, C., Kattsov, V., Reason, C. and Rummukainen, M.: Evaluation of climate models, Cambridge University Press, Cambridge, United Kingdom and New York, NY, USA., 2013.

Fuglestvedt, J., Berntsen, T., Myhre, G., Rypdal, K. and Skeie, R. B.: Climate forcing from the transport sectors, Proc. Natl. Acad. Sci. U. S. A., 105(2), 454–458, doi:10.1073/pnas.0702958104, 2008.

Fung, F., Lopez, A. and New, M.: Water availability in +2 C and +4 C worlds, Philos. Trans. R. Soc. A Math. Phys. Eng. Sci., 369(1934), 99–116, doi:10.1098/rsta.2010.0293, 2011.

Funk, C., Hoell, A. and Stone, D.: Examining the Contribution of the Observed Global Warming Trend to the California Droughts of 2012/13 and 2013/14, Bull. Am. Meteorol. Soc., 95(9), S11–S15, doi:10.1175/1520-0477-95.9.S1.1, 2014.

G. T. Walker: Correlation in seasonal variations of weather - A further study of world weather., Indian Meteorol. Mem., XXI, Part, 275–332 [online] Available from: ftp://ftp.library.noaa.gov/docs.lib/htdocs/rescue/mwr/053/mwr-053-06-0252.pdf, 1925.

Ganguly, D., Rasch, P. J., Wang, H. and Yoon, J. H.: Climate response of the South Asian monsoon system to anthropogenic aerosols, J. Geophys. Res. Atmos., 117(13), doi:10.1029/2012JD017508, 2012.

García-Herrera, R., Díaz, J., Trigo, R. M., Luterbacher, J. and Fischer, E. M.: A Review of the European Summer Heat Wave of 2003, Crit. Rev. Environ. Sci. Technol., 40(4), 267–306, doi:10.1080/10643380802238137, 2010.

Geethalakshmi, V., Yatagai, A., Palanisamy, K. and Umetsu, C.: Impact of ENSO and the Indian Ocean Dipole on the north-east monsoon rainfall of Tamil Nadu State in India, Hydrol. Process., 23(4), 633–647, doi:10.1002/hyp.7191, 2009.

Gilleland, E. and Katz, R. W.: New software to analyze how extremes change over time, Eos (Washington. DC)., 92(2), 13–14, doi:10.1029/2011EO020001, 2011.

GoB: Climate Fiscal Framework. Government of Bangladesh. [online] Available from: http://www.climatefinance-developmenteffectiveness.org/archive/documents/Bangladesh_Climate_Fiscal_Framework_271014.pdf, 2014.

Gordon, C., Cooper, C., Senior, C. A., Banks, H., Gregory, J. M., Johns, T. C., Mitchell, J. F. B. and Wood, R. A.: The simulation of SST, sea ice extents and ocean heat transports in a version of the Hadley Centre coupled model without flux adjustments, Clim. Dyn., 16(2–3), 147–168, doi:10.1007/s003820050010, 2000.

Goswami, B. B., Deshpande, M., Mukhopadhyay, P., Saha, S. K., Rao, S. A., Murthugudde, R. and Goswami, B. N.: Simulation of monsoon intraseasonal variability in NCEP CFSv2 and its role on systematic bias, Clim. Dyn., 43(9–10), 2725–2745, doi:10.1007/s00382-014-2089-5, 2014.

Goswami, B. N., Venugopal, V., Sangupta, D., Madhusoodanan, M. S. and Xavier, P. K.: Increasing trend of extreme rain events over India in a warming environment, Science (80-.)., 314(5804), 1442–1445,

doi:10.1126/science.1132027, 2006.

Guillod, B. P., Jones, R. G., Bowery, A., Haustein, K., Massey, N. R., Mitchell, D. M., Otto, F. E. L., Sparrow, S. N., Uhe, P., Wallom, D. C. H., Wilson, S. and Allen, M. R.: Weather@home 2: Validation of an improved global-regional climate modelling system, Geosci. Model Dev., 10(5), 1849–1872, doi:10.5194/gmd-10-1849-2017, 2017.

Guo, J., Deng, M., Lee, S. S., Wang, F., Li, Z., Zhai, P., Liu, H., Lv, W., Yao, W. and Li, X.: Delaying precipitation and lightning by air pollution over the pearl river delta. Part I: Observational analyses, J. Geophys. Res., 121(11), 6472–6488, doi:10.1002/2015JD023257, 2016.

Guo, L., Highwood, E. J., Shaffrey, L. C. and Turner, A. G.: The effect of regional changes in anthropogenic aerosols on rainfall of the East Asian Summer Monsoon, Atmos. Chem. Phys., 13(3), 1521–1534, doi:10.5194/acp-13-1521-2013, 2013.

Gutro, R.: Bangladesh's Heavy Rainfall Examined With NASA's IMERG, Nasa Gpm [online] Available from: https://www.nasa.gov/feature/goddard/2017/bangladeshs-heavy-rainfall-examined-with-nasas-imerg (Accessed 14 November 2017), 2017.

Habiba, U. and Shaw, R.: Drought scenario in Bangladesh, in Community, Environment and Disaster Risk Management, vol. 13, edited by M. A. Abedin, U. Habiba, and R. Shaw, pp. 213–245, Emerald Group Publishing Limited., 2013.

Hasan, M. A. and Islam, A. K. M. S.: Evaluation of Microphysics and Cumulus Schemes of WRF for Forecasting of Heavy Monsoon Rainfall over the

Southeastern Hilly Region of Bangladesh, Pure Appl. Geophys., 175(12), 4537–4566, doi:10.1007/s00024-018-1876-z, 2018.

Hasan, M. A., Islam, A. K. M. S. and Bhaskaran, B.: Validation of seasonal temperature , precipitation and mean sea level pressure of the multi-member ensemble scenarios over Bangladesh using PRECIS model, 4th Int. Conf. Water Flood Manag., 565–574, 2013.

Hassan, M., Penfei, D., Iqbal, W., Can, W., Wei, F. and Ba, W.: Temperature and Precipitation Climatology Assessment over South Asia using the Regional Climate Model (RegCM4.3): An Evaluation of the Model Performance, J. Earth Sci. Clim. Change, 05(07), 214, doi:10.4172/2157-7617.1000214, 2014.

Hatsuzuka, D., Yasunari, T. and Fujinami, H.: Characteristics of Low Pressure Systems Associated with Intraseasonal Oscillation of Rainfall over Bangladesh during Boreal Summer, Mon. Weather Rev., 142(12), 4758–4774, doi:10.1175/MWR-D-13-00307.1, 2014.

Hauser, M., Gudmundsson, L., Orth, R., Jézéquel, A., Haustein, K., Vautard, R., van Oldenborgh, G. J., Wilcox, L. and Seneviratne, S. I.: Methods and Model Dependency of Extreme Event Attribution: The 2015 European Drought, Earth's Futur., 5(10), 1034–1043, doi:10.1002/2017EF000612, 2017.

Haustein, K., Uhe, P. F., Rimi, R. H., Islam, A. S. and Otto, F. E. L.: Is the wettest place on Earth getting wetter?, Geophys. Res. Lett., n.d.

He, J. and Soden, B. J.: Does the lack of coupling in SST-forced atmosphere-only models limit their usefulness for climate change studies?, J. Clim., 29(12), 4317–4325, doi:10.1175/JCLI-D-14-00597.1, 2016.

He, J., Soden, B. J. and Kirtman, B.: The robustness of the atmospheric circulation and precipitation response to future anthropogenic surface warming, Geophys. Res. Lett., 41(7), 2614–2622, doi:10.1002/2014GL059435, 2014.

Heede, R.: Tracing anthropogenic carbon dioxide and methane emissions to fossil fuel and cement producers, 1854-2010, Clim. Change, 122(1–2), 229–241, doi:10.1007/s10584-013-0986-y, 2014.

Herring, S. C., Christidis, N., Hoell, A., Kossin, J. P., III, C. J. S. and Stott, P. A.: EXPLAINING EXTREME EVENTS OF 2016 FROM A CLIMATE PERSPECTIVE., 2017.

Hirons, L. C., Klingaman, N. P. and Woolnough, S. J.: The Impact of Air-Sea Interactions on the Representation of Tropical Precipitation Extremes, J. Adv. Model. Earth Syst., 10(2), 550–559, doi:10.1002/2017MS001252, 2018.

Höfer, T. and Messerli, B.: Floods in Bangladesh: history, dynamics and rethinking the role of the Himalayas, United Nations University Press, Tokyo., 2006.

Hosking, J. R. M.: L-moments: Analysis and Estimation of Distributions Using Linear Combinations of Order Statistics, J. R. Stat. Soc. (Series B), 52(1), 105–124, 1990.

Hossain, A. N. H. A.: Flood management. [online] Available from: http://www.apfm.info/publications/casestudies/cs_bangladesh_sum.pdf, 1998.

Houze, R. A., Rasmussen, K. L., Medina, S., Brodzik, S. R. and Romatschke, U.: Anomalous atmospheric events leading to the summer 2010 floods in Pakistan, Bull. Am. Meteorol. Soc., 92(3), 291–298, doi:10.1175/2010BAMS3173.1, 2011.

Huang, B., Thorne, P. W., Banzon, V. F., Boyer, T., Chepurin, G., Lawrimore, J. H., Menne, M. J., Smith, T. M., Vose, R. S. and Zhang, H. M.: Extended reconstructed Sea surface temperature, Version 5 (ERSSTv5): Upgrades, validations, and intercomparisons, J. Clim., 30(20), 8179–8205, doi:10.1175/JCLI-D-16-0836.1, 2017.

Huang, J., Wang, T., Wang, W., Li, Z. and Yan, H.: Climate effects of dust aerosols over east asian arid and semiarid regions, J. Geophys. Res., 119(19), 11,398-11,416, doi:10.1002/2014JD021796, 2014.

Huffman, G. J., Adler, R. F., Bolvin, D. T., Gu, G., Nelkin, E. J., Bowman, K. P., Hong, Y., Stocker, E. F. and Wolff, D. B.: The TRMM Multi-satellite Precipitation Analysis: Quasi-Global, Multi-Year, Combined-Sensor Precipitation Estimates at Fine Scale, J. Hydrometeorol., 8, 38–55, doi:10.1175/JHM560.1, 2007.

Imada, Y., Shiogama, H., Takahashi, C., Watanabe, M., Mori, M., Kamae, Y. and Maeda, S.: Climate Change Increased the Likelihood of the 2016 Heat Extremes in Asia, Bull. Am. Meteorol. Soc., 98(12), S97–S101, doi:10.1175/BAMS-D-17-0109.1, 2017.

Immerzeel, W.: Historical trends and future predictions of climate variability, Int. J. Clim., 28(2), 243–254, doi:10.1002/joc, 2008.

IPCC: AR5 - Summary for Policymakers, in CLIMATE CHANGE 2013 - The Physical Science Basis, Contribution of Working Group I to the Fifth Assessment Report of the Intergovernmental Panel on Climate Change, vol. 9, p. 78., 2013a.

IPCC: Climate Change 2013: The Physical Science Basis. Contribution of Working Group I to the Fifth Assessment Report of the Intergovern- mental Panel on

Climate Change, edited by T. F. Stocker, D. Qin, G.-K. Plattner, M. Tignor, S. K. Allen, J. Boschung, A. Nauels, Y. Xia, V. Bex, and P. M. Midgley, Cambridge University Press Cambridge, UK, and New York., 2013b.

IPCC, 2013: The Physical Science Basis. Contribution of Working Group I to the Fifth Assessment Report of the Intergovernmental Panel on Climate Change, Cambridge University Press, Cambridge, United Kingdom and New York, NY, USA. [online] Available from: http://scholar.google.nl/scholar?hl=nl&q=climate+change&btnG=&lr=&oq=climate+ca#2, 2013c.

Islam, M. A., Ahmed, A., Munir, M. M. and Khandakar, Z. Z.: Verification of APHRODITE Precipitation Data Sets over Bangladesh, in Proceedings of the 4th International Conference on Civil Engineering for Sustainable Development (ICCESD, 2018), pp. 1–9, Khulna University of Engineering & Technology, Khulna, Bangladesh. [online] Available from: http://www.iccesd.com/proc_2018/Papers/r_p4584.pdf, 2018.

Islam, M. N.: Rainfall and Temperature Scenario for Bangladesh, Open Atmos. Sci. J., 3(1), 93–103, doi:10.2174/1874282300903010093, 2009.

Islam, M. N., Rafiuddin, M., Ahmed, A. U. and Kolli, R. K.: Calibration of PRECIS in employing future scenarios in Bangladesh, Int. J. Climatol., 28(5), 617–628, doi:10.1002/joc.1559, 2008a.

Islam, M. N., Rafiuddin, M., Ahmed, A. U. and Kolli, R. K.: Calibration of PRECIS in employing future scenarios in Bangladesh, Int. J. Clim., 28, 617–628, doi:10.1002/joc.1559, 2008b.

Iversen, T., Bentsen, M., Bethke, I., Debernard, J. B., Kirkevåg, A., Seland, Ø., Drange, H., Kristjansson, J. E., Medhaug, I., Sand, M. and Seierstad, I. A.: The Norwegian Earth System Model, NorESM1-M – Part 2: Climate response and scenario projections, Geosci. Model Dev., 6(2), 389–415, doi:10.5194/gmd-6-389-2013, 2013.

James, R., Otto, F., Parker, H., Boyd, E., Cornforth, R., Mitchell, D. and Allen, M.: Characterizing loss and damage from climate change, Nat. Clim. Chang., 4(11), 938–939, doi:10.1038/nclimate2411, 2014.

James, R., Washington, R., Schleussner, C. F., Rogelj, J. and Conway, D.: Characterizing half-a-degree difference: a review of methods for identifying regional climate responses to global warming targets, Wiley Interdiscip. Rev. Clim. Chang., 8(2), doi:10.1002/wcc.457, 2017.

James, R., Washington, R., Abiodun, B., Kay, G., Mutemi, J., Pokam, W., Hart, N., Artan, G. and Senior, C.: Evaluating climate models with an African lens, Bull. Am. Meteorol. Soc., 99(2), 313–336, doi:10.1175/BAMS-D-16-0090.1, 2018.

James, R. A., Jones, R. G., Boyd, E., Young, H. R., Otto, F. E. L., Huggel, C. and Fuglestvedt, J. S.: Attribution: How Is It Relevant for Loss and Damage Policy and Practice?, in Loss and Damage from Climate Change: Concepts, Methods and Policy Options, edited by R. Mechler, L. M. Bouwer, T. Schinko, S. Surminski, and J. Linnerooth-Bayer, pp. 113–154, Springer International Publishing, Cham., 2019.

Janes, T. and Bhaskaran, B.: Evaluation of regional model performance in simulating key climate variables over Bangladesh, Met Office, Exeter, United Kingdom., 2012.

Jones, A., Roberts, D. L., Woodage, M. J. and Johnson, C. E.: Indirect sulphate aerosol forcing in a climate model with an interactive sulphur cycle, J. Geophys. Res. Atmos., 106(D17), 20293–20310, doi:10.1029/2000JD000089, 2001.

Jones, R. G., M, N., DC, H., D, H., S S, W., G J, J. and B, M. J. F.: Generating high resolution climate change scenarios using PRECIS, Exeter, UK., 2004.

Kay, A. L., Crooks, S. M., Pall, P. and Stone, D. A.: Attribution of Autumn/Winter 2000 flood risk in England to anthropogenic climate change: A catchment-based study, J. Hydrol., 406(1–2), 97–112, doi:10.1016/j.jhydrol.2011.06.006, 2011.

Kenyon, J. and Hegerl, G. C.: Influence of modes of climate variability on global precipitation extremes, J. Clim., 23(23), 6248–6262, doi:10.1175/2010JCLI3617.1, 2010.

Khandu, Awange, J. L. and Forootan, E.: An evaluation of high-resolution gridded precipitation products over Bhutan (1998-2012), Int. J. Climatol., 36(3), 1067–1087, doi:10.1002/joc.4402, 2016.

Kharin, V. V., Zwiers, F. W., Zhang, X. and Hegerl, G. C.: Changes in temperature and precipitation extremes in the IPCC ensemble of global coupled model simulations, J. Clim., 20(8), 1419–1444, doi:10.1175/JCLI4066.1, 2007.

Kharin, V. V., Zwiers, F. W., Zhang, X. and Wehner, M.: Changes in temperature and precipitation extremes in the CMIP5 ensemble, Clim. Change, 119(2), 345–357, doi:10.1007/s10584-013-0705-8, 2013.

King, A. D., Lewis, S. C., Perkins, S. E., Alexander, L. V., Donat, M. G., Karoly, D. J. and Black, M. T.: Limited Evidence of Anthropogenic Influence on the 2011-12 Extreme Rainfall over Southeast Australia [in "Explaining Extreme Events

of 2012 from a Climate Perspective"], Bull. Am. Meteorol. Soc., 94, S55–S58, 2013.

King, A. D., Van Oldenborgh, G. J. and Karoly, D. J.: Climate change and El Niño increase likelihood of Indonesian heat and drought, Bull. Am. Meteorol. Soc., 97(12), S113–S117, doi:10.1175/BAMS-D-16-0164.1, 2016.

Kirkevåg, A., Iversen, T., Seland, Ø., Hoose, C., Kristjánsson, J. E., Struthers, H., Ekman, A. M. L., Ghan, S., Griesfeller, J., Nilsson, E. D. and Schulz, M.: Aerosol–climate interactions in the Norwegian Earth System Model – NorESM1-M, Geosci. Model Dev., 6(1), 207–244, doi:10.5194/gmd-6-207-2013, 2013.

Klimont, Z., Smith, S. J. and Cofala, J.: The last decade of global anthropogenic sulfur dioxide: 2000-2011 emissions, Environ. Res. Lett., 8(1), doi:10.1088/1748-9326/8/1/014003, 2013.

Knutson, T. R., Kam, J., Zeng, F. and Wittenberg, A. T.: CMIP5 Model-based Assessment of Anthropogenic Influence on Record Global Warmth During 2016, Bull. Am. Meteorol. Soc., 98(12), S11–S15, doi:10.1175/BAMS-D-17-0104.1, 2017.

Kripalani, R. H., Oh, J. H., Kulkarni, A., Sabade, S. S. and Chaudhari, H. S.: South Asian summer monsoon precipitation variability: Coupled climate model simulations and projections under IPCC AR4, Theor. Appl. Climatol., 90(3–4), 133–159, doi:10.1007/s00704-006-0282-0, 2007.

Kumar, D. and Dimri, A. P.: Sensitivity of convective and land surface parameterization in the simulation of contrasting monsoons over CORDEX-South Asia domain using RegCM-4.4.5.5, Theor. Appl. Climatol.,

doi:10.1007/s00704-019-02976-9, 2019.

Kumar, D., Arya, D. S., Murumkar, A. R. and Rahman, M. M.: Impact of climate change on rainfall in Northwestern Bangladesh using multi-GCM ensembles, Int. J. Climatol., 34(5), 1395–1404, doi:10.1002/joc.3770, 2014.

Kumar, K. K., Kamala, K., Rajagopalan, B., Hoerling, M. P., Eischeid, J. K., Patwardhan, S. K., Srinivasan, G., Goswami, B. N. and Nemani, R.: The once and future pulse of Indian monsoonal climate, Clim. Dyn., 36(11–12), 2159–2170, doi:10.1007/s00382-010-0974-0, 2011.

Kumar, P., Wiltshire, A., Mathison, C., Asharaf, S., Ahrens, B., Lucas-Picher, P., Christensen, J. H., Gobiet, A., Saeed, F., Hagemann, S. and Jacob, D.: Downscaled climate change projections with uncertainty assessment over India using a high resolution multi-model approach, Sci. Total Environ., 468–469, doi:10.1016/j.scitotenv.2013.01.051, 2013.

Lau, K. M. and Kim, K. M.: Observational relationships between aerosol and Asian monsoon rainfall, and circulation, Geophys. Res. Lett., 33(21), doi:10.1029/2006GL027546, 2006.

Lau, K. M. and Yu, J.-Y.: Contrasting Indian Ocean SST variability with and without ENSO influence: A coupled atmosphere-ocean GCM study, Meteorol. Atmos. Phys., 90(3–4), 179–191, doi:10.1007/s00703-004-0094-7, 2005.

Lau, K. M., Kim, M. K. and Kim, K. M.: Asian summer monsoon anomalies induced by aerosol direct forcing: The role of the Tibetan Plateau, Clim. Dyn., 26(7–8), 855–864, doi:10.1007/s00382-006-0114-z, 2006.

Lau, W. K. M. and Kim, K. M.: Fingerprinting the impacts of aerosols on long-term trends of the Indian summer monsoon regional rainfall, Geophys. Res. Lett.,

37(16), n/a-n/a, doi:10.1029/2010GL043255, 2010.

Lee, D., Min, S.-K., Fischer, E. M., Shiogama, H., Bethke, I., Lierhammer, L. and Scinocca, J.: Impacts of half a degree additional warming on the Asian summer monsoon rainfall characteristics, Environ. Res. Lett., doi:10.1088/1748-9326/aab55d, 2018.

Lewis, S. C. and Karoly, D. J.: Anthropogenic contributions to Australia's record summer temperatures of 2013, Geophys. Res. Lett., 40(14), 3708–3709, doi:10.1002/grl.50673, 2013.

Li, S., Mote, P. W., Rupp, D. E., Vickers, D., Mera, R. and Allen, M.: Evaluation of a regional climate modeling effort for the western United States using a superensemble from weather@home, J. Clim., 28(19), 7470–7488, doi:10.1175/JCLI-D-14-00808.1, 2015.

Li, S., Rupp, D. E., Hawkins, L., Mote, P. W., McNeall, D., Sparrow, S. N., Wallom, D. C. H., Betts, R. A. and Wettstein, J. J.: Improving climate model accuracy by exploring parameter space with an O(10_5) member ensemble and emulator, Geosci. Model Dev. Discuss., 1–67, doi:10.5194/gmd-2018-198, 2018.

Li, T., Wang, B., Chang, C.-P. and Zhang, Y.: A Theory for the Indian Ocean Dipole–Zonal Mode*, J. Atmos. Sci., 60(17), 2119–2135, doi:10.1175/1520-0469(2003)060<2119:ATFTIO>2.0.CO;2, 2003.

Li, W., Fu, R., Juarez, R. I. N. and Fernandes, K.: Observed change of the standardized precipitation index, its potential cause and implications to future climate change in the Amazon region, Philos. Trans. R. Soc. B Biol. Sci., 363(1498), 1767–1772, doi:10.1098/rstb.2007.0022, 2008.

Li, Z., Li, C., Chen, H., Tsay, S. C., Holben, B., Huang, J., Li, B., Maring, H., Qian, Y., Shi, G., Xia, X., Yin, Y., Zheng, Y. and Zhuang, G.: East Asian Studies of Tropospheric Aerosols and their Impact on Regional Climate (EAST-AIRC): An overview, J. Geophys. Res. Atmos., 116(4), doi:10.1029/2010JD015257, 2011a.

Li, Z., Niu, F., Fan, J., Liu, Y., Rosenfeld, D. and Ding, Y.: Long-term impacts of aerosols on the vertical development of clouds and precipitation, Nat. Geosci., 4(12), 888–894, doi:10.1038/ngeo1313, 2011b.

Li, Z., Lau, W. K. M., Ramanathan, V., Wu, G., Ding, Y., Manoj, M. G., Liu, J., Qian, Y., Li, J., Zhou, T., Fan, J., Rosenfeld, D., Ming, Y., Wang, Y., Huang, J., Wang, B., Xu, X., Lee, S. S., Cribb, M., Zhang, F., Yang, X., Zhao, C., Takemura, T., Wang, K., Xia, X., Yin, Y., Zhang, H., Guo, J., Zhai, P. M., Sugimoto, N., Babu, S. S. and Brasseur, G. P.: Aerosol and monsoon climate interactions over Asia, Rev. Geophys., 54(4), 866–929, doi:10.1002/2015RG000500, 2016a.

Li, Z., Lau, W. K. M., Ramanathan, V., Wu, G., Ding, Y., Manoj, M. G., Liu, J., Qian, Y., Li, J., Zhou, T., Fan, J., Rosenfeld, D., Ming, Y., Wang, Y., Huang, J., Wang, B., Xu, X., Lee, S. S., Cribb, M., Zhang, F., Yang, X., Zhao, C., Takemura, T., Wang, K., Xia, X., Yin, Y., Zhang, H., Guo, J., Zhai, P. M., Sugimoto, N., Babu, S. S. and Brasseur, G. P.: Aerosol and monsoon climate interactions over Asia, Rev. Geophys., 54(4), 866–929, doi:10.1002/2015RG000500, 2016b.

Li, Z., Cai, W. and Lin, X.: Dynamics of changing impacts of tropical Indo-Pacific variability on Indian and Australian rainfall, Sci. Rep., 6, 1–7,

doi:10.1038/srep31767, 2016c.

Liesch, T., Simone Ruiz-Vergote, Tewari, R., Höhne, N., Burck, J. and Freundt, M.: Deep Dive. What do current policy developments in China, India and the US mean for investing in renewables? [online] Available from: https://newclimateinstitute.files.wordpress.com/2017/04/allianz-climate-and-energy-monitor-deep-dive-2017.pdf, 2017.

Lim, E.-P. and Hendon, H. H.: Causes and Predictability of the Negative Indian Ocean Dipole and Its Impact on La Niña During 2016, Sci. Rep., 7(1), 12619, doi:10.1038/s41598-017-12674-z, 2017.

Lott, F. C., Christidis, N. and Stott, P. A.: Can the 2011 East African drought be attributed to human-induced climate change?, Geophys. Res. Lett., 40(6), 1177–1181, doi:10.1002/grl.50235, 2013.

Lucas-Picher, P., Christensen, J. H., Saeed, F., Kumar, P., Asharaf, S., Ahrens, B., Wiltshire, A. J., Jacob, D. and Hagemann, S.: Can Regional Climate Models Represent the Indian Monsoon?, J. Hydrometeorol., 12(5), 849–868, doi:10.1175/2011JHM1327.1, 2011.

Ma, J., Xie, S. P. and Kosaka, Y.: Mechanisms for tropical tropospheric circulation change in response to global warming, J. Clim., 25(8), 2979–2994, doi:10.1175/JCLI-D-11-00048.1, 2012.

Macadam, I. and Janes, T.: Validation of Regional Climate Model simulations for the DECCMA project, DECCMA Working Paper, Deltas, Vulnerability and Climate Change: Migration and Adaptation, IDRC Project Number 107642, www.deccma.com., 2017.

Mahfouz, P., Mitri, G., Jazi, M. and Karam, F.: Investigating the Temporal Variability of the Standardized Precipitation Index in Lebanon, Climate, 4(2), 2016.

Mani, M., Bandyopadhyay, S., Chonabayashi, S., Markandya, A. and Mosier, T.: South Asia's Hotspots: The Impact of Temperature and Precipitation Changes on Living Standards, World Bank, Washington, DC., 2018.

Manoharan, V. S., Kotamarthi, R., Feng, Y. and Cadeddu, M. P.: Increased absorption by coarse aerosol particles over the Gangetic-Himalayan region, Atmos. Chem. Phys., 14(3), 1159–1165, doi:10.5194/acp-14-1159-2014, 2014.

Marthews, T. R., Otto, F. E. L., Mitchell, D., Dadson, S. J. and Jones, R. G.: The 2014 drought in the horn of Africa: Attribution of meteorological drivers, Bull. Am. Meteorol. Soc., 96(12), S83–S88, doi:10.1175/BAMS-D-15-00115.1, 2015.

Martins, E. S. P. R., Coelho, C. A. S., Haarsma, R., Otto, F. E. L., King, A. D., Jan van Oldenborgh, G., Kew, S., Philip, S., Vasconcelos Júnior, F. C. and Cullen, H.: A Multimethod Attribution Analysis of the Prolonged Northeast Brazil Hydrometeorological Drought (2012–16), Bull. Am. Meteorol. Soc., 99(1), S65–S69, doi:10.1175/BAMS-D-17-0102.1, 2018.

Massey, N., Jones, R., Otto, F. E. L., Aina, T., Wilson, S., Murphy, J. M., Hassell, D., Yamazaki, Y. H. and Allen, M. R.: Weather@Home-Development and Validation of a Very Large Ensemble Modelling System for Probabilistic Event Attribution, Q. J. R. Meteorol. Soc., 141(690), 1528–1545, doi:10.1002/qj.2455, 2015.

Massey, N. R.: Validation of a climate model for extreme event attribution studies, University of Oxford. [online] Available from: https://ora.ox.ac.uk/objects/uuid:a2f23b37-6148-4e1b-90b2-becc09791ad8,

2015.

Masson-Delmotte, V., Zhai, P., Pörtner, H.-O., Roberts, D., Skea, J., Shukla, P. R., Pirani, A., Moufouma-Okia, W., Péan, C., Pidcock, R., Connors, S., Matthews, J. B. R., Chen, Y., Zhou, X., Gomis, M. I., Lonnoy, E., Maycock, T., Tignor, M. and Waterfield, T.: Global warming of 1.5°C An IPCC Special Report., 2018.

Mathison, C., Wiltshire, A., Dimri, A. P., Falloon, P., Jacob, D., Kumar, P., Moors, E., Ridley, J., Siderius, C., Stoffel, M. and Yasunari, T.: Regional projections of North Indian climate for adaptation studies, Sci. Total Environ., 468–469, S4–S17, doi:10.1016/j.scitotenv.2012.04.066, 2013.

Matsumoto, J.: Seasonal transition of summer rainy season over Indochina and adjacent monsoon region, Adv. Atmos. Sci., 14(2), 231–245, doi:10.1007/s00376-997-0022-0, 1997.

Matthews, H. D.: Quantifying historical carbon and climate debts among nations, Nat. Clim. Chang., 6(1), 60–64, doi:10.1038/nclimate2774, 2016.

May, W.: Potential future changes in the Indian summer monsoon due to greenhouse warming: Analysis of mechanisms in a global time-slice experiment, Clim. Dyn., 22(4), 389–414, doi:10.1007/s00382-003-0389-2, 2004.

Mckee, T. B., Doesken, N. J. and Kleist, J.: The relationship of drought frequency and duration to time scales, in AMS 8th Conference on Applied Climatology, vol. 17, pp. 179–184, American Meteorological Society Boston, MA., 1993.

McKee, T. B., Doesken, N. J. and Kleist, J.: Drought Monitoring with Multiple Time Scales, in Proceedings of the 9th AMS Conference on Applied Climatology, pp. 233–236, American Meteorological Society Dallas, Boston, MA., 1995.

McPhillips, L. E., Chang, H., Chester, M. V., Depietri, Y., Friedman, E., Grimm, N. B., Kominoski, J. S., McPhearson, T., Méndez-Lázaro, P., Rosi, E. J. and Shafiei Shiva, J.: Defining Extreme Events: A Cross-Disciplinary Review, Earth's Futur., 6(3), 441–455, doi:10.1002/2017EF000686, 2018.

Menon, A., Levermann, A., Schewe, J., Lehmann, J. and Frieler, K.: Consistent increase in Indian monsoon rainfall and its variability across CMIP-5 models, Earth Syst. Dyn. Discuss., 4(1), 1–24, doi:10.5194/esdd-4-1-2013, 2013.

Meyers, G., McIntosh, P., Pigot, L. and Pook, M.: The years of El Niño, La Niña and interactions with the tropical Indian Ocean, J. Clim., 20(13), 2872–2880, doi:10.1175/JCLI4152.1, 2007.

Min, S.-K., Kim, Y.-H., Kim, M.-K. and Park, C.: Assessing Human contribution to the summer 2013 Korean heat wave [In "Explaining extreme events of 2013 from a climate perspective"], Bull. Am. Meteorol. Soc., 95(9), S48–S51, 2014.

Mitchell, D., Heaviside, C., Vardoulakis, S., Huntingford, C., Masato, G., P Guillod, B., Frumhoff, P., Bowery, A., Wallom, D. and Allen, M.: Attributing human mortality during extreme heat waves to anthropogenic climate change, Environ. Res. Lett., 11(7), doi:10.1088/1748-9326/11/7/074006, 2016a.

Mitchell, D., James, R., Forster, P. M., Betts, R. A., Shiogama, H. and Allen, M.: Realizing the impacts of a 1.5 °C warmer world, Nat. Clim. Chang., 6(8), 735–737, doi:10.1038/nclimate3055, 2016b.

Mitchell, D., AchutaRao, K., Allen, M., Bethke, I., Beyerle, U., Ciavarella, A., Forster, P. M., Fuglestvedt, J., Gillett, N., Haustein, K., Ingram, W., Iversen, T., Kharin, V., Klingaman, N., Massey, N., Fischer, E., Schleussner, C. F., Scinocca, J., Seland, Ø., Shiogama, H., Shuckburgh, E., Sparrow, S., Stone, D.,

Uhe, P., Wallom, D., Wehner, M. and Zaaboul, R.: Half a degree additional warming, prognosis and projected impacts (HAPPI): Background and experimental design, Geosci. Model Dev., 10(2), 571–583, doi:10.5194/gmd-10-571-2017, 2017.

Mote, P. W., Allen, M. R., Jones, R. G., Li, S., Mera, R., Rupp, D. E., Salahuddin, A. and Vickers, D.: Superensemble regional climate modeling for the western United States, Bull. Am. Meteorol. Soc., 97(2), 203–215, doi:10.1175/BAMS-D-14-00090.1, 2016.

Murata, F., Terao, T., Hayashi, T., Asada, H. and Matsumoto, J.: Relationship between atmospheric conditions at Dhaka, Bangladesh, and rainfall at Cherrapunjee, India, Nat. Hazards, 44(3), 399–410, doi:10.1007/s11069-007-9125-2, 2008.

Murshed, S. B., Islam, A. K. M. and Khan, M. S. A.: Impact of climate change on rainfall intensity in Bangladesh, Dhaka, Bangladesh. [online] Available from: http://teacher.buet.ac.bd/akmsaifulislam/reports/Heavy_Rainfall_report.pdf, 2011.

Nakajima, T., Yoon, S. C., Ramanathan, V., Shi, G. Y., Takemura, T., Higurashi, A., Takamura, T., Aoki, K., Sohn, B. J., Kim, S. W., Tsuruta, H., Sugimoto, N., Shimizu, A., Tanimoto, H., Sawa, Y., Lin, N. H., Lee, C. Te, Goto, D. and Schutgens, N.: Overview of the Atmospheric Brown Cloud East Asian Regional Experiment 2005 and a study of the aerosol direct radiative forcing in east Asia, J. Geophys. Res. Atmos., 112(24), doi:10.1029/2007JD009009, 2007.

Naresh Kumar, M., Murthy, C. S., Sesha sai, M. V. R. and Roy, P. S.: On the use of Standardized Precipitation Index (SPI) for drought intensity assessment,

Meteorol. Appl., 16(3), 381–389, doi:10.1002/met.136, 2009.

National Academies of Sciences, Engineering, and M.: Attribution of Extreme Weather Events in the Context of Climate Change, National Academies Press, Washington, D.C., 2016.

Natsuko, Y., Atsushi, H. and Yatagai, A.: Development of a Long-term Daily Gridded Temperature Dataset and Its Application to Rain/Snow Discrimination of Daily Precipitation, Glob. Environ. Res., 15, 165–172 [online] Available from: http://st.hirosaki-u.ac.jp/~aphrodite2/data/Yasutomi2011GER.pdf, 2011.

Neale, R. B., Richter, J., Park, S., Lauritzen, P. H., Vavrus, S. J., Rasch, P. J. and Zhang, M.: The Mean Climate of the Community Atmosphere Model (CAM4) in Forced SST and Fully Coupled Experiments, J. Clim., 26(14), 5150–5168, doi:10.1175/JCLI-D-12-00236.1, 2013.

Nirapad: Bangladesh: Flash Flood Situation - April 19, 2017, Situat. Rep., 7 [online] Available from: https://reliefweb.int/sites/reliefweb.int/files/resources/Flash_Flood%2C Updated %28April 19%29%2C 2017.pdf (Accessed 14 November 2017), 2017.

Nowreen, S., Murshed, S. B., Islam, A. K. M. S., Bhaskaran, B. and Hasan, M. A.: Changes of rainfall extremes around the haor basin areas of Bangladesh using multi-member ensemble RCM, Theor. Appl. Climatol., 119(1–2), 363–377, doi:10.1007/s00704-014-1101-7, 2015.

Van Oldenborgh, G. J., Van Urk, A. and Allen, M.: The absence of role of climate change in the 2011 Thailand floods, Bull. Am. Meteorol. Soc., 93(7), 1047–1049, doi:10.1175/BAMS-D-12-00021.1, 2012.

Van Oldenborgh, G. J., Philip, S., Kew, S., Van Weele, M., Uhe, P., Otto, F., Singh, R., Pai, I., Cullen, H. and Achutarao, K.: Extreme heat in India and anthropogenic climate change, Nat. Hazards Earth Syst. Sci., 18(1), 365–381, doi:10.5194/nhess-18-365-2018, 2018.

van Oldenborgh Geert J.: How unusual was autumn 2006 in Europe?, Clim. Past, 3, 659–668, 2007.

Otto, F., Rachel, J. and Allen, M.: The science of attributing extreme weather events and its potential contribution to assessing loss and damage associated with climate change impacts. [online] Available from: https://unfccc.int/files/adaptation/workstreams/loss_and_damage/application/pdf/attributingextremeevents.pdf, 2015a.

Otto, F. E. L.: Attribution of Weather and Climate Events, Annu. Rev. Environ. Resour., 42(1), 627–646, doi:10.1146/annurev-environ, 2017.

Otto, F. E. L., Massey, N., Van Oldenborgh, G. J., Jones, R. G. and Allen, M. R.: Reconciling two approaches to attribution of the 2010 Russian heat wave, Geophys. Res. Lett., 39(4), doi:10.1029/2011GL050422, 2012.

Otto, F. E. L., Jones, R. G., Halladay, K. and Allen, M. R.: Attribution of changes in precipitation patterns in African rainforests, Philos. Trans. R. Soc. Lond. B. Biol. Sci., 368(1625), 20120299, doi:10.1098/rstb.2012.0299, 2013.

Otto, F. E. L., Rosier, S. M., Allen, M. R., Massey, N. R., Rye, C. J. and Quintana, J. I.: Attribution analysis of high precipitation events in summer in England and Wales over the last decade, Clim. Change, 132(1), 77–91, doi:10.1007/s10584-014-1095-2, 2015b.

Otto, F. E. L., Boyd, E., Jones, R. G., Cornforth, R. J., James, R., Parker, H. R. and Allen, M. R.: Attribution of extreme weather events in Africa: a preliminary exploration of the science and policy implications, Clim. Change, 132(4), 531–543, doi:10.1007/s10584-015-1432-0, 2015c.

Pall, P., Aina, T., Stone, D. A., Stott, P. A., Nozawa, T., Hilberts, A. G. J., Lohmann, D. and Allen, M. R.: Anthropogenic greenhouse gas contribution to flood risk in England and Wales in autumn 2000, Nature, 470(7334), 382–385, doi:10.1038/nature09762, 2011a.

Pall, P., Aina, T., Stone, D. A., Stott, P. A., Nozawa, T., Hilberts, A. G. J., Lohmann, D. and Allen, M. R.: Anthropogenic greenhouse gas contribution to flood risk in England and Wales in autumn 2000, Nature, 470(7334), 382–385, doi:10.1038/nature09762, 2011b.

Parker, H. R., Cornforth, R. J., Boyd, E., James, R., Otto, F. E. and Allen, M. R.: Implications of event attribution for loss and damage policy, Weather, 70(9), 268–273, doi:10.1002/wea.2542, 2015.

Paul, R. and Hussain, Z.: Landslide, floods kill 156 in Bangladesh, India; toll could rise, Reuters, 14th June [online] Available from: https://uk.reuters.com/article/uk-bangladesh-landslides/landslide-floods-kill-156-in-bangladesh-india-toll-could-rise-idUKKBN1950AG, 2017.

Perkins, S., Lewis, S., King, A. and Alexander, L.: Increased simulated risk of the hot Australian summer of 2012/13 due to anthropogenic activity as measured by heatwave intensity and frequency, Bull. Am. Meteorol. Soc., 95(9), S34-37, doi:10.1175/1520-0477-95.9.s1.1, 2014.

Peterson, T. C., Stott, P. A. and Herring, S., Eds.: Explaining Extreme Events of 2011 from a Climate Perspective, Bull. Am. Meteorol. Soc., 1–28 [online] Available from: https://journals.ametsoc.org/doi/pdf/10.1175/BAMS-D-12-00021.1, 2012.

Philip, S., Sparrow, S., Kew, S. F., van der Wiel, K., Wanders, N., Singh, R., Hassan, A., Mohammed, K., Javid, H., Haustein, K., Otto, F. E. L., Hirpa, F., Rimi, R. H., Islam, A. S., Wallom, D. C. H. and van Oldenborgh, G. J.: Attributing the 2017 Bangladesh floods from meteorological and hydrological perspectives, Hydrol. Earth Syst. Sci. Discuss., 1–32, doi:10.5194/hess-2018-379, 2018.

Philip, S., Sparrow, S., Kew, S. F., Van Der Wiel, K., Wanders, N., Singh, R., Hassan, A., Mohammed, K., Javid, H., Haustein, K., Otto, F. E. L., Hirpa, F., Rimi, R. H., Saiful Islam, A. K. M., Wallom, D. C. H. and Jan Van Oldenborgh, G.: Attributing the 2017 Bangladesh floods from meteorological and hydrological perspectives, Hydrol. Earth Syst. Sci., 23(3), 1409–1429, doi:10.5194/hess-23-1409-2019, 2019.

Prakash, S., Mitra, A. K., Momin, I. M., Rajagopal, E. N., Basu, S., Collins, M., Turner, A. G., Achuta Rao, K. and Ashok, K.: Seasonal intercomparison of observational rainfall datasets over India during the southwest monsoon season, Int. J. Climatol., 35(9), 2326–2338, doi:10.1002/joc.4129, 2015.

Rahman, M. R. and Lateh, H.: Climate change in Bangladesh: a spatio-temporal analysis and simulation of recent temperature and rainfall data using GIS and time series analysis model, Theor. Appl. Climatol., 128(1–2), 27–41, doi:10.1007/s00704-015-1688-3, 2017.

Rajeevan, M. and Bhate, J.: A High Resolution Daily Gridded for Mesoscale Meteorological Studies. National Climate Centre Research Report No. 9. Indian Meteorological Department, Pune, India. [online] Available from: http://www.imdpune.gov.in/ncc_%0A910%0Arept/RESEARCH REPORT 9.pdf, 2008.

Ramage, C. S.: Monsoon Meteorology, Academic Press, New York., 1971.

Ramanathan, V. and Carmichael, G.: Global and regional climate changes due to black carbon, Nat. Geosci., 1(4), 221–227, doi:10.1038/ngeo156, 2008.

Ramanathan, V. and Feng, Y.: Air pollution, greenhouse gases and climate change: Global and regional perspectives, Atmos. Environ., 43(1), 37–50, doi:10.1016/j.atmosenv.2008.09.063, 2009.

Ramanathan, V., Chung, C., Kim, D., Bettge, T., Buja, L., Kiehl, J. T., Washington, W. M., Fu, Q., Sikka, D. R. and Wild, M.: Atmospheric brown clouds: Impacts on South Asian climate and hydrological cycle, Proc. Natl. Acad. Sci., 102(15), 5326–5333, doi:10.1073/pnas.0500656102, 2005.

Rashid, H. E.: Geography of Bangladesh, The University Press Ltd., Dhaka, Dhaka, Bangladesh., 1991.

Rawlani, A. K. and Sovacool, B. K.: Building responsiveness to climate change through community based adaptation in Bangladesh, Mitig. Adapt. Strateg. Glob. Chang., 16(8), 845–863, doi:10.1007/s11027-011-9298-6, 2011.

Rayner, N. A., Parker, D. E., Horton, E. B., Folland, C. K., Alexander, L. V., Rowell, D. P., Kent, E. C. and Kaplan, A.: Global analyses of sea surface temperature, sea ice, and night marine air temperature since the late nineteenth century, J. Geophys. Res., 108, 4407, doi:10.1029/2002JD002670, 2003.

Rimi, R. H., Haustein, K., Barbour, E. J., Jones, R. G., Sparrow, S. N. and Allen, M. R.: Evaluation of a large ensemble regional climate modelling system for extreme weather events analysis over Bangladesh, Int. J. Climatol., 39(6), 2845–2861, doi:10.1002/joc.5931, 2019a.

Rimi, R. H., Haustein, K., Barbour, E. J. and Allen, M. R.: Risks of Pre-Monsoon Extreme Rainfall Events of Bangladesh: Is Anthropogenic Climate Change Playing a Role?, Bull. Am. Meteorol. Soc., 100(1), S61–S65, doi:10.1175/BAMS-D-18-0152.1, 2019b.

Risser, M. D., Stone, D. A., Paciorek, C. J., Wehner, M. F. and Angélil, O.: Quantifying the effect of interannual ocean variability on the attribution of extreme climate events to human influence, Clim. Dyn., 49(9–10), 3051–3073, doi:10.1007/s00382-016-3492-x, 2017.

Robine, J. M., Cheung, S. L. K., Le Roy, S., Van Oyen, H., Griffiths, C., Michel, J. P. and Herrmann, F. R.: Death toll exceeded 70,000 in Europe during the summer of 2003, Comptes Rendus - Biol., 331(2), 171–178, doi:10.1016/j.crvi.2007.12.001, 2008.

Ropelewski, C. F. and Halpert, M. S.: Global and Regional Scale Precipitation Patterns Associated with the El Niño/Southern Oscillation, Mon. Weather Rev., 115(8), 1606–1626, doi:10.1175/1520-0493(1987)115<1606:GARSPP>2.0.CO;2, 1987.

Rosenfeld, D.: Suppression of rain and snow by urban and industrial air pollution, Science (80-.)., 287(5459), 1793–1796, doi:10.1126/science.287.5459.1793, 2000.

Rowlands, D. J., Frame, D. J., Ackerley, D., Aina, T., Booth, B. B. B., Christensen, C., Collins, M., Faull, N., Forest, C. E., Grandey, B. S., Gryspeerdt, E., Highwood, E. J., Ingram, W. J., Knight, S., Lopez, A., Massey, N., McNamara, F., Meinshausen, N., Piani, C., Rosier, S. M., Sanderson, B. M., Smith, L. A., Stone, D. A., Thurston, M., Yamazaki, K., Hiro Yamazaki, Y. and Allen, M. R.: Broad range of 2050 warming from an observationally constrained large climate model ensemble, Nat. Geosci., 5(4), 256–260, doi:10.1038/ngeo1430, 2012.

Runge, J., Petoukhov, V. and Kurths, J.: Quantifying the strength and delay of climatic interactions: The ambiguities of cross correlation and a novel measure based on graphical models, J. Clim., 27(2), 720–739, doi:10.1175/JCLI-D-13-00159.1, 2014.

Rupp, D. E., Mote, P. W., Massey, N., Rye, C. J. and Allen, M.: Did Human influence on climate make the 2011 Texas drought more probable?, Bull. Am. Meteorol. Soc., 93(July), 1052–1054, doi:10.1175/BAMS-D-12-00021.1., 2012.

Saeed, F., Hagemann, S. and Jacob, D.: A framework for the evaluation of the South Asian summer monsoon in a regional climate model applied to REMO, Int. J. Climatol., 32(3), 430–440, doi:10.1002/joc.2285, 2012.

Saha, S. K., Pokhrel, S., Chaudhari, H. S., Dhakate, A., Shewale, S., Sabeerali, C. T., Salunke, K., Hazra, A., Mahapatra, S. and Rao, A. S.: Improved simulation of Indian summer monsoon in latest NCEP climate forecast system free run, Int. J. Climatol., 34(5), 1628–1641, doi:10.1002/joc.3791, 2014.

Saji, N. H. and Yamagata, T.: Possible impacts of Indian Ocean Dipole mode events on global climate, Clim. Res., 25(2), 151–169, doi:10.3354/cr025151, 2003a.

Saji, N. H. and Yamagata, T.: Structure of SST and surface wind variability during Indian Ocean Dipole mode events: COADS observations, J. Clim., 16(16), 2735–2751, doi:10.1175/1520-0442(2003)016<2735:SOSASW>2.0.CO;2, 2003b.

Saji, N. H., Goswami, B. N., Vinayachandran, P. N. and Yamagata, T.: A dipole mode in the tropical Indian ocean, Nature, 401(6751), 360–363, doi:10.1038/43854, 1999a.

Saji, N. H., Goswami, B. N., Vinayachandran, P. N. and Yamagata, T.: A dipole mode in the tropical Indian Ocean, Nature, 401, 360–363, doi:10.1038/43854, 1999b.

von Salzen, K., Scinocca, J. F., McFarlane, N. A., Li, J., Cole, J. N. S., Plummer, D., Verseghy, D., Reader, M. C., Ma, X., Lazare, M. and Solheim, L.: The Canadian fourth generation atmospheric global climate model (CanAM4). Part I: Representation of physical processes, Atmos. - Ocean, 51(1), 104–125, doi:10.1080/07055900.2012.755610, 2013.

Samset, B. H., Sand, M., Smith, C. J., Bauer, S. E., Forster, P. M., Fuglestvedt, J. S., Osprey, S. and Schleussner, C. F.: Climate Impacts From a Removal of Anthropogenic Aerosol Emissions, Geophys. Res. Lett., 45(2), 1020–1029, doi:10.1002/2017GL076079, 2018.

Sanderson, M. and Ahmed, R.: Pre-monsoon rainfall and its variability in Bangladesh: A trend surface analysis, Hydrol. Sci. Bull., 24(3), 277–287, doi:10.1080/02626667909491867, 1979.

Sarraf, M., Dasgupta, S. and Adams, N.: Bangladesh Development Series: The Cost of Adapting to Extreme Weather Events in a Changing Climate, Washington, DC., 2011.

Sawe, B. E.: Wettest Places On Earth By Annual Rainfall, [online] Available from: http://www.worldatlas.com/articles/the-ten-wettest-places-in-the-world.html, 2017.

Scaife, A. A., Woollings, T., Knight, J., Martin, G. and Hinton, T.: Atmospheric blocking and mean biases in climate models, J. Clim., 23(23), 6143–6152, doi:10.1175/2010JCLI3728.1, 2010.

Schaller, N., Otto, F. E. L., van Oldenborgh, G. J., Massey, N. R., Sparrow, S. and Allen, M. R.: The heavy precipitation event of May–June 2013 in the upper Danube and Elbe basins, Bull. Amer. Meteor. Soc., 95(9), S69–S72, 2014.

Schaller, N., Kay, A. L., Lamb, R., Massey, N. R., Van Oldenborgh, G. J., Otto, F. E. L., Sparrow, S. N., Vautard, R., Yiou, P., Ashpole, I., Bowery, A., Crooks, S. M., Haustein, K., Huntingford, C., Ingram, W. J., Jones, R. G., Legg, T., Miller, J., Skeggs, J., Wallom, D., Weisheimer, A., Wilson, S., Stott, P. A. and Allen, M. R.: Human influence on climate in the 2014 southern England winter floods and their impacts, Nat. Clim. Chang., 6(6), 627–634, doi:10.1038/nclimate2927, 2016.

Schamm, K., Ziese, M., Becker, A., Finger, P., Meyer-Christoffer, A., Schneider, U., Schröder, M. and Stender, P.: Global gridded precipitation over land: A description of the new GPCC First Guess Daily product, Earth Syst. Sci. Data, 6(1), 49–60, doi:10.5194/essd-6-49-2014, 2014.

Schamm, K., Ziese, M., Raykova, K., Becker, A., Finger, P., Meyer-Christoffer and Anja; Schneider, U.: GPCC Full Data Daily Version 1.0 at 1.0°: Daily Land-Surface Precipitation from Rain-Gauges built on GTS-based and Historic Data, , doi:10.5676/DWD_GPCC/FD_D_V1_100, 2015.

Schleussner, C. F., Lissner, T. K., Fischer, E. M., Wohland, J., Perrette, M., Golly, A., Rogelj, J., Childers, K., Schewe, J., Frieler, K., Mengel, M., Hare, W. and Schaeffer, M.: Differential climate impacts for policy-relevant limits to global warming: The case of 1.5 °c and 2 °c, Earth Syst. Dyn., 7(2), 327–351, doi:10.5194/esd-7-327-2016, 2016.

Schneider, U., Becker, A., Finger, P., Meyer-Christoffer, A., Ziese, M. and Rudolf, B.: GPCC's new land surface precipitation climatology based on quality-controlled in situ data and its role in quantifying the global water cycle, Theor. Appl. Climatol., 115(1), 15–40, doi:10.1007/s00704-013-0860-x, 2014.

Schott, F. A., Xie, S. P. and McCreary, J. P.: Indian ocean circulation and climate variability, Rev. Geophys., 47(1), doi:10.1029/2007RG000245, 2009.

Sellers, P. J., Dickinson, R. E., Randall, D. A., Betts, A. K., Hall, F. G., Berry, J. A., Collatz, G. J., Denning, A. S., Mooney, H. A., Nobre, C. A., Sato, N., Field, C. B. and Henderson-Sellers, A.: Modeling the exchanges of energy, water, and carbon between continents and the atmosphere, Science (80-.)., 275(5299), 502–509, doi:10.1126/science.275.5299.502, 1997.

Shahid, S.: Rainfall variability and the trends of wet and dry periods in Bangladesh, Int. J. Climatol., 30(15), 2299–2313, doi:10.1002/joc.2053, 2010a.

Shahid, S.: Recent trends in the climate of Bangladesh, Clim. Res., 42(3), 185–193, doi:10.3354/cr00889, 2010b.

Shiogama, H., Watanabe, M., Imada, Y., Mori, M., Kamae, Y., Ishii, M. and Kimoto, M.: Attribution of the june-july 2013 heat wave in the southwestern United States, Sci. Online Lett. Atmos., 10(1), 122–126, doi:10.2151/sola.2014-025, 2014.

Singh, D., Bollasina, M., Ting, M. and Diffenbaugh, N. S.: Disentangling the influence of local and remote anthropogenic aerosols on South Asian monsoon daily rainfall characteristics, Clim. Dyn., doi:10.1007/s00382-018-4512-9, 2018.

Sippel, S. and Otto, F. E. L.: Beyond climatological extremes - assessing how the odds of hydrometeorological extreme events in South-East Europe change in a warming climate, Clim. Change, 125(3–4), 381–398, doi:10.1007/s10584-014-1153-9, 2014.

Sippel, S., Otto, F. E. L., Forkel, M., Allen, M. R., Guillod, B. P., Heimann, M., Reichstein, M., Seneviratne, S. I., Thonicke, K. and Mahecha, M. D.: A novel bias correction methodology for climate impact simulations, Earth Syst. Dyn., 7(1), 71–88, doi:10.5194/esd-7-71-2016, 2016.

Skeie, R. B., Fuglestvedt, J., Berntsen, T., Peters, G. P., Andrew, R., Allen, M. and Kallbekken, S.: Perspective has a strong effect on the calculation of historical contributions to global warming, Environ. Res. Lett., 12(2), doi:10.1088/1748-9326/aa5b0a, 2017.

Solomon, S., Qin, D., Manning, M., Chen, Z., Marquis, M., Averyt, K. B., Tignor, M. and Miller, H. L.: Climate Change 2007 - The Physical Science Basis: Working Group I Contribution to the Fourth Assessment Report of the IPCC, edited by S. Solomon, D. Qin, M. Manning, Z. Chen, M. Marquis, K. B. Averyt, M. Tignor, and H. L. Miller, Cambridge University Press, Cambridge, UK and New York, NY, USA. [online] Available from: https://books.google.com/books?hl=nl&lr=&id=8-m8nXB8GB4C&pgis=1, 2007.

Srivastava, A., Naresh Kumar, S. and Aggarwal, P. K.: Assessment on vulnerability of sorghum to climate change in India, Agric. Ecosyst. Environ., 138(3–4), 160–169, doi:10.1016/j.agee.2010.04.012, 2010.

Stainforth, D. A., Aina, T., Christensen, C., Collins, M., Faull, N., Frame, D. J., Kettleborough, J. A., Knight, S., Martin, A., Murphy, J. M., Piani, C., Sexton, D., Smith, L. A., Splcer, R. A., Thorpe, A. J. and Allen, M. R.: Uncertainty in predictions of the climate response to rising levels of greenhouse gases, Nature, 433(7024), 403–406, doi:10.1038/nature03301, 2005.

Stark, J. D., Donlon, C. J., Martin, M. J. and McCulloch, M. E.: OSTIA: An Operational, high resolution, real time, global sea surface temperature analysis system., in Oceans 2007 - Marine Challenges: Coastline to Deep Sea, pp. 1–4, IEEE., 2007.

Stott, P. A. and Walton, P.: Attribution of climate-related events: Understanding stakeholder needs, Weather, 68(10), 274–279, doi:10.1002/wea.2141, 2013.

Stott, P. A., Stone, D. A. and Allen, M. R.: Human contribution to the European heatwave of 2003, Nature, 432(7017), 610–614, doi:10.1038/nature03089, 2004a.

Stott, P. A., Stone, D. A. and Allen, M. R.: Human contribution to the European heatwave of 2003, Nature, 432(7017), 610–614, doi:10.1038/nature03089, 2004b.

Stott, P. A., Stone, D. A. and Allen, M. R.: Human Contribution to the Heat wave of 2003, Nature, 432(7017), 610–614, 2004c.

Stott, P. A., Allen, M., Christidis, N., Dole, R., Hoerling, M., Huntingford, C., Pall, P., Perlwitz, J. and Stone, D.: Attribution of Weather and Climate-Related

Extreme Events, in In Monograph : “Climate Science for Serving Society: Research, Modelling and Prediction Priorities,” edited by G. R. Asrar and J. W. Hurrell, pp. 1–44, Springer., 2013a.

Stott, P. A., Allen, M., Christidis, N., Dole, R. M., Hoerling, M., Huntingford, C., Pall, P., Perlwitz, J. and Stone, D.: Climate Science for Serving Society, edited by G. R. Asrar and J. W. Hurrell, Springer Netherlands, Dordrecht., 2013b.

Stott, P. A., Christidis, N., Otto, F. E. L., Sun, Y., Vanderlinden, J. P., van Oldenborgh, G. J., Vautard, R., von Storch, H., Walton, P., Yiou, P. and Zwiers, F. W.: Attribution of extreme weather and climate-related events, Wiley Interdiscip. Rev. Clim. Chang., 7(1), 23–41, doi:10.1002/wcc.380, 2016.

Sugimoto, S. and Takahashi, H. G.: Seasonal differences in precipitation sensitivity to soil moisture in Bangladesh and surrounding regions, J. Clim., 30(3), 921–938, doi:10.1175/JCLI-D-15-0800.1, 2017.

Sun, Q. and Miao, C.: Extreme Rainfall (R20mm, RX5day) in Yangtze–Huai, China, in June–July 2016: The Role of ENSO and Anthropogenic Climate Change, in Bulletin of the American Meteorological Society, vol. 98, pp. S102–S106., 2017.

Surminski, S. and Lopez, A.: Concept of loss and damage of climate change ??? a new challenge for climate decision-making? A climate science perspective, Clim. Dev., 7(3), 267–277, doi:10.1080/17565529.2014.934770, 2015.

Syed, M. and Al Amin, M.: Geospatial Modeling for Investigating Spatial Pattern and Change Trend of Temperature and Rainfall, Climate, 4(2), 21, doi:10.3390/cli4020021, 2016.

Taylor, K. E., Stouffer, R. J. and Meehl, G. A.: An overview of CMIP5 and the experiment design, Bull. Am. Meteorol. Soc., 93(4), 485–498, doi:10.1175/BAMS-D-11-00094.1, 2012.

The World Bank: Turn Down Heat: Why a 4 degree warmer world must be avoided. A Report for the World Bank by the Potsdam Institute for Climate Impact Research and Climate Analytics, Washington, DC : World Bank. [online] Available from: http://climatechange.worldbank.org/sites/default/files/Turn_Down_the_heat_Why_a_4_degree_centrigrade_warmer_world_must_be_avoided.pdf, 2012.

Thiele-Eich, I., Burkart, K. and Simmer, C.: Trends in water level and flooding in Dhaka, Bangladesh and their impact on mortality, Int. J. Environ. Res. Public Health, 12(2), 1196–1215, doi:10.3390/ijerph120201196, 2015.

Trenberth, K. E., Fasullo, J. T. and Shepherd, T. G.: Attribution of climate extreme events, Nat. Clim. Chang., 5(8), 725–730, doi:10.1038/nclimate2657, 2015.

Turner, A. G. and Annamalai, H.: Climate change and the South Asian summer monsoon, Nat. Clim. Chang., 2(8), 587–595, doi:10.1038/NCLIMATE1495, 2012.

UNFCCC: Paris Agreement, in 21st Conference of the Parties, vol. 2017, p. 3., 2015.

UNFPA: State of World Population 2014. [online] Available from: http://www.unfpa.org/sites/default/files/pub-pdf/EN-SWOP14-Report_FINAL-web.pdf, 2014.

van Vuuren, D. P., Edmonds, J., Kainuma, M., Riahi, K., Thomson, A., Hibbard, K., Hurtt, G. C., Kram, T., Krey, V., Lamarque, J. F., Masui, T., Meinshausen, M., Nakicenovic, N., Smith, S. J. and Rose, S. K.: The representative

concentration pathways: An overview, Clim. Change, 109(1), 5–31, doi:10.1007/s10584-011-0148-z, 2011.

Walsh, J. E., Thoman, R. L., Bhatt, U. S., Bieniek, P. A., Brettschneider, B., Brubaker, M., Danielson, S., Lader, R., Fetterer, F., Holderied, K., Iken, K., Mahoney, A., McCammon, M. and Partain, J.: The High Latitude Marine Heat Wave of 2016 and Its Impacts on Alaska, Bull. Am. Meteorol. Soc., 98(12), S39–S43, doi:10.1175/BAMS-D-17-0105.1, 2017.

Wang, B.: Climatic Regimes of Tropical Convection and Rainfall, J. Clim., 7(7), 1109–1118, doi:10.1175/1520-0442(1994)007<1109:CROTCA>2.0.CO;2, 1994.

Wang, B. and Ding, Q.: Global monsoon: Dominant mode of annual variation in the tropics, Dyn. Atmos. Ocean., 44(3–4), 165–183, doi:10.1016/j.dynatmoce.2007.05.002, 2008.

Wang, B., Liu, J., Yim, P. J. W. S. and Kiefer, T.: Recent change of the global monsoon precipitation (1979 – 2008), Clim. Dyn., 39(5), 1123–1135, doi:10.1007/s00382-011-1266-z, 2012.

Watanabe, M., Suzuki, T., O'Ishi, R., Komuro, Y., Watanabe, S., Emori, S., Takemura, T., Chikira, M., Ogura, T., Sekiguchi, M., Takata, K., Yamazaki, D., Yokohata, T., Nozawa, T., Hasumi, H., Tatebe, H. and Kimoto, M.: Improved climate simulation by MIROC5: Mean states, variability, and climate sensitivity, J. Clim., 23(23), 6312–6335, doi:10.1175/2010JCLI3679.1, 2010.

Webster, P. J.: The variable and interactive monsoon., in Monsoon, edited by J. Fein and P. Stephens, pp. 269–330, J. Wiley Company, Hoboken, New Jersey, USA., 1987.

Webster, P. J., Magaña, V. O., Palmer, T. N., Shukla, J., Tomas, R. A., Yanai, M. and Yasunari, T.: Monsoons: Processes, predictability, and the prospects for prediction, J. Geophys. Res. Ocean., 103(C7), 14451–14510, doi:10.1029/97JC02719, 1998.

Webster, P. J., Moore, A. M., Loschnigg, J. P. and Leben, R. R.: Coupled ocean-atmosphere dynamics in the Indian Ocean during 1997-98, Nature, 401(6751), 356–360, doi:10.1038/43848, 1999.

Webster, P. J., Toma, V. E. and Kim, H. M.: Were the 2010 Pakistan floods predictable?, Geophys. Res. Lett., 38(4), doi:10.1029/2010GL046346, 2011.

Wilks, D. S.: Comparison of three-parameter probability distributions for representing annual extreme and partial duration precipitation series, Water Resour. Res., 29(10), 3543–3549, doi:10.1029/93WR01710, 1993.

Wilks, D. S.: Statistical Methods in the Atmospheric Sciences, Academic Press, 2011., 2011.

Willmott, C. J., Rowe, C. M. and Philpot, W. D.: Small-scale climate maps: A sensitivity analysis of some common assumptions associated with grid-point interpolation and contouring, Am. Cartogr., 12(1), 5–16, doi:10.1559/152304085783914686, 1985.

WMO: Standardized Precipitation Index : User Guide, WMO-No. 1090, World Meteorological Organization, Geneva, Switzerland., 2012.

Wu, G., Liu, Y., Zhang, Q., Duan, A., Wang, T., Wan, R., Liu, X., Li, W., Wang, Z. and Liang, X.: The Influence of Mechanical and Thermal Forcing by the Tibetan Plateau on Asian Climate, J. Hydrometeorol., 8(4), 770–789, doi:10.1175/JHM609.1, 2007.

Xie, S. P., Annamalai, H., Schott, F. A. and McCreary, J. P.: Structure and mechanisms of South Indian Ocean climate variability, J. Clim., 15(8), 864–878, doi:10.1175/1520-0442(2002)015<0864:SAMOSI>2.0.CO;2, 2002.

Xie, S. P., Deser, C., Vecchi, G. A., Ma, J., Teng, H. and Wittenberg, A. T.: Global warming pattern formation: Sea surface temperature and rainfall, J. Clim., 23(4), 966–986, doi:10.1175/2009JCLI3329.1, 2010.

Xu, X., Lu, C., Shi, X. and Ding, Y.: The large-scale topography of China: A factor for seasonal march of the Meiyu-Baiu-Changma in East Asia., J. Geophys. Res. Atmos, 115, doi:10.1029JD012444, 2010.

Yang, Y., Xie, S. P., Wu, L., Kosaka, Y., Lau, N. C. and Vecchi, G. A.: Seasonality and predictability of the Indian Ocean dipole mode: ENSO forcing and internal variability, J. Clim., 28(20), 8021–8036, doi:10.1175/JCLI-D-15-0078.1, 2015.

Yatagai, A., Kamiguchi, K., Arakawa, O., Hamada, A., Yasutomi, N. and Kitoh, A.: Aphrodite constructing a long-term daily gridded precipitation dataset for Asia based on a dense network of rain gauges, Bull. Am. Meteorol. Soc., 93(9), 1401–1415, doi:10.1175/BAMS-D-11-00122.1, 2012.

Yeh, S.-W., Cai, W., Min, S.-K., McPhaden, M. J., Dommenget, D., Dewitte, B., Collins, M., Ashok, K., An, S.-I., Yim, B.-Y. and Kug, J.-S.: ENSO atmospheric teleconnections and their response to greenhouse gas forcing, Rev. Geophys., 56, 185–206, doi:10.1002/2017RG000568, 2018.

Yiou, P. and Cattiaux, J.: Contribution of atmospheric circulation to wet North European summer precipitation of 2012, Bull. Am. Meteorol. Soc., 94(9), S39–S41, doi:http://dx.doi.org/10.1108/17506200710779521, 2013.

Yiou, P. and Cattiaux, J.: Contribution of atmospheric circulation to wet southern European winter of 2013, Bull. Amer. Meteor. Soc., 95, S66–S69, 2014.

Yuan, X., Wang, L. and Wood, E. F.: Anthropogenic Intensification of Southern African Flash Droughts as Exemplified by the 2015/16 Season, in Explaining Extreme Events of 2016 From a Climate Perspective, vol. 98, pp. S1–S157., 2017a.

Yuan, X., Wang, S. and Hu, Z.-Z.: Do Climate Change and El Niño Increase Likelihood of Yangtze River Extreme Rainfall?, in Bulletin of the American Meteorological Society, vol. 98, pp. S113–S117., 2017b.

Zhang, C.: Madden-julian oscillation: Bridging weather and climate, Bull. Am. Meteorol. Soc., 94(12), 1849–1870, doi:10.1175/BAMS-D-12-00026.1, 2013.

Zhang, Q., Li, J., Singh, V. P., Xu, C. Y. and Deng, J.: Influence of ENSO on precipitation in the East River basin, south China, J. Geophys. Res. Atmos., 118(5), 2207–2219, doi:10.1002/jgrd.50279, 2013.

Zhang, W., Wang, Y., Jin, F. F., Stuecker, M. F. and Turner, A. G.: Impact of different El Niño types on the El Niño/IOD relationship, Geophys. Res. Lett., 42(20), 8570–8576, doi:10.1002/2015GL065703, 2015.

Zhang, X., Wang, J., Zwiers, F. W. and Groisman, P. Y.: The influence of large-scale climate variability on winter maximum daily precipitation over North America, J. Clim., 23(11), 2902–2915, doi:10.1175/2010JCLI3249.1, 2010.

Zhao, A. D., Stevenson, D. S. and Bollasina, M. A.: The role of anthropogenic aerosols in future precipitation extremes over the Asian Monsoon Region, Clim. Dyn., 52(9–10), 6257–6278, doi:10.1007/s00382-018-4514-7, 2019.

Zheng, X. T., Xie, S. P., Vecchi, G. A., Liu, Q. and Hafner, J.: Indian ocean dipole response to global warming: Analysis of ocean-atmospheric feedbacks in a coupled model, J. Clim., 23(5), 1240–1253, doi:10.1175/2009JCLI3326.1, 2010.

Zwiers, F. W., Zhang, X. and Feng, Y.: Anthropogenic influence on long return period daily temperature extremes at regional scales, J. Clim., 24(3), 881–892, doi:10.1175/2010JCLI3908.1, 2011.